ISOTOPIC OXYGEN EXCHANGE REACTIONS ON MAGNESIUM OXIDE

IAN MELLOR

A thesis submitted in partial fulfilment of the requirements of The Nottingham Trent University for the degree of Doctor of Philosophy

December 1999

ProQuest Number: 10290295

ProQuest 10290295

Abstract

Isotopic oxygen exchange is a very useful tool in probing the reactivity of the surface oxygen of metal oxide catalysts. From this it is possible to obtain information regarding the mechanism of oxygen activation, obtaining a fundamental understanding of how catalysts operate. This is of importance since, for example, oxygen activation may be the rate determining step in oxidation catalysis, where the Mars-van Krevelen mechanism occurs.

In this thesis isotopic oxygen exchange reactions have been performed on magnesium oxide (MgO). This material was chosen as its defect chemistry is well understood, and it can be prepared with well defined surfaces exhibiting variations in the relative numbers of co-ordinatively unsaturated ions present at the surface. Each of these may differ in their reactivity towards exchange, hence measuring the activity of a series of MgO samples exposing different populations of co-ordinatively unsaturated surface ions, can lead to the elucidation of the most reactive site.

Three sets of MgO catalysts have been tested in this study. Initially the exchange characteristics of commercial MgO samples donated by Ube Industries of Japan were determined. These catalysts were observed to expose the (100) face and comparison of specific rates of exchange indicated structure insensitivity. MgO was also prepared from magnesium ribbon, magnesium hydroxide and magnesium basic carbonate precursors, looking at the influence of starting material upon isotopic oxygen exchange properties. The ex basic carbonate showed an activity five times that of the other two materials, which were found to be very similar. Finally an attempt was made to produce (111) terminated MgO surfaces, which are generally not observed due to their relative instability. Upon stabilisation of these planes rates of isotopic oxygen exchange were subsequently measured, comparing them to those obtained previously. Suprisingly the (111) terminated surface showed a higher specific rate than expected, as it exposed predominantly low co-ordinated ions.

Each of the MgO catalysts used has been extensively characterised using techniques such as surface area determination, TEM, powder XRD and XPS. Also the relative populations of 3, 4 and 5 co-ordinated sites have been determined for the commercial Ube samples from UV/VIS/NIR diffuse reflectance, photoluminescence and FTIR spectroscopies.

Acknowledgements

List Of Abbreviations

BET	Brunauer, Emmett and Teller
E_a	Activation Energy
EPR	Electron Paramagnetic Resonance
ESR	Electron Spin Resonance
FTIR	Fourier Transform Infra Red
FWHM	Full Width Half Maximum
JCPDS	Joint Committee On Powder Diffraction Standards
MCT	Mercury Cadmium Telluride
NIR	Near Infra Red
RDS	Rate Determining Step
SEM	Scanning Electron Microscopy
SSITKA	Steady State Isotopic Transient Kinetic Analysis
TCD	Thermal Conductivity Detector
TEM	Transmission Electron Microscopy
UV	Ultra Violet
VIS	Visible
XPS	X-Ray Photoelectron Spectroscopy
XRD	X-Ray Diffraction

Addendum

The term "*structure sensitivity*" as used in this thesis, is defined as the dependence of rate of reaction per unit area, upon the crystallographic face and/or particle size of the MgO samples used in this study. Correspondingly, "*structure insensitivity*" is the lack of dependence of reaction rate per unit area, upon these parameters.

Contents

1. Introduction

1.1 Scope Of Thesis

Isotopic oxygen exchange is a very useful tool in probing the reactivity of the surface oxygen of metal oxide catalysts. From this it is possible to obtain information regarding the mechanism of oxygen activation, obtaining a fundamental understanding of how catalysts operate. This is of importance since, for example, oxygen activation may be the rate determining step in oxidation catalysis, where the Mars-van Krevelen mechanism occurs.

Isotopic oxygen exchange has been utilised to great effect by several researchers over the past 50 years, highlighting metal oxide catalysts exhibiting a high oxidation potential. During a reaction an isotope of oxygen (generally ^{18}O) in the gaseous phase, exchanges with normal (^{16}O) on the oxide surface. The activity is measured by continuously monitoring the concentration of the oxygen species present in the gaseous mixture.

However to date there has been little or no work performed investigating exchange over a single oxide, taking into account differences in co-ordination environment of oxygen anions on the surface. Therefore the aim of the present work is to determine if isotopic oxygen exchange is structure sensitive over magnesium oxide (MgO), chosen as it has the ability to possess a perfectly cubic morphology. Another advantage of using this material is that its defect chemistry is well understood. Altering the crystallite size will lead to variations in the relative numbers of co-ordinatively unsaturated ions exposed at the surface. If each of these differ in their reactivity towards exchange, using a range of samples allows the determination of the most active.

In this study isotopic oxygen exchange was followed on three sets of MgO catalysts. Initially perfectly cubic crystallites were investigated differing only in their length, affecting the surface populations of co-ordinatively unsaturated sites. Consequently the environment of the most reactive oxygen anion or defect will be elucidated. Secondly catalysts were prepared from alternative precursor materials, yielding MgO possessing different morphologies. Again this will effect the co-ordination of the surface ions. Finally an attempt was made to produce (111) terminated MgO surfaces, which are generally not observed due to their relative instability. Also extensive characterisation of the MgO used was performed, providing valuable information which can help describe the measured rates of exchange.

1.2 Magnesium Oxide

MgO "periclase" is an alkaline earth oxide possessing a NaCl rock salt type structure [1], with a lattice parameter of 4.2 Å [2]. In its equilibrium state it exhibits a perfectly cubic structure, as indicated below.

(a) 3 co-ordinated
(b) 4 co-ordinated
(c) 5 co-ordinated
(d) 6 co-ordinated

4.2 Å
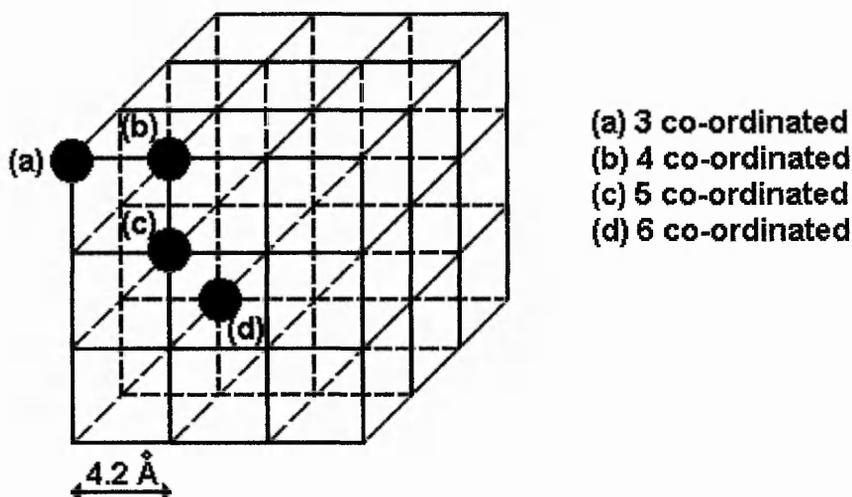
Fig 1.2.1   The NaCl Rock Salt Structure Of Magnesium Oxide.

From Fig 1.2.1 it can be seen that the co-ordination environment of Mg^{2+} or O^{2-} ions vary depending upon their lattice position. Close inspection indicates there are sites exhibiting 3, 4 and 5 fold co-ordination present at corners, edges and on the flat surface respectively. Fully saturated ions having six nearest neighbours are found in the bulk.

The usual termination plane of MgO is (100) which has been verified by electron microscopy studies [3-8]. It has also been demonstrated that small cublets can form aggregates, with growth observed at different orientations to each other [3, 9]. This results in the crystals produced exposing higher mean index planes, such as (110) and (111) [3, 6, 7, 9], as well as the predominant (100). It is reported a greater density of lower co-ordinated surface ions are evident, in the presence of higher order Miller indices [7, 10, 11].

For a crystallite of length (l) the number of ions (n) along the breadth of a single cube can be calculated from knowing the unit cell dimensions, thus populations of each individual site type can be determined. These are tabulated below.

Co-ordination Number	Number Of Ions Exhibiting Co-ordination
3	8
4	$12(n - 2)$
5	$6(n - 2)^2$
Total Surface	$2(3n^2 - 6n + 4)$

Table 1.2.1   **Populations Of Co-ordinatively Unsaturated Surface Sites Present On A Single MgO Cube.**

However it must be stressed that the above values are only applicable for a perfectly cubic morphology, generally this is not the case with surface defects being apparent.

1.2.1 Steps At The MgO Surface

It is not uncommon to find steps at the surface of a magnesium oxide crystal [5, 7], with a pictorial representation of this given in Fig 1.2.1.1.

(a) 3 co-ordinated
(b) 4 co-ordinated
(c) 5 co-ordinated
(d) 6 co-ordinated
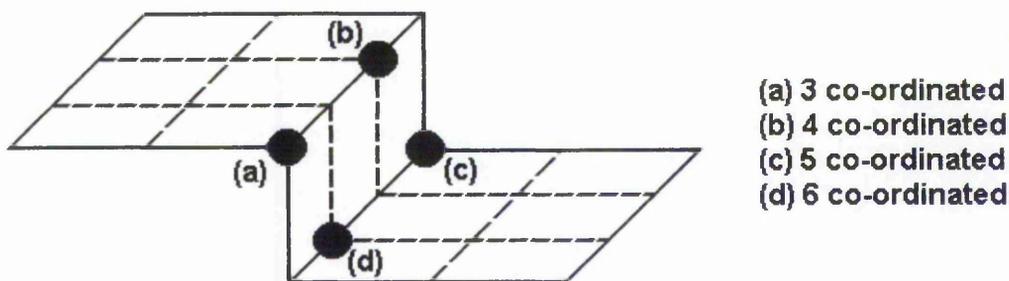
Fig 1.2.1.1   **A Step At The Magnesium Oxide Surface.**

As it can be seen inclusion of a step, equivalent to only a single unit cell, considerably changes the co-ordination environment of the surface ions. Populations of 3C and 6C sites increase, the latter not being exposed with a perfectly cubic system (Fig 1.2.1), at the expense of 4C which subsequently decrease. Interestingly the number of 5C remain the same.

1.2.2 Kinks And Terraces At The MgO Surface

Kinks and terraces are formed extensively at the MgO surface from the agglomeration of small crystallites, giving larger ones exhibiting high irregularity. They can also be observed following water vapour and carbon dioxide attack of MgO, caused by erosion of the surface (see Section 1.3). Evidence of kink and terrace formation by faceting was first reported by Moodie and Warble [3, 9], on preparing MgO from magnesium basic carbonate. They found that upon heating to elevated temperatures, small cubes typically 200-400 Å in length were microfaceting, giving both perfect and imperfect alignment. As a result bunches were formed possessing a greater average crystallite size.

(a) 3 co-ordinated
(b) 4 co-ordinated
(c) 5 co-ordinated
(d) 6 co-ordinated
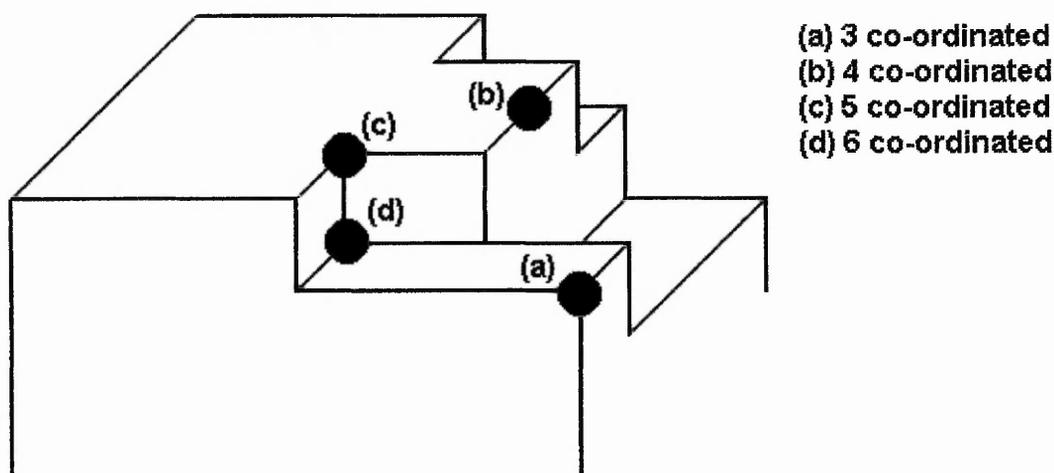
Fig 1.2.2.1   An Example Of An Irregular MgO Crystal Formed From The Annealing Of Several Small Cubes.

It is apparent from Fig 1.2.2.1 that construction of such a crystallite, has a dramatic effect upon the surface in terms of the numbers of different co-ordinated ions present. Both 3 and 6C populations are greater, compared to a perfect cube. Consequently a net reduction in 5C are observed, whilst 4 remain relatively unchanged [12].

1.3   Adsorption Of H_2O And CO_2 On The MgO Surface

It is found that both water vapour [4, 8, 13-19] and carbon dioxide [11, 20-27] readily attack MgO, causing surface modification upon desorption. Results show interaction with H_2O occurs at a greater rate than with CO_2 [22, 23].

1.3.1 Water Vapour Adsorption On The MgO Surface

One of the first reports of the dissociation of water vapour on the MgO surface was by Anderson *et al* [16]. It was found that during the initial stages of hydration a chemisorbed layer was formed, consisting of hydroxyl groups. Further H_2O addition led to the production of a weakly adsorbed monolayer of undissociated water molecules. These results were later verified by Coluccia and co-workers [17].

The mechanism of the dissociative chemisorption reaction is given below, it is interesting to note that an oxygen anion of the lattice is active in the formation of one of the hydroxyl ions.

Fig 1.3.1.1   The Dissociative Chemisorption Of A Water Molecule At The MgO Surface.

During the early studies, Anderson [16] made no attempt to measure differences in reactivity between surface ions of different co-ordination, concentrating only upon the degree of coverage. However Kuroda *et al* [8] and other studies [11, 15, 17, 28-30] showed that the 3C sites were the most active for water vapour dissociation, followed closely by 4C and finally 5C. Attack of the latter was found to be slow but significant at room temperature [8].

Similar work by Jones *et al* [31] did not subscribe to this view, stating that ions exhibiting 5 fold co-ordination were unable to dissociate H_2O on the MgO surface. They thought that the reaction occurred only at the more highly unsaturated sites, located at corners, steps and edges. On the flat (100) plane adsorption was thought to occur in small pits along the surface formed by abrasion due to H_2O contact, the degree of which could be enhanced by increasing the water vapour pressure. Consequently this increased the exposure of 3 and 4 co-ordinated ions on the surface. These sites were then responsible for the hydroxyls found on the (100) face. Such channels could not be detected through surface area measurements, using nitrogen physisorption at 77 K, since they were inaccessible to the incoming nitrogen molecule.

More recently theoretical calculations have been performed by Langel and Parrinello [32] and de Leeuw *et al* [33] on this system, agreeing with the findings of Jones *et al* [31] that 5 co-ordinated ions were unable to dissociate water vapour. Simulations showed 3 and 4 co-ordinated ions to be the preferential sites for chemisorption. It was also found that 5C ions held an undissociated physisorbed layer of H_2O, however this desorbed upon room temperature outgassing. Unlike the previous experimental work which indicated a hydroxyl group was bound to one Mg^{2+}_{LC} cation (Fig 1.3.1.1), it appeared the most stable configuration involved OH^- interaction with two cations exhibiting low co-ordination at a stepped surface.
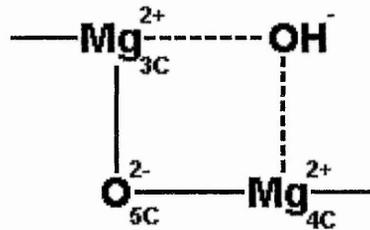
Fig 1.3.1.2   **Proposed Stable Configuration Of Hydroxyl Group Adsorption On The Stepped MgO Surface.**

1.3.2 Water Vapour Desorption On The MgO Surface

Desorption of water vapour from MgO can cause the formation of kinks and terraces, altering the co-ordination environment of the surface. Anderson [16] proposed that desorption following the initial loss of the physisorbed overlayer, was realised by interaction of two adjacent OH groups, that associated with the Mg^{2+}_{LC} leaving more easily. However desorption of the other hydroxide ion resulted in removal of a O^{2-}_{LC} of the lattice, giving the observed kink and terrace formation.
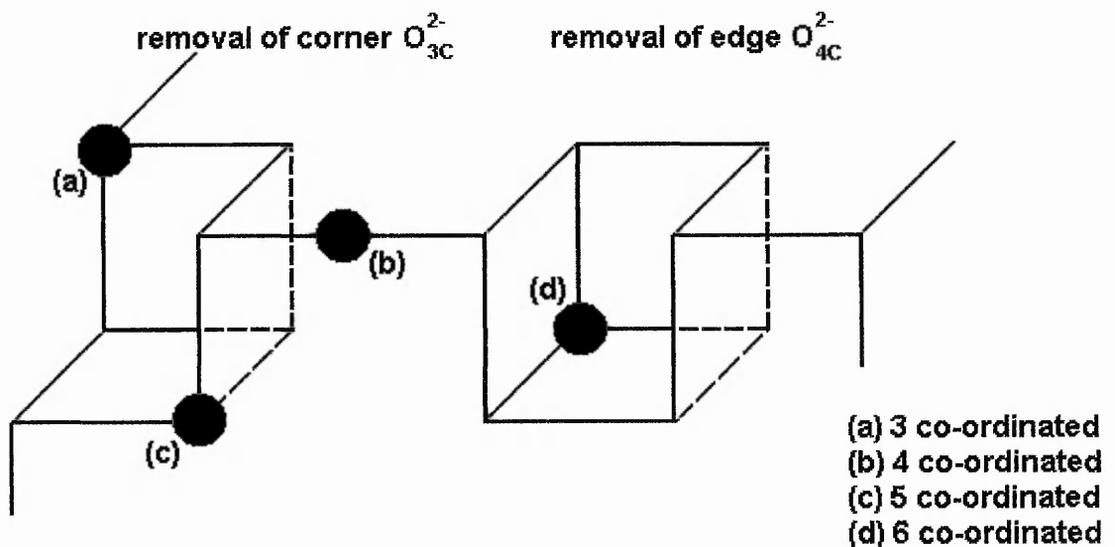
Fig 1.3.2.1   **Kink Formation On The Surface Of MgO Due To The Removal Of O^{2-}_{LC} Anions From The Lattice Through Water Vapour Desorption.**

As Fig 1.3.2.1 shows removal of O^{2-}_{LC} anions situated at a corner and edge position (sometimes termed a valley site [11]) respectively, change the distribution of co-ordinatively unsaturated sites present on the surface. Considering this desorption a common trend is apparent, applicable to both cases. There is an increase in populations of 3 and 6C sites at the surface, at the expense of 4C. Subsequently ions exhibiting 5 fold co-ordination remain constant, however their exposure towards reacting species is altered. These findings are similar to those for irregular MgO cublets, formed by the annealing of several small crystallites (Section 1.2.2). However in this situation it is also possible to remove an oxygen atom from the surface whilst leaving the electrons in the vacancy, thus forming an F centre (two electrons trapped in an anion vacancy).

It is well documented the desorption temperature of water vapour from MgO, is determined by the lattice ion co-ordination environment, to which the hydroxide group is adsorbed. Most studies are not concerned with comprehensive details of this reaction [4, 8, 13-17, 19, 29], only mentioning that an OH associated with an O^{2-}_{3C} is the hardest to remove, requiring heating to 1073 K. The only work to provide an extensive account of this process was by Coluccia *et al* [17], on a high surface area MgO derived from magnesium hydroxide. They constructed the following table, indicating the percentage of surface hydroxyl groups remaining as a function of temperature.

Outgassing Temperature / K	Percentage of OH groups remaining / %
373	100
473	55
573	36
673	25
773	15
873	9
973	3
1073	0

Table 1.3.2.1   Percentage Of Surface Hydroxyl Groups Remaining At A MgO Surface As A Function Of Temperature. - Taken From Ref [17].

Clearly this cannot be directly related to populations of 3, 4 and 5 co-ordinated sites present, as these vary between individual samples, the latter generally constituting roughly 95 % of the total surface.

Finally it can be noted that all kinks and terraces covered in this section are formed irrespective of the model assumed for H_2O vapour adsorption (Section 1.3.1). This is because in all studies, it is accepted the heterolytic water dissociation product H^+ is associated with one O^{2-}_{LC} anion of the oxide.

1.3.3 Carbon Dioxide Adsorption On The MgO Surface

As well as possessing the ability to adsorb water vapour, CO_2 interacts with the MgO surface, but to a lesser extent [22] at room temperature. The occurrence of physically adsorbed CO_2 [20, 24, 34], unidentate [21, 22, 24, 26, 27, 34] and bidentate [20-22, 24, 26, 27, 34] species have been identified using IR spectroscopy. Evans and Whateley [21] found it was also possible to form hydrogen bicarbonate ions, upon adsorbing CO_2 on hydroxylated MgO. The CO_2 species observed on the clean surface are shown below, interacting with both Mg^{2+}_{LC} and O^{2-}_{LC} ions.

<center>unidentate   bidentate</center>
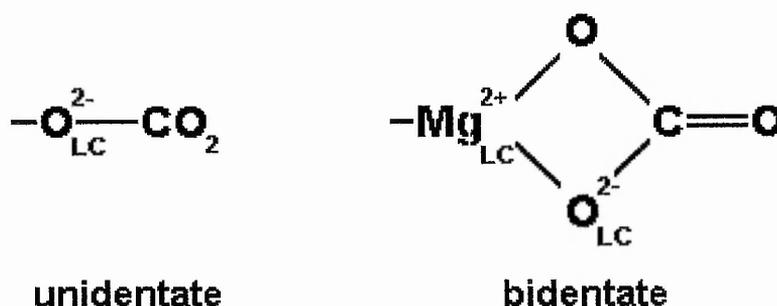
Fig 1.3.3.1   **Species Formed On The MgO Surface Upon Interaction With Carbon Dioxide.**

Even though the literature indicates the formation of the above two chemisorbed groups, there are discrepancies between researchers. Evans and Whateley [21] and other workers [22, 24, 26, 34] were in agreement that both uni- and bidentate ions were formed, but the latter only at room temperature and above. Gregg [20] was only able to identify bidentate species on MgO, which may be attributed to the sensitivity of his IR measurements, as Tsuji

et al [26] found unidentate coverage to be sparse on the surface. Gregg [20] also showed that unlike water vapour attack which caused bulk MgO rehydration, $MgCO_3$ was only evident in the outermost layers of the solid. There are few examples highlighting the preferential sites for CO_2 adsorption, however Onishi *et al* [11] reported low co-ordinated ions to have the greatest reactivity.

1.3.4 Carbon Dioxide Desorption On The MgO Surface

As with H_2O removal, CO_2 desorption can promote kink and terrace formation on the MgO surface. Loss of an oxygen anion of the oxide is possible, with one of the adsorbed carbon dioxide taking an adjacent position [22, 35], providing overall neutrality. The net result is similar to that illustrated in Figs 1.2.2.1 and 1.3.2.1. Smart *et al* [24] found all surface carbonate species could be removed by evacuation at 723 K, bidentate ions being the most tightly bound. Tsuji *et al* [26] were in agreement with this first statement, but saw temperatures of 1000 K were required for total bicarbonate desorption.

1.4   Isotopic Oxygen Exchange

Isotopic oxygen exchange is a useful diagnostic tool for investigating the reactivity of surface oxygen, enabling comparison of different catalysts. Ever since the earliest reports of Allen and Lauder [36], considerable attention has been paid to this reaction, with the publication of several reviews on this topic [37-39].

Exchange is known to proceed via two pathways, the first between ^{18}O in the gas phase and ^{16}O of the oxide, is known as heterophase (or heterolytic) exchange. The other termed equilibration (sometimes called homophase, homolytic or homomolecular exchange) does not involve exchange with the surface, it actually catalyses the mixing of ^{18}O and ^{16}O. The extent of reaction is generally monitored by measuring the changing composition of the gaseous phase with time using mass spectrometry.

The main technique for following exchange is through thermal activation, however more recently it has been shown illumination at room temperature can also provide the desired energy for initiation [40, 41]. The most common origin of the isotopic oxygen is $^{18}O_2$, however on occasions other probe molecules such as $H_2{}^{18}O$ [37, 42, 43], $C^{18}O_2$ [26]

and C^{18}O [44] have been used in heterophase reactions. The kinetics of exchange have generated much interest [38, 45-49], substantial analysis being performed by many workers.

Many pure, doped and metal supported oxides have been tested for their exchange capabilities. Also metals coated with thin oxide films have been investigated [38, 50-52]. Isotopic exchange activities of materials have been compared to their ability to oxidise numerous reactions, in an attempt to find a correlation between the two processes [38, 43, 53-57].

1.4.1 Conditions Of Pre-treatment

In investigating either homo or heterophase isotopic oxygen exchange, oxides are subjected to high temperature treatment, removing adsorbed species from the surface. This was to in an attempt to prevent them from contributing to the measured rate of exchange.

The initial procedure used by Winter [37, 54, 58-63] and other workers [36, 43, 50, 52, 64, 65] was to heat the sample in vacuum to 673-973 K, depending on the nature of the oxide, over a 8-16 hour period. On completion of this ^{18}O was admitted into the system, with exchange being followed.

On interpreting these early results, Winter [48] found an initial rapid decrease in ^{18}O, during the initial stages of reaction. There was concern that high temperature vacuum heating caused F centre (two electrons trapped at a surface anion vacancy) and other defect formation. Therefore at this point, the only process being measured was the filling of such sites, not proper exchange.

At a similar time Popovskii [55] and Boreskov [38], thought it would be of interest to pre-treat in an atmosphere of normal (^{16}O) oxygen, thus giving a stoichiometric surface layer. Winter [48] subsequently adopted this approach, concluding that ^{16}O filled the F centres, giving an equilibrium amount of oxygen in the lattice. Subsequently the initial drop in ^{18}O on the commencement of exchange was less pronounced, compared to that following vacuum treatment, leading to the claim of successful F centre eradication.

As a greater understanding of the effects of pre-treatment has been developed, researchers now use either method to tailor their specific needs, depending if they wish to investigate reduced or oxidised surfaces.

1.4.2 Reaction Mechanisms Of Isotopic Oxygen Exchange

As briefly mentioned above isotopic oxygen exchange can be divided into two main groups, that with or without the participation of oxygen of the oxide. These will now be dealt with in more detail.

The first report of equilibration (homophase exchange) was by Winter [61], on MgO and ZnO. In this reaction the oxide surface catalyses the scrambling of a ^{16}O and ^{18}O gas phase mixture, until equilibrium is attained. Winter found equilibration could be described by the following equation :

$$^{18}O_{2\,(g)} + {}^{16}O_{2\,(g)} \quad \longrightarrow \quad 2\,^{16}O^{18}O_{(g)} \qquad (R_0)$$

The R_0 termination was added at a later date by Cunningham [41, 66, 67], the zero indicating no exchange with the lattice, which was subsequently adopted by most workers. There are also instances with R_3 [40, 48] and R [46] being used to identify this reaction.

Early experiments by Winter [37, 51, 61] and others [50, 52, 56], were performed at temperatures lower than those where exchange with the surface layer was evident. This enabled homophase exchange to be measured, without any contributions from heterophase reactions. During their equilibration studies Boreskov [38, 65] and other workers [68, 69], initially brought the surface to equilibrium with respect to ^{18}O, hence oxygen atoms of the oxide participated in this type of reaction.

Later Klier *et al* [46], followed by Winter [48] and Boreskov [38, 47], provided a more extensive study of the kinetics of exchange. This allowed the measurement of rates of equilibration and heterophase exchange, when occurring simultaneously on a catalyst surface.

Early heterophase isotopic oxygen exchange experiments involving the lattice [36, 70] made no attempt to consider any reaction mechanisms, primary objectives were to show exchange between ^{18}O and ^{16}O on catalyst surfaces was evident.

Winter [58-60, 62] was the first worker to make any attempt to quantify the actual mechanism of exchange, as shown below.

$$^{18}O_{(g)} + {}^{16}O_{(surface)} \quad \longrightarrow \quad {}^{16}O_{(g)} + {}^{18}O_{(surface)}$$
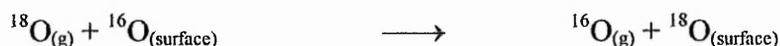
As it can be seen this only offers a crude explanation regarding the exchange of the heavy isotope with the oxide lattice, however this was found sufficient at the time.

Not until an extensive analysis of the kinetics of exchange was provided by Klier *et al* [46], Boreskov *et al* [38, 47] and Winter [48], were any mechanisms associated with exchange involving surface oxygen presented. Boreskov [38, 47] thought three pathways were available, the first being equilibration (R_0) as discussed above, proceeding through an adsorption/desorption mechanism. Reactions could also be realised with the participation of either one or two surface oxygen anions, given the name heterophase (heterolytic) exchange. The former process, which was assumed to be occurring previously when studying simple kinetics [58-60, 62], was now called R_1 exchange. In this one atom of the adsorbed $^{18}O_2$ molecule replaced a single ^{16}O of the oxide lattice, as indicated below.

$$^{18}O_{2\,(g)} + {}^{16}O_{(surface)} \longrightarrow {}^{16}O^{18}O_{(g)} + {}^{18}O_{(surface)} \qquad (R_1)$$

Reactions involving both atoms of the isotopic oxygen was termed R_2 exchange.

$$^{18}O_{2\,(g)} + 2\,^{16}O_{(surface)} \longrightarrow {}^{16}O_{2\,(g)} + 2\,^{18}O_{(surface)} \qquad (R_2)$$

Clearly after a certain time period, there will be a significant concentration of ^{18}O present in the surface layer or in the gaseous phase, which itself is capable of undergoing exchange. Therefore further mechanisms were constructed allowing the possibility of this occurring.

$$^{16}O^{18}O_{(g)} + {}^{16}O_{(surface)} \longrightarrow {}^{16}O_{2\,(g)} + {}^{18}O_{(surface)} \qquad (R_1)$$

$$^{16}O^{18}O_{(g)} + {}^{18}O_{(surface)} \longrightarrow {}^{18}O_{2\,(g)} + {}^{16}O_{(surface)} \qquad (R_1)$$

Similarly for R_2.

$$^{16}O^{18}O_{(g)} + 2\,^{16}O_{(surface)} \longrightarrow {}^{16}O_{2\,(g)} + {}^{16}O_{(surface)} + {}^{18}O_{(surface)} \qquad (R_2)$$

$$^{16}O^{18}O_{(g)} + 2\,^{18}O_{(surface)} \longrightarrow {}^{18}O_{2\,(g)} + {}^{18}O_{(surface)} + {}^{16}O_{(surface)} \qquad (R_2)$$

Routes are available where exchange occurs but does not lead to a change in isotopic composition, for this reason they are not given here.

13

These alternative exchange pathways will not be evident during the early stages of a reaction, since they require either ^{18}O on the oxide surface or $^{16}O^{18}O$ present in the gas phase. However their concentrations will increase with time during an experiment, allowing exchange to be realised via these routes. Cunningham *et al* [41] were able to follow the alternative R_1 and R_2 reactions on ZnO and TiO$_2$ samples. They measured rates of heterophase exchange after a pre-equilibration of $^{16}O_2$ and $^{18}O_2$ on the surface. Under such conditions initial $^{16}O_2$, $^{18}O_2$ and $^{16}O^{18}O$ levels will be appreciable in the gas phase, allowing the new R_1 and R_2 reactions to proceed. Using this mixture allows different heterophase pathways to be readily distinguished, by the effect each has upon the isotopic composition of the gas phase.

When reinvestigating the modes of exchange, Winter [48] postulated R_2 exchange was possible through the formation and subsequent decomposition of a four atom complex $(^{16}O^{16}O^{18}O^{18}O)_{surface}$. This led to two new mechanisms.

$$^{18}O_{2\,(g)} + 2\,^{16}O_{(surface)} \longrightarrow \quad ^{16}O^{18}O_{(g)} + ^{16}O_{(surface)} + ^{18}O_{(surface)} \quad (R_2)$$

$$^{16}O_{2\,(g)} + 2\,^{18}O_{(surface)} \longrightarrow \quad ^{16}O^{18}O_{(g)} + ^{16}O_{(surface)} + ^{18}O_{(surface)} \quad (R_2)$$
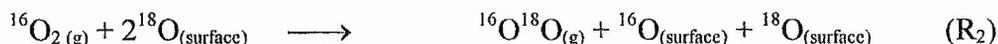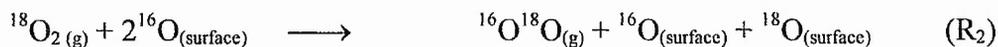
Winter subsequently reinvestigated the kinetics of exchange taking into account these two new R_2 processes. However problems arose when considering certain experimental conditions where $R_0 = 0$ and $R_1 = R_2$, and the number of exchangeable atoms on the oxide surface were greater than in the gaseous phase. It was found that no value of R_2 could simultaneously account for the total number of ^{18}O atoms in the gas phase or total rate of exchange. Therefore contributions from the above R_2 mechanisms were discarded, concluding exchange was not possible through a four atom complex.

More recently a reaction termed place exchange has been identified [41, 71]. It was found a metal oxide could carry an appreciable amount of non-dissociatively chemisorbed $^{16}O_2$ from pre-oxidation (Section 1.4.1), thought to be in the form of an O^-_2 species [71]. Upon commencement of a reaction this layer could exchange with the admitted $^{18}O_2$, changes in the gas phase may be represented by the following equations.

$$^{16}O_{2\,(chem)} + ^{18}O_{2\,(g)} \longrightarrow \quad ^{18}O_{2\,(chem)} + ^{16}O_{2\,(g)} \quad (R_2)$$

$$^{16}O_{2\,(chem)} + ^{16}O^{18}O_{(g)} \longrightarrow \quad ^{16}O^{18}O_{(chem)} + ^{16}O_{2\,(g)} \quad (R_2)$$

Due to the nature of this it is sometimes likened to a R_2 mechanism.

In studying the characteristics of CaO, Cunningham [72] found that adsorbed hydroxyl groups on the surface were capable of undergoing oxygen exchange. New mechanisms were formulated to account for these observations.

$$^{18}O_{2\,(g)} + {}^{16}OH^-_{(surface)} \longrightarrow {}^{16}O^{18}O_{(g)} + {}^{18}OH^-_{(surface)} \qquad (R_1)$$

$$^{18}O_{2\,(g)} + 2{}^{16}OH^-_{(surface)} \longrightarrow {}^{16}O_{2\,(g)} + 2{}^{18}OH^-_{(surface)} \qquad (R_2)$$

It was found that the occurrence of oxygen exchange, with either hydroxyl groups or the surface, was dependent upon the initial outgassing conditions of CaO.

1.4.3 Kinetics Of Isotopic Oxygen Exchange

When measuring rates of equilibration over MgO and several first row transition metal oxides [37, 54, 61], Winter found the decrease in $^{18}O_2$ to obey a first order rate equation :

$$-\frac{dx}{dt} = k_e' x$$

Equation 1.4.3.1   **First Order Rate Equation For Isotopic Oxygen Equilibration On Metal Oxide Catalysts.**

where   x   = excess abundance of mass 36 in the gaseous phase

     t   = time

     k_e' = experimental rate constant for equilibration

This was later verified by further studies of Margolis [52] and Boreskov *et al* [38, 56, 64, 65], on V_2O_5 and some other first row transition metal oxides. Antoshin *et al* [68] also showed this to be true for homophase exchange on rare earth oxides. The only exception to this rule was CuO, found by Margolis [50] not to follow first order kinetics. However Boreskov did not subscribe to this view [65], reporting a lack of reproducibility of results

on this sample. Similarly the process can also be followed by monitoring the increase in $^{16}O^{18}O$ with time [38, 47, 56, 65, 69].

Early heterophase experiments of Allen and Lauder [36] made no attempt to quantify the kinetics of isotopic oxygen exchange, the object of the work was to show that the reaction was proceeding. The first attempt to model the kinetics of exchange was by Winter [37, 58-60, 62, 63, 70], in measuring the disappearance of mass 36 in the gaseous phase on several metal oxide specimens. From this a first order kinetic expression was postulated [58, 59, 63] :

$$-\frac{d^{18}O_t}{dt} = k_e(^{18}O_t - {}^{18}O_\infty)$$

Equation 1.4.3.2   **First Order Rate Equation For Isotopic Oxygen Exchange On Metal Oxide Catalysts.**

where $^{18}O_t$ = amount of ^{18}O in the gaseous phase at time t

$^{18}O_\infty$ = amount of ^{18}O in the gaseous phase at the end of reaction (∞ time)

k_e = experimental rate constant

t   = time

It was shown that plotting $\log_{10}(^{18}O_t - {}^{18}O_\infty)$ versus time yielded a straight line [37, 62, 70], demonstrating the validity of the equation. This was subsequently verified by Cameron *et al* [43] and Boreskov [55].

As briefly discussed above Winter was only concerned with monitoring changes in mass 36 the gas phase, assuming that a single ^{18}O exchanged with one ^{16}O of the lattice (later called R_1 exchange, Section 1.4.2). No consideration was made towards the simultaneous occurrence of this reaction with double exchange reactions (R_2) or equilibration (R_0). The possibility of new routes led Boreskov *et al* [38, 47] and Klier *et al* [46] to further investigate the kinetics of exchange, where all three mechanisms could be measured simultaneously.

Klier *et al* [46] formulated the rates of change in the number of molecules of a given composition, using the different exchange mechanisms (Section 1.4.2) and the following expression.

$$\text{Rate of change in the number of} \quad = \left(\frac{1}{n}\right) \times K \times p_1 \times p_2$$
$$\text{molecules of a given composition}$$

Equation 1.4.3.3   **Equation Showing The Rate Of Change In The Number Of Molecules Of A Given Composition During An Exchange Reaction.**

where $K =$ rate constant for R_0, R_1 and R_2 respectively.

$n =$ number of molecules converted in the chosen reaction per molecule of the isotopic species whose conversion is followed.

$p_1 =$ probability of the simultaneous presence of molecules and atoms of the given isotopic composition in the chosen reaction.

$p_2 =$ probability that when exchange occurs between molecules and/or atoms of the given isotopic composition in the chosen reaction, it will also lead to the change in the number of molecules of the isotopic composition followed.

From knowing the contributions from each individual mechanism, the kinetics of exchange could be formulated, making the following assumptions. Initially it is believed that different isotopes undergo reaction at the same rate, neglecting isotope effects. Secondly transport phenomena are considerably faster than exchange, and finally, all exchangeable atoms of the solid oxide are equivalent. Generally this last statement is not true, as most surfaces are not uniform for exchange [55]. However this problem is easily overcome, with the kinetics measured corresponding to the most active regions of the oxide [38, 47, 48].

In deriving expressions from Equation 1.4.3.3 the symbols presented below were introduced.

$x =$ number of $^{18}O_2$ molecules in the gas phase.

$y =$ number of $^{16}O^{18}O$ molecules in the gas phase.

$z =$ number of $^{16}O_2$ molecules in the gas phase.

$w =$ number of ^{18}O atoms in the gas phase.

$u =$ number of exchangeable ^{18}O atoms in the solid oxide.

$v =$ number of exchangeable ^{16}O atoms in the solid oxide.

c = total number of exchangeable atoms in the system.

m = total number of exchangeable atoms in the solid.

a = total number of oxygen molecules in the gaseous phase.

It also holds that :

a = x + y + z

w = 2x + y

m = v + u

c = w + u

Therefore the change in $^{18}O_2$ molecules in the gas phase can be described by the equation below.

$$-\frac{dx}{dt} = \frac{R_0}{a}\left[x - \frac{1}{a}\left(\frac{w}{2}\right)^2\right] + \frac{R_1}{a}\left[x - \frac{w(c-w)}{2m}\right] + \frac{R_2}{a}\left[x - \frac{a(c-w)^2}{m^2}\right]$$

Equation 1.4.3.4   **Equation Showing The Change In $^{18}O_2$ Molecules In The Gas Phase With Time.**

It can also be shown that a similar expression holds for $^{16}O^{18}O$ molecules.

The variation of ^{18}O atoms in the gas phase with time is given by :

$$\frac{dw}{dt} = 2\frac{dx}{dt} + \frac{dy}{dt}$$

Therefore substituting Equation 1.4.3.4 and that corresponding to $^{16}O^{18}O$ molecules into the above, then integrating between t = 0 and t, yields the following.

$$w - w_\infty = (w - w_\infty) \exp\left[-(2R_2 + R_1)\left(\frac{2a+m}{2am}\right)t\right]$$

Equation 1.4.3.5   **Equation Showing The Change In The Number Of ^{18}O Atoms In The Gas Phase.**

where $w_0 = w$ at $t = 0$ and $w_\infty = \dfrac{2ac}{(2a+m)}$

Now substituting the value of w from Equation 1.4.3.5 into Equation 1.4.3.4 and integrating between the limits of $t = 0$ and t, we obtain an expression describing the dependence of the number of $^{18}O_2$ molecules in the gas phase with time.

$$x = \frac{ac^2}{(2a+m)^2} + (w_0 - w_\infty)\left(\frac{c}{2a+m}\right)\exp\left[-(2R_2+R_1)\left(\frac{2a+m}{2am}\right)t\right] -$$

$$\left\{\frac{1}{2m}(w_0 - w_\infty)^2 \frac{\left[1 + \left(\frac{m^2 R_0}{4a^2 R_2}\right) - \left(\frac{mR_1}{2aR_2}\right)\right]}{\left[2 + \left(\frac{m}{2a}\right) - \left(\frac{mR_0}{2aR_2}\right) + \left(\frac{R_1}{R_2}\right)\right]} \times \exp\left[-(2R_2+R_1)\left(\frac{2a+m}{am}\right)t\right]\right\}$$

$$+\left\{x_0 - \frac{ac^2}{(2a+m)^2} - (w_0 - w_\infty)\left(\frac{c}{2a+m}\right) + \frac{1}{2m}(w_0 - w_\infty)^2\right.$$

$$\left.\times\frac{\left[1 + \left(\frac{m^2 R_0}{4aR_2}\right) - \left(\frac{mR_1}{2aR_2}\right)\right]}{\left[2 + \left(\frac{m}{2a}\right) - \left(\frac{mR_0}{2aR_2}\right) + \left(\frac{R_1}{R_2}\right)\right]}\right\} \times \exp\left[-\frac{1}{a}(R_0 + R_1 + R_2)t\right]$$

where x_0 is the value of x at $t = 0$.

Equation 1.4.3.6   **Equation Showing The Dependence Of The Number Of $^{18}O_2$ Molecules In The Gas Phase With Time.**

Following the same procedure yields a similar result for the change in $^{16}O^{18}O$ molecules with time, as illustrated by Boreskov *et al* [38, 47].

From measuring the isotopic composition of the gaseous phase throughout an experiment, contributions of R_0, R_1 and R_2 exchange can be determined during a reaction. It is found the most convenient method of calculating these values is by the aid of a computer [45].

Subsequently Boreskov *et al* [38, 47] and Winter [48] both made a comprehensive study of the kinetics of isotopic oxygen exchange, comparing their findings to those of Klier *et al* earlier [46]. Even though slightly different methods were adopted in both cases, it was demonstrated that all solutions generated were equivalent.

Finally in considering exchange kinetics the quantity given below is of importance, as it is the measure of deviation of the reaction from equilibrium, where it has a value of 4 [38, 41, 46-48, 66].

$$\frac{y^2}{xz}$$

If the contribution from R_2 is zero a value of 4 is observed throughout exchange. Consequently if both R_1 and R_0 are absent, the function passes through a minimum, before reaching a steady state. All other pathways lie between these two extremes.

1.4.4 Determination Of The Rate Determining Step Of Isotopic Oxygen Exchange

Since the kinetics of isotopic oxygen exchange have been studied, activation energies (E_a) of this process have been determined. As a result of this there has been considerable discussion, regarding the nature of the rate determining step (RDS) of this reaction.

Winter [59, 60] and Boreskov [47, 65] provided a sequence of events, describing all the stages necessary in an exchange reaction, as shown overleaf.

(1)   Transportation of reactants towards the surface.

(2)   Adsorption of oxygen molecules.

(3)   Dissociation of adsorbed molecules into atoms.

(4)   Diffusion of adsorbed atoms or molecules over the oxide surface into cracks or
        pores.

(5)   Exchange proper involving electron transfer between adsorbed and lattice oxygen or
        suitable surface defects.

(6)   Recombination of adsorbed atoms into molecules.

(7)   Desorption of oxygen molecules.

(8)   Transportation of products away from the surface.

From these attempts were made to quantify the nature of each process, elucidating the RDS
of exchange.

        Gaseous diffusion through the powdered oxide (diffusion limitation, steps 1 and 8),
becomes the limiting step of the reaction, when the transportation of reactants/products
either to/from the catalyst is the slow stage. When apparent it is normally characterised by a
low E_a, typically in the range 10-15 kJ mol^{-1} [73]. It can generally be prevented by
improving the movement of the catalyst with respect to the gas, or vice versa [73].
However the catalyst particle size can also influence diffusion limitation depending upon its
nature.

        During isotopic oxygen exchange studies on many oxides, Winter found that at high
temperatures the E_a of reaction suddenly decreased to a value of approximately 10 kJ mol^{-1}
[37, 54, 58-60, 63]. It was suggested that the results could not be diffusion limited, as the
catalyst was spread loosely over the vessel, allowing adequate transportation of the gaseous
mixture to/from the reaction zone. However this still led to Boreskov claiming Winter's
results were subject to diffusion limitation [38, 65]. Using a gas circulating pump, hence
improving the movement of the isotopic mixture with respect to the catalyst, Popovskii and
Boreskov [38, 55] did not witness a decrease in E_a with increasing temperature, showing
that it is likely Winter's results were diffusion limited.

        Winter investigated the adsorption of normal oxygen on both MgO [60] and ZnO
[63], attempting to determine its influence on heterophase exchange. Rates of uptake were
appreciable even at 10^{-3} Torr and liquid oxygen temperatures and hence it was concluded it
was not to be the slow stage under exchange conditions.

However, on measuring rates of both hetero and homophase reactions on NiO, Fe_2O_3 and Cr_2O_3 [37, 54], Winter found the E_a's of both processes to be equal. Since adsorption and desorption were common to both, it was now thought one of these were the RDS in isotopic oxygen exchange. Interestingly oxygen adsorption on the same catalysts, at exchange temperatures and pressures, gave similar results. Consequently, it was proposed that the earlier measurements on MgO [60] and ZnO [63] were misleading, and did not accurately simulate exchange conditions. Consequently homophase exchange E_a's of these two samples [61] were different to those measured regarding heterophase exchange [60, 63]. Boreskov [38] also expressed doubts regarding the validity of comparing oxygen adsorption and equilibration rates as a means of determining the RDS. It was thought that high temperature treatment of the oxides, prior to adsorption, would lead to a defective surface. Upon oxygen admission filling of such sites would occur prior to adsorption, giving an inaccurate measurement of this value.

Subsequently numerous workers showed rates of hetero and homophase exchange to be equivalent, on many first row transition [38, 55, 56, 65], rare earth [68] and other oxides [38]. Naturally there are a few reports with conflicting views. Margolis [52] found differences on V_2O_5, whereas Boreskov *et al* [38, 55, 56, 65], showed rates to be equal. These researchers reached the same conclusion regarding MgO [38] and ZnO [65], disagreeing with Winter [61]. From their studies Boreskov and co-workers were in general agreement with Winter [37, 52] that the RDS of isotopic exchange is the adsorption of oxygen on the catalyst surface, with dissociation into atoms or ions.

In investigating isotopic exchange on numerous metal oxides, Winter [48] now demonstrated desorption to be the RDS, previously not being able to distinguish between this and adsorption [37, 52]. If adsorption were the limiting stage the E_a of exchange could be determined using the gas kinetic expression:

$$Rate = (B\sigma)e^{\left(\frac{-E_a}{RT}\right)}$$

Equation 1.4.4.1   **Kinetic Expression For Calculating The E_a Of Exchange Assuming Oxygen Adsorption As The RDS. - Taken From Ref [48].**

where E_a = activation energy for exchange / kJ mol^{-1}

   R = molar gas constant / 0.008314 kJ K^{-1} mol^{-1}

   T = temperature / K

   σ = degree of surface available for adsorption (total coverage = 1)

and

$$B = \frac{PN}{\left(2\pi MRT\right)^{0.5}}$$

where P = oxygen pressure

   N = Avogadro's number

   M = molecular weight of oxygen

Using Equation 1.4.4.1 Winter [48] found that of the 38 oxides studied, the maximum calculated E_a of exchange was only 42 kJ mol^{-1}. He therefore concluded that desorption must be the slow stage, since measured E_a's were much higher.

Later Boreskov [64] followed equilibration on the surface of V_2O_5, comparing rates with those for hydrogen oxidation, on the same catalyst. Results indicated E_a's did not coincide, which was suprising as oxygen adsorption was a common step in both reactions. If this were the slow stage, one would expect the measured rate of hydrogen oxidation to be comparable to that of exchange. Since this was not the case, it was now thought the RDS of exchange, to be the actual exchange between adsorbed oxygen and the oxide lattice. In the case of Boreskov's [38, 65, 69] and others [68] homophase experiments, they argued that pre-treatment of the surface in ^{18}O allowed equilibration to proceed via exchange with the lattice. Hence it was possible that this was the slow stage. Clearly this indicates a change in view from their earlier work, showing adsorption followed by dissociation as being the determining step. However in this study Boreskov did not consider either hydrogen dissociation or H_2O desorption as possible limiting stages, casting doubts over the validity of the results. Also the above suggestion does not account for the equivalence of homo and heterophase rates, calculated by Winter [37, 54], without participation of surface oxygen.

From these studies it is difficult to determine the RDS of isotopic oxygen exchange with any certainty. Evidence exists indicating both adsorption/desorption and exchange

proper as being possible candidates. It appears further investigations are required, in understanding this process fully.

1.5   The History of Isotopic Oxygen Exchange On MgO

Magnesium oxide has played a significant role in measurements of isotopic oxygen exchange over metal oxides, being the subject of many investigations. A high proportion of these experiments were conducted in a static reactor at elevated temperatures, with a small quantity of the isotopic mixture bled into a mass spectrometer for analysis. This is the method adopted in the current study. However more recently different approaches have been used, including the use of illumination for initiating exchange [40] and continuous flow microreactors [74, 75], where ^{18}O is periodically pulsed into the system.

A chronological summary of literature concerned with isotopic oxygen exchange on MgO, using $^{18}O_2$ as the probe molecule and the three methods outlined above, is tabulated overleaf.

These results from Table 1.5.1.1 will now be discussed in greater detail.

1.5.1 Isotopic Oxygen Exchange On MgO Performed In A Static System

The first measurement of isotopic oxygen exchange over MgO was published by Winter [58-60]. Following heating of the sample under vacuum overnight, exchange was found to proceed rapidly on the catalyst surface. Construction of an Arrhenius plot indicated a change in slope, hence a change in mechanism, at approximately 693 K. The E_a of reaction was calculated to be 142 and 13 kJ mol^{-1}, below and above this point. Winter attributed these two processes to exchange with the oxide and migration either across the surface or into the bulk respectively. In a subsequent study, Winter [37] presented further data regarding the same sample. The reaction of high E_a was comparable to that given previously, however the lower value was approximately 20 kJ mol^{-1} higher, out of the range of experimental error.

After this Winter next performed equilibration (homophase) reactions on an evacuated MgO surface [37, 61], involving mixing of $^{16}O_2$ and $^{18}O_2$ on the sample.

Publisher and Reference	Experiment Type	MgO Precursor	Treatment	Reaction	E_a / kJ mol^{-1}
Winter [58] [59] [60]	Static	$MgCO_3$	673-873 K in vac 16 hr	Heterophase	142 < 693 K 13 > 693 K
Winter [61] [37]	Static	$MgCO_3$	813 K in vac 16 hr	Homophase	113
Winter [37]	Static	$MgCO_3$	813 K in vac 16 hr	Heterophase	150 < 693 K 32 > 693 K
Boreskov [38]	Static	No reference	773 K in vac 4 hr	Homophase Heterophase	167 167
Muzykantov [45] [46]	Static	No reference	Vac then O_2 at exch. temp	$2R_2 = R_1$	-
Winter [48]	Static	$MgCO_3$	783 K in vac 753 K in O_2	R_1(little R_0) R_1	159[a] 159[a]
Martin and Duprez [71]	Static	Commercial 100 Å Ube	Vac then O_2 / H_2 at 723 K	R_1	166
Kalenik and Wolf [75]	Continuous flow	No reference	No reference	Heterophase	-
Peil [74]	Continuous flow	No reference	O_2 at exch. temp 30 min	Heterophase	265

a - diffusion limitation still apparent at higher temperatures but magnitude not specified.

Table 1.5.1   A Summary Of The Literature Regarding Isotopic Oxygen Exchange Experiments On MgO.

Oxygen of the oxide did not participate in the reaction, only catalysing the integration of the two isotopes (Section 1.4.2). An E_a of 113 kJ mol^{-1} was obtained in the range 298-523 K, a range chosen where no exchange with the surface was evident. These early experiments indicated rates of equilibration were quicker than their heterophase counterpart.

The early interest shown by Winter, led Boreskov [38] to study the exchange characteristics of MgO. Boreskov cited two main differences between his results, to those

presented by Winter [37, 58-61]. Firstly the E_a of equilibration was found to be 167 kJ mol^{-1}, which is 54 kJ mol^{-1} greater than that of Winter [37, 61]. Boreskov attributed this to differences in treatment conditions. After vacuum heating Boreskov allowed the surface to react with ^{18}O. This gave both a stoichiometric surface oxide layer, and one having an equilibrium ^{18}O content with respect to the gas phase prior to exchange. Upon evacuation and admission of the reaction mixture, this form of equilibration involved the lattice, unlike that of Winter's [37, 61]. In addition Boreskov's catalyst was not active at 298 K. It was thought the higher activity obtained by Winter was due to defects such as F centres not present with Boreskov's MgO, formed during vacuum heating. Boreskov [38] demonstrated this by reproducing the earlier findings of Winter under the same conditions. Later Winter [48] agreed with this statement, distinguishing a lack of homophase exchange after prolonged ^{16}O treatment.

Unlike Winter, Boreskov did not observe a break in the heterophase Arrhenius plot in the 693 K region. Boreskov found the E_a of this reaction to be 167 kJ mol^{-1} throughout the 673-773 K range studied, being similar to the high value E_a of Winter. It was concluded that as Winter increased the temperature, the results became diffusion limited, the slow stage being transportation of reactants/products either to/from the catalyst [73]. Boreskov overcame this by forcing the movement of the gaseous phase, with the aid of a circulating pump [55].

Klier *et al* [46] and Muzykantov [45] provided an in depth investigation of the kinetics of isotopic exchange, providing a better understanding of mechanisms. In this they introduced the concept of R_1 and R_2 pathways, whereas Winter only acknowledged reaction involving the oxide (Section 1.4.2). Their report for MgO is only brief, only offering the fact that both R_1 and R_2 processes were occurring, the former being twice that of the latter.

As a consequence of the increased literature regarding MgO, Winter [48] reinvestigated oxygen exchange on MgO, in an attempt to substantiate the earlier claims. Even though experiments were performed using a dynamic system, a low E_a was still reported above ca. 693 K, however Winter still believed his apparatus not to be diffusion limited. A value of 159 kJ mol^{-1} was obtained at lower temperatures, after both vacuum and ^{16}O treatment, agreeing with his earlier work [37, 58-60] and that of Boreskov [38]. Reactions now took into account the possibility of the R_2 mechanism occurring, but detailed analysis could not find any evidence of this, unlike Klier [46] and Muzykantov [45] before.

A slight contribution from R_0 exchange was observed following vacuum, but not ^{16}O treatment. This was in accordance with the results of Boreskov [38].

Both Boreskov [38] and Winter [48] compared rates of exchange, at an extrapolated temperature of 573 K, providing a relative scale of catalytic activity between oxides. Values of 1.95×10^{12} and 1.8×10^{11} atoms s^{-1}/m^2 were published, by Winter [48] and Boreskov [38] respectively. This is interesting as the rate measured by Winter, is nearly an order of magnitude greater than Boreskov at 573 K.

The most recent report of isotopic exchange on MgO was by Martin and Duprez [71], using 100 Å crystals of MgO, supplied by Ube Industries of Japan. This is of particular interest, as it is one of the samples under investigation, in the present study (Chapter 3). They found after an initial treatment in vacuum then O_2 and H_2 at 723 K, an E_a of 166 kJ mol^{-1} was obtained, being close to the earlier findings of Winter [37, 48, 58-60] and Boreskov [38]. Another conclusion from this was that only R_1 exchange was observed, agreeing with Winter [48], but not Klier and co-workers [45, 46]. Finally this is one of only a few publications claiming to have exchanged more than a monolayer for this type of investigation.

In all isotopic oxygen exchange experiments performed the rate is independent of oxygen pressure over the whole range studied. Therefore it can be concluded even at the lowest quantity studied, 10 Torr [38], all sites responsible for exchange are saturated.

1.5.2 Isotopic Oxygen Exchange On MgO Performed Under The Influence Of Illumination

As with thermally activated samples, exchange under the influence of illumination is followed in a static system. Most of the work involving MgO in this area has been performed by Cunningham *et al* [61]. Pre-treating a sample in vacuum at 923-1123 K, caused anion vacancy (F centre) formation, in accordance with the earlier findings of Winter [58-60]. Subsequent admission of an equimolar mixture of $^{16}O_2$ and $^{18}O_2$, causes rapid equilibration at 298 K, similar to Winter's homophase experiments [37, 61]. However subjecting the catalyst to darkness causes exchange to cease, with illumination required to restart activity. Photons in the range 340-640 nm, incident to the sample promote electrons from F centres into the surface state, which then contribute to exchange.

$$hv$$
$$F \ Centre_{(surface)} \quad \longrightarrow \quad F^+ \ Centre_{(surface)} + electron$$

It is interesting to note the wavelengths used are longer than those required to excite co-ordinatively unsaturated O^{2-}_{LC} on the MgO surface (190-265 nm, see Section 4.1), hence any contribution from these can be discarded.

Upon illumination both homo and heterophase exchange was observed, but it was difficult to quantify contributions from individual mechanisms. Also under these conditions reactions did not follow the simple kinetics, as devised earlier by many workers [38, 46-48].

1.5.3 Isotopic Oxygen Exchange On MgO Performed In A Continuous Flow System

In the case of a continuous flow isotopic oxygen exchange experiment, normal ^{16}O is initially passed over the catalyst, followed by an abrupt switch to ^{18}O. Isotopic switches are considered to be very useful during mechanistic studies of reaction pathways without affecting the steady state equilibrium.

Steady state isotopic transient kinetic analysis (SSITKA) has been performed most recently by Peil *et al* [74] and Kalenik and Wolf [75]. Peil *et al* [74] found flowing 2 ml/min $^{18}O_2$ over MgO at atmospheric pressure, allowed exchange of 1.2 monolayers at 898 K. Subsequent calculations showed this process as having an E_a of 265 kJ mol^{-1}, being 100 kJ mol^{-1} greater than that reported for the static system [37, 38, 48, 58-60]. Due to the high temperatures used, the RDS was attributed to diffusion of ^{18}O into the bulk lattice, replenishing the surface with ^{16}O available for further exchange.

1.6   The Mars-van Krevelen Mechanism

Oxidation reactions play an important role in heterogeneous catalysis and many of these processes are thought to occur via a Mars- van Krevelen mechanism [76]. In this an adsorbed species (often a hydrocarbon, depicted by R below), combines with oxygen of the lattice, giving a product and a lattice vacancy :

$$R_{(ads)} + O^{2-}_{(lattice)} \longrightarrow products + 2e^-$$

Oxygen from the gas phase then fills this vacancy :

$$\tfrac{1}{2}O_{2\,(g)} + 2e^- \longrightarrow O_{(lattice)}$$

A graphical representation of these events is shown below.
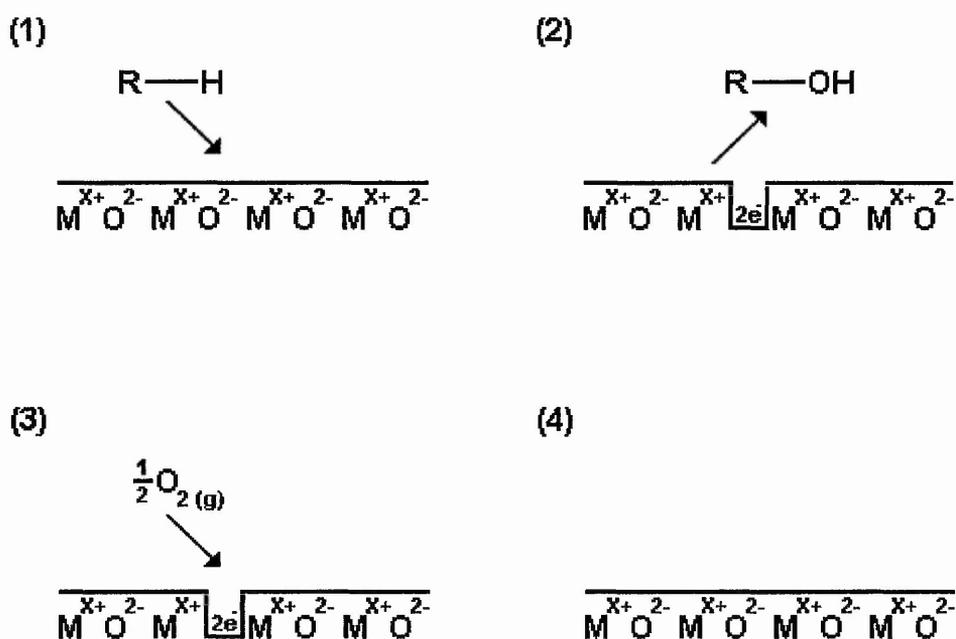
Fig 1.6.1   Stages Of An Oxidation Reaction Following A Mars-van Krevelen Type Mechanism.

No assumption is made regarding the form of the catalyst oxygen, it can either be chemisorbed or in the lattice. The rate of reoxidation is taken to be proportional to the fraction of sites on the catalyst and to oxygen pressure to the power n. Under steady state conditions :

$$Rate = kP(1 - \theta)$$

Equation 1.6.1   **Kinetics Of The Mars-van Krevelen Mechanism.**

where P = partial pressure of reactant species

k = rate constant for oxidation

θ = fraction of active sites

Lattice oxygen appears to follow this model in a general way. It is thought that the limiting stage of this type of oxidation is oxygen activation, the O^{2-} ion being the active species.

The above statement is of particular interest in terms of isotopic oxygen exchange, as reaction with the lattice could possibly be the RDS of this reaction (Section 1.4.4). This fact could bear significance in the search for new catalysts in oxidation reactions. If both share a common determining step, an oxide exhibiting a high exchange activity, may exhibit similar properties in an actual process.

Winter [37, 53] demonstrated with NiO, Fe_2O_3 and Cr_2O_3, all showing moderate exchange capabilities, that CO oxidation followed a Mars-van Krevelen type mechanism on these oxides. In using a surface enriched with heavy oxygen, it was found the initial ^{18}O content of CO_2 to be unusually high, which decreased during the run. The reason for this was that in the early stages CO was removing ^{18}O from the lattice, with the active site replenished by ^{16}O from the gas phase. Due to this all the subsequently formed CO_2, constituted of only normal oxygen. Another interesting finding from this study was that the amount of ^{18}O in the CO_2 was considerable less than that exchanged on the surface previously. This indicated that only a small portion of the surface was available for CO oxidation, constantly undergoing the reaction cycle.

1.7   Comparison Of Isotopic Oxygen Exchange Rates With Those In Oxidation Reactions

Since isotopic oxygen exchange can sometimes be used as a diagnostic tool in determining oxide activity, it would be of interest to compare trends, with those available for specific

oxidation reactions. Such work has been performed by several researchers [38, 55, 56], mostly involving first row transition metal oxides.

Before attempting to draw any conclusions, Boreskov [38] stated comparisons were only valid between exchange results after ^{16}O treatment and oxidation reactions, having an excess of oxygen in the mixture. It was found hydrogen [38, 55], carbon monoxide [38] and hydrocarbon total oxidation reactions [38], followed a similar sequence to exchange rates [65], as indicated below.

$$Co_3O_4 > MnO_2 > NiO = CuO > Fe_2O_3 > ZnO > Cr_2O_3 > V_2O_5 > TiO_2$$
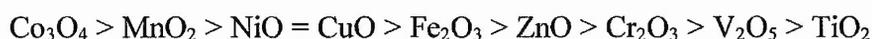
This was also illustrated graphically.
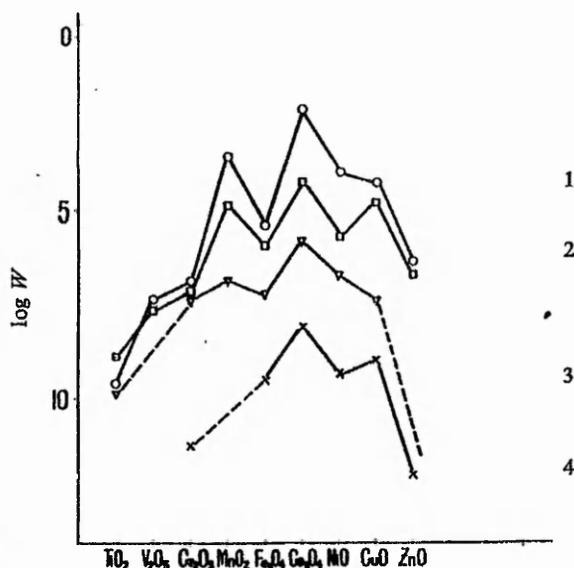
FIG. 8.—The catalytic activity of oxides of the elements of the fourth period in the homomolecular exchange of oxygen (1), oxidation of hydrogen (2), oxidation of methane (3) and nitrogen oxide decomposition (4) at 300°C.

Fig 1.7.1   **Plot Showing Similarities Between Isotopic Oxygen Exchange Rates And Those In Specific Oxidation Reactions. - Taken From Ref [57].**

Dzisyak [56] and Boreskov [38] also attempted to measure SO_2 oxidation over the same transition metal catalysts, however they encountered problems as each formed an inactive sulfate. The exception to this was V_2O_5, which when doped with alkali metal sulfates showed a comparable order to isotopic oxygen exchange activities.

2. Experimental

2.1 Surface Area Determination

Physisorption of an inert gas (generally nitrogen at 77 K) onto a surface and plotting the volume adsorbed as a function of equilibrium pressure allows the construction of an isotherm. Determination of surface area from this is possible, by the application of a linearising mathematical procedure to the initial part. The approach most commonly used was devised by Brunauer, Emmett and Teller [77], giving the following expression :

$$\frac{P}{V(P_0 - P)} = \frac{1}{V_M C} + \frac{(C-1)P}{V_M C P_0}$$

Equation 2.1.1   **The BET Equation.**

where   V = volume of gas adsorbed at equilibrium pressure P

   V_M = volume necessary to form a monolayer

   P_O = saturated vapour pressure of the adsorbent gas at the temperature of
      measurement

   C = constant

Plotting $P/V(P_O-P)$ as ordinate and P/P_O as abscissa yields a straight line, the slope is given by $(C-1)/V_M C$ and the intercept by $1/V_M C$.

Five types of isotherm have been identified [78, 79], reflecting the nature of the adsorbent and adsorbate under study. However the BET equation can only be applied to types II and IV, also it is only valid for a limited part of the isotherm, in the range $0.05 < P/P_O < 0.3$. MgO can generally exhibit either a type II or IV isotherm, depending upon preparation techniques.

Samples were initially outgassed at 473 K, to a pressure of 5×10^{-2} Torr to remove any adsorbed species from the surface. Measurements were performed using a Digisorb instrument, helium being used as calibrant and nitrogen as adsorbate at 77 K. Surface areas

were calculated assuming the average cross sectional area of a nitrogen molecule to be 0.162 nm^2.

2.1.1 Surface Area Determination Of Exchanged Samples

It is desirable to measure the surface areas of both exchanged and oxygen pre-treated samples, to seek evidence of sintering. The Digisorb (Section 2.1) is inadequate for such an application due to the small masses involved, typically 25-100 mg, as it can only measure surface areas greater than 10 m^2 in the bulb. For this reason a Quantasorb instrument was used.

Samples were heated at 423 K for 1 hour in a 20 ml/min continuous flow of gas (90 % He and 10 % N$_2$), to remove any adsorbed species from the surface. Nitrogen adsorption was then performed at 77 K, at several points on the isotherm where the BET equation is valid. For each individual pressure nitrogen was initially adsorbed on the surface at 77 K. Heating the catalyst to room temperature caused this amount to be desorbed, which was subsequently measured using a TCD (Thermal Conductivity Detector), allowing determination of the degree of coverage.

2.2 Transmission Electron Microscopy (TEM)

Transmission electron microscopy is a technique which can be employed to examine sample morphology. Electron micrographs of MgO can give valuable information regarding crystallite shape, presence of steps, terraces and kinks on the surface and particle size distribution.

Micrographs were obtained using a Jeol, JEM-2010 electron microscope operating at 200 kV. Prior to analysis samples were dispersed in chloroform, the resulting sample being mounted onto a 3 mm diameter copper grid with 200 mesh carbon film.

2.3   Powder X-Ray Diffraction (XRD)

The powder X-ray diffraction pattern can be used as a fingerprint for the identification of many compounds. Diffraction occurs when the angle of incidence of X-rays, satisfies the Bragg equation :

$$n\lambda = 2d \sin\theta$$

Equation 2.3.1   **The Bragg Equation.**

where   n = a small integer

λ = wavelength of X-ray source

d = separation between planes in crystal

θ = angle of incidence of X-Rays

Reflections from the pattern can be compared to those in a standard powder diffraction file [80], enabling structure identification. The presence of different phases can also be determined. Measurements were performed using a Philips 3510 diffractometer with a Cu Kα source, wavelength 1.5418 Å. A scan range of $5° < 2\theta < 80°$ was used, with step size 0.02° and counting time of 0.5 s. The pattern is obtained by rotating the sample through an angle θ while the detector is rotated through 2θ.

2.3.1 Determination Of Crystallite Size

Crystallite size can be calculated by measuring the full width at half maximum (FWHM) of a peak, then applying the Scherrer equation :

$$d = \frac{k\lambda}{B \cos\theta}$$

Equation 2.3.1.1   **The Scherrer Equation.**

where   d = particle size diameter / Å

         k = constant / 57.29578°

         λ = wavelength of X-Ray source / 1.5418 Å

         B = full width at half maximum / degrees

         θ = diffraction angle / degrees (results are given as 2θ)

This is only an approximate method and can be influenced by various factors, such as instrument parameters and lattice distortions.

2.3.2 Determination Of Particle Shape

A method of deducing mean crystallite shape was developed by Berry [81], using the dependence of line breadth on the indices of reflection. This was achieved by calculating the ratio between the breadths of two lines produced by a specimen, by rearrangement of the Scherrer equation :

$$R = \frac{B_1}{B_2} = \frac{k_1 \cos \theta_2}{k_2 \cos \theta_1}$$

Equation 2.3.2.1   **Equation For Determining Crystal Shape As Devised By Berry [81].**

where   R = ratio between the breadths of two lines

         B = full width at half maximum / degrees

         k = coefficient depending on the shape of the particles and the Miller indices of the reflection

         θ = diffraction angle / degrees

Comparing experimental ratios with theoretical ones, determined from the above equation, taking values of k as used by Berry [81], gives information regarding crystal morphology. When investigating cubic shape, the sample showing the closest ratio to unity, corresponds to the one exhibiting the greatest cubic character.

2.4   X-Ray Photoelectron Spectroscopy (XPS)

Electrons present in the core levels within a sample may absorb photons, causing excitation to occur. The result of this is the emission of a photoelectron, possessing a certain amount of kinetic energy, the magnitude of which is given by the following expression.

$$kinetic\ energy = photon\ energy - (binding\ energy + \phi)$$

Equation 2.4.1   **Correlation Between Kinetic Energy And Binding Energy.**

where ϕ = work function / eV

The work function is typically 5eV, which is negligible compared to the photon energy, therefore it can be treated as constant.

Spectrometers are used to measure kinetic energies, making the calculation of binding energies simple using Equation 2.4.1. Data is then presented as the number of electrons with a specific energy versus binding energy. Each element in the periodic table has a unique set of binding energies, making XPS an excellent technique for near surface elemental analysis.

Photoelectrons collide with other electrons, being inelastic in nature, hence energy loss is incurred. The average distance travelled before this event takes place is roughly 5-15 Å and is termed the inelastic mean free path (escape depth). Therefore only electrons near the surface can escape and be detected, making XPS surface sensitive.

2.4.1 Experimental Procedure

XPS was used as a means of identifying impurities present in MgO. Measurements were recorded using a VG ESCA 3 instrument. Initially powdered samples were mounted onto a probe using double sided adhesive tape, then introduced into the vacuum system. Spectra were not recorded until the base pressure of the analyser chamber was in the region of 10^{-8} Torr.

Aluminium Kα radiation was used, giving photons of energy 1486.6 eV incident to the sample. Peak positions were corrected for changes relative to Mg 1s, as this was the most intense. Subsequent identification was possible by reference to the Handbook of Photoelectron Spectroscopy [82].
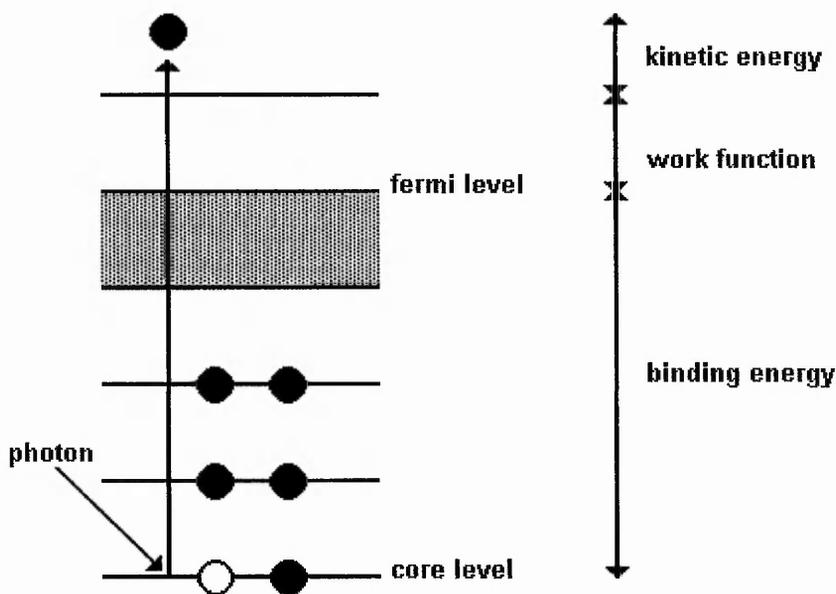
Fig 2.4.1.1   **Principles Of Photoelectron Spectroscopy.**

2.4.2 Determination Of The Surface Concentration Impurities

The ratio of impurities present compared to either magnesium or oxygen can be determined by comparison of peak areas, using the following expression :

$$\frac{I_A}{I_B} = \frac{N_A}{N_B} \times \frac{\delta_A}{\delta_B}\left[\frac{E_A}{E_B}\right]^{0.6}$$

Equation 2.4.2.1   **Surface Ratio Determination Of Two Elements.**

where   A = element A

B = element B

I = peak area corrected for the number of scans / arbitrary units

N_A/N_B = surface ratio of element A to B

δ = photoionisation cross sectional area / arbitrary units

E = kinetic energy / eV

0.6 = calibration factor of the instrument

With calculations cross sectional areas reported by Scofield were used [83].

2.5   Sample Pre-treatment For Spectroscopic Measurements

Prior to UV/VIS/NIR diffuse reflectance, FTIR and photoluminescence spectroscopy measurements, MgO was subjected to a pre-treatment. This was in an attempt to obtain a clean surface, by removal of hydroxyl groups, as water attack of MgO is evident at room temperature [4, 8, 13-19].

Samples were treated in a cell, its design dependent on the characterisation method used, connected to a glass vacuum line. Initially the sample was heated in vacuum ($<10^{-4}$ Torr) to 723 K at a rate of 10 K/min. On attainment of this temperature 10 Torr O_2 was brought into contact with the surface and left for 30 minutes, with the intention of removing any residual hydrocarbons present. Further heating in vacuum to 1093 K at the same rate followed then the catalyst was left for 30 minutes at this temperature. Finally the sample was cooled to room temperature, the cell then being transferred to the appropriate instrument so measurements could be made.

2.5.1 Adsorption Measurements

Photoluminescence, UV/VIS/NIR diffuse reflectance and FTIR spectra of MgO were recorded after reactions with hydrogen, oxygen or carbon monoxide. The probe gases were admitted in situ using a glass dosing system, connected to the cell. Measurements were taken at pressures ranging from 10^{-3}-100 Torr.

2.6   Photoluminescence Spectroscopy

The absorption of ultra-violet radiation by molecules of a solid causes the promotion of electrons to an excited state. Fluorescence occurs when the electron loses energy and reverts back to the ground electronic state.

a : absoption
b : fluorescence
c : collisonal deactivation
d : intersystem crossing
e : phosphorescence
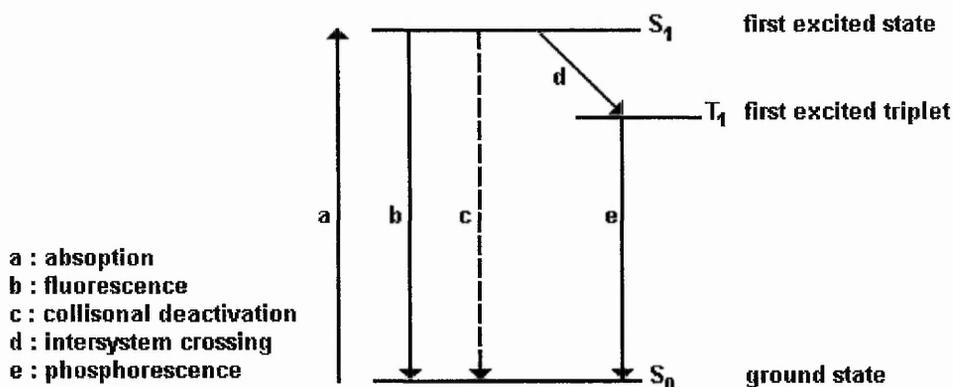
Fig 2.6.1   Principles Of Fluorescence.

Phosphorescence and collisonal deactivation also occur. The possibility exists for the spin of the excited electron to be reversed, with movement to the triplet state, this process being termed intersystem crossing. Phosphorescence is then observed with the subsequent loss of energy. Because a change of spin is necessary, the probability of phosphorescence occurring is low. Fluorescence and phosphorescence are easily distinguishable by their decay times, lifetimes being in the range 10^{-9}-10^{-7} and 10^{-4}-10 seconds respectively.

Collisional deactivation offers a decay pathway minimising the lifetime of the excited state, spanning approximately 10^{-12} seconds. The excess energy is transferred to other molecules through collisions, by means of a radiationless process, on dropping to the ground state. Due to this fact collisional deactivation is undetectable.

2.6.1 Experimental Procedure

Powdered MgO was pre-treated as described previously (Section 2.5). Measurements were obtained using a Spex Fluorolog 1680, 0.22 m, single beam spectrometer, with double grating excitation and emission monochromators. A 450 W Xenon lamp was used as source, producing radiation that extends from 300-1300 nm.

Radiation was passed to the sample via an excitation monochromator, giving the desired scanning wavelength but excluding others. The transmitted fluorescence travels through an emission monochromator to a photomultiplier and is consequently recorded.

Both excitation and emission spectra were obtained. An excitation spectrum is obtained by measuring the emission intensity at a fixed wavelength whilst the excitation wavelength is varied. Emission spectra involve excitation at a fixed wavelength whilst recording the emission intensity.

Results were normalised using Rhodamine B as a reference. Exciting this compound at 250 nm yields a well defined emission peak in the 500-700 nm region, the maximum intensity of which is used in standardising all experimental values.

2.7   Diffuse Reflectance Spectroscopy

In UV/VIS/NIR diffuse reflectance spectroscopy, samples with irregular surfaces, are irradiated with narrow bands of radiation. The incident light penetrates the surface, exciting vibrational modes of the analyte and is reflected in all directions. This phenomenon is termed diffuse reflectance.

Light travels from the sample and is reflected on the walls of an integrating sphere, coated with a nearly perfect diffuse reflector (generally $BaSO_4$) and eventually enters the detector.

A spectrum is initially recorded with a $BaSO_4$ reference in place, which is then replaced by the sample. Usually the ratio of the intensity of radiation reflected from the sample to that of the reference (R), is plotted as a function of the wavelength of the incident light.

detector
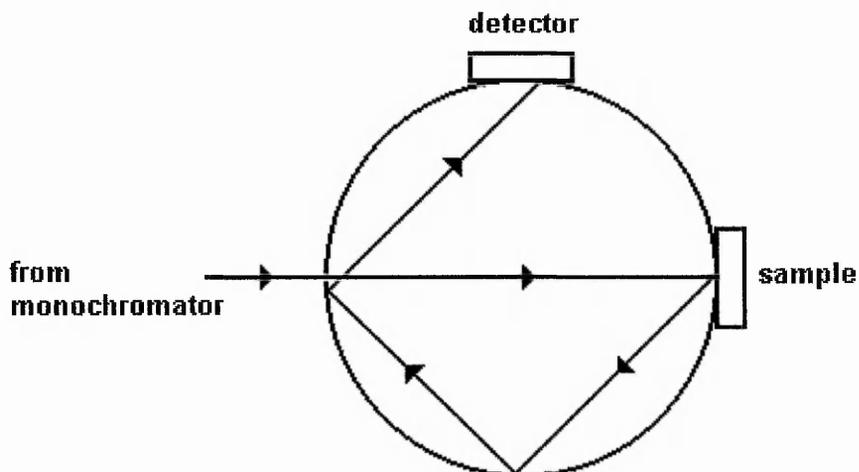
Fig 2.7.1   An Integrating Sphere.

2.7.1 Experimental Procedure

Spectra were obtained in the UV/VIS/NIR region of the electromagnetic spectrum, in the range 190-2500 nm, using a Perkin Elmer Lambda 19 UV/VIS/NIR spectrometer (NIR = Near Infra Red). The instrument consisted of two sources, a deuterium lamp for the UV and a halogen lamp for the VIS/NIR region. Similarly two detectors were employed, a photomultiplier and a PbS detector, functioning in the UV/VIS and NIR ranges respectively. In determining reflectance spectra $BaSO_4$ was used as reference.

2.8   Fourier Transform Infra Red Spectroscopy (FTIR)

Fourier Transform Infra Red (FTIR) spectroscopy is a technique which can be used to identify adsorbed species at the catalyst surface. A distinct advantage of using FTIR is that it allows the measurement of all wavelengths of absorption simultaneously.

The basis of an FTIR instrument is the interferometer, operating on a principle developed by Michelson :
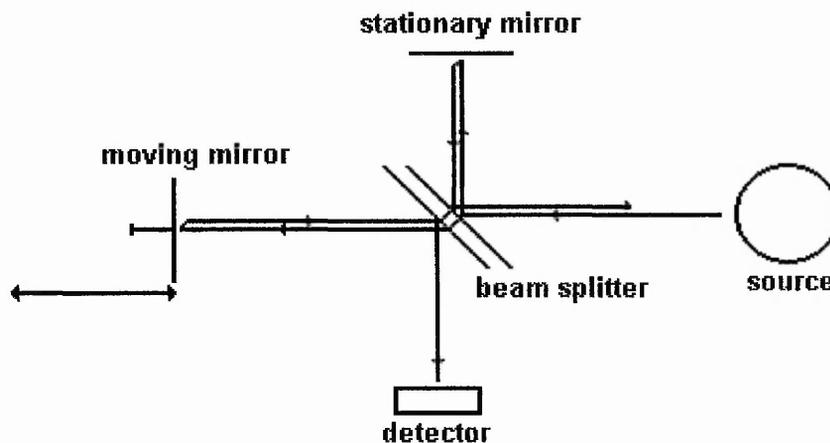
Fig 2.8.1   Principles Of The Michelson Interferometer.

Radiation emitted from the IR source makes contact with the beam splitter, a half silvered plane mirror. This causes half of the radiation to be transmitted to the moving mirror, whilst the other half is reflected, hitting the stationary mirror. Light reflected from the mirrors recombines and enters the detector, interfering constructively or destructively depending on the position of the moving mirror.

Plotting the intensity of radiation as a function of the moving mirror's position gives an interferogram, taking the Fourier transform of this yields the intensity of the source. Inserting a sample, between either of the two mirrors and the beam splitter, modifies the interferogram, resulting in a complete infra red spectrum.

2.8.1 Experimental Procedure

IR spectra were recorded using a Bruker IFS 48 instrument, using a SiC glowbar as source, capable of emitting radiation in the range 4000-400 cm^{-1}. Detection was achieved using a MCT (mercury cadmium telluride) photoconducting device, cooled at 77 K. Experiments were performed in transmission mode, with a resolution of 4 cm^{-1}.

MgO in the form of rectangular pellets, dimensions 18 mm x 10 mm, were supported in a cell, designed so measurements could be made at room temperature or 77 K. This was then attached to a glass dosing line, as described previously (Section 2.5),

allowing adsorption of probe molecules in situ. In all cases the thickness of each pellet was assumed to be equal.

A diagram of the IR cell can be seen below :
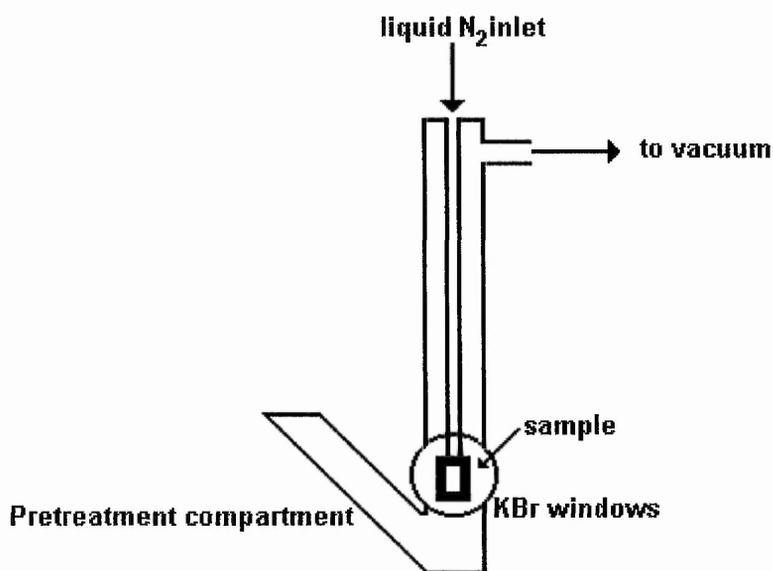
Fig 2.8.1.1   Cell Used In IR Experiments.

2.9   Isotopic Oxygen Exchange Reactions - Reactor Design

Reactions were followed using a specifically designed microreactor, taking into account systems used by other workers in the field [37, 43, 55, 62]. A schematic diagram of the system can be seen overleaf.
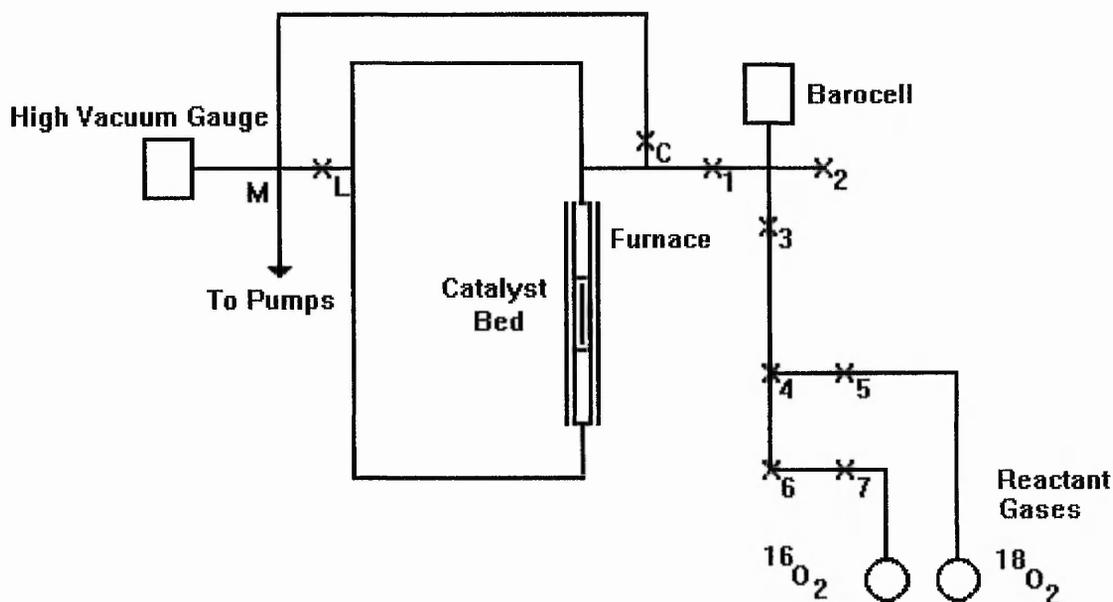
Fig 2.9.1   Layout Of The Reactor System Used For Isotopic Oxygen Exchange Experiments.

where X_{1-7} = toggle valves

X_C = high conductance valve

X_L = leak valve

M   = mass spectrometer

The reactor, volume 24 cm^3, was built using standard 1/4" stainless steel tubing. The catalyst was housed in 1/2" tubing equipped with a silica insert, employed as stainless steel could possibly promote exchange at high temperature. Silica wool plugs were used to position the sample, ensuring it remained central in the uniform heated zone of the furnace.

The system was outgassed using the high conductance valve, X_C (Caburn AV150M). Reactant gases were admitted via the dosing line, X_{1-3}, of known volume (7.5 cm^3) and pressure, measured using a barocell (Edwards W600-41-111, 0-1000 Torr). This was also used to monitor the system pressure during the course of a reaction. Temperatures were maintained by use of a furnace (LPC Elements) coupled to a Eurotherm 818 controller.

A small quantity of reaction mixture was continually bled to a quadrupole mass spectrometer (Hiden HAL 201.5), through a leak valve (Balzers UDV 040). The volume of gas is so small, typically corresponding to a pressure drop of 0.5 Torr/h, that the reactor conditions may be assumed to be constant.

When in the mass spectrometer, the sample can be analysed to determine which exchange mechanism is being followed. Setting the instrument to detect changes in masses 32 ($^{16}O_2$), 34 ($^{16}O^{18}O$) and 36 ($^{18}O_2$) will enable reaction types to be distinguished. Masses 18 (H_2O) and 28 (N_2) were also recorded to monitor that the system was leak free. A high vacuum gauge (Balzers IKR 60, cold cathode gauge) allowed measurement of the operating pressure of the mass spectrometer.

Early studies by Boreskov [38, 65] highlighted diffusion limitation to be of concern. Taking a circular design allows circulation of the reaction mixture by convection, shown by Cameron *et al* [43], avoiding this phenomenon. This approach was adopted in the current investigations.

2.9.1 Experimental Procedure

Powdered MgO samples (25-100 mg) were loaded into the reactor and pre-treated before commencement of exchange. This involved heating at elevated temperatures (generally 733 K) for 16 hours in either vacuum or approximately 120 Torr of $^{16}O_2$ (Air Products) prior to exchange, followed by evacuation. The system was allowed to reach reaction temperature and left for 1 hour. Pure $^{18}O_2$ (CK Gas Products Ltd, 99.2 %) was then dosed into the system, giving reaction pressures of either 20 or 80 Torr, dependent upon the type of experiment under consideration. Exchange was subsequently monitored by following changes in masses 32, 34 and 36 recorded by the mass spectrometer.

3. Characterisation And Isotopic Oxygen Exchange Reactions On Ube MgO

3.1   General Introduction

An important main aim of this work was to determine whether MgO catalysed isotopic oxygen exchange is structure sensitive. A possible answer to this can be provided by comparing rates of exchange on a series of MgO catalysts, of varying surface area. Samples used for this purpose were donated by Ube Industries of Japan.

These specimens are of particular interest because it is claimed that they can be produced exhibiting a perfect cubic morphology and narrow size distribution, and therefore there would be large differences in the relative and absolute numbers of 3 (corner) and 4 (edge) co-ordinate ions. Also in principle this allows calculation of the populations of 3, 4 and 5 co-ordinated sites on the surface, with a high degree of accuracy. Using such samples should have an advantage over MgO prepared from burning magnesium ribbon in air [4-6, 12]. Even though this route gives the desired morphology, cube lengths vary by approximately two orders of magnitude within a sample.

Ube Industries prepare the MgO samples by a build up process [84, 85]. Crystals are grown in a diffusing turbulent flow where magnesium vapour is brought into contact with oxygen in a controlled atmosphere. Four such materials have been provided, having nominal cube lengths of 100, 500, 1000 and 2000 Å. Characterisation was performed using techniques such as surface area determination, TEM, powder XRD and XPS. These provided valuable information about the morphology, cube length, size distribution and purity of the Ube MgO samples used. Kinetics of isotopic oxygen exchange reactions were determined using a specifically constructed microreactor, as detailed in Section 2.9.

3.2   Surface Area Determination

Surface areas of the Ube MgO samples were measured by nitrogen physisorption at 77 K, using a semi-automated 5 point BET instrument as described previously (Section 2.1). Each

was determined three times and the average taken. These values can then be compared to those calculated theoretically, on the basis of crystallite size, taking the density of MgO to be 3.58 g/cm^3 [86].

Cube Length / Å	Surface Area / m^2g^{-1}	
	Experimental	Calculated
100	98	168
500	31	34
1000	26	17
2000	12	8

Table 3.2.1   **Experimental And Calculated Surface Areas Determined For The Ube MgO Samples.**

In general, except in the case of the 100 Å material, there is good agreement between the two values, accounting for errors associated with the measured areas. Takayasu [87] also saw this discrepancy when using various Ube MgO samples as catalyst supports. In this study the surface area of 100 Å MgO was determined to be 90 m^2g^{-1}, similar to that reported above. Also both 500 and 2000 Å MgO gave values comparable to those in Table 3.2.1. However in separate investigations by Martin [71] and Matsuura *et al* [84, 85], surface areas of 150 and 144 m^2g^{-1} were quoted for 100 Å MgO respectively, which are much closer to the expected 168 m^2g^{-1}.

3.3   Transmission Electron Microscopy (TEM) Studies

Electron microscopy provides an excellent means of examining sample morphology. This is an important consideration since imperfections such as kinks, steps and terraces, alter the relative populations of 3, 4 and 5 co-ordinated sites on the surface. It also highlights any distribution of size within a sample. Micrographs of each of the Ube MgO samples are presented overleaf.
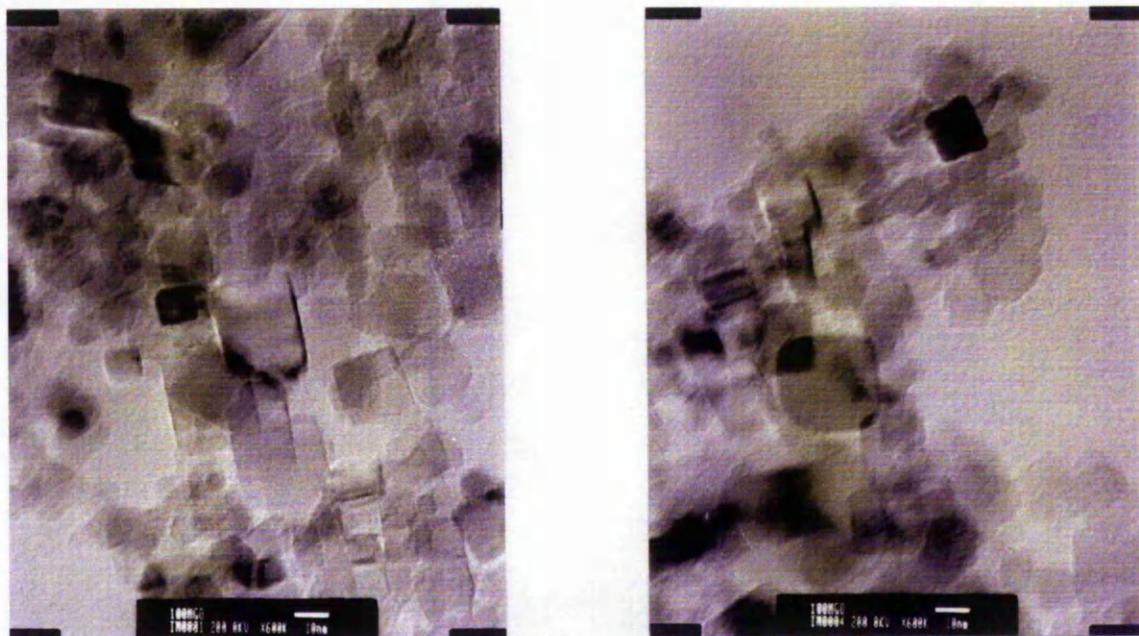
Fig 3.3.1   **Transmission Electron Micrographs Of 100 Å MgO. - Magnification x 600K, Scale 5mm = 10nm.**
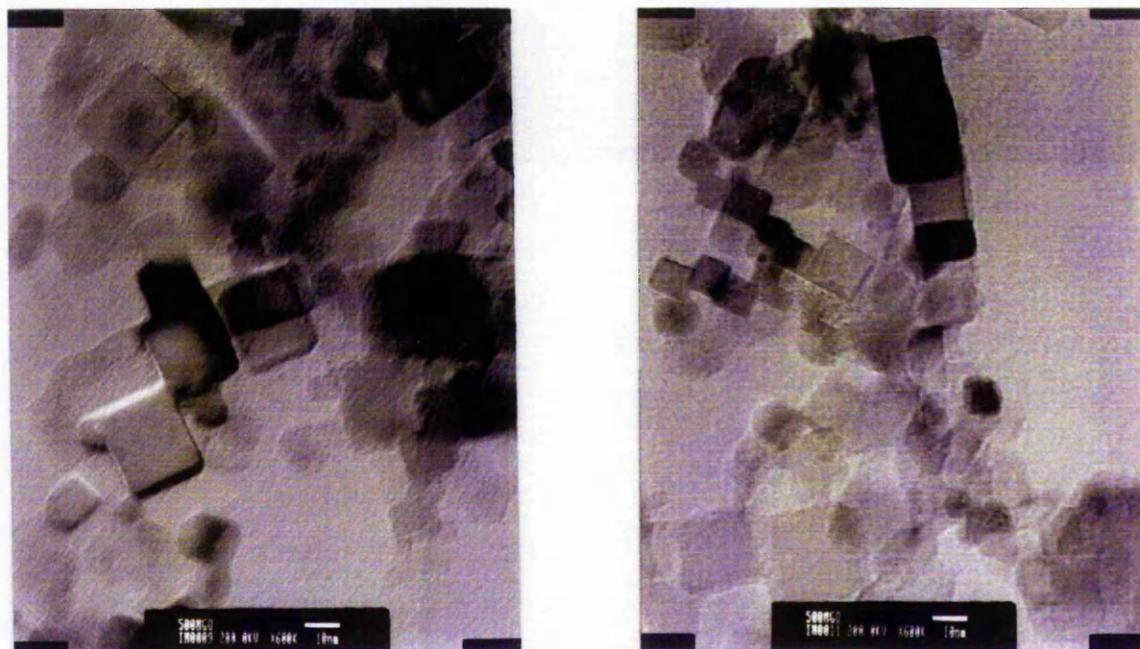
Fig 3.3.2   **Transmission Electron Micrographs Of 500 Å MgO. - Magnification x 600K, Scale 5mm = 10nm.**
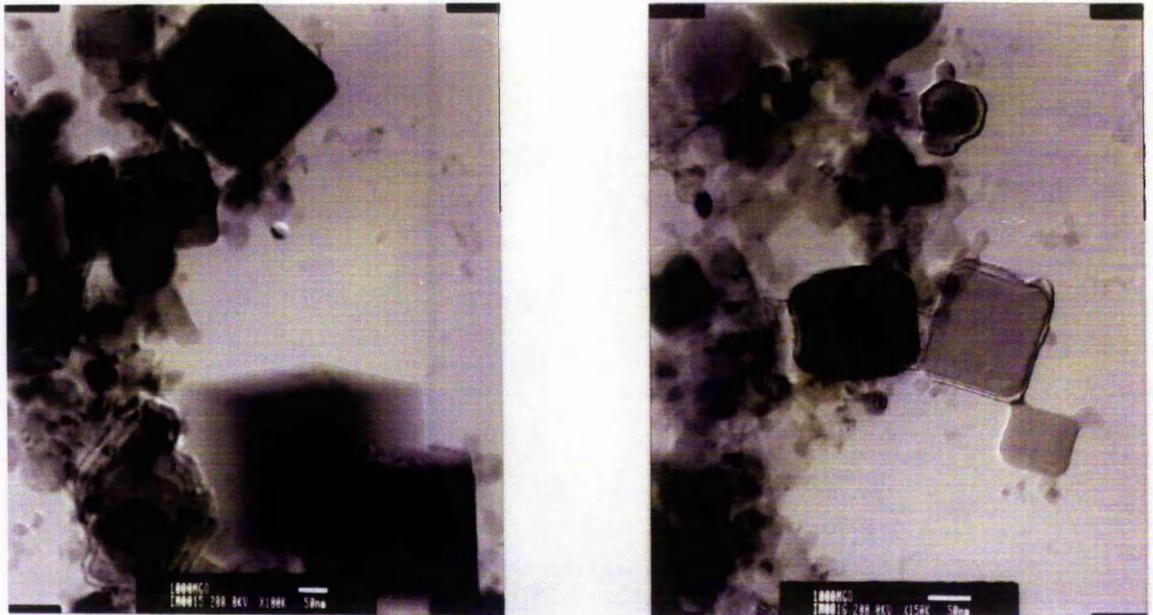
Fig 3.3.3   **Transmission Electron Micrographs Of 1000 Å MgO. - (a) Magnification x 100K, Scale 5mm = 50nm, (b) Magnification x 150K, Scale 7mm = 50nm.**
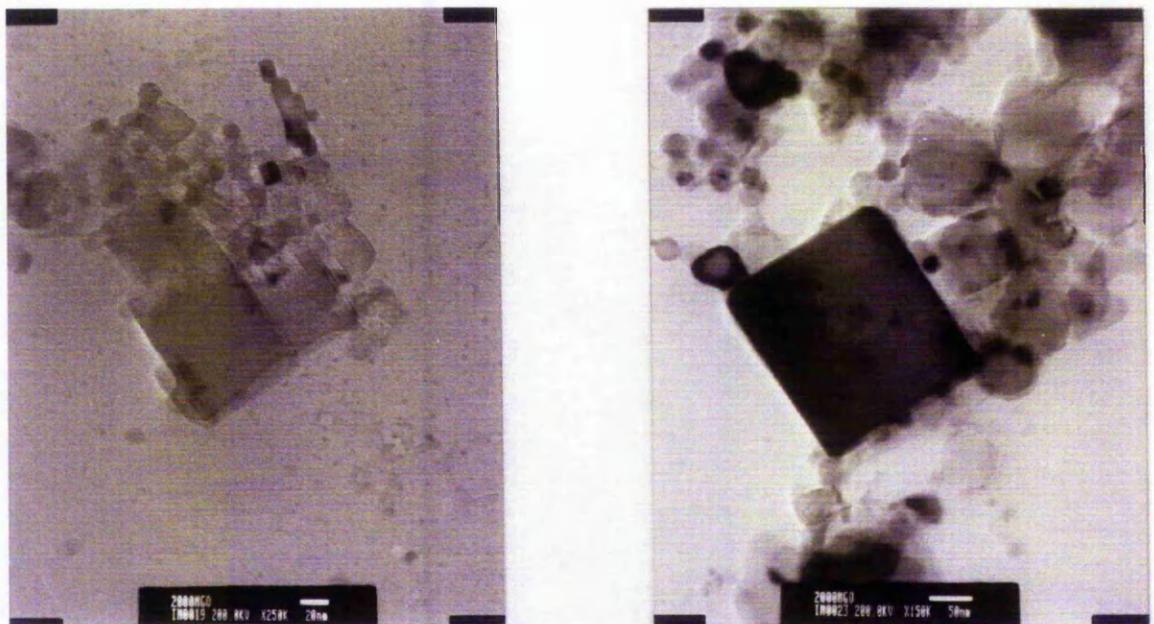
Fig 3.3.4   **Transmission Electron Micrographs Of 2000 Å MgO. - (a) Magnification x 250K, Scale 5mm = 20nm, (b) Magnification x 150K, Scale 7mm = 50nm.**

There are three main features of the above micrographs. The first is sintered intergrowth of cubes, where both perfect and imperfect alignment is evident. This is more pronounced with samples having smaller dimensions, as highlighted by Figs 3.3.1 and 3.3.2. This effect was also observed by Moodie and Warble [3, 9], in preparing MgO from magnesium basic carbonate. They found small cubelets were bunching together, giving larger crystals. Where apparent one would expect this to decrease the measured surface area, having the greatest effect on smaller sized cubes. This is in accordance with the current results (Section 3.2), for 100 Å MgO.

Secondly, close inspection of individual crystals indicate that most lack the expected perfect cubic morphology. It is clear that a high proportion of the cubes have distinct rounded edges, indicative of attack by water vapour [12]. As a result kinks, steps and terraces are formed on the surface as shown by Figs 3.3.3 and 3.3.4, changing the proportions of 3, 4 and 5 co-ordinated sites from their calculated ideal values.

Finally size distributions of cubes within a sample requires discussion. A claim made by Ube is that MgO can be produced whilst controlling the crystallite size, a major contributing factor to them being used in the current study. From the above figures this is not the case for the samples as received by us, as illustrated by Fig 3.3.4.

3.3.1 Evaluation Of Cube Size Distribution Within The Ube MgO Samples Using TEM

The sizes of 100 individual crystals were measured for each of the 100, 500, 1000 and 2000 Å MgO samples using a number of micrographs, to give a more accurate representation of size distribution within each sample. Such variations are depicted graphically below.
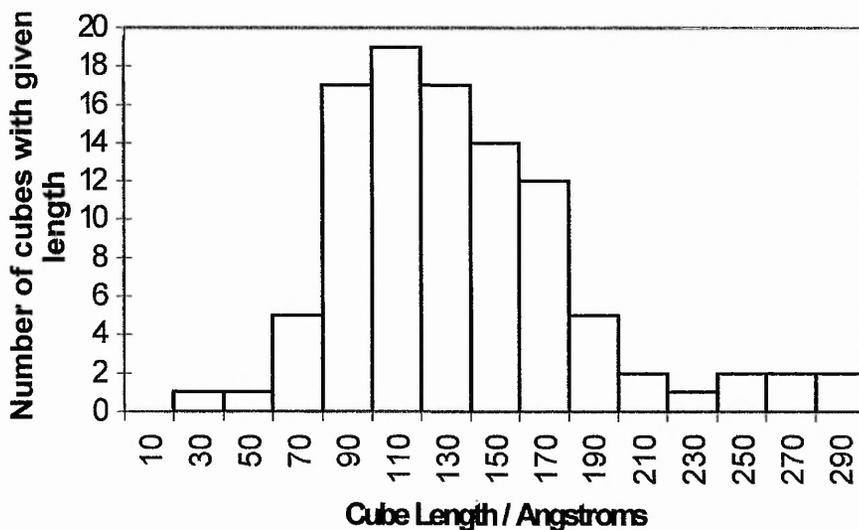
Fig 3.3.1.1   Histogram Showing The Distribution Of Cube Size For 100 Å Ube MgO.
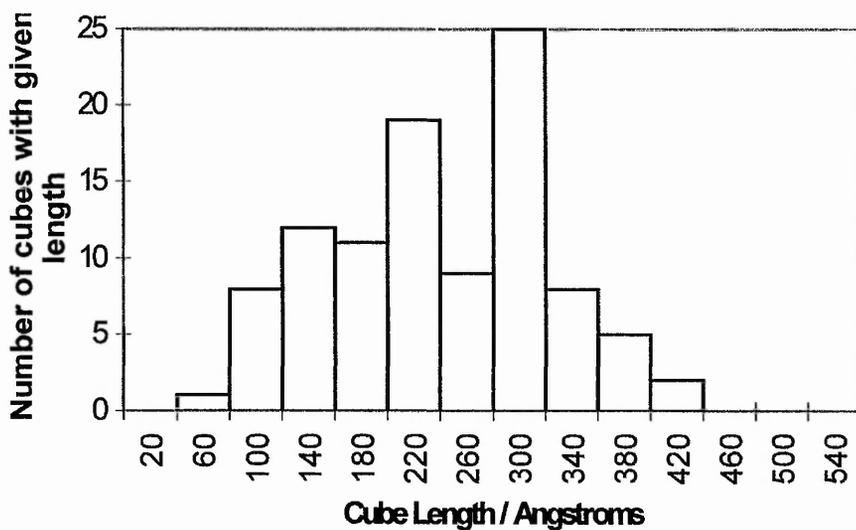
Fig 3.3.1.2   Histogram Showing The Distribution Of Cube Size For 500 Å Ube MgO.
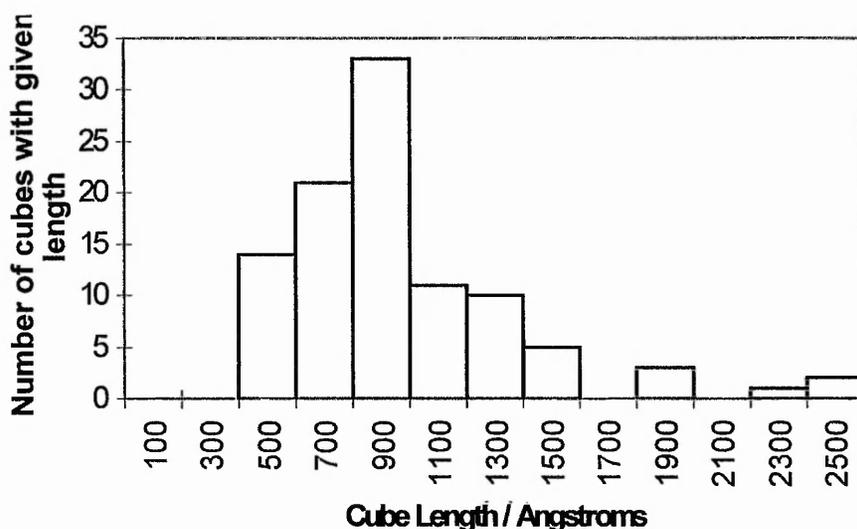
Fig 3.3.1.3 **Histogram Showing The Distribution Of Cube Size For 1000 Å Ube MgO.**
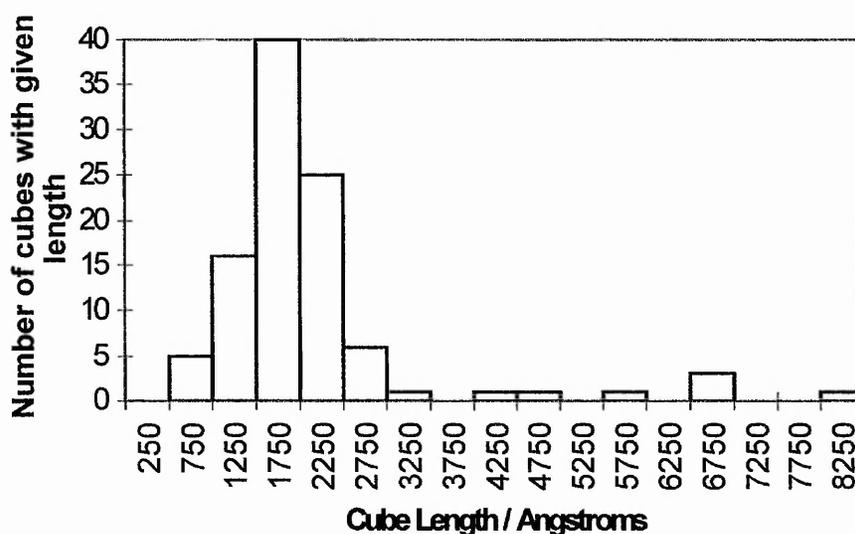
Fig 3.3.1.4 **Histogram Showing The Distribution Of Cube Size For 2000 Å Ube MgO.**

From Figs 3.3.1.1 to 3.3.1.4 the average crystallite size for each of the Ube MgO samples was determined, the results of which are tabulated below, together with the corresponding root mean square ($\sqrt{x^2}$) and cube root mean ($\sqrt[3]{x^3}$) values. The average volume and surface area of a particle are $(\sqrt[3]{x^3})^3$ and $(\sqrt{x^2})^2$ respectively, therefore from knowing these and

taking the density (ρ) of MgO to be 3.58 g/cm^3 [86], the surface area of each individual sample can be calculated using the following expression.

$$surface\, area\, per\, gram = \frac{6\left(\sqrt{x^2}\right)^2}{\rho\left(\sqrt[3]{x^3}\right)^3}$$

Equation 3.3.1.1   **General Expression For Determining The Surface Area Of The MgO Samples From The Electron Micrographs.**

These values are also presented in Table 3.3.1.1.

Ube MgO Sample / Å	Average Cube Length (x) / Å	Root Mean Square ($\sqrt{x^2}$) / Å	Cube Root Mean ($\sqrt[3]{x^3}$) / Å	Surface Area[a] / m^{2}g^{-1}
100	150	145	155	92
500	250	255	265	59
1000	1000	1050	1145	12
2000	2200	2475	2945	4

a - determined from Equation 3.3.1.1.

Table 3.3.1.1   **Table Showing Average Cube Lengths And Associated Surface Areas Of The Ube MgO Samples Measured From TEM Micrographs.**

As the above table and cube size distribution figures show, the average lengths of the crystallites differ considerably to those reported by Ube, particularly in the case of both 100 and 500 Å batches. Inspection of electron micrographs of 100 Å MgO give a mean crystallite size of 150 Å, giving a corresponding surface area of 92 m^{2}g^{-1}. Interestingly this is close to the measured value of 98 m^{2}g^{-1}, observed by Takayasu [87]. However both Martin [71] and Matsuura *et al* [84, 85] found the surface area of 100 Å MgO to be in the region of 150 m^{2}g^{-1}, near to that calculated on the assumption of a perfect morphology. These results indicate it could appear difficult for Ube to synthesise MgO samples,

possessing small crystallite sizes with any great consistency. Clearly independent batches of 100 Å MgO have been produced where the actual cube lengths differ by approximately 50 Å.

The average value of 250 Å generated from measuring the dimensions of 500 Å cubes is quite suprising. This would lead to the sample having a surface area of 59 m^2g^{-1}, whereas it was shown to be 31 m^2g^{-1}, agreeing more with the one calculated. An explanation for this could be that the micrographs obtained for 500 Å MgO do not give a true representation of the sample as a whole, hence giving an incorrect crystallite distribution.

Average cube lengths measured for both 1000 and 2000 Å MgO are in good agreement with the actual values, indicating their size can possibly be regulated more easily than with smaller crystals. The findings of Takayasu [87] also support this claim.

3.4   Powder X-Ray Diffraction (XRD) Studies

The principles and method of obtaining a powder X-ray diffraction pattern have been described previously (Section 2.3). Reflections can be compared with those tabulated in standard powder X-ray diffraction pattern files [80], allowing identification of the different phases present. Patterns have been obtained for each of the Ube MgO samples, the results of which are given overleaf:
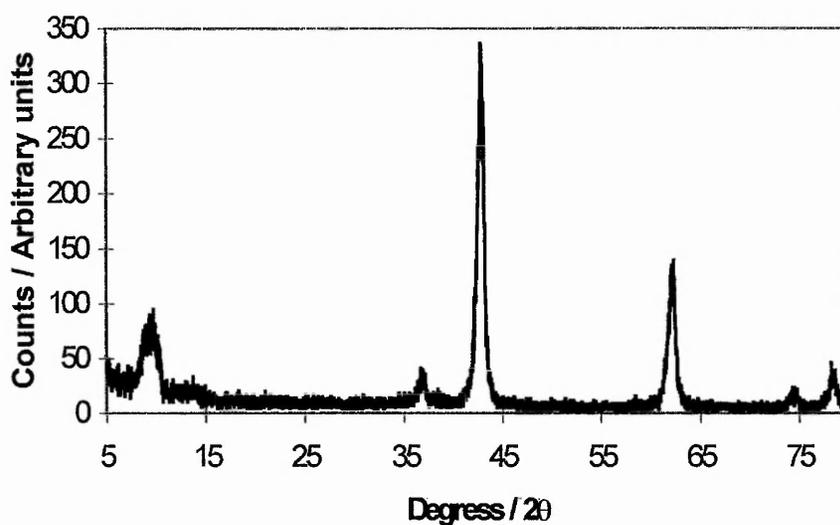
Fig 3.4.1   Powder X-Ray Diffraction Pattern Of 100 Å MgO.
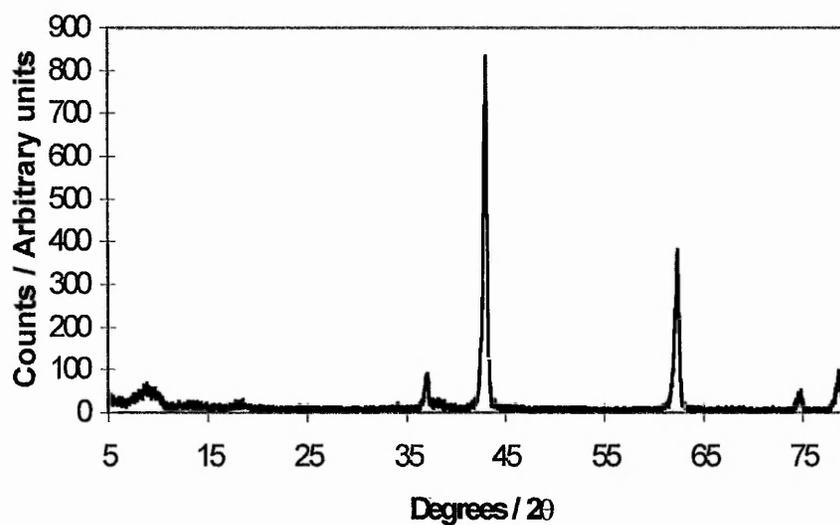
Fig 3.4.2   Powder X-Ray Diffraction Pattern Of 500 Å MgO.
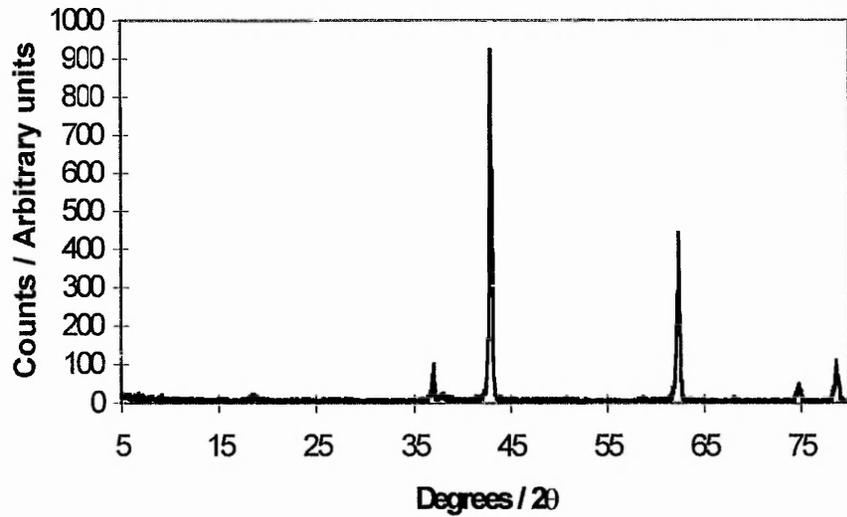
Fig 3.4.3   Powder X-Ray Diffraction Pattern Of 1000 Å MgO.
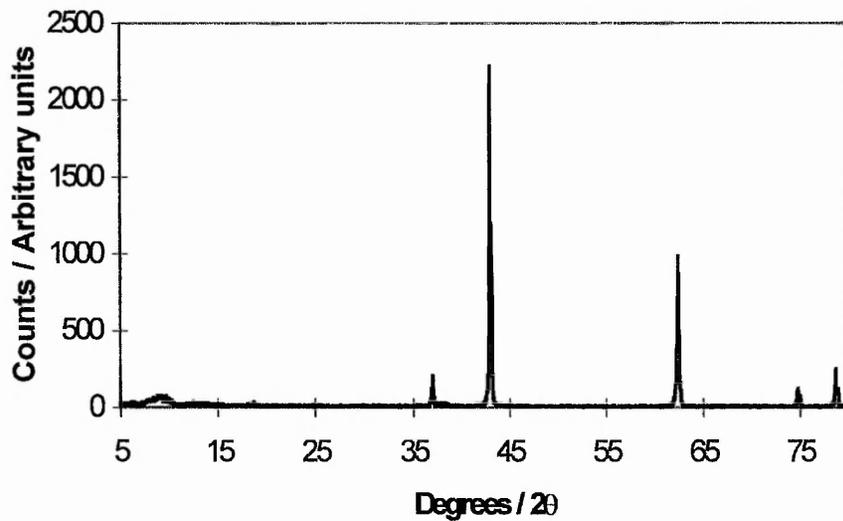
Fig 3.4.4   Powder X-Ray Diffraction Pattern Of 2000 Å MgO.

The positions and intensities of the individual reflections from each pattern are tabulated below, together with the values taken from the standard files [80].

Tabulated[a]			Experimental								
			100 Å		500 Å		1000 Å		2000 Å		
{hkl}	d / Å	Int[b]	d / Å	Int[b]	d / Å	Int[b]	d / Å	Int[b]	d / Å	Int[b]	
MgO											
111	2.431	10			2.482	11	2.426	11	2.428	9	
200	2.106	100	2.111	100	2.104	100	2.103	100	2.102	100	
220	1.489	52	1.489	42	1.488	46	1.489	48	1.488	45	
311	1.270	4			1.269	6	1.269	6	1.269	6	
222	1.216	12			1.215	12	1.213	5	1.215	11	
$Mg(OH)_2$											
111	1.494	18	1.493	40							
$MgCO_3$											
122	1.488	6							1.484	22	
Unidentified											
-	-	-	2.127	57							
-	-	-							1.212	6	

a - values taken from the JCPDS standard X-Ray diffraction files [80]. MgO : no 4-829;

    $Mg(OH)_2$: no 7-239; $MgCO_3$: 8-479.

b - Int = Intensity / Arbitrary units.

Table 3.4.1   **Comparison Of Tabulated And Experimental Reflections Obtained From The Powder XRD Patterns Of The Ube Samples.**

As expected, Table 3.4.5 shows magnesium oxide is the major phase present in each of the Ube MgO catalysts. However reflections indicative of $Mg(OH)_2$ and $MgCO_3$ were detected in 100 and 2000 Å MgO. Appearance of the hydroxide phase in the diffraction pattern of 100 Å MgO was also observed by Martin and Duprez [71]. The presence of these may account for the spherical crystals observed with the TEM micrographs, especially magnesium carbonate in 2000 Å MgO (Fig 3.3.4).

Since impurities such as magnesium hydroxide and carbonate could affect the rates of oxygen exchange, catalysts were calcined before use at 733 K, a temperature sufficiently high to decompose these impurity phases.

3.4.1 Determination Of Crystallite Size From Powder XRD Patterns

The Scherrer equation (Equation 2.3.1.1) has been used to calculate the average crystallite size of a each sample, using the full width-half maximum (FWHM) of a reflection in the diffraction pattern. Generally the most intense is used, for MgO this has a d-spacing of 2.106 Å. Cube lengths determined for each of the Ube MgO catalysts are tabulated below.

Ube Cube Length / Å	D-Spacing / Å	FWHM / °	Crystallite Size[a] / Å
100	2.111	0.764	124
500	2.104	0.426	222
1000	2.103	0.296	320
2000	2.102	0.170	558

a - determined using the Scherrer equation.

Table 3.4.1.1   MgO Crystallite Sizes Calculated From Powder XRD Patterns Using The Scherrer Equation.

As the cube length increases from 100 to 2000 Å the value of the FWHM gradually decreases, indicating increasing crystallite size. However calculation of these using the Scherrer equation, shows poor correlation between them and those stipulated by Ube, for the larger cubes. In this instance it would appear unwise to quote the results obtained using the Scherrer equation, as they do not bear much resemblance to the actual values. Generally crystallite sizes determined using this method are very approximate, as they also depend on other variables such as instrument factors and lattice distortions, which need to be accounted for. This results in an underestimation of size, a trend which appears to be followed in Table 3.4.1.1.

3.5   X-Ray Photoelectron Spectroscopy (XPS)

XPS is a useful means of determining the elemental composition of a catalyst surface. This is important for catalytic studies such as isotopic oxygen exchange, as impurities such as sodium and potassium, may affect the exchange characteristics of MgO. Cunningham *et al* [67] and Duprez [71] have also demonstrated that chloride ions inhibit the rate of isotopic oxygen exchange on various metal oxide catalysts.

A brief account of the theory behind XPS, its instrumentation and operating procedures are reported previously (Section 2.4). Spectra were recorded for each of the Ube samples, with a typical spectrum of MgO shown below.
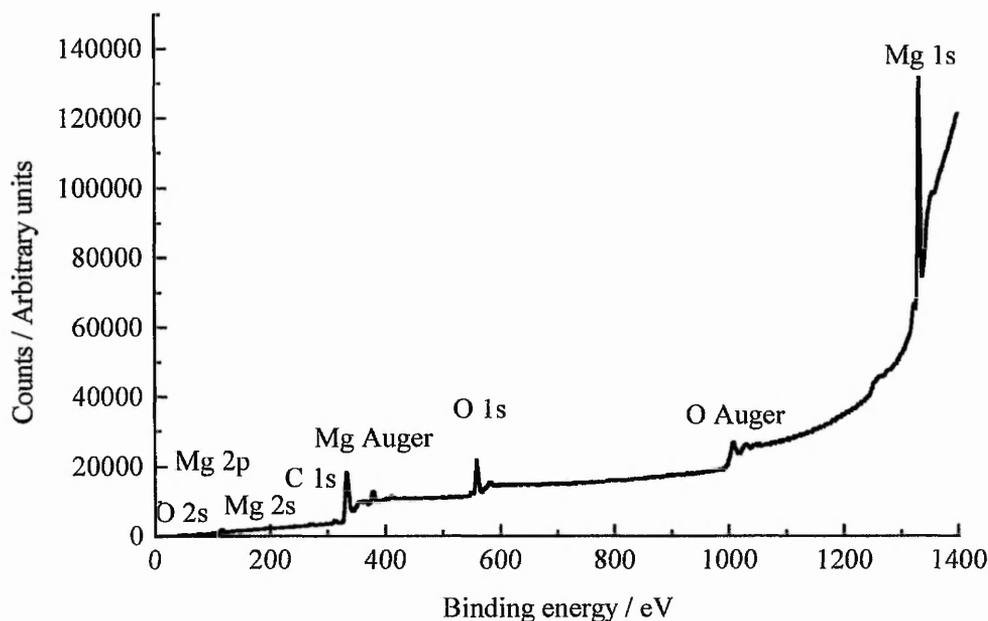
Fig 3.5.1   **XP Spectrum Of 2000Å MgO.**

Individual peaks can be identified by reference to the Handbook of Photoelectron Spectroscopy [82], as indicated by the above figure. The binding energy of each line was calculated using the Mg 1s at 1305.0 eV as reference, which was chosen because it is the most intense. A small peak due to carbon at ca. 284.6 eV is present with every sample,

originating from the tape used to mount the powdered MgO on the probe and pump oil etc. Positions of the maxima in the XP spectra of the Ube MgO catalysts are tabulated below.

Peak	Tabulated BE[a] / eV	Ube MgO - Experimental BE / eV			
		100 Å	500 Å	1000 Å	2000 Å
O 2s	23.0	-	-	-	23.9
Mg 2p	49.8	48.2	-	-	50.1
Mg 2s	90.0	87.5	87.6	-	88.9
C 1s	284.6	285.1	285.1	285.3	286.0
O 1s	531.0	531.2	531.6	531.5	532.2
Mg 1s	1305.0	1305.0	1305.0	1305.0	1305.0
Unknown	-	None	None	None	None

a - Taken from the Handbook of Photoelectron Spectroscopy [82].

Table 3.5.1   Table Showing The Binding Energy Positions Of The Maxima Of The Ube MgO Catalysts From The XP Spectra - Highlighting Any Impurities.

As one would expect, the experimental and tabulated values coincide well. Within the detection limits of the ESCA3 spectrometer, no peaks were observed corresponding to any of the impurities discussed above. Similar findings were reported by Martin and Duprez [71], with bulk levels of calcium and silicon to be as low as 20 ppm on 100 Å Ube MgO.

3.6   Isotopic Oxygen Exchange On The Ube MgO Samples

A detailed account of the history of isotopic oxygen exchange on magnesium oxide is given in the introduction (Section 1.5). Rates of isotopic exchange were measured after one of two pre-treatments, either in vacuum or in oxygen of normal isotopic composition, using procedures of earlier workers in the field (Section 1.4.1).

To determine that exchange was not promoted by the reaction vessel a blank reaction was run, admitting $^{18}O_2$ at 773 K. This is 50 K higher than the maximum temperature used during experiments. No changes in the composition of the gas phase were

observed even after 5 hours, indicating that background effects from the empty reactor tube can be neglected.

During a typical exchange reaction $^{18}O_2$ was dosed into the system at the temperature under study and variations in partial pressures of masses 32, 34 and 36 constantly monitored over periods of 8-24 hours, using a quadrupole mass spectrometer connected to the reactor by a leak valve. When plotting these changes in the gaseous products each is expressed as a mole fraction of the total oxygen species, as the sensitivity of the mass spectrometer varied with time, typically 25 % during an experiment. The change in mole fraction of a given oxygen isotope throughout a reaction, can be calculated from the equation below.

$$mole\ fraction\ (X) = \frac{P_X}{P_{32} + P_{34} + P_{36}}$$

Equation 3.6.1   **Equation To Determine The Mole Fractions Of The Oxygen Species During An Exchange Reaction.**

where X = oxygen isotope under consideration (i.e. mass 32, 34 or 36)

   P = partial pressure of the oxygen isotope under consideration

The results obtained from such a reaction are shown overleaf. From Fig 3.6.1 a trace of mass 32 ($^{16}O_2$) was present, remaining constant throughout the experiment at around 5 % of the reaction mixture, attributed to a residual amount in the mass spectrometer.

As the figure clearly shows there is a gradual decrease in mass 36 ($^{18}O_2$) with an equal and opposite increase in mass 34 ($^{16}O^{18}O$), indicating the occurrence of R_1 exchange only. This is in accordance with the earlier findings of Winter [58-60] and Boreskov [38]. However Klier et al [45, 46] reported MgO also catalysed R_2 exchange in conjunction with R_1, but the present results do not support this claim.
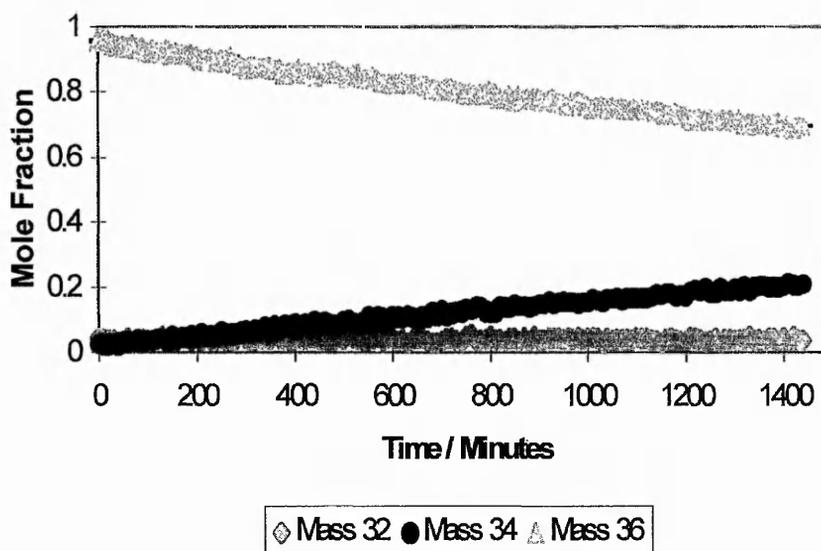
Fig 3.6.1   **A Typical Plot Showing How The Mole Fractions Of The Different Oxygen Species Vary During A Reaction - Experiment 100 Å MgO Treated In Vacuum At 733 K Then Exchanged At 688 K And An Oxygen Pressure Of 20 Torr.**

This observation can be verified by plotting the atomic fraction 18 (AF 18) present in the gaseous phase during the course of a reaction, using the following expression [40, 71].

$$AF\,18 = \frac{P_{34} + 2\,P_{36}}{2(P_{32} + P_{34} + P_{36})}$$

Equation 3.6.2   **Equation To Determine The Atomic Fraction 18 Present In The Gaseous Phase During An Exchange Reaction.**

where P = partial pressure of the oxygen isotope under consideration

A plot of AF 18 against time is given overleaf for the data presented in Fig 3.6.1.
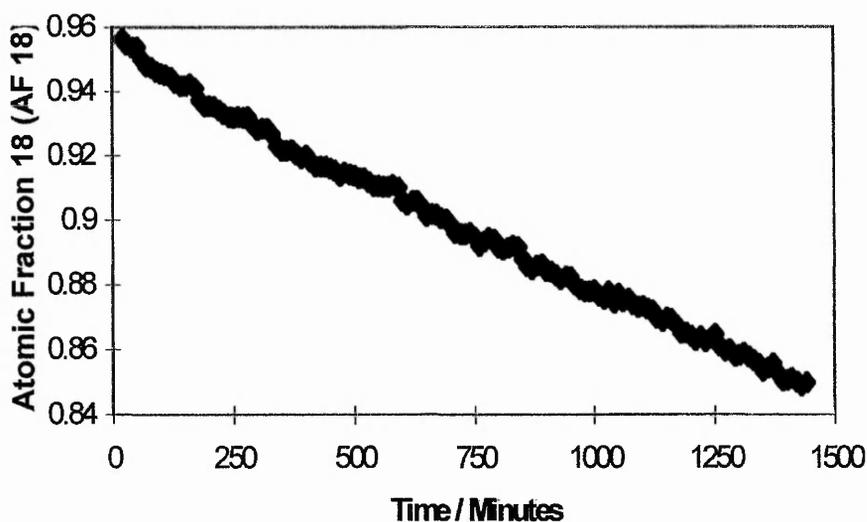
Fig 3.6.2   **A Typical Plot Showing How The AF 18 Varies During A Reaction - Experiment 100 Å MgO Treated In Vacuum At 733 K Then Exchanged At 688 K And An Oxygen Pressure Of 20 Torr.**

If the increase in mole fraction 34 (Fig 3.6.1) arose from equilibration (R_0) the AF 18 would be constant throughout an experiment, as all the ^{18}O remains in the gas phase. However if heterophase exchange were occurring (R_1 in this instance), the AF 18 would decrease as the reaction progresses, since ^{18}O is being incorporated into the MgO lattice. Clearly from Fig 3.6.2 the latter scenario is true.

3.6.1 Kinetics Of Isotopic Oxygen Exchange On Ube MgO

It is of interest to model the kinetics of isotopic oxygen exchange, in an attempt to fit the data to a rate equation. As with previous studies [37, 46, 48, 58-60, 71] it was thought isotopic oxygen exchange on MgO followed a first order rate equation, according to an R_1 mechanism. It is also assumed that only the surface monolayer is exchangeable, a result which is verified by subsequent experiments (Table 3.7.1.2).

$$\frac{-dP}{dt} = kP_{O_2}(1 - \vartheta_t)$$

Equation 3.6.1.1   **Proposed First Order Rate Equation For Isotopic Oxygen Exchange On MgO Assuming An R_1 Mechanism.**

where $-dP/dt$ = change in pressure of $^{18}O_2$ with time

     k   = rate constant

     P_{O_2} = $^{18}O_2$ partial pressure

     θ_t = fraction of oxygen in the sample that has been exchanged at time t

From Equation 3.6.1.1 :

$$\vartheta_t = \frac{P_I - P_t}{P_I - P_f}$$

where P_I = initial pressure of mass 36

     P_f = final pressure of mass 36

     P_t = pressure of mass 36 at time t

We are working at low oxygen conversions therefore P_{O_2} may be assumed to be constant throughout a reaction, we can therefore define a new rate constant, k', such that k' = kP_{O_2}. Substituting into Equation 3.6.1.1 gives :

$$\frac{-dP}{dt} = k' \frac{(P_t - P_f)}{(P_I - P_f)}$$

On integration   - (P_I-P_f) ln (P_t-P_f) = k't + c

At t = 0   c = - (P_I-P_f) ln (P_I-P_f)

Finally substitution and rearrangement gives :

$$k't = (P_I - P_f)\ln\frac{(P_I - P_f)}{(P_t - P_f)}$$

Equation 3.6.1.2   **Expression For The Universal Rate Constant Of Isotopic Oxygen Exchange On MgO.**

If the rate equation and the underlying assumptions are correct, plotting $(P_I-P_f)\ln(P_I-P_f)/(P_t-P_F)$ against time for the experimental data should yield a straight line with gradient k'. The result of this for a typical experiment is shown below.
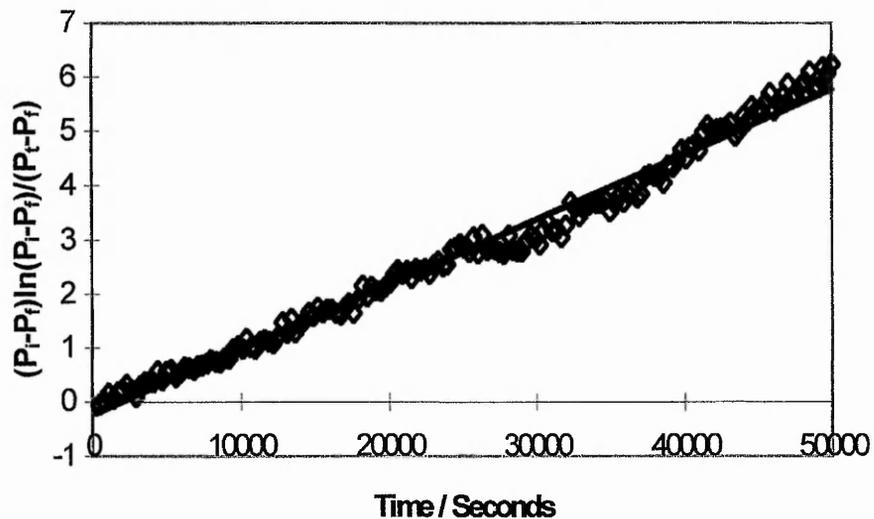
Fig 3.6.1.1   **A Typical Plot Of The First Order Kinetics Of Isotopic Oxygen Exchange On MgO For Determining The Universal Rate Constant - Experiment 100 Å MgO Treated In Vacuum At 733 K Then Exchanged At 688 K And An Oxygen Pressure Of 20 Torr.**

It is clear that the data in Fig 3.6.1.1 follows a straight line, indicating the reaction satisfies the proposed first order kinetics. However the line fails to pass through the origin, attributed to a slight experimental error in the value of P_I. Since exchange could not be carried out to completion, P_f was treated as a disposable parameter.

From the universal rate constant (k') the specific rate constant (rate constant normalised to unit surface area of sample) of exchange can be calculated.

3.6.2 Method Of Measuring Initial Rates Of Isotopic Oxygen Exchange

Knowing the changes in mole fraction of the different oxygen species and the initial system pressure, the number of $^{16}O^{18}O$ molecules (mass 34) formed with time can be calculated. This provides an alternative and simpler means of determining the specific rate of reaction, without the need of extensive kinetic analysis. The results of this are shown below.
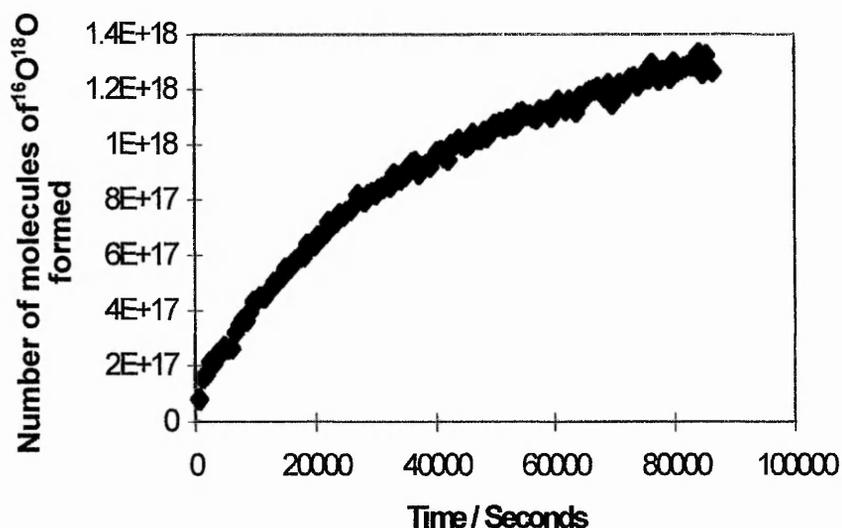
Fig 3.6.2.1   **A Typical Plot Showing The Number Of $^{16}O^{18}O$ Molecules Formed During An Exchange Reaction - Experiment 2000 Å MgO Treated In Vacuum At 733 K Then Exchanged At 708 K And An Oxygen Pressure Of 20 Torr.**

From Fig 3.6.2.1 it is clear that as the reaction progresses the rate of exchange gradually decreases, indicating a finite number of exchangeable sites. Therefore when attempting to draw conclusions using this technique, it is important to state at which stage the rate of reaction was calculated.

Taking the gradient of this line for the first 10000 s gives a value for the initial rate of exchange, which is subsequently referred to as rate throughout this work. This method was used in all cases. These yield activation energies directly comparable to those obtained

from using the specific rate constant (Section 3.6.1), measuring the disappearance in $^{18}O_2$ (mass 36). This is expected since only R_1 exchange is occurring.

This approach of calculating the rate is the one adopted throughout the current work.

3.7   Isotopic Oxygen Exchange On The Ube MgO Samples After Vacuum Pre-treatment

For each experiment, a fresh batch of 20-100 mg powdered MgO was loaded into the reactor, the weight depending upon the sample under investigation, to give a surface area of approximately 2 m^2. The system was then outgassed to elevated temperatures, at the ultimate vacuum obtainable in the turbomolecular pumped system, estimated at ca. 7.5 x 10^{-6} Torr for 16 hours, following the procedure of previous workers [36, 37, 42, 43, 50, 52, 54, 55, 58-65].

Initially experiments were performed at both 20 and 80 torr, in the range 688-733 K, to determine whether changes in the oxygen partial pressure influenced the measured rate of exchange. An evacuation temperature of 733 K was adopted in all cases.

Secondly the effect of outgassing temperature, upon the isotopic oxygen exchange characteristics of MgO was investigated, in the range 733-923 K. Reactions were followed using the 2000 Å sample at a pressure of 20 torr and 708 K.

3.7.1 Measured Rates Of Exchange At Oxygen Partial Pressures Of 80 Torr

Specific rates of isotopic oxygen exchange were measured at 80 torr and in the range 688-733 K following outgassing at 733 K, over a reaction period of 8 hours. The results of such experiments are shown overleaf. The errors quoted were calculated taking into account discrepancies in surface area measurements, reaction temperature and the mass spectrometer response.

Temperature / K	Specific Rate Of Isotopic Oxygen Exchange / x 10^{13} atoms s^{-1} / m^2			
	100 Å	500 Å	1000 Å	2000 Å
688	1.41 ± 0.32	2.34 ± 0.35	1.18 ± 0.54	1.02 ± 0.50
708	3.61 ± 0.33	3.74 ± 0.37	1.94 ± 0.23	1.73 ± 0.26
723	3.74 ± 0.37	6.12 ± 0.55	2.69 ± 0.30	2.35 ± 0.33
733	6.22 ± 0.44	8.52 ± 0.60	5.74 ± 0.40	4.96 ± 0.45

Table 3.7.1.1   **Specific Rates Of Isotopic Oxygen Exchange On The Ube MgO Samples At An Oxygen Pressure Of 80 Torr Following Vacuum Pre-treatment At 733 K.**

A plot of the values given in Table 3.7.1.1 is shown overleaf.

It is interesting to compare the specific rates of exchange presented above with those obtained by Winter [48] and Boreskov [38]. Both workers made an extensive study of isotopic oxygen exchange over a wide range of metal oxides. Extrapolating the measured rate to a common temperature of 573 K then served as an indication of surface oxygen reactivity between catalysts. Rates of exchange were found to be 1.95×10^{12} and 1.8×10^{11} atoms s^{-1}/m^2 by Winter [48] and Boreskov [38] for MgO respectively. The current results show that with 500 Å MgO, the most reactive Ube catalyst, the rate of exchange would be 5.48×10^{11} atoms s^{-1}/m^2 at 573 K. Also, in studying the exchange characteristics of 100 Å MgO Martin and Duprez [71] found a rate of 6.5×10^{16} atoms s^{-1}/m^2 at 763 K, being much higher than 1.41×10^{14} atoms s^{-1}/m^2 obtained from the values above (Table 3.7.1.1) using an extrapolated value.

More recently Karasuda and Aika [137] determined the rate of isotopic oxygen exchange with the MgO surface to be 4.68×10^{13} atoms s^{-1}/m^2 at 773 K. This equates to 4.44×10^{13} atoms s^{-1}/m^2 at 733 K, agreeing well with the 4.96×10^{13} atoms s^{-1}/m^2, observed on 2000 Å MgO at the same temperature in the present investigation (Table 3.7.1.1).

It is apparent that the present results are of similar magnitude to those quoted by Winter [48], Boreskov [38] and Karasuda and Aika [137], but are considerably lower than those reported by Martin and Duprez [71].

Fig 3.7.1.1   Plot Showing The Specific Rates Of Isotopic Oxygen Exchange On The Ube MgO Samples At An Oxygen Pressure Of 80 Torr Following Vacuum Pre-treatment At 733K.

Following a reaction the percentage of exchange was calculated, providing valuable information regarding the extent of surface oxygen anions which are actually exchangeable. This figure for each of the Ube samples is given overleaf.

As Table 3.7.1.2 shows the greatest amount of exchange is achieved with 100 and 500 Å MgO, accounting for 9 % of the total surface. In the temperature range under consideration it is thought diffusion into the bulk is negligible, a result verified by Peil *et al* [74], requiring at least 823 K for total monolayer exchange. Consequently Kalenik and Wolf [75] found only 7 % of the oxide lattice was exchangeable at 1023 K.

Cube Length / Å	Total No Of Atoms Exchanged[a]	Total No Of Surface Ions Present[b]	Percentage Of The Surface Exchanged
100	3.82×10^{18}	4.40×10^{19}	9
500	3.19×10^{18}	3.50×10^{19}	9
1000	2.88×10^{18}	4.64×10^{19}	6
2000	2.21×10^{18}	2.72×10^{19}	8

a - Results from reactions at 733 K for 8 hours.

b - Calculated from the measured surface areas presented in Table 3.2.1 and on the basis that the masses of catalyst charged to the reactor were adjusted to give roughly the same area loaded (see Section 3.7).

Table 3.7.1.2   Table Showing The Percentage Of The Surface Exchanged On The Ube MgO Samples At An Oxygen Pressure Of 80 Torr And 733 K Following Treatment In Vacuum At 733 K.

3.7.2 Calculation Of The Activation Energy Of Exchange At Oxygen Partial Pressures Of 80 Torr

By applying the Arrhenius equation (Equation 3.7.2.1) to the rates of isotopic oxygen exchange on the Ube MgO samples (Table 3.7.1.1), their activation energy can be determined.

$$k = Ae^{\frac{-Ea}{RT}}$$

Equation 3.7.2.1   The Arrhenius Equation.

where k = rate of reaction at temperature T / atoms s^{-1}

A = pre-exponential factor / atoms s^{-1}

E_a = activation energy / kJ mol^{-1}

R = molar gas constant / 0.008314 kJ K^{-1} mol^{-1}

T = reaction temperature / K

Plotting ln k against 1/T yields a straight line with gradient -E_a/R and intercept ln A. This has been done using the rates given in Table 3.7.1.1, the results of which are shown below.
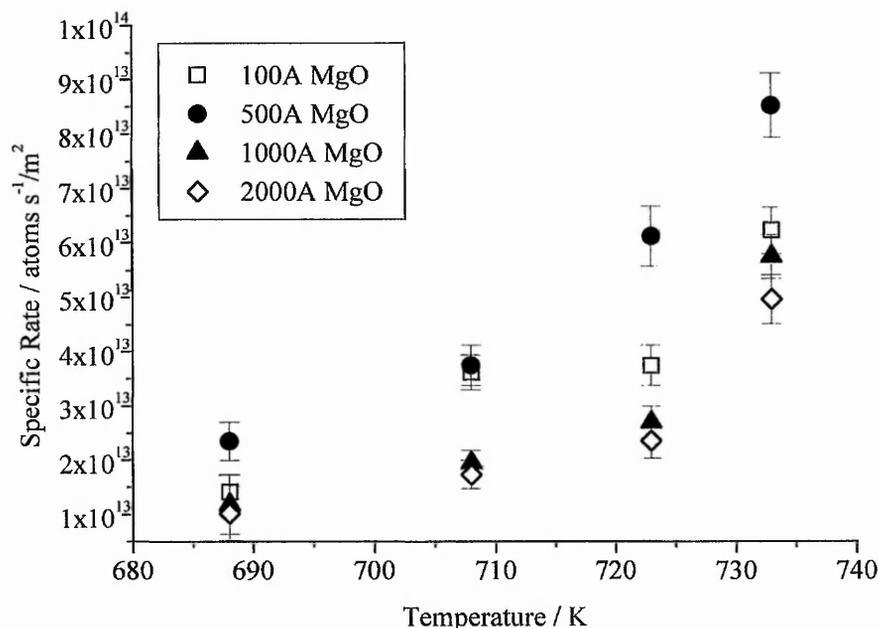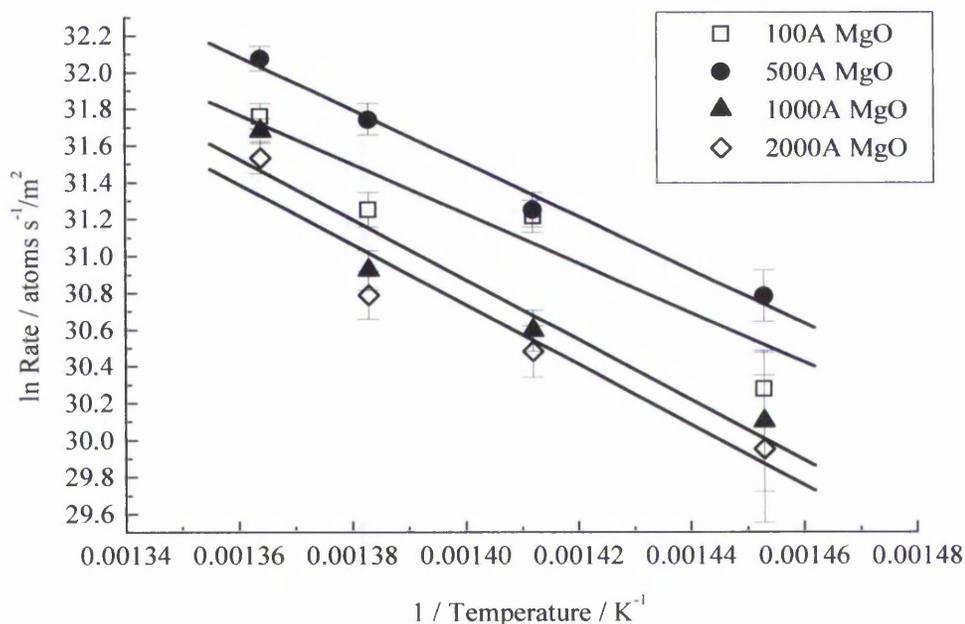

Fig 3.7.2.1   **Arrhenius Plot Of Isotopic Oxygen Exchange On The Ube MgO Samples At An Oxygen Pressure Of 80 Torr Following Vacuum Pre-treatment At 733 K.**

Calculating the gradient and intercept for each of the Ube MgO samples gives the following values.

Ube MgO Sample / Å	E_a / kJ mol^{-1}	A x 10^{22}/ atoms s^{-1}/m^2
100	127 ± 27	6.48 ± 0.58
500	120 ± 9	3.08 ± 0.09
1000	136 ± 30	21.1 ± 1.89
2000	135 ± 29	18.0 ± 1.62

Table 3.7.2.1   **Table Showing Activation Energies And Pre-exponential Terms Of Isotopic Oxygen Exchange On The Ube MgO Samples At An Oxygen Pressure Of 80 Torr Following Vacuum Pre-treatment At 733 K.**

As with the measured rates of isotopic oxygen exchange (Section 3.7.1), calculated activation energies and pre-exponential factors for the Ube MgO samples are lower than those previously reported in the literature [38, 48, 71]. These studies showed each term to be in the region 160-170 kJ mol^{-1} and 2-3 x 10^{26} atoms s^{-1}/m^2 respectively. It is interesting to note however that during his early experiments, Winter [58-60], found oxygen exchange to have an activation energy of 142 kJ mol^{-1}, being much closer to the current value.

An early concern of this work was that diffusion limitation may be apparent in the system (Section 1.4.4), when dealing with high exchange temperatures. In the region 693 K and above Winter [37, 48, 58-60] observed a change in slope of the Arrhenius plot compared to lower temperatures, corresponding to an activation energy of 13 kJ mol^{-1} for isotopic oxygen exchange on MgO. This led to the suggestion that these results were subject to diffusion limitation above 693 K, due to the unexpectedly low value quoted. From close inspection of the Arrhenius plot in Fig 3.7.2.1 it is evident that this is not the case regarding the present data, with no break in the line.

3.7.3 Characterisation After Oxygen Exchange At Partial Pressures Of 80 Torr

Following reaction, the MgO catalysts were removed from the reactor and characterised. Surface area measurements, investigating the effects of sintering, and XP spectra, looking at segregation of impurities to the surface during heating were recorded.

Ube MgO Sample	Surface Area / m^{2}g^{-1}		Percentage Decrease
/ Å	Prior To Exchange	Following Exchange	In Surface Area / %
100	98	79	19
500	31	22	29
1000	26	15	42
2000	12	7	42

Table 3.7.3.1   Surface Areas Of The Ube MgO Samples Following Vacuum Treatment And Isotopic Oxygen Exchange At 733 K And An Oxygen Partial Pressure Of 80 Torr.

From Table 3.7.3.1 it is clear that sintering has occurred during the treatment or exchange process, resulting in a 20-40 % decrease in surface area. Winter [37, 58, 59, 70] showed that sintering was apparent during high temperature vacuum heating of MgO. However this was negligible in the region 673-773 K, a result which was later confirmed by Ito *et al* [35] and Razouk and Mikhail [89]. Therefore it would appear the loss of surface area can be attributed to annealing via interaction with oxygen during an exchange reaction, which has been demonstrated by Coluccia *et al* [13].

A sintering mechanism of MgO in water vapour has been proposed by several authors [22, 35] following an adsorption-desorption cycle (anion exchange mechanism), offering a mode of transport for an oxygen ion in the surface layer. Upon desorption a H_2O molecule may remove an anion from the surface, thus leaving its original O^{2-} in an adjacent position. The movement of oxygen ions on the surface is realised by the repeated adsorption-desorption of water molecules. This enhanced surface mobility causes the disappearance of smaller crystallites and the growth of larger ones, resulting in a reduction of surface area. Later Ito [22] expanded this theory to other oxygen containing molecules, including oxygen itself, highlighting its ability to promote MgO sintering.

By its definition it is clear that an anion exchange mechanism involving oxygen constitutes isotopic exchange, therefore if it is evident there should be a direct relationship between the two. If this were the case the percentage of exchange (Table 3.7.2.1), should be comparable to the surface area lost (Table 3.7.3.1), during a reaction. Rates of both surface exchange and sintering are tabulated below.

Ube MgO Sample / Å	Rate Of Surface Oxygen Exchange / m^2/s	Rate Of Sintering / m^2/s
100	3.13×10^{-4}	6.60×10^{-4}
500	3.13×10^{-4}	1.01×10^{-3}
1000	2.08×10^{-4}	1.46×10^{-3}
2000	2.78×10^{-4}	1.46×10^{-3}

Table 3.7.3.2   Table Comparing The Rates Of Isotopic Oxygen Exchange And Sintering Assuming An Anion Exchange Mechanism.

Inspection of Table 3.7.3.2 shows no simple connection between the two, indicating continuous oxygen adsorption/desorption does not account for the sintering measured on these samples. Consequently it would appear annealing is manifested during either vacuum pre-treatment or via an alternative mechanism involving oxygen.

XP spectra of the exchanged Ube MgO samples after vacuum pre-treatment were recorded, the findings of which are summarised below.

Peak	Tabulated BE[a] / eV	BE Exchanged Ube MgO At 733 K/ eV			
		100 Å	500 Å	1000 Å	2000 Å
O 2s	23.0	-	-	-	-
Mg 2p	49.8	-	48.5	48.5	-
Mg 2s	90.0	87.7	87.6	87.8	88.2
C 1s	284.6	285.5	285.3	285.0	285.2
O 1s	531.0	531.7	531.3	531.3	531.3
Mg 1s	1305.0	1305.0	1305.0	1305.0	1305.0
Unknown	-	None	None	None	None

a - Taken from the handbook of Photoelectron Spectroscopy [82].

Table 3.7.3.3   Table Showing The Binding Energy Positions Of The Maxima Of The Ube MgO Catalysts From The XP Spectra After Vacuum Pre-treatment And Exchange At 733 K And Oxygen Partial Pressures Of 80 Torr - Highlighting Any Impurities.

As Table 3.7.3.3 shows heating has no appreciable effect on surface composition, giving results comparable to those presented in Table 3.5.2 for the untreated catalysts. As a consequence isotopic oxygen exchange can be explained solely in terms of reaction with MgO, without any promotional effects from surface impurities.

3.7.4 Measured Rates Of Exchange At Oxygen Partial Pressures Of 20 Torr

To determine if the exchange rate was dependent on the pressure of oxygen, experiments were performed at 20 torr, which could then be compared to the previous results obtained

at 80 torr (Section 3.7.1). Reactions were followed on 100 and 2000 Å MgO in the range 688-733 K, and the full set of Ube samples at 708 K, after an initial vacuum pre-treatment at 733 K.

Specific rates of isotopic oxygen exchange (Section 3.6.2), measured on both 100 and 2000 Å MgO are tabulated below.

Temperature / K	Specific Rate Of Exchange / x 10^{13} atoms s^{-1} / m^2	
	100 Å	2000 Å
688	1.46 ± 0.20	1.35 ± 0.22
708	3.51 ± 0.35	2.27 ± 0.25
723	3.65 ± 0.40	3.23 ± 0.42
733	5.95 ± 0.65	4.69 ± 0.39

Table 3.7.4.1   **Specific Rates Of Isotopic Oxygen Exchange On 100 And 2000 Å MgO At An Oxygen Pressure Of 20 Torr Following Vacuum Pre-treatment At 733 K.**

Similarly values for all the Ube samples obtained at a common exchange temperature of 708 K are summarised in Table 3.7.4.2.

Cube Length / Å	Specific Rate Of Exchange / x 10^{13} atoms s^{-1} / m^2
100	3.51 ± 0.35
500	2.50 ± 0.25
1000	2.82 ± 0.31
2000	2.27 ± 0.25

Table 3.7.4.2   **Specific Rates Of Isotopic Oxygen Exchange On The Ube MgO Samples At 708 K And An Oxygen Pressure Of 20 Torr Following Vacuum Pre-treatment At 733 K.**

A graphical representation of the specific rates measured on both 100 and 2000 Å MgO, as given in Table 3.7.4.1, is shown overleaf.
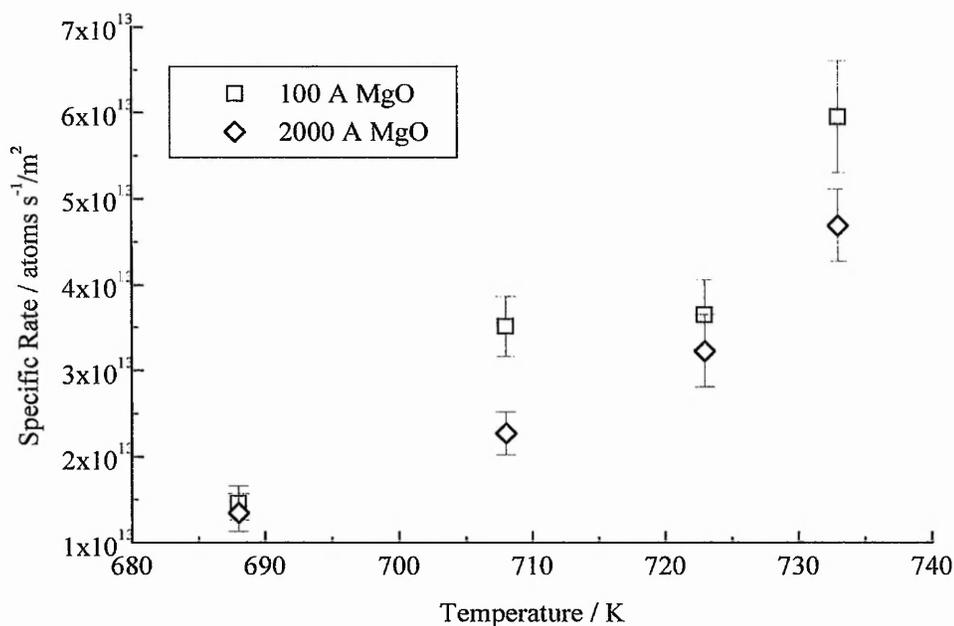
Fig 3.7.4.1   Plot Showing The Specific Rates Of Isotopic Oxygen Exchange On 100 And 2000 Å MgO At An Oxygen Pressure Of 20 Torr Following Vacuum Pre-treatment At 733 K.

It is interesting to compare the results at 20 (Table 3.7.4.1) and 80 (Table 3.7.1.1) torr, investigating the influence of oxygen partial pressure on the rate of isotopic oxygen exchange. Inspection of the data would suggest that rates measured at both 20 and 80 torr are close within the limits of experimental error, suggesting the reaction is independent of oxygen pressure within the range studied. This is in agreement with the earlier work of Winter [48], stating exchange on MgO was zero order with respect to oxygen pressure between 10-140 torr, and Boreskov [38], who found the rate to be independent of oxygen pressure in the region of 10-100 torr.

3.7.5 Calculation Of The Activation Energy Of Exchange At Oxygen Partial Pressures Of 20 Torr

As with the experiments performed at 80 torr (Section 3.7.2), activation energies of exchange were calculated for reactions run at 20 torr. An Arrhenius plot of the specific

76

rates given in Table 3.7.4.1 for 100 and 2000 Å MgO is presented below.
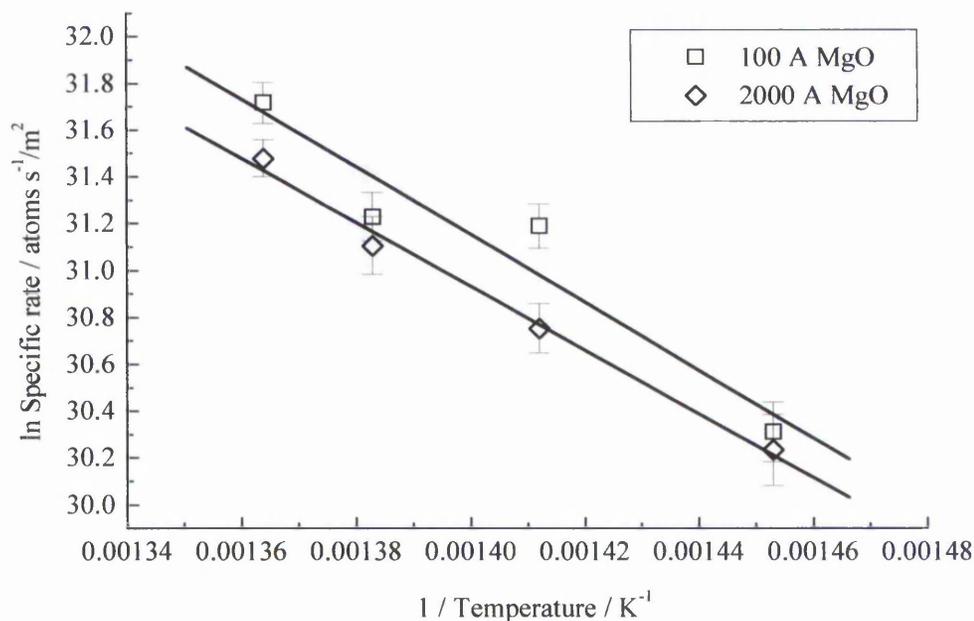
Fig 3.7.5.1   **Arrhenius Plot Of Isotopic Oxygen Exchange Derived From The Specific Rates On 100 And 2000 Å MgO At An Oxygen Pressure Of 20 Torr Following Vacuum Pre-treatment At 733 K.**

From the Arrhenius plot (Fig 3.7.5.1), activation energies and pre-exponential terms of isotopic oxygen exchange can be determined, as given in Table 3.7.5.1.

Cube Length / Å	E_a / kJ mol^{-1}	$A \times 10^{21}$ / atoms s^{-1}/m^2
100	120 ± 25	20.2 ± 0.16
2000	113 ± 8	0.44 ± 0.01

Table 3.7.5.1   **Table Showing Activation Energies And Pre-exponential Terms Of Isotopic Oxygen Exchange Derived From The Specific Rates On 100 And 2000 Å MgO At An Oxygen Pressure Of 20 Torr Following Vacuum Pre-treatment At 733 K.**

Comparison of the activation energies and pre-exponential terms obtained at 20 torr (Table 3.7.5.1), with those determined for reactions performed at 80 torr (Table 3.7.2.1), indicates a close agreement between the two data sets. Such a finding would be expected, since the measured rates of exchange at both 20 and 80 torr were found to be equal, within the limits of experimental error (Section 3.7.4). This can be confirmed by the literature, as the rate of isotopic oxygen exchange on MgO, was found to be independent of oxygen pressure in the range 10-140 torr [38, 48].

3.7.6 Influence Of Outgassing Temperature On The Measured Rate Of Exchange

A concern of Winter [48] was that the high temperature evacuation promoted surface F-centre formation, in the case of MgO this is two electrons trapped at an anion vacancy. Upon $^{18}O_2$ admission the initial reaction observed was the filling of these centres with isotopic oxygen, which was then followed by exchange on their saturation. Clearly if this were true the measured value of the rate would be inaccurate as initially it does not involve isotopic exchange. In an attempt to further investigate this phenomenon, exchange reactions were conducted on 2000 Å MgO at 708 K and 20 torr after evacuation at 873 and 1023 K, as well as 733 K adopted in the preceding experiments (Section 3.7.4).

It may also be possible to elucidate the role played by surface F-centres in the exchange process, by determining the number formed during pre-treatment using the Boltzmann distribution (Equation 3.7.6.1). The energy of formation of such a centre at high densities (the worst possible scenario) was taken to be 3.8 eV, as calculated by Castanier and Noguera [88]. If molar energies are used with the Boltzmann distribution, the Boltzmann constant (K) can be replaced by the molar gas constant (R).

$$\frac{N_1}{N_2} = e^{\left(\frac{-\Delta E}{RT}\right)}$$

Equation 3.7.6.1　　　　**The Boltzmann Distribution.**

where N_1/N_2 = ratio of vacancies to non-vacancies

ΔE = energy of formation of an F-centre / kJ mol^{-1} (1 eV = 96.485 kJ mol^{-1})

R = molar gas constant / 0.008314 kJ K^{-1} mol^{-1}

T = outgassing temperature / K

The ratio of vacancies formed relative to the number of surface ions present are tabulated below for all of the outgassing temperatures studied.

Outgassing Temperature / K	Ratio Of Vacancies To Non-Vacancies (N_1/N_2)
733	7.57×10^{-27}
873	1.15×10^{-22}
1023	1.90×10^{-19}

Table 3.7.6.1   Ratio Of Vacancies To Non-Vacancies Formed On The MgO Surface During Outgassing At Elevated Temperatures.

Inspection of Table 3.7.6.1 shows that as the evacuation temperature is progressively increased, the probability of surface F-centre formation is enhanced. The occurrence of this is insignificant at 733 K, as the ratio of vacancies to surface ions was found to be 7.57×10^{-27}. Consequently rates obtained at this outgassing temperature (Sections 3.7.1 and 3.7.4), can be described solely in terms of exchange between oxygen of the gas phase and the MgO lattice. However quite a different chain of events are observed for reactions where evacuation was performed at higher temperatures.

Upon admission of 20 torr $^{18}O_2$ on 2000 Å MgO at 708 K after vacuum heating at 873 K, a small but significant decrease in oxygen pressure was initially observed, as indicated by the barocell. Following this period, the pressure reading stabilised, with any further changes corresponding only to the bleed rate set by the leak valve. Such an observation could imply that surface F-centres are manifested during the vacuum pre-treatment, which are subsequently filled on the addition of isotopic oxygen, after which exchange proceeds.

Changes in masses 32, 34, and 36 were monitored over 16 hours, with a plot of the number of $^{16}O^{18}O$ molecules formed with time given below.
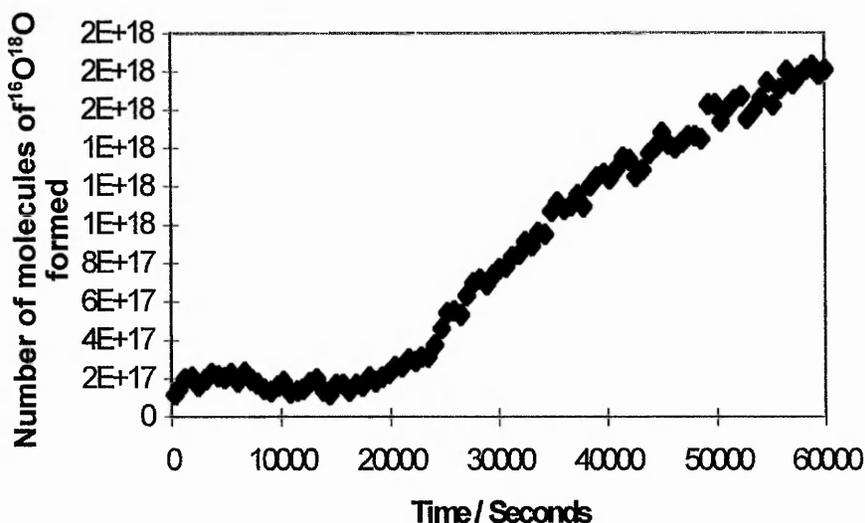
Fig 3.7.6.1   **Plot Showing The Number Of $^{16}O^{18}O$ Molecules Formed On 2000 Å MgO At 708 K And An Oxygen Pressure Of 20 Torr Following Vacuum Pre-treatment At 873 K.**

As Figure 3.7.6.1 shows during the initial stages of reaction no $^{16}O^{18}O$ formation is observed, however following this period the catalyst exhibits exchange characteristics very similar to those witnessed in previous experiments. Calculation of the specific rate gave a value of 2.50 x 10^{13} atoms s^{-1}/m^2, being close to that obtained under the same reaction conditions, but at the lower outgassing temperature of 733 K (Table 3.7.4.3).

After evacuation of 2000 Å MgO at 1023 K and subsequent addition of 20 torr $^{18}O_2$, the pressure initially dropped so much at 708 K, due to interaction with the MgO, that the rate of exchange could not be measured. Therefore the reaction was conducted at 80 torr. With the introduction of 80 torr $^{18}O_2$ into the system a sharp decrease in pressure was recorded before levelling out, comparable to the previous experiment. A reaction profile similar to that shown in Figure 3.7.6.1 was observed, yielding an exchange rate of 2.61 x 10^{13} atoms s^{-1}/m^2.

A summary of the results obtained at 708 K and 20 torr on 2000 Å MgO at various outgassing temperatures is tabulated below.

Outgassing Temperature / K	Measured Rate Of Exchange / x 10^{13} atoms s^{-1}/m^2
733	2.27 ± 0.25
873	2.50 ± 0.28
1023	2.61 ± 0.31^a

a - experiment run at an oxygen pressure of 80 torr.

Table 3.7.6.2   Specific Rates Of Isotopic Oxygen Exchange On 2000 Å MgO At 708 K And 20 Torr Following Vacuum Pre-treatment At Elevated Temperatures.

From Table 3.7.6.2 it is evident that in each particular case, even when $^{16}O^{18}O$ formation is initially delayed, measured rates of exchange are similar within the limits of experimental error.

In an attempt to determine the nature of the species released from the surface during the high temperature outgassing at 1023 K, the desorption products were analysed using the mass spectrometer. Main peaks were found at masses 18 (H_2O) and 28 (CO), the latter arising from reactions between oxygen entities and carbonaceous residues present in the vacuum system. Under no circumstances was any mass 32 ($^{16}O_2$) observed, agreeing with the findings of Karasuda *et al* [137, 138]. However in related work Martens *et al* [96] did report evolution of atomic oxygen in the 873-1173 K region when decomposing brucite.

3.8   Isotopic Oxygen Exchange On The Ube MgO Samples At Partial Pressures Of 80 Torr After Oxygen Pre-treatment

Following isotopic oxygen exchange reactions after heating in vacuum, Boreskov [38, 55] and Winter [48] changed the pre-treatment method (Section 1.4.1), now using an atmosphere of normal oxygen ($^{16}O_2$), before the commencement of exchange. The aim of this was to attain a stoichiometric amount of oxygen in the surface layer of the oxide, as at the time there was concern about the presence of F-centres (Section 3.7.6), enhancing the rate of exchange.

In this study, experiments were carried out in the same manner as those previously (Section 3.7), the only difference being pre-treatment was performed in an oxygen environment of ca. 120 Torr $^{16}O_2$. Following the 16 hour heating period at 733 K the gaseous phase was evacuated for 5 minutes, after which 80 torr of $^{18}O_2$ was admitted and exchange measured.

3.8.1 Characterisation After Oxygen Treatment

As indicated with earlier isotopic exchange reactions (Section 3.7.3), sintering occurs during either vacuum pre-treatment or upon oxygen interaction with the MgO surface. Therefore it is of interest to obtain further information regarding this process, hence catalysts were removed from the reactor following treatment but prior to exchange and their surface areas determined.

Ube MgO Sample	Surface Area / m^2g^{-1}		Percentage Decrease
/ Å	Prior To Treatment	Following Treatment	In Surface Area / %
100	98	69	30
500	31	29	6
1000	26	15	42
2000	12	5	58

Table 3.8.1.1   Surface Areas Of The Ube MgO Samples Following Oxygen Pre-treatment And Prior To Isotopic Exchange.

As expected, there has been a decrease in surface area, in some cases up to 60 %, following pre-treatment in oxygen at elevated temperature. These changes are similar in magnitude to the samples treated in vacuum then exchanged (Table 3.7.3.1), bar 100 and 500 Å MgO, sintering being more prominent with the former and barely influencing the latter. Since there is no vacuum heating stage here, it cannot account for the loss in surface area. Therefore oxygen may play some part in the annealing process.

During this type of treatment an alternative possibility arises where H_2O vapour and CO_2 could promote sintering. Each readily adsorbs on the MgO surface at ambient

temperatures and pressures (Section 1.3), therefore it is possible they are present on the Ube samples, although care was taken to prevent this by storage in a desiccator when not in use. Since oxygen treatment is performed under static conditions, such adsorbates on the catalyst surface would remain in the system upon desorption. It is well documented both H_2O and CO_2 are more effective at promoting sintering than oxygen alone [22, 23, 35], hence they may contribute to surface area loss. Both are thought to initiate annealing via the anion exchange mechanism [22, 35], as described previously (Section 3.7.3). However this was shown not to account for sintering between oxygen and the MgO surface. Unfortunately no further comment can be made regarding reaction of H_2O vapour and CO_2 by this pathway, as there is insufficient evidence available.

Clearly there is no simple explanation regarding the mechanism of sintering during oxygen pre-treatment. It is possible water vapour, carbon dioxide, or oxygen itself could account for the diminished surface areas observed.
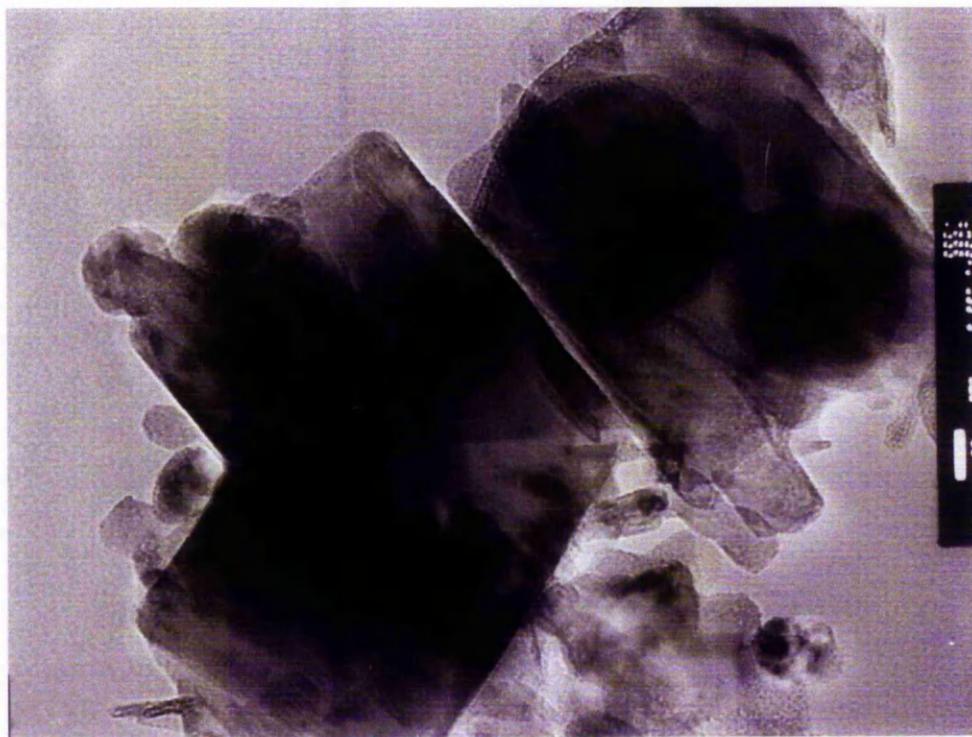
Fig 3.8.1.1   Transmission Electron Micrograph Of 1000 Å MgO Following Oxygen Pre-
treatment At 733K Prior To Exchange. - Magnification x 100 K, Scale 8 mm =
100 nm.

TEM studies were also performed following oxygen pre-treatment in an attempt to highlight any sintering present. Micrographs were obtained for each of the four MgO catalysts, crystallites of the 1000 Å MgO catalyst being represented on the preceding page.

It is evident from Fig 3.8.1.1 that sintering between individual 1000 Å cubes has occurred, during the treatment process, compared to the as received sample (Fig 3.3.3). Clearly fusion between crystallites is apparent generally causing imperfect alignment, leading to the formation of irregularly shaped particles.

This annealing will lead to the observed reduction in surface area. Similar results were obtained for the remaining Ube MgO catalysts.

3.8.2 Measured Rates Of Exchange At Oxygen Partial Pressures Of 80 Torr

The specific rates of isotopic oxygen exchange measured in the range 688-733 K and 80 torr, after oxygen pre-treatment at 733 K, are given below.

Temperature / K	Specific Rate Of Isotopic Oxygen Exchange / x 10^{13} atoms s^{-1} / m^2			
	100 Å	500 Å	1000 Å	2000 Å
688	1.45 ± 0.20	2.59 ± 0.31	1.06 ± 0.24	1.07 ± 0.43
708	3.16 ± 0.22	4.52 ± 0.32	1.42 ± 0.23	1.46 ± 0.48
723	4.51 ± 0.32	6.01 ± 0.42	1.98 ± 0.24	2.25 ± 0.10
733	6.03 ± 0.30	9.66 ± 0.48	5.52 ± 0.39	4.55 ± 1.41

Table 3.8.2.1   Specific Rates Of Isotopic Oxygen Exchange On The Ube MgO Samples At Partial Pressures Of 80 Torr Following Oxygen Pre-treatment At 733 K.

A plot of the above values is given overleaf. Comparison of these values with those in Table 3.7.1.1 following heating in vacuum indicates that the rates of isotopic exchange are similar, irrespective of the pre-treatment method adopted, after normalising for surface area. This is as expected since the reason behind treating in an oxygen environment was to eradicate any

surface F-centres, which were shown by use of the Boltzmann distribution (Table 3.7.6.1) to be barely formed during evacuation at 733 K.

These results coincide with the findings of Winter [48], reporting that rates of exchange were essentially the same after both treatment in vacuum and oxygen. However it was mentioned that the rate was initially higher following vacuum evacuation before levelling out, a result not reproduced here.
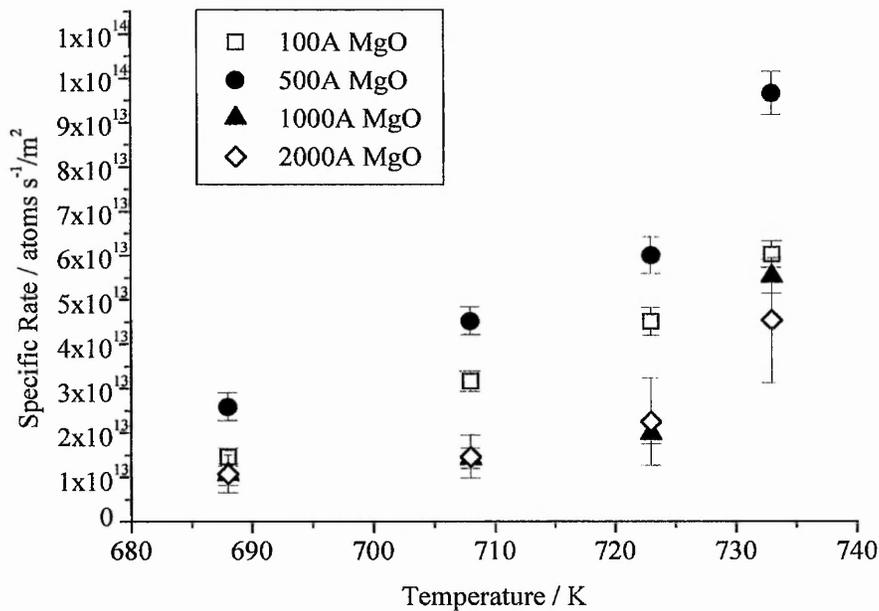
Fig 3.8.2.1   Plot Showing The Specific Rates Of Isotopic Oxygen Exchange On The Ube MgO
Samples At Partial Pressures Of 80 Torr Following Oxygen Pre-treatment At 733 K.

3.8.3 Calculation Of The Activation Energy Of Exchange At Oxygen Partial Pressures Of 80 Torr

From the specific rates of isotopic exchange measured after oxygen pre-treatment (Table 3.8.2.1), the following Arrhenius plot is obtained.
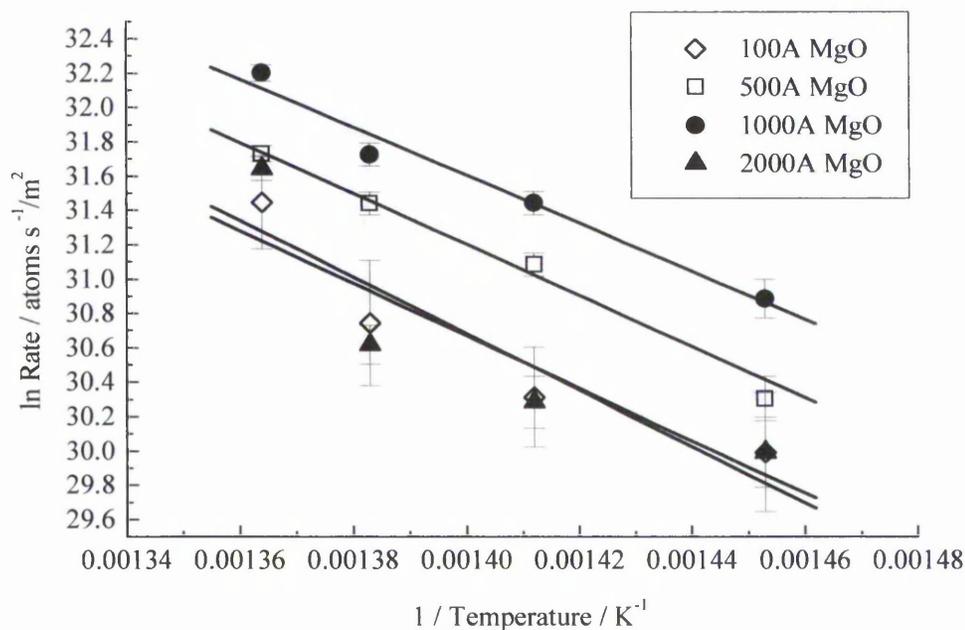
Fig 3.8.3.1   Arrhenius Plot Of Isotopic Oxygen Exchange On The Ube MgO Samples At Partial Pressures Of 80 Torr Following Oxygen Pre-treatment At 733 K.

From Fig 3.8.3.1 the activation energies and pre-exponential terms for exchange on the Ube MgO samples after oxygen pre-treatment can be calculated, as presented below.

Ube MgO Sample / Å	E_a / kJ mol^{-1}	A x 10^{22} / atoms s^{-1}/m^2
100	131 ± 9	13.7 ± 0.41
500	116 ± 13	1.68 ± 0.07
1000	136 ± 50	20.4 ± 3.26
2000	127 ± 32	3.90 ± 0.39

Table 3.8.3.1   Table Showing Activation Energies And Pre-exponential Terms Of Isotopic Oxygen Exchange On The Ube MgO Samples At Partial Pressures Of 80 Torr Following Oxygen Pre-treatment At 733 K.

Since the rates of isotopic exchange are comparable after both vacuum and oxygen treatment, one would also expect the activation energies and pre-exponential factors to follow the same trend. This is shown to be the case on inspection of Tables 3.7.2.1 and 3.8.3.1. It is important to stress again that these values are lower than those previously reported in the literature.

3.8.4 Characterisation After Oxygen Exchange

As with the vacuum treated samples, once isotopic oxygen exchange was complete, the MgO catalysts were removed from the reactor for characterisation. Again surface area measurements and XP spectra were obtained.

The surface areas of the exchanged samples are given below, together with those recorded following oxygen treatment but prior to exchange (Table 3.8.1.1) for comparison.

Ube MgO Sample / Å	Surface Area / m^2g^{-1}	
	Following Treatment	Following Exchange
100	69	73
500	29	28
1000	15	16
2000	5	8

Table 3.8.4.1   Surface Areas Of The Ube MgO Samples Following Oxygen Pre-treatment And Isotopic Oxygen Exchange At 80 Torr And 733 K.

From inspection of Table 3.8.4.1 surface areas of the Ube MgO samples remain relatively unchanged following isotopic exchange. It appears however that some of these have slightly increased, which can be attributed to errors in obtaining the experimental measurements. Equivalence of these two sets of values would suggest that sintering had ceased by the end of the oxygen pre-treatment period.

The positions of the binding energies observed in the XP spectra of the MgO catalysts after exchange at 733 K are summarised below.

Peak	Tabulated BE[a] / eV	BE Exchanged Ube MgO At 733 K/ eV			
		100 Å	500 Å	1000 Å	2000 Å
O 2s	23.0	-	-	-	-
Mg 2p	49.8	-	-	-	-
Mg 2s	90.0	88.0	87.9	-	-
C 1s	284.6	285.1	285.3	285.2	284.8
O 1s	531.0	531.7	531.4	531.3	531.1
Mg 1s	1305.0	1305.0	1305.0	1305.0	1305.0
Unknown	-	None	None	None	None

a - Taken from the handbook of Photoelectron Spectroscopy [82].

Table 3.8.4.2   Table Showing The Binding Energy Positions Of The Maxima Of The Ube MgO Catalysts From The XP Spectra After Oxygen Pre-treatment And Exchange At 80 Torr And 733 K - Highlighting Any Impurities.

Even after a total reaction time of 24 hours at 733 K (16 hours treatment, 8 hours exchange), there is no appreciable change in composition of the surface layer. Hence it can be concluded that the surfaces are impurity free, indicating that the initial rates of isotopic oxygen exchange depend only on interactions with MgO.

3.9   Isotopic Switching Experiments

In an attempt to obtain a greater understanding of the structure sensitivity of oxygen exchange on the MgO surface, an isotopic switching experiment was performed, to determine the degree of reversibility of exchange. This can also provide valuable information regarding surface migration and bulk diffusion contributions during a reaction. The outline of the method used is given below.

Initially an exchange reaction was carried out, using procedures already described, at 80 torr and 733 K, after treatment in vacuum at 733 K (Section 3.7). Once the 9 hour reaction period was complete the gaseous phase was evacuated and replaced by an

equivalent amount of normal oxygen ($^{16}O_2$). Again changes in masses 32, 34 and 36 were monitored over a further 9 hours.

As concluded previously (Section 3.6) the initial exchange on Ube MgO is occurring via an R_1 type mechanism (Section 1.4.2) :

$$^{18}O_{2\,(g)} + {}^{16}O_{(surface)} \longrightarrow {}^{16}O^{18}O_{(g)} + {}^{18}O_{(surface)} \qquad (R_1)$$

The aim of the switching experiment is to determine how much of the ^{18}O incorporated into the surface layer during the first exchange, can be displaced upon subsequent $^{16}O_2$ admission, i.e. :

$$^{16}O_{2\,(g)} + {}^{18}O_{(surface)} \longrightarrow {}^{16}O^{18}O_{(g)} + {}^{16}O_{(surface)} \qquad (R_1)$$

Reactions were performed on both 100 and 2000 Å MgO, the samples possessing the highest and lowest surface areas respectively.

3.9.1 Switching Experiments On 100 And 2000 Å MgO

A plot showing the numbers of $^{16}O^{18}O$ molecules formed, when initially using 80 torr $^{18}O_2$, then evacuating and switching to $^{16}O_2$ on 100 Å MgO at 733 K, is given overleaf.

Following the switch to normal oxygen, the total $^{16}O^{18}O$ concentration measured at the end of the run, was greater than that which would account for the number of ^{18}O atoms exchanged during the initial reaction. This indicates some error in obtaining the measurements. It was found that during the first exchange $^{18}O_2$ was adsorbed on either the walls, or the filament, of the mass spectrometer, which is quite possible since it constitutes approximately 90 % of the gas phase. Then upon the isotopic switch, the $^{16}O_2$ exchanges with this $^{18}O_2$, releasing $^{16}O^{18}O$ into the chamber of the mass spectrometer, where it is detected.

Therefore an experiment was run in the absence of a catalyst, with the rate of $^{16}O^{18}O$ formed by displacement reactions measured, allowing determination of the true rate of

re-exchange. It must be noted that the data presented in Fig 3.9.1.1 has already been adjusted for this.
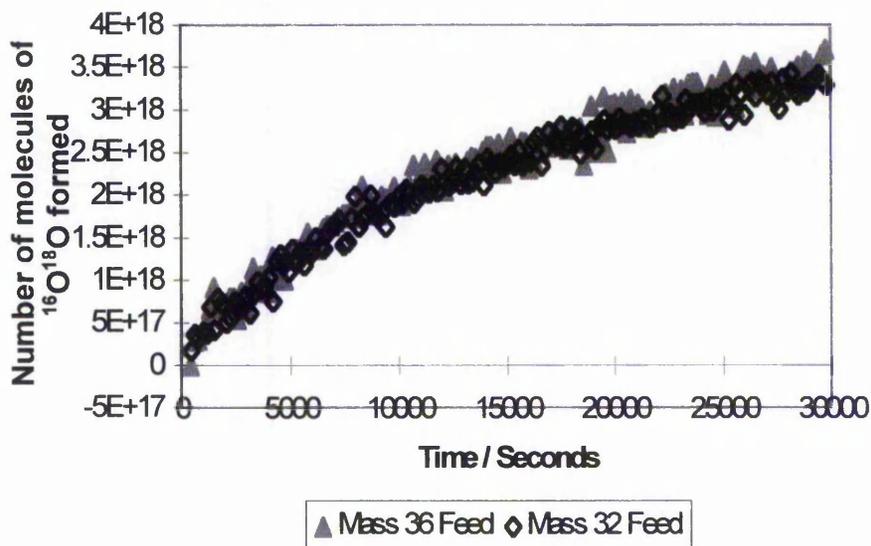
Fig 3.9.1.1   **An Isotopic Switching Experiment On 100 Å MgO At Partial Pressures Of 80 Torr And 733 K Following Vacuum Pre-treatment At 733 K.**

The rate of isotopic oxygen exchange of the two processes are tabulated below, together with those for a similar experiment on 2000 Å MgO.

Ube MgO Sample / Å	Specific Rate Of Oxygen Exchange x 10^{13} / atoms s^{-1}/m^2	
	Mass 36 Feed	Mass 32 Feed
100	6.17 ± 0.435	6.43 ± 0.435
2000	4.72 ± 0.446	4.17 ±0.446

Table 3.9.1.1   **Specific Rates Of Isotopic Oxygen Exchange From Switching Experiments On 100 And 2000 Å MgO At Partial Pressures Of 80 Torr And 733 K Following Vacuum Pre-treatment At 733 K.**

Inspection of Fig 3.9.1.1 and Table 3.9.1.1 shows the rates of both reactions are equal, within the limits of experimental error. This suggests that there are a set number of fixed sites available on the surface for exchange, which then re-exchange sequentially upon admission of $^{16}O_2$.

3.10 Discussion

3.10.1 Characterisation Of The Ube Samples

The first properties of the MgO catalysts to be discussed are the average crystallite lengths and apparent size distribution within a sample. From the various techniques adopted the following table can be constructed.

Theoretical Values		N$_2$ Adsorption		TEM		Powder XRD	
Size / Å	SA / m^{2}g^{-1}	Size / Å^a	SA / m^{2}g^{-1}	Size / Å	SA / m^{2}g$^{-1 b}$	Size / Å	SA / m^{2}g$^{-1 c}$
100	168	171	98	150	92	124	135
500	34	541	31	250	59	222	75
1000	17	645	26	1000	12	320	52
2000	8	1397	12	2200	4	558	30

a - calculated assuming the measured surface area from N$_2$ adsorption.

b - calculated using the measured cube lengths from electron micrographs.

c - calculated from the average crystallite size from the diffraction pattern.

Table 3.10.1.1   **Comparison Of The Calculated And Experimentally Determined Cube Lengths And Associated Surface Areas Of The Ube MgO Catalysts.**

Before discussing these results it is important to draw attention to the values obtained using powder XRD. As mentioned previously (Section 3.4.1) crystallite sizes determined from applying data to the Scherrer equation are only very approximate, depending on a number of variables such as instrument factors and lattice distortions. As a consequence the Scherrer equation generally underestimates cube lengths, when these are not taken into account. The effect due to lattice distortions becomes more pronounced as particle size increases, a trend which is followed in Table 3.10.1.1, as both 1000 and 2000 Å MgO give values much lower than expected. Due to the limited accuracy of these current results, they will be omitted from any subsequent arguments concerning the size and surface area of the Ube samples.

It was hoped that the four MgO catalysts exhibited a perfect cubic morphology, having a narrow size distribution around the quoted value. Unfortunately electron microscopy (Section 3.3) and surface area measurements (Table 3.10.1.1) shows neither is the case. Firstly considering 100 Å MgO it is clear both nitrogen adsorption and TEM give similar results, indicating a crystallite size in the region of 150 Å and surface area 100 m^2g^{-1}. Such findings have also been reported by other workers [87], who have studied 100 Å Ube MgO. However there are instances where the surface area has been much closer to its actual value of 168 m^2g^{-1} [71, 84, 85].

In explaining these conflicting observations it would appear that problems may arise when attempting to control crystal growth, using the build up process, in the smallest size range. It is apparent on occasions cubes larger than desired are produced, leading to a decreased surface area as shown in Table 3.10.1.1. In addition sintered intergrowth could account for the discrepancies between these values. Moodie and Warble [3, 9] saw annealing between individual cubes of MgO prepared from a magnesium basic carbonate precursor, with both perfect and imperfect alignment observed. Gregg [90] also reported that small crystals in close proximity, favour adhesion even at room temperature. Electron micrographs of 100 Å MgO (Fig 3.3.1) are consistent with this finding.

It is also clear from the TEM of 100 Å MgO, as with the remainder of the samples, the surface has undergone etching. Evidence of this is supplied by kink, step and terrace formation present, being typical of those caused by the interaction with water vapour and carbon dioxide. Interestingly these have been shown to have no effect upon the surface area [12, 31]. This is due to their relatively small size, making them insensitive towards nitrogen during physisorption at 77 K [31].

Except for minor deviations, the remainder of the catalysts possess both cube sizes and surface areas comparable to those given by Ube, a result which is consistent with the literature [87]. One such anomaly which requires discussion is the crystallite size of only 250 Å measured for 500 Å MgO, from TEM studies. If this were correct the surface area should be 67 m^2g^{-1}, twice that obtained from nitrogen physisorption, which agrees well with the theoretical value. Therefore one can conclude problems were encountered when performing the electron microscopy of 500 Å MgO. It may be that the electron micrographs of this sample are not properly representative of the sample as a whole.

Finally as Table 3.10.1.1 shows, lengths calculated for 1000 and 2000 Å MgO from surface area experiments are lower than anticipated. This is probably due to the error associated with the measurements which is at best 10 %, subsequently giving inaccurate cube dimensions. Alternatively surface roughness could account for some of the observed surface area, which would give a smaller crystallite size than expected.

The main conclusions from powder XRD patterns of the received catalysts is that reaction with CO_2 and H_2O at room temperature is apparent. Reflections from 100 and 2000 Å MgO indicate bulk hydroxide and carbonate formation respectively, in addition to magnesium oxide. The presence of these phases will not affect rates of isotopic oxygen exchange, as they begin to decompose at 623 K [86], which is 110 K lower than the 733 K pre-treatment temperature used in the majority of the experiments (Section 3.7). Therefore on the commencement of exchange the bulk phases should have been removed, however H_2O vapour and CO_2 still may be adsorbed on the surface.

Finally from recording the XP spectra of the Ube samples it is evident that there are no impurities present within the detectable limits of the spectrometer. As a consequence there are no foreign ions which could alter the exchange characteristics of MgO.

3.10.2   Effect Of Water Attack On The Cubic Morphology

As mentioned in Section 3.10.1 it was hoped the Ube MgO catalysts would exhibit a perfect cubic morphology with a narrow size distribution range. If this had been the case, calculation 3, 4 and 5 co-ordinated sites on the surface would have been simple, yielding the results shown overleaf.

Correlation of these values with measured rates of isotopic oxygen exchange can indicate any structure sensitivity of this reaction between samples.

Unfortunately water vapour attack and its subsequent loss leads to the removal of a surface oxygen (Section 1.3.2), thus altering the populations of the ions present in the outermost layer. Coluccia *et al* [12] reported that in general a net increase in 3 co-ordinated ions are observed at the expense of 5, with 4 remaining unchanged.

Consequently the proportions of each site present do not coincide with those calculated for a perfect system (Table 3.10.2.1), therefore comparisons cannot be made

Cube Length / Å	Percentage Of Total Surface Sites		
	3C	4C	5C
100	0.06	4.2	95.74
500	0.002	0.8	99.198
1000	0.0006	0.4	99.5994
2000	0.0001	0.2	99.7999

Table 3.10.2.1   Table Showing Proportions Of Each Site Type On The Different Ube MgO Catalysts.

between these values and the rates of isotopic exchange.

However techniques such as photoluminescence, UV/VIS/NIR diffuse reflectance and FTIR spectroscopy offer a means of determining numbers of 3, 4 and 5 co-ordinated sites experimentally. This alternative will give the necessary information required to answer the question regarding structure sensitivity of oxygen exchange on MgO. Such measurements are dealt with in Chapter 4.

3.10.3   Isotopic Oxygen Exchange On The Ube Samples

In accordance with the findings of Winter [48], the present results show the initial rates of isotopic oxygen exchange are not dependent on the pre-treatment method used. However extrapolation of our initial rates to 763 K, shows they are an order of magnitude lower than those of Martin and Duprez [71], on 100 Å Ube MgO.

The current results point to an activation energy of approximately 130 kJ mol^{-1} for isotopic oxygen exchange on MgO, compared to 160-170 kJ mol^{-1} reported elsewhere [38, 48, 71]. Pre-exponential factors are roughly 4 orders of magnitude lower than those presented in the literature [38, 48].

Initially it was thought that the reason for such discrepancies is that exchange proceeds via ^{18}O with ^{16}O of adsorbed hydroxyl groups, not oxygen in the surface layer of the oxide. As indicated in Section 3.10.1 the Ube samples have most probably been hydroxylated, making the possibility of this reaction occurring quite feasible.

It is well documented that temperatures in excess of 1073 K are required for the total removal of surface hydroxyl groups on MgO [15-17, 91-96], associated with desorption from ions in low co-ordination [15, 17, 95]. By analogy to work by Coluccia *et al* [17], in the 733 K region used for outgassing (Section 3.7), approximately 25 % of the surface will retain hydroxyl groups (Table 1.3.2.1). Since 3 and 4 co-ordinated sites constitute less than 5 % of the total surface of 100 Å MgO (Table 3.10.2.1), which represent the highest population, it is clear that hydroxyls are adsorbed on all types of co-ordinatively unsaturated surface sites. However recent modelling studies of H_2O chemisorption on MgO [32], indicate ions exhibiting 5 fold co-ordination are unable to dissociate a water molecule, contradicting the experimental findings of Coluccia [17]. Therefore it is uncertain if 5C sites are covered by hydroxyl groups.

Upon dissociation of water vapour two types of hydroxyl groups are formed, as indicated below :
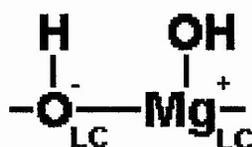
Fig 3.10.3.1   **Different Hydroxyl Groups Formed On The MgO Surface.**

It would be expected that the oxygen of the Mg — OH group would exchange more readily than that of the O — H, since the latter is associated with an anion of the oxide, making it harder to remove. Also increasing the co-ordination number of the Mg^{2+}_{LC} cation decreases its acidic character, leading to a weaker bond to the hydroxyl group, hence being available for reaction more readily. Therefore it seems reasonable to assume that isotopic oxygen exchange would preferentially occur at a Mg — OH site, with the Mg^{2+}_{LC} exhibiting the highest co-ordination available. A similar conclusion was reached by Cunningham *et al* [72], when investigating exchange reactions on CaO. Exchange involving hydroxyl groups led to a new R_1 route to be proposed (Section 1.4.2).

$$^{18}O_{2\,(g)} + {}^{16}OH_{(ads)} \quad \longrightarrow \quad {}^{16}O^{18}O_{(g)} + {}^{18}OH_{(ads)} \quad\quad (R_1)$$

In an attempt to verify this theory, isotopic exchange was monitored using IR spectroscopy [139], at 80 torr after vacuum pre-treatment, under the same conditions as adopted previously (Section 3.7).

It is widely accepted the ^{16}OH stretch of adsorbed water on MgO is located in the 3750 cm^{-1} region of the spectrum [8, 16, 17, 21, 94], which upon exchange with ^{18}O would shift to lower wavenumbers. The results of such an experiment are shown below.
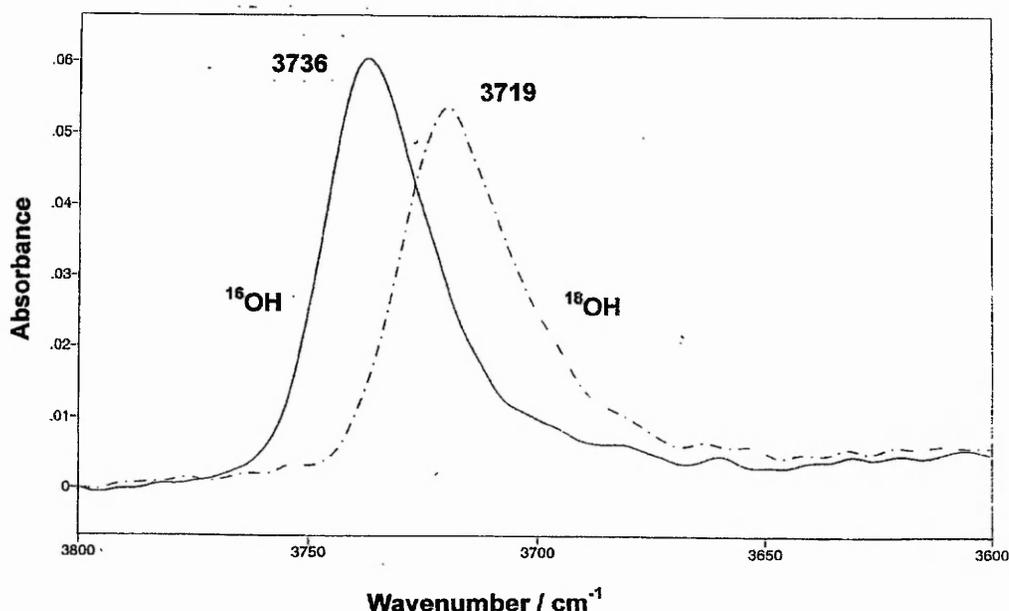
Fig 3.10.3.2   Isotopic Oxygen Exchange On MgO At 740 K And 80 Torr Following Vacuum Treatment Probed Using IR Spectroscopy.

As Fig 3.10.3.2 shows upon admission of $^{18}O_2$ a new band appears at 3719 cm^{-1}, its intensity increasing with time, providing evidence of hydroxyl group exchange. The observed shift of 17 cm^{-1} compares reasonably well with the 13 cm^{-1}, calculated assuming a harmonic oscillator [140]. However the reaction is complete within a minute, which cannot explain the observed kinetics (Fig 3.6.2.1), where activity is sustained over a much longer time period. Therefore exchange between ^{18}O and ^{16}O of hydroxyls, does not provide a

satisfactory isotopic oxygen exchange mechanism regarding the Ube MgO samples, but they are still thought to play a significant role in the exchange process.

It is possible that the active site is an O⁻ ion, formed during pre-treatment, via a pathway proposed by Martens *et al* [96]. In their studies the decomposition of brucite at elevated temperatures led to the evolution of the following species :
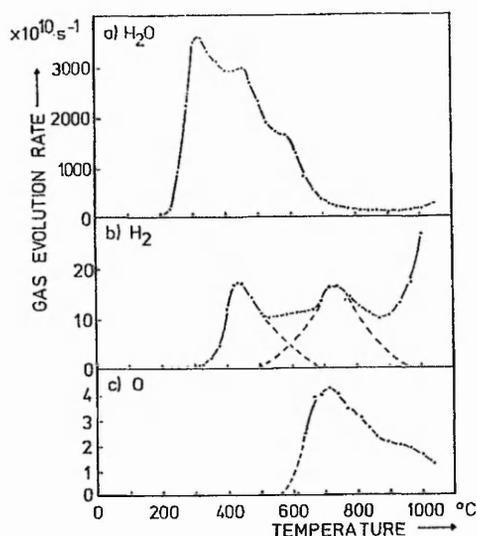
Fɪɢ. 1. Gas evolution curves as a function of the dehydration temperature for 38μg Mg(OH)₂ (heating rate: 2°C min⁻¹): (a) water, (b) hydrogen, (c) atomic oxygen.

Fig 3.10.3.3   Evolution Of Different Species From The Decomposition Of Brucite At Elevated Temperatures - Taken From Ref [96].

The appearance of hydrogen (part b) was attributed to a two stage process, the route being sensitive to decomposition temperature, as indicated below. Such reactions were also responsible for the simultaneous surface O⁻ formation.

$$2OH^- \longrightarrow 2O^- + H_2 \qquad 573\text{-}873 \text{ K}$$
$$OH^- \longrightarrow O^- + \tfrac{1}{2}H_2 \qquad 873\text{-}1173 \text{ K}$$
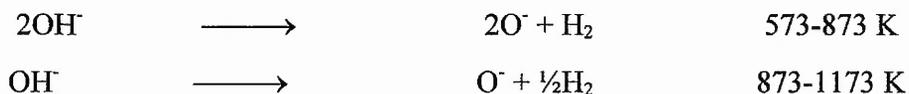
It is believed that a similar phenomenon is occurring with OH⁻ groups present on the Ube MgO samples, as they are considered to be highly hydroxylated. In related work

Karasuda *et al* [137, 138] did not observe hydrogen release until temperatures of 973 K were reached, however the degree of hydroxyl coverage on their MgO is unclear.

By analogy to hydroxyl exchange work [72], it is regarded that the active O^- site is formed by removing a hydrogen atom from the OH^- located on a Mg^{2+}_{LC} cation (Fig 3.10.3.1), exhibiting the highest possible co-ordination available.

Inspection of Fig 3.10.3.3 indicates that at 733 K, the temperature adopted for pre-treatment, there is a significant O^- presence on the catalyst surface from hydroxyl disproportionation. It is well documented that O^- is highly reactive towards oxygen [141, 142], forming an ozonide ion (O_3^-), which has been verified on MgO using EPR spectroscopy [143-147].

It is also thought that this process is easily reversible, providing a suitable pathway for exchange reactions to take place [148, 149]. Nikisha *et al* [148] proposed the following route for a partially reduced silica-supported vanadium pentoxide system.

$$^{16}O^-_{(surface)} + {}^{18}O_{2\,(g)} \longrightarrow ({}^{16}O^{18}O^{18}O)^-_{(surface)} \longrightarrow {}^{18}O^-_{(surface)} + {}^{16}O^{18}O_{(g)} \quad (R_1)$$

It is envisaged that this sequence of events can explain the isotopic exchange characteristics observed with the current Ube MgO samples.
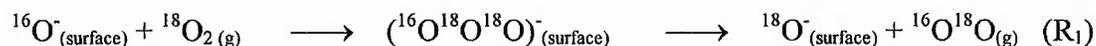
Figure 3.6.2.1 indicates isotopic oxygen exchange follows first order kinetics and the rate of reaction steadily decreases until it finally stops. Therefore there are a fixed number of sites available for exchange. After 20 hours the curve has nearly reached its plateau, according to Figure 3.6.2.1 this accounts for approximately 6 % of the total surface. If the experimental findings of Coluccia [17] are correct, there are sufficient OH^- groups present able to form O^-, which in turn are able to undergo exchange on the Ube catalysts, following a pre-treatment temperature of 733 K. Also since the measured rate was independent of oxygen pressure in the 20-80 torr range studied (Section 3.7.4), it would appear that desorption is the rate determining step of the reaction.

In addition to explaining the current observations, it is thought this exchange mechanism can account for the results obtained by Martin and Duprez [71]. In their studies the optimal exchange rate on MgO was measured at 763 K, coinciding well with the maximum O^- concentration present on the surface from Figure 3.10.3.3 [96]. Therefore it is possible that the two phenomena are related. What is also striking from the study of Martin

and Duprez [71], is that the 100 Å Ube MgO used was highly hydroxylated, showing evidence of a bulk $Mg(OH)_2$ phase in the powder XRD pattern. The presence of brucite considerably enhances the probability of O^- formation in their system.

3.10.4   Structure Sensitivity Of Isotopic Oxygen Exchange On The Ube MgO Samples

Inspection of Figures 3.7.2.1, 3.7.5.2 and 3.8.3.1 at pressures of both 20 and 80 torr, indicates no differences in the rates and activation energies of isotopic oxygen exchange on magnesium oxide, within the limits of experimental error. This result is quite suprising since there is an order of magnitude difference between the highest and lowest surface area samples, 100 and 2000 Å MgO respectively. From this it can be concluded that this reaction rate is not influenced by variations in the relative and absolute number of 3 and 4 co-ordinate ions.

Considering each of the catalysts it is apparent that an increase in crystallite size leads to a decrease in the populations of ions exhibiting 3 and 4 co-ordination (Fig 3.10.2.1), hence populations will vary between samples. Since the exchange does not depend upon the surface area of the Ube samples, it would appear that such ions do not participate alone in the reaction. Therefore the O^- active site is thought to be situated on a Mg^{2+}_{5C} cation.

However it is also feasible that exchange occurs simultaneously at 3, 4 and 5 co-ordinated sites with equal rates, making each type indistinguishable.

Previous work published by this group [7], concerning methane coupling on various MgO catalysts, made a similar observation regarding structure sensitivity. Amongst catalysts of cube like morphologies, differences in populations of 3 and 4 co-ordinated ions did not change reactivity.

3.10.5   Isotopic Switching Experiments

From Fig 3.9.1.1 it is clear that the rates of the initial and the re-exchange reactions are very similar. It is apparent from this plot, as mentioned in Section 3.10.3, that the process

eventually stops, indicating there are a finite number of active species. Also it appears that the same number of exchange events are observed in both the forward and back reaction.

Therefore it can be speculated that during the first reaction ^{18}O exchanges with $^{16}O^-$ adsorbed on a $Mg^{2+}{}_{5C}$ site (Sections 3.10.3 and 3.10.4). Then on switching to ^{16}O each $^{18}O^-$ re-exchanges at the same rate in a sequential manner, showing the equivalence of each active site.

Due to the similarity between both measured rates it is unlikely that migration across the surface or diffusion into the bulk are apparent. If the movement of an adsorbed ^{18}O across the surface or into the lattice followed by exchange were occurring, the probability of the exact opposite happening upon ^{16}O admission is negligible. If this were the case, behaviour as in Fig 3.9.1.1 would not be observed.

The difficulty of migration of adsorbed oxygen species across the MgO surface was demonstrated by Kantorovich *et al* [97]. They concluded that for this to occur on an MgO terrace a change in spin state is required, the timescale of which is very long for an isolated atom, compared to that of an exchange event. Therefore the process would have to rely on interactions with other adsorbed species or defects to proceed. If the spin state remained the same, migration would be very slow well above room temperature.

3.10.6   Influence Of High Temperature Outgassing On The Rate Of Isotopic Oxygen Exchange

As shown in Section 3.7.6, increasing the vacuum pre-treatment temperature, affected the exchange characteristics of MgO. Evacuating a sample of 2000 Å MgO to 873 or 1023 K, appears to promote F-centre formation, which are subsequently filled upon admission of $^{18}O_2$. After this there is a short period of inactivity, before which exchange proceeds at a rate comparable to that when no such vacancies are present (Table 3.7.6.2), as with outgassing at 733 K (Table 3.7.6.1).

It is thought that oxygen is lost from the surface layer of the oxide and not from the O$^-$ active site, as shown overleaf.
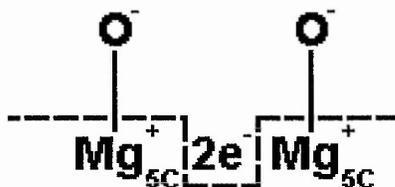
Fig 3.10.6.1   **Proposed Surface F-centre Formation On The Ube MgO Catalysts.**

The reasoning behind this is that if a re-population of O^- were occurring, it would be labelled with ^{18}O on oxygen contact. Subsequently no changes in mole fractions 32, 34 and 36 would be observed, once exchange commences.

It is tentatively suggested that the onset of exchange is delayed, because the presence of surface F-centres increases the strength O_3^- binding towards Mg^{2+}_{5C}. Therefore the reaction switches off until a certain degree of filling occurs, following which $^{16}O^{18}O$ desorption is then possible.

4. Spectroscopic Measurements

4.1   General Introduction

Characterisation of the Ube MgO samples (Chapter 3) showed they neither exhibit a perfect cubic morphology, nor possess a narrow size distribution, around the quoted value. Consequently calculations of the populations of 3, 4 and 5 co-ordinated sites on the surface becomes virtually impossible. Quantification of these values are desirable, as they enable confirmation of the conclusions of Chapter 3, showing the lack of structure sensitivity regarding oxygen exchange on the Ube MgO samples.

Techniques such as photoluminescence, UV/VIS/NIR diffuse reflectance and FTIR spectroscopies were adopted to determine the relative numbers of co-ordinatively unsaturated sites on the surface of the Ube MgO samples. This involved measurements upon both clean surfaces and the use of probe molecules such as oxygen, hydrogen and carbon monoxide. It is envisaged that results from such studies will help in understanding the isotopic oxygen exchange characteristics of MgO.

4.2   UV/VIS/NIR Diffuse Reflectance Spectroscopy

There have been many investigations involving UV/VIS/NIR diffuse reflectance spectroscopy on MgO [4, 15, 28, 98-100], all indicating the absorption of light in the UV/Visible region of the electromagnetic spectrum. During early measurements, Nelson and Hale [98] observed fluorescence using absorption wavelengths around 250 nm. This gave reflectances greater than 100 %, attributed to the emitted light entering the instrument photomultiplier [15]. It was found that a small amount of oxygen quenched this fluorescence [98], revealing the true absorption spectrum. Therefore all experiments are performed in a slight pressure of oxygen.

Two bands were found on MgO, occurring at 37000 and 46000 cm^{-1}, thought to be related to 3 and 4 co-ordinated ions respectively [4, 15, 28, 99, 100]. This was confirmed using MgO from different precursors, varying in surface area [4] and sintering experiments

[15], where populations of 3 and 4 sites differed. Garrone *et al* [28] summarised the diffuse reflectance absorption bands on MgO :

Co-ordination Number	Energy Of Transition / eV	Absorption Band / cm⁻¹
Band Gap	8.7	71700
First Exciton (6C)	7.7[a]	63500
5C	6.6[b]	54400
4C	5.75	46000
3C	4.62	37000

a - value taken from single crystal data.

b - extrapolated value.

Table 4.2.1   Table Showing The Absorptions Present On MgO Due To Unsaturated Surface Ions.

In an attempt to verify the correct assignment of the bands, each was subjected to the Mollwo-Ivey relation, which determines the degree of freedom of an exciton.

$$\lambda_m = ka^m$$

Equation 4.2.1   The Mollwo-Ivey Relationship.

where λ_m = wavelength of the absorption peak

   k   = constant

   a   = cation-anion distance

   m   = constant

If an exciton is bound (i.e. localised at a position on the surface), a plot of $\log_{10} \lambda$ against $\log_{10} a$, should yield a straight line. Therefore one would expect 3 co-ordinated ions to follow this relationship closely, as they have little scope for movement. The converse should be true regarding 5C sites, as they possess a greater degree of translational freedom. A plot for 3, 4, 5 and 6C ions showed the assignments to be true, the former two following a linear

relation, whilst the latter indicating no apparent correlation. The bulk excition is said to be free as it has the ability to travel through the crystal as a whole.

The positions of these bands should be identical to the excitation maxima of the corresponding photoluminescence spectra (Section 4.3), as the same process is being followed. Energies in Table 4.2.1 are very similar to those at 5.40 and 4.52 eV for 4 and 3 co-ordinated ions from the luminescence.

Unlike its photoluminescence counterpart, the nature of diffuse reflectance bands are straightforward, with their assignment being completely agreed by all workers.

4.2.1 UV/VIS/NIR Diffuse Reflectance Spectra Of 100 Å MgO

Sample treatment and recording of spectra are described elsewhere (Sections 2.5 and 2.7). The figure below shows the spectrum of 100 Å MgO in 10 Torr O_2 :
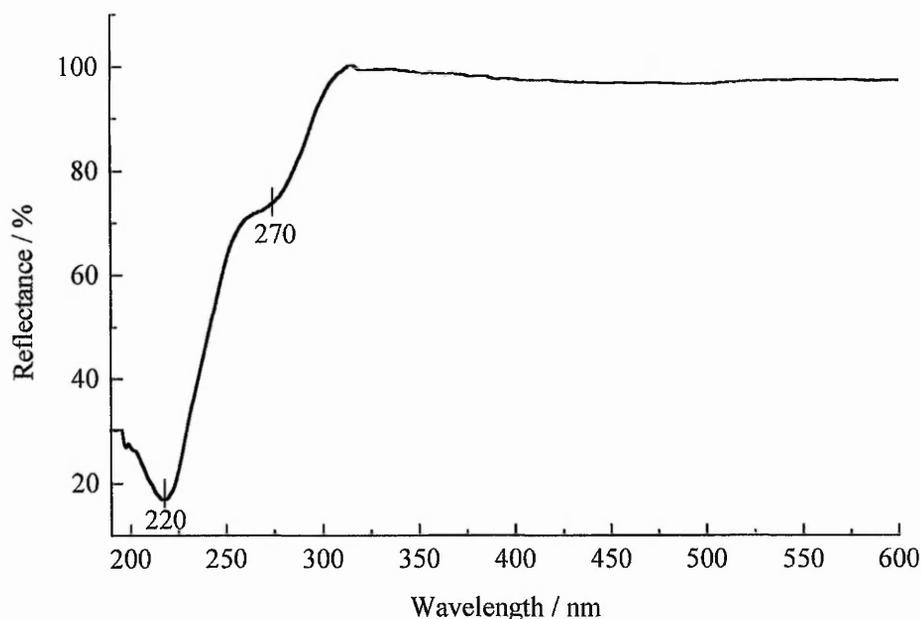
Fig 4.2.1.1   UV/VIS/NIR Diffuse Reflectance Spectrum Of 100 Å MgO At 298 K In 10 Torr O_2.

Consistent with the literature oxygen addition quenches fluorescence, yielding an absorption band at 220 nm with a shoulder at 270 nm. Spectra were recorded for the remaining Ube

samples, to compare the relative intensities of the two bands, giving an insight to the populations of 3 and 4 co-ordinated sites on the surface.

4.2.2 UV/VIS/NIR Diffuse Reflectance Spectra Of The Ube Samples

In addition to 100 Å MgO the diffuse reflectance spectra were recorded for the other samples, as shown below :
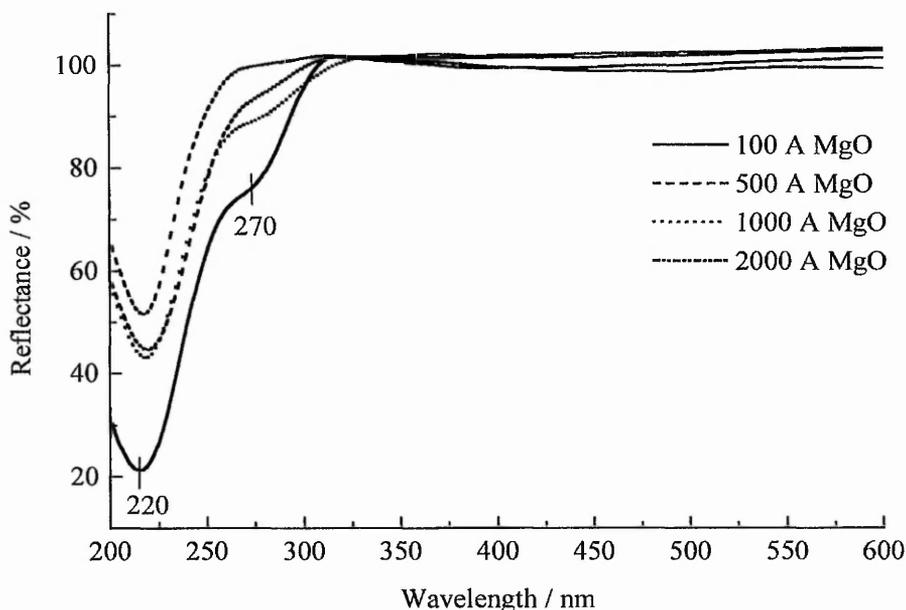
Fig 4.2.2.1   **UV/VIS Diffuse Reflectance Spectra Of The Ube Samples At 298 K In 10 Torr O₂.**

From the shoulder at 270 nm it is clear that the numbers of 3 co-ordinated sites decrease in the following manner :

$$100 \text{ Å} > 1000 \text{ Å} > 500 \text{ Å} > 2000 \text{ Å}$$

Similarly the absorption band at 220 nm gives a sequence for the 4 co-ordinated sites :

$$100 \text{ Å} > 500 \text{ Å} \approx 1000 \text{ Å} > 2000 \text{ Å}$$

Unfortunately UV/VIS/NIR diffuse reflectance measurements only provide a qualitative indication of the co-ordinatively unsaturated surface sites, hence exact populations cannot be determined. However it gives a good approximation as to how the numbers of 3 and 4 co-ordinated sites vary within the samples.

It has been previously shown [98] that the % reflectance is related to the absorption coefficient (k) by the Kubelka-Munk equation :

$$\frac{(1-R)^2}{2R} = \frac{k}{s}$$

Equation 4.2.2.1   The Kubelka-Munk Equation.

where   R = % reflectance

   k = absorption coefficient

   s = scattering coefficient

Application of the Kubelka-Munk equation to the reflectance data in Fig 4.2.2.1 is plotted overleaf.

The advantage of plotting the results in this manner is that the relative intensity reflects the actual populations of sites within a sample. Therefore comparison of the maximum values, can provide information regarding the surface ratio of 4 to 3 co-ordinated ions [4]. The results obtained from Fig 4.2.2.2 are presented below.

Cube Size / Å	4C Maxima at 46000 cm^{-1}	3C Maxima at 37000 cm^{-1}	Ratio 4C/3C
100	2.049	0.051	40.18
500	0.892	0.017	52.47
1000	0.631	0.017	37.12
2000	0.533	0.005	106.60

Table 4.2.2.1   Table Showing The Ratio Of 4 To 3 Co-ordinated Sites On The Ube Samples From The UV/VIS/NIR Diffuse Reflectance Spectra.
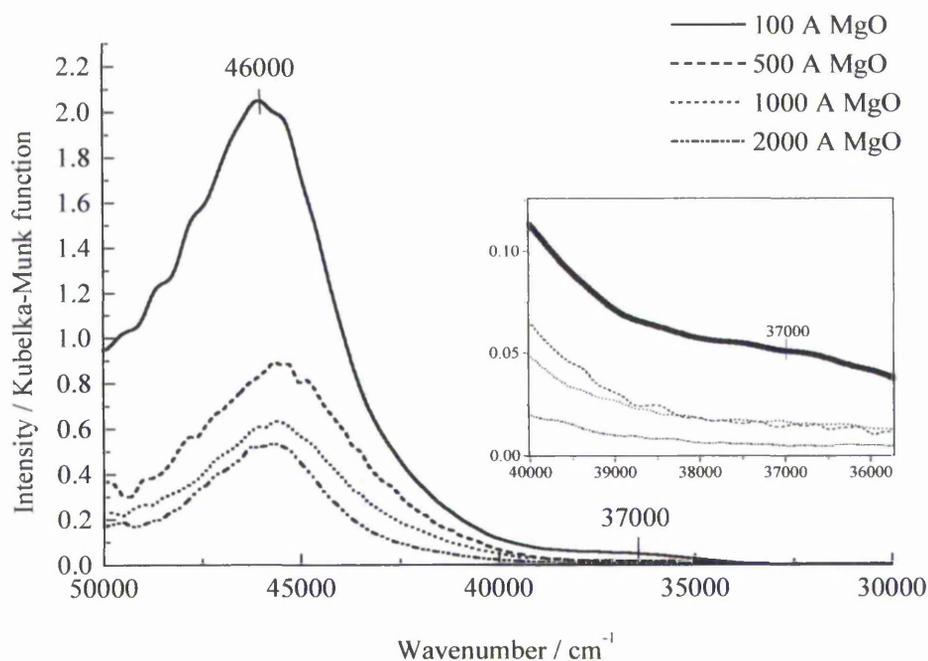
Fig 4.2.2.2   Plot Of Kubelka-Munk Function Against Wavenumber For The Ube Samples.

From Fig 4.2.2 it is also possible to determine differences in population of a particular site, between the Ube samples. This can be achieved by assuming the packing of the powder is essentially the same for each sample, with a constant area of the cell exposed to the radiation. The ratios, compared to that of 100 Å MgO, are tabulated below for the data from Table 4.2.2.1.

Ratio	Ratio 3C	Ratio 4C
100:500	3.0	2.30
100:1000	3.0	3.25
100:2000	10.2	3.84

Table 4.2.2.2   Table Showing The Ratios Of Each Different Co-ordination Site Type From The UV/VIS/NIR Diffuse Reflectance Spectra.

4.3   Photoluminescence Spectroscopy

The photoluminescence properties of powdered MgO were first reported by Nelson and Hale [7], during a UV/VIS/NIR diffuse reflectance spectroscopy study. As stated earlier they found that when using absorption wavelengths in the region of 250 nm the reflectance was greater than 100%. This was attributed to the absorption and re-emission of light, i.e. luminescence. Subsequently many studies have been made investigating this phenomenon [4, 12-14, 91, 95, 101-108].

Tench and Pott [101] expanded upon this initial observation, devoting a study to the photoluminescence behaviour of MgO. With an excitation wavelength of 250 nm in vacuum at 298 K, an emission peak with maximum 440 nm and a shoulder at 400 nm was observed. Further excitation at 320 nm gave an emission at 535 nm. Consequently a spectrum with maxima at 247 and 292 nm was produced, when recording excitation wavelengths whilst measuring emission at 400 nm. This result was quite suprising since single crystals of pure MgO show no absorption of light in the near UV region. Therefore excitations were deemed not to be due to transitions involving the bulk ions but ones on surface sites of low co-ordination.

Effects of hydroxylation on the photoluminescence of MgO has been investigated [14, 91]. Coluccia [91] found highly dehydroxylated surfaces in vacuo at 254 nm gave results in agreement to those previously [101]. Contact of water vapour with the sample led to the gradual disappearance of these bands, new ones being formed at 435 and 465 nm when exciting at 365 nm. This further reinforced the theory that emissions were from surface ions in low co-ordination, as hydroxyl groups covering these sites quenched their luminescence. Removal of the hydroxyl groups by re-heating in vacuum restored the original spectrum. Similar trends were found by Duley [14] during the progressive decomposition of $Mg(OH)_2$ at temperatures up to 1200 K. In this study the band at 465 nm was assigned to hydroxyl groups present on four co-ordinated oxygen anions.

The photoluminescence process occurring was thought to proceed via a charge transfer complex by the following pathway [13, 102, 103] :

$$(Mg^{2+}_{LC} - O^{2-}_{LC}) \longrightarrow (Mg^{+}_{LC} - O^{-}_{LC})^{*}$$
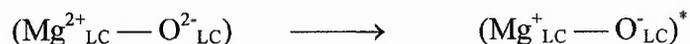
The observed photoluminescence is the light emitted by the excited complex reverting to the ground state. It was postulated that absorption occurred on an O^{2-}_{LC} anion with electron transfer to a neighbouring Mg^{2+}_{LC} cation where luminescence then takes place [13, 92]. Excitation will be characteristic of the O^{2-}_{LC}, whereas the emission will tend to reflect more the environment of the $Mg^{2+}_{LC}O^{2-}_{LC}$ ion pair. Duley however was not in total agreement with this [106]. It was acknowledged that the absorbing sites were the oxygen anions in low co-ordination, but suggested emission occurred through a charge transfer to an adjacent F^{+}_{S} centre (an electron trapped at a surface anion vacancy), rather than an Mg^{+*}_{LC} cation.

Experiments involving MgO prepared from different precursors, each having varying populations of co-ordinatively unsaturated type sites, were performed to determine their role in the photoluminescence [4, 12]. It was found that ions in 4 and 3 co-ordination were responsible for excitation spectra at 230 (5.40) and 274 nm (4.52 eV) respectively. Contributions from ions in 5 fold co-ordination were not seen [4, 13], as they lie outside the lower detectable limits of the instrument. Spectra could only be recorded above 230 nm because of the low intensity of the excited light at shorter wavelengths. However 5 co-ordinated ions of other alkaline earth oxides, lying at lower energies than for MgO, have been identified using this technique [13, 103].

Contributions from surface point defects, such as F^{+}_{S} centres were unclear, Tench and Pott [101] were unsure if they led to the observed emissions. During UV/VIS/NIR diffuse reflectance studies Nelson and Hale [98] purposely produced surface F^{+}_{S} centres by γ-irradiation in vacuo, finding they had an absorption at 600 nm, associated with a blue/purple colouration of the sample. However the original MgO showed no sign of this band. Since the photoluminescence gave no excitation maximum in this 600 nm region, their presence was discounted.

Shvets and co-workers [104] were not in agreement with the band assignments by Coluccia, claiming emissions at 415-480 nm were due to F^{+}_{S} centres and that at 530 nm F^{0}_{S} centres (a surface anion vacancy with two trapped electrons). Interestingly Tench and Pott [2] also observed the second band at 535 nm.

This led to a re-investigation of photoluminescence on MgO by Anpo *et al* [102]. They observed both short (10^{-4} s) and long ($1\text{-}10^{4}$ s) lived emissions at excitation wavelengths of 240-280 and 340-450 nm respectively. The latter were thought to originate from F^{+}_{S} centres, formed due to unusually high levels of impurity in the sample. Similar long

lived emissions at 535 nm have been reported by Yanagisawa and Huzimura [107]. Anpo concluded the earlier theory was correct and that Shvets [104] had actually seen this long lived emission due to F^+_s centres and the assignment made of the 415-480 nm bands were incorrect.

The current results, showing emissions in the region 350-450 nm, will be explained in terms of excitations of 3 and 4 co-ordinated ions.

4.3.1 Photoluminescence Spectra Of 100 Å MgO

Sample treatment (Section 2.5) and the recording of spectra (Section 2.6) have been described previously. Results for 100 Å MgO can be seen below :
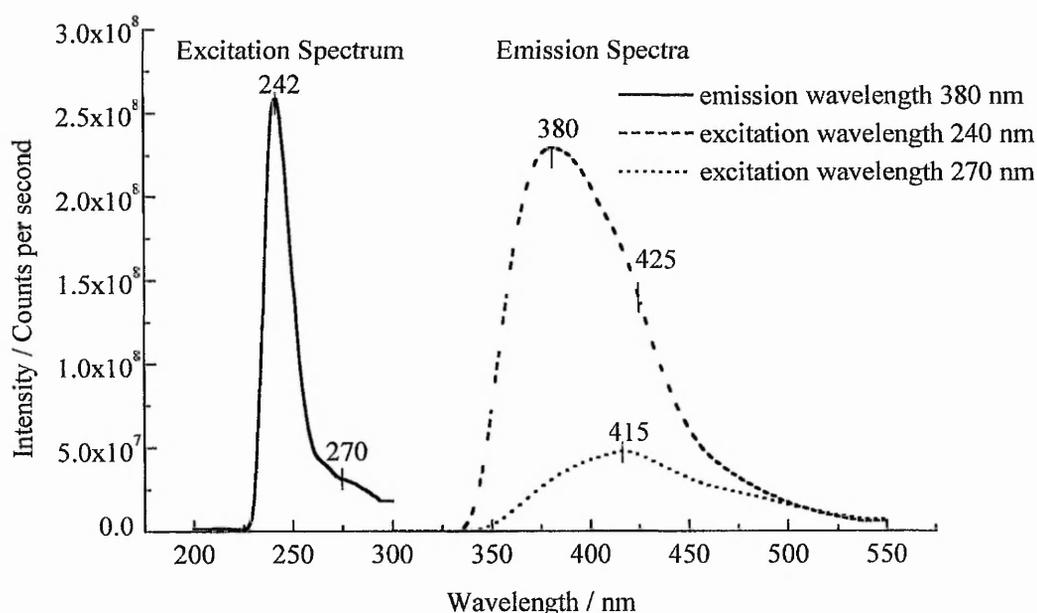
Fig 4.3.1.1   Excitation And Emission Spectra Of 100 Å MgO In Vacuum At 298 K.

It is evident that these spectra are in agreement with those of previous workers. When using excitation wavelengths of 240 and 270 nm emission maxima are present at 380 and 415 nm, corresponding to ions in 4 and 3 fold co-ordination respectively. However a shoulder at

425 nm is also observed in the spectrum irradiated at 240 nm, indicating an emission from 3 fold sites even though 4C are being excited.
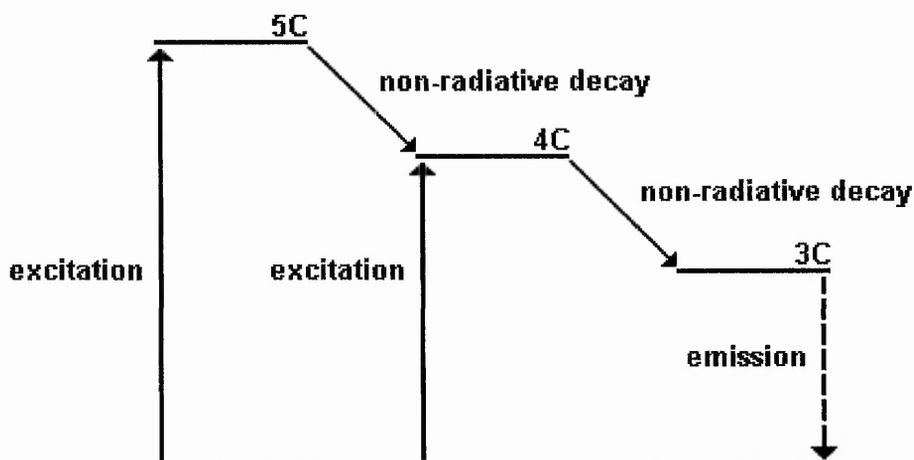
Consequently an absorption maximum is present at 242 nm, with a shoulder at 270 nm, when using a constant emission of 380 nm.

With SrO at room temperature [103, 105, 108] it was found when exciting 5 and 4 co-ordinated sites a non-radiative decay from these to the 3 co-ordinated sites was occurring, where emission then took place. This can be seen diagramatically below :

Fig 4.3.1.2   Non-radiative Decay Pathways Following Absorption On MgO.

Radiative decay is more efficient from 3 co-ordinated sites, explained in terms of bonding to the lattice. Ions in higher co-ordination have more bonds to the oxide, increasing the number of possible non-radiative decay pathways available. Mobility at the lowest co-ordinated sites is more constrained and they act as sinks for the energy absorbed by other surface centres. Suprisingly a slight effect due to the reverse process was observed [108], when exciting the 4 co-ordinated sites emissions from both 3 and 5 co-ordinated ions were seen.

When non-radiative decay is evident it does not give a true reflection of the populations of each site type. However this energy transfer is largely suppressed at 77 K

[103, 108], hence 100 Å MgO spectra were recorded at this temperature. Results obtained were very similar to those observed at 298 K, indicating that non-radiative decay was not apparent on MgO.

4.3.2 Photoluminescence Spectra Of The Ube Samples

The excitation and emission spectra of each of the Ube samples can be seen below :
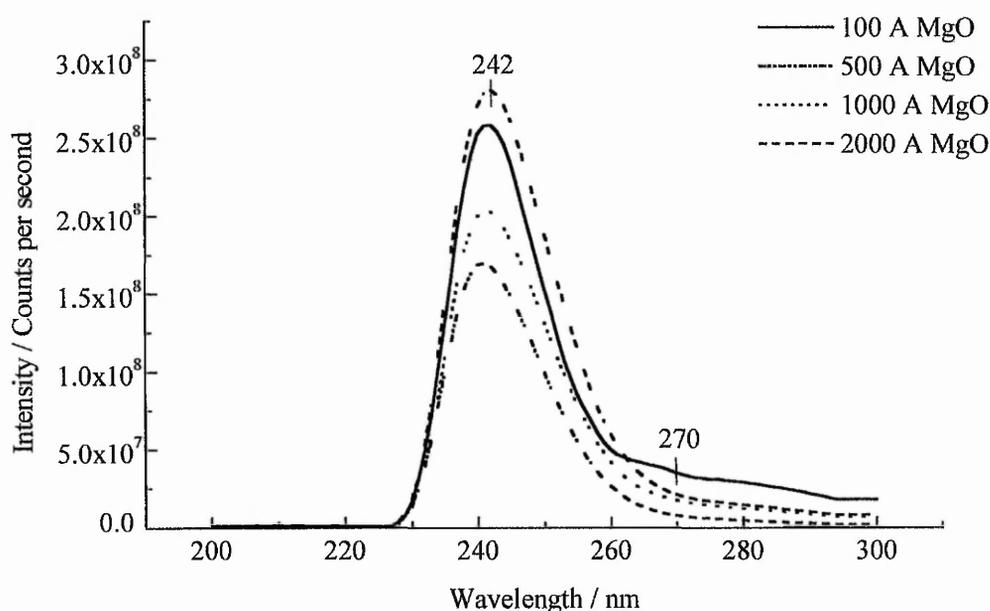
Fig 4.3.2.1   **Excitation Spectra Of The Ube Samples At 298 K In Vacuum. Measured Using A Constant Emission Of 380 nm.**
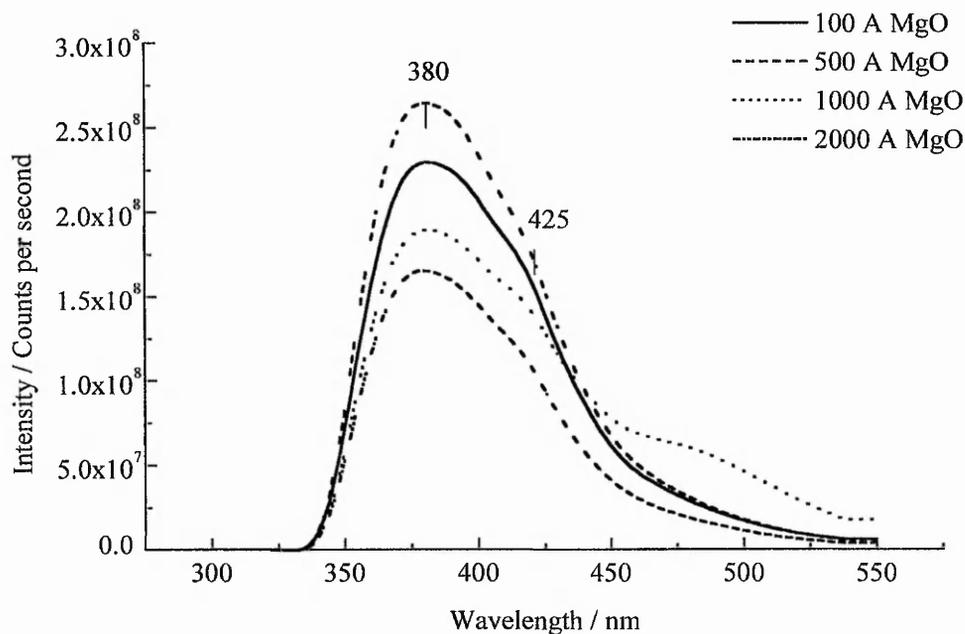
Fig 4.3.2.2   Emission Spectra Of The Ube Samples At 298 K In Vacuum Using An Excitation Wavelength Of 240 nm. Mainly Probing 4 Co-ordinated Sites.
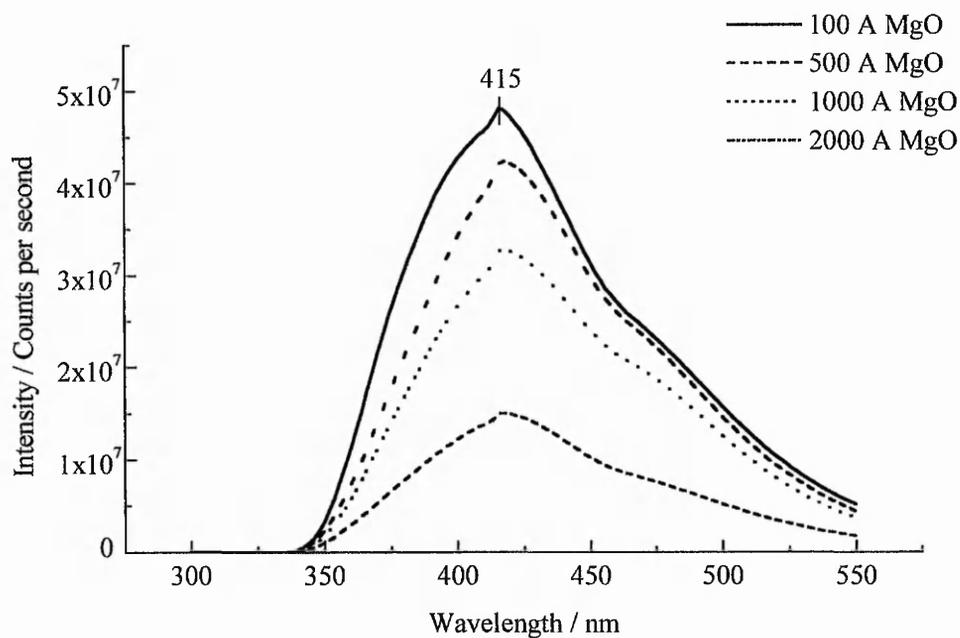
Fig 4.3.2.3   Emission Spectra Of The Ube Samples At 298 K In Vacuum Using An Excitation Wavelength Of 270 nm. Probing 3 Co-ordinated Sites.

As with UV/VIS/NIR diffuse reflectance spectroscopy (Section 4.2.2), comparison of the relative number of 4 to 3 co-ordinated sites within a series of samples, can be achieved by comparing the ratio of the intensity maxima of these two site types. These results are summarised below :

Cube Size / Å	Excitation Spectra		Ratio I_{240}/I_{270}	Emission Spectra		Ratio I_{380}/I_{415}
	Max (242 nm)	Max (270 nm)		Max (380 nm)	Max (415 nm)	
100	2.58×10^8	3.79×10^7	6.81	2.29×10^8	4.82×10^7	4.75
500	2.81×10^8	2.46×10^7	11.42	2.64×10^8	4.24×10^7	6.23
1000	2.03×10^8	1.98×10^7	10.25	1.89×10^8	3.27×10^7	5.78
2000	1.70×10^8	9.38×10^6	18.12	1.65×10^8	1.50×10^7	11.00

Table 4.3.2.1   Table Showing The Ratio Of 4 To 3 Co-ordinated Sites On The Ube Samples From The Photoluminescence Spectra.

Similarly it is possible to calculate the differences in population of a single site on the MgO surface, using the same assumptions as those previously in constructing Table 4.2.2.2.

Ratio	Excitation Spectra		Emission Spectra		Average	
	3C	4C	3C	4C	3C	4C
100 : 500	1.54	0.92	1.14	0.87	1.27	0.90
100 : 1000	1.92	1.27	1.47	1.21	1.66	1.24
100 : 2000	4.04	1.52	3.21	1.39	3.38	1.46

Table 4 3.2.2   Table Showing The Ratios Of Each Different Co-ordination Site Type From The Photoluminescence Spectra.

4.3.3 Reactions Of The Surface With Oxygen

UV/VIS/NIR diffuse reflectance experiments (Section 4.2) showed fluorescence was quenched on the addition of a small amount of oxygen, allowing a true absorption spectrum to be obtained. Photoluminescence measurements gave further evidence of this

[4, 12, 13, 91, 102]. The exact nature of the interaction of oxygen with the surface is unclear, with two different mechanisms being presented [91, 102].

(1)   Collisional (weak interaction) quenching where the gaseous molecules interact with the emitting sites in a metastable excited state.

(2)   Quenching due to the formation of a complex between the adsorbed oxygen and the excited emitting site.

Both these are thought to give a non-radiative deactivation pathway to the ground state, however there is no direct evidence supporting either. Anpo [102] thought the former was predominant because of the reversible nature of quenching, suggesting the oxygen molecules interact weakly with the active surface. Coluccia [91] favoured the latter as oxygen quenching was irreversible at 77 K, due to the formation of a weak charge transfer complex, giving a non-radiative pathway for the energy to be absorbed. Nelson and Hale [98] found quenching responded to changes in oxygen pressure up to 0.3 Torr. If both 3 and 4 co-ordinated ions adsorb oxygen forming a complex, all the sites will be saturated at much lower pressures than 0.3 Torr, as they account for less than 1 % of the total surface ions. Since oxygen addition enhanced quenching, it appears to be due an increased collisional effect, according to the first proposal.

Results of oxygen quenching experiments on 100 Å MgO can be seen overleaf. From Fig 4.3.3.1 dosing 15 Torr O_2 completely destroys luminescence. Subsequent evacuation of oxygen led to the restoration of the original spectrum. Separate studies [13] showed that pumping off the oxygen led to the intensity reaching 80 % of its original value, a small amount being irreversible at room temperature. Absorbed oxygen on the sites of lowest co-ordination was thought to account for this observation.
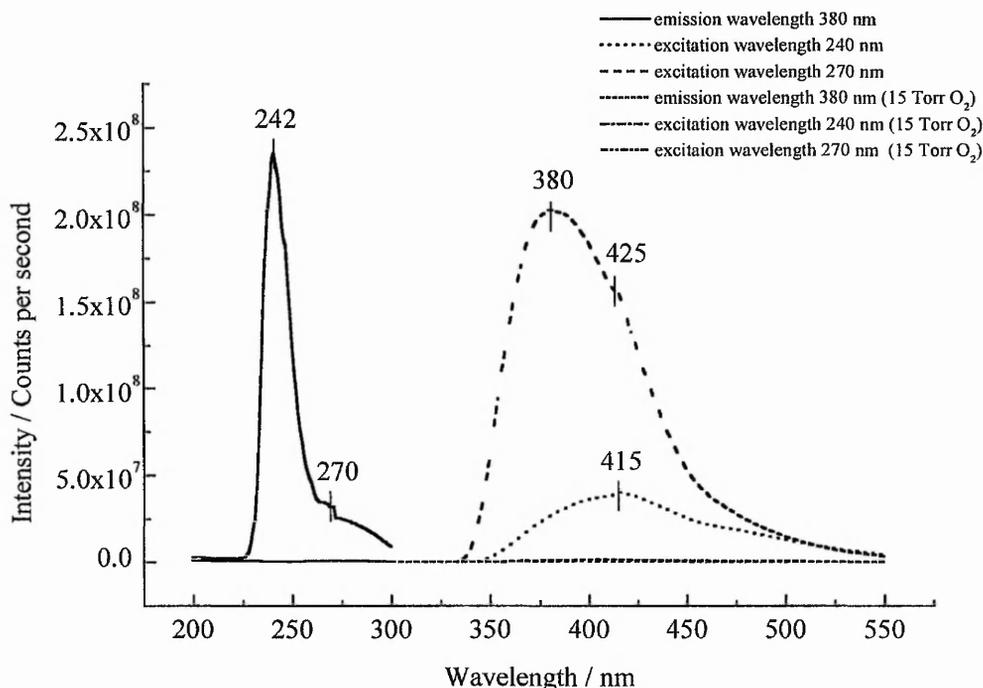
Fig 4.3.3.1   **Influence Of Oxygen On The Photoluminescence Properties Of 100 Å MgO At 298 K.**

4.3.4 Reactions Of The Surface With Hydrogen

The reactivity and nature of the interaction of hydrogen with MgO is of great interest as it is an integral step in many catalytic reactions, with photoluminescence spectroscopy playing an important role in determining this [12, 13, 92, 102, 104, 106, 107]. Coluccia [12, 13, 92] found the emission at 415 nm and a slight amount on the low energy shoulder of the 380 nm peak, were irreversible on evacuation, after hydrogen adsorption at 298 K. It was concluded that this occurred on the 3 co-ordinated sites [92]. $Mg^{2+}_{4C}O^{2-}_{3C}$ and related pairs also played a part, accounting for the loss in intensity on the 380 nm emission. However these assignments were tentative as the spectra were complex. Further photoluminescence [102, 106] and UV/VIS/NIR diffuse reflectance experiments supported this claim [100].

Shvets [11] could not reproduce these results, attributing the findings of Coluccia to CO impurities in the hydrogen. In separate studies [107], Yanagisawa found hydrogen adsorption increased the luminescence of MgO, associating it to interactions with surface F-

centres. Since Shvet's samples were considered rich in such centres [104], this would explain why no reduction in photoluminescence was observed.

The exact nature of hydrogen interaction with the surface is unclear, with workers in favour of both homolytic [10, 109, 110] and heterolytic [92-94, 109, 111] dissociation. Early studies of Boudart *et al* [10] following H_2-D_2 equilibration reactions on the MgO surface, highlighted the O^- ion as a site promoting homolytic hydrogen dissociation. The active site was thought to be a hydroxyl ion adjacent to a triangular array of O^- anions, simulating a (111) orientated microplane, where a Mg^{2+}_{3C} cation had been removed from a corner position. Evidence of these (111) planes were demonstrated using SEM (Scanning Electron Microscopy). This active site was considered equivalent to a surface V centre (a magnesium cation vacancy), showing similar characteristics. This was verified by EPR (Electron Paramagnetic Resonance) spectroscopy, a signal due to the O^- complex being identified at a position associated with V centres.

Cordischi [110] also shared this view when determining the irreversible nature of hydrogen adsorption on MgO. In addition to Boudart's suggestion [10] he believed individual O^- ions, present on the surface, were able to dissociate hydrogen homolytically. According to Martens [96] these ions were formed during the thermal evacuation of hydroxylated MgO, by the following mechanism :

$$[O^{2-}_{LC} \!-\!\!\!-\ H^+]^- \qquad \longrightarrow \qquad O^-_{LC} + \tfrac{1}{2}H_2$$

Subsequent hydrogen admission caused the reverse of the above reaction to occur. However these ions only constitute a small proportion of the surface, typically 0.3 %.

Coluccia [92] proposed a mechanism for heterolytic hydrogen dissociation (Fig 4.3.4.1, overleaf). This was later verified by IR spectroscopy [93, 94] where bands were identified in both O-H and Mg-H regions. Clearly the latter would not be observed if only homolytic dissociation occurred on surface O^- anions. Coluccia acknowledged a homolytic process could be present [94], however the heterolytic pathway was the major contributing factor.

$$H_{2(g)}$$

$$O^{2-}_{3C} - Mg^{2+}_{3C} \longrightarrow \overset{\overset{\delta+}{H}----\overset{\delta-}{H}}{O^{2-}_{3C} - Mg^{2+}_{3C}} \longrightarrow \left[\begin{array}{c|c} \overset{H^+}{\underset{|}{O^{2-}_{3C}}} & \overset{H^-}{\underset{|}{Mg^{2+}_{3C}}} \end{array} \right]^+$$
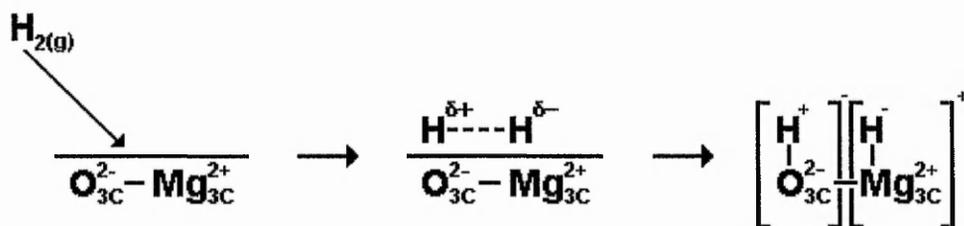
Fig 4.3.4.1   Mechanism Proposed For The Heterolytic Dissociation Of Hydrogen On The MgO Surface.

TPD studies by Ito [111, 112] reinforced these ideas. In this MgO samples were exposed to hydrogen at 173 K, cooled to 77 K, then the TPD was followed. There were three main types of site present, desorbing at 673, 823 and 923 K, attributed to $Mg^{2+}_{3C}O^{2-}_{4C}$, $Mg^{2+}_{4C}O^{2-}_{3C}$ and $Mg^{2+}_{3C}O^{2-}_{3C}$ ion pairs respectively.

IR studies by Knözinger [109] indicated the presence of both homo and heterolytic hydrogen dissociation on MgO. There was agreement with Coluccia [92-94] and Ito [111, 112] that heterolytic dissociation only involved ions exhibiting low co-ordination. However where Coluccia [12, 13, 92] found hydrogen adsorption to be irreversible after prolonged room temperature evacuation, Knözinger [109] considered it to be reversible. It was believed that the irreversible part was associated with hydrogen dissociated homolytically on O^- anions, previously shown to be active by Boudart [10] and Cordischi [110].

In addition Knözinger [109] proposed homolytic dissociation was possible on Mg^+ cations, formed in an analogous manner to O^- anions [96], during high temperature heating of hydroxylated MgO.

$$[\, Mg^{2+} - OH^- \,]^+ \qquad \longrightarrow \qquad Mg^{+\bullet} + OH^\bullet$$

The resulting radical cations are then able to reduce hydrogen to H^-.

$$Mg^{+\bullet} + H_2 \qquad \longrightarrow \qquad Mg^{2+} + H^- + H^\bullet$$
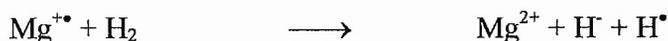
Clearly there are conflicting views concerning the exact mechanism and irreversibility of hydrogen dissociation on MgO, however it is evident that an adsorbed species is formed on the surface. Photoluminescence spectroscopy supports this view as luminescence is partially quenched as the active sites are blocked due to the adsorption process.

## 4.3.5 Hydrogen Adsorption On 100 Å MgO

Effects of hydrogen adsorption on 100 Å MgO were studied using photoluminescence spectroscopy. Hydrogen gas, 75 Torr, was brought into contact with the clean surface and allowed to react for 1 hour. The excess hydrogen was then evacuated prior to obtaining the spectra, since it promotes the formation of F^+_S centres in the presence of UV light on MgO [7, 13]. Once the luminescence had been recorded the reactivity of the irreversible hydrogen towards oxygen was determined, using the same procedure as described above. The results are shown overleaf.

In accordance with the previous literature the emission of the 415 nm peak diminished, due to hydrogen adsorption on $Mg^{2+}_{3C}O^{2-}_{3C}$ pairs (Fig 4.3.5.2), as did the low energy shoulder of the 380 nm band, from reaction with $Mg^{2+}_{3C}O^{2-}_{4C}$ and $Mg^{2+}_{4C}O^{2-}_{3C}$ sites (Fig 4.5.3.1). The overall loss in intensity can be increased by prolonging the exposure time [13, 100].

Subsequent oxygen addition had little or no effect on the photoluminescence spectra. Previous studies of the reaction of oxygen with hydrogen adsorbed on MgO indicated the formation of O_2^- ions using ESR (Electron Spin Resonance) spectroscopy [94, 110, 113]. Ito [113] thought this to proceed initially via electron transfer to molecular oxygen from a H^- ion, which then releases its electron. Surface migration of the H atom to an appropriate O^{2-}_{LC} anion follows. The free electron is donated to either a surface anion vacancy or another Mg^{2+}_{LC} cation, forming a $F^+_S(H)$ centre. This immediately gives up its electron to an oxygen molecule, giving a second O_2^- ion.
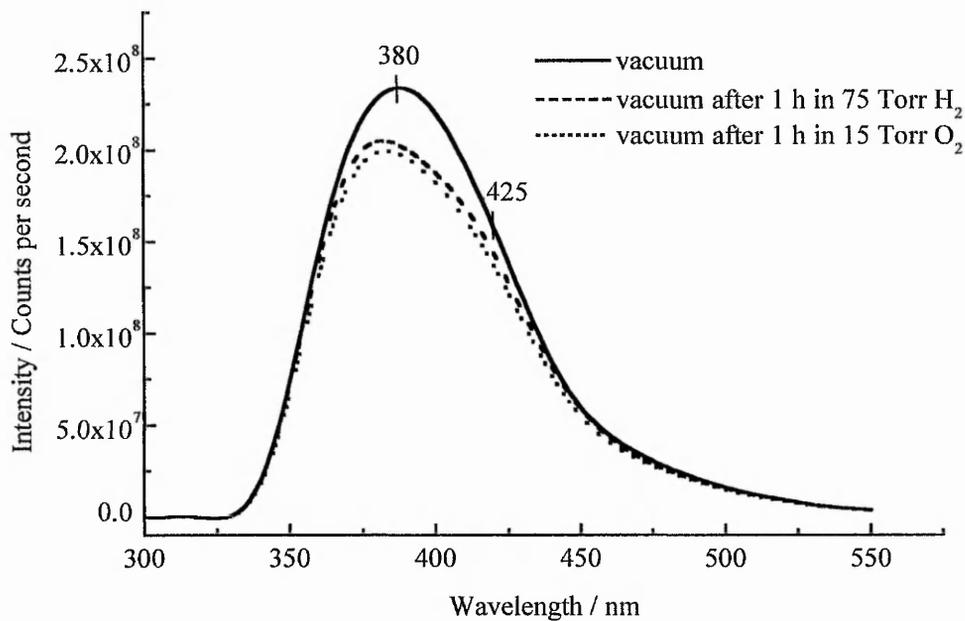
Fig 4.3.5.1 **Emission Spectra At 380 nm Of 100 Å MgO At 298 K After Reaction With Hydrogen And Oxygen.**
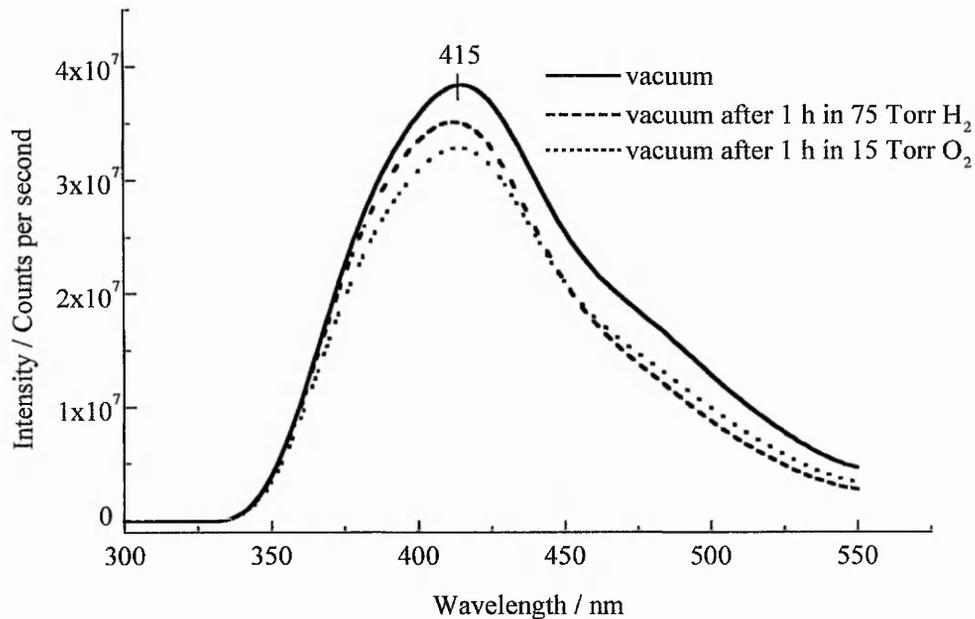
Fig 4.3.5.2 **Emission Spectra At 415 nm Of 100 Å MgO At 298 K After Reaction With Hydrogen And Oxygen.**

The overall process is shown below :

$$O^{2-} + H_2 \longrightarrow OH^- + H^-$$

$$H^- + 2O_2 + O^{2-} \longrightarrow 2O_2^- + OH^-$$
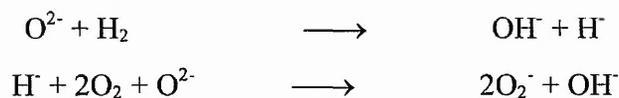
From IR studies Coluccia [94] proposed the following reaction.

$$Mg^{2+} \text{-----} H^- + O_{2\,(g)} \longrightarrow Mg^{2+} \text{-----} O_2^- + \tfrac{1}{2}H_{2\,(g)}$$
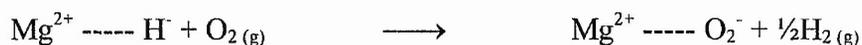
However Cordischi [110] believed the $[O^{2-}_{LC} \text{---} H^+]$ sites were active for O_2^- production, giving a surface complex by interaction with a Mg^{2+} cation :
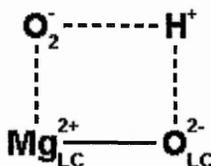
Clearly such differences in mechanism cannot be resolved using photoluminescence spectroscopy, however both indicate a reaction with the pre-adsorbed hydrogen blocking the luminescent sites. Since complex formation or a displacement reaction follows at the same site no new surface ions are involved , therefore no changes are observed in the photoluminescence.

4.4   Reactions Of The Surface With CO

The adsorption of CO onto the clean MgO surface can provide valuable information regarding the co-ordination environment of both the Mg^{2+} and O^{2-} unsaturated surface ions. Such interactions have been extensively studied using UV/VIS/NIR diffuse reflectance and FTIR spectroscopy.

4.4.1 Reactions With The Mg^{2+}_{LC} (Acidic) Sites

Only recently has the interaction of CO with Mg^{2+}_{LC} cations been utilised [5, 114-118], indicating the populations of 3, 4 and 5 co-ordinated sites on the MgO surface. Adsorption occurs at an appreciable extent on all Mg^{2+}_{LC} cations at 77 K, however only coverage of Mg^{2+}_{3C} has been observed at room temperature [119].

The incoming CO molecule adsorbs linearly to the Mg^{2+}_{LC} site, with the carbon pointing towards the cation, forming a σ bond [5, 114-117], with the polarisation of CO towards Mg^{2+}.
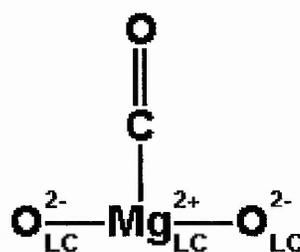
Fig 4.4.1.1   **Interaction Of CO With The Co-ordinatively Unsaturated Mg^{2+} Cations.**

At 77 K initial adsorption occurs at the most acidic sites, cations with the lowest co-ordination, until total coverage of these is attained. Further CO addition follows at 4 and subsequently 5 co-ordinated sites in a sequential manner. Also a CO molecule was able to adsorb on a Mg^{2+} ion pair, present at kinks and steps formed on the MgO surface [5, 115].
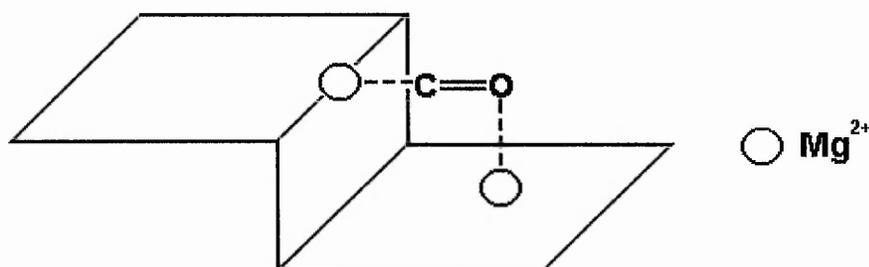
Fig 4.4.1.2   **CO Adsorption On A Mg^{2+}_{LC} Ion Pair At A Surface Imperfection.**

Assignment of these species was rather tentative. Also their detection, associated with a maximum at 2148 cm^{-1}, was masked by the more prominent Mg^{2+}_{5C} — CO band, found in the 2158-2148 cm^{-1} region [5]. All the interactions reported with Mg^{2+}_{LC} cations are considered to be weak, as all are reversible upon evacuation at 77 K [5, 117].

Clearly CO adsorption at 77 K on the Ube MgO samples will give an insight of the proportions of 3, 4 and 5 co-ordinated Mg^{2+} sites on the surface. This is of particular interest regarding 5C ions, since of the spectroscopic techniques used, it is the only one capable of probing ions in this environment.

4.4.2 Reaction With The O^{2-}_{LC} (Basic) Sites

Adsorption of CO on O^{2-}_{LC} anions at both 77 and 298 K has attracted much interest, with measurements performed using UV/VIS/NIR diffuse reflectance [10, 26, 36, 41, 43] and FTIR [37, 38, 39, 40, 42, 43, 44, 48] spectroscopy. It was found that only oxygen anions in 3 fold co-ordination were capable of interacting with CO, as absorptions at 46000 cm^{-1} due to O^{2-}_{4C} remained unchanged during UV/Visible diffuse reflectance experiments [99, 100, 120, 121]. This is attributed to the fact that only 3 co-ordinated anions possess sufficient electron donor properties to react with CO [120].

The first species observed on contact of CO with an O^{2-}_{3C} site is the carbonite (CO_2^{2-}) ion [5, 114, 118, 122, 123]. Its presence has only been detected at low coverages at 77 K [5, 114, 118, 123], or at pressures below ca. 2 Torr at room temperature [122]. This entity is the precursor to all subsequent surface species. According to Zecchina *et al* [114] it is generated by the nucleophilic attack of a surface O^{2-}_{3C} by CO bonded on an Mg^{2+}_{LC} cation in an adjacent position, via the following mechanism :
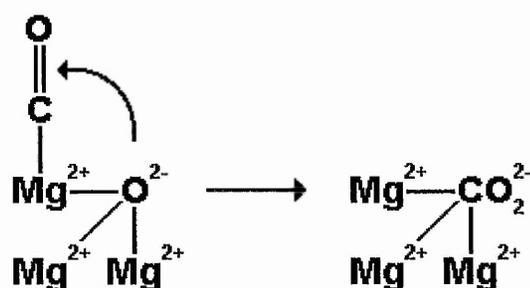
Fig 4.4.2.1   **Formation Of The Carbonite Ion On The O^{2-}_{3C} Anion Of MgO.**

Stepwise addition of CO to the CO_2^{2-} ion leads to dimer ($C_2O_3^{2-}$) and trimer ($C_3O_4^{2-}$) formation, such species are termed "ketenic" due to their ketene like structure.

dimer   trimer
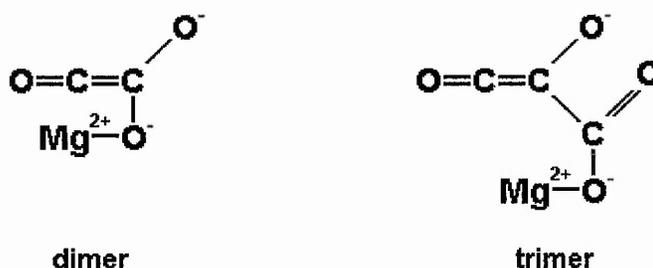
Fig 4.4.2.2   **$C_2O_3^{2-}$ And $C_3O_4^{2-}$ Species Formed On The MgO Surface During CO Addition.**

At 77 K the reaction proceeds no further [114, 116, 118, 122], however at room temperature the ketenic species can react yielding ring structures [99, 100, 121]. A slight pink colouration of the sample is observed [99, 100, 114, 120, 122], associated with a rhodizonate ion ($C_6O_6^{2-}$). The parallel formation of an oxidised component was found under these conditions by Babaeva *et al* [118] and Guglielminotti and co-workers [119] during early investigations. Zecchina subsequently believed these oxidised species originated from disproportionation reactions occurring at the surface [114]. Also a 5 membered ring species, the croconate ion ($C_5O_5^{2-}$), was identified by a green/yellow colour [100] over long reaction periods, being a fragmentation product of the less stable rhodizonate ion.

croconate   **rhodizonate**
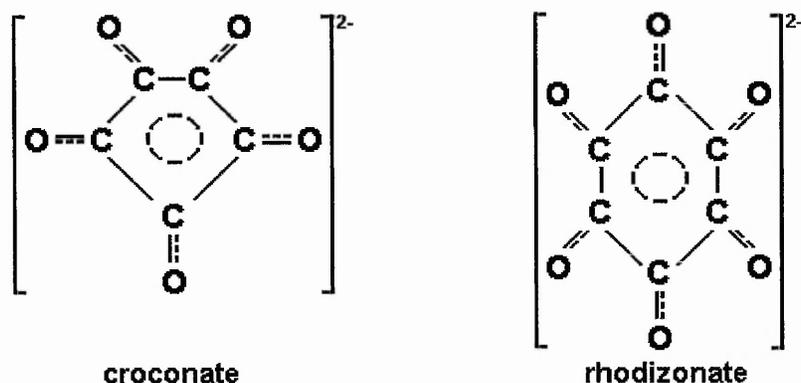
Fig 4.4.2.3   **Rhodizonate And Croconate Ring Structures Formed On The Surface Of MgO During CO Addition.**

The ketenic species are known to be responsible for cyclic ring formation [114, 119], but not all are capable of undergoing this reaction, only ones at special sites are able to react with CO [119]. It was concluded that CO bridged two neighbouring ketenic species found on steps and kinks on the highly irregular surface, giving the desired structure [114].
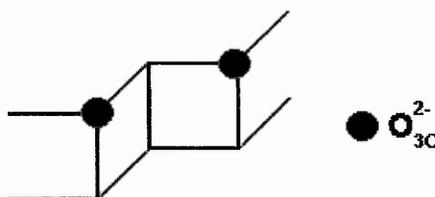
Fig 4.4.2.4   **Sites Responsible For Cyclic Ring Formation On The MgO Surface.**

The insertion of a CO molecule between the two ketenic species, giving the desired ring structure, was thought to proceed via the following pathway.
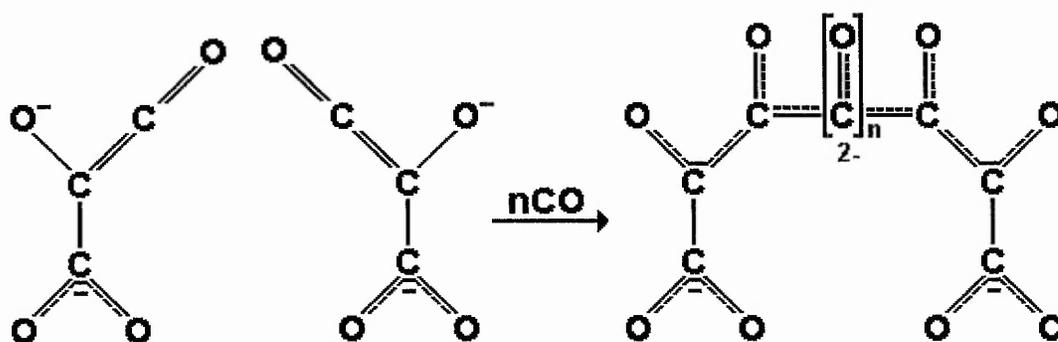
Fig 4.4.2.5   Formation Of A Cyclic Ring Structure From Ketenic Species.

Since only a proportion of the total ketenic species lie on these sites, not all are capable of undergoing such an addition.

Disproportionation of cyclic ring and ketenic structures is common over long reaction periods, giving both oxidised and reduced species [114, 119, 121], with carbonate ions [114, 118, 119] and solid carbon [119] being identified.

The relative stability of the anionic species was tested by both treatment in vacuum and oxygen [114, 118, 119, 121, 123]. At 77 K the carbonite ion is very unstable [114, 118, 123], being reversible on outgassing and reacting immediately upon oxygen admission, yielding an oxidised product [118]. Both ketenic and aromatic structures are stable to evacuation at room temperature [118, 119, 121], however on prolonged pumping the latter decompose, leading to an enhancement of the former. The cyclic rings are susceptible to oxygen attack, disappearing on contact [118, 119, 121]. Ketenic species are unaffected by oxygen, remaining relatively unchanged even after reaction times of 18 hours or longer [121].

4.5   FTIR Spectra Of CO Interaction With Mg^{2+}_{LC} Sites

There are several examples illustrating the adsorption of CO on the Mg^{2+}_{LC} ions at 77 K [5, 114-118]. The assignment and position of these bands are tabulated below :

126

Band Position / cm^{-1}	Assignment	Reference
2200	Mg^{2+}_{3C}	[5] [114] [115] [116]
2165-2159	Mg^{2+}_{4C}	[5] [115] [116] [118]
2157-2148	Mg^{2+}_{5C}	[5] [115] [116] [117]
2148	CO on a Mg^{2+}_{LC} ion pair	[5] [115] [117] [119]
2143	Free CO molecule	[116] [124]

Table 4.5.1   **Position And Assignment Of Mg^{2+}_{LC} Bands Of CO Adsorption On MgO At 77 K.**

Later theoretical work by Pelmenschikov *et al* [124], using a quantum chemical method of frequency calculation by the molecular approach, found band positions due to Mg^{2+}_{3C} and Mg^{2+}_{4C} were very similar to those determined experimentally.

From Table 4.5.1 it is evident that the maxima associated with both Mg^{2+}_{4C} and Mg^{2+}_{5C} cations varies, decreasing in wavenumber with increasing CO coverage. This is attributed to adsorbate-adsorbate interactions (dipolar coupling), at the surface [5, 115-118]. As CO is progressively adsorbed on the Mg^{2+}_{LC} sites, a situation arises where two cationic sites in close proximity, may both hold a CO molecule. These can subsequently couple and oscillate in tandem, consequently decreasing their frequency of oscillation. As the coverage is increased the probability of coupling is enhanced, leading to a further downward shift in wavenumber. As saturation of a given Mg^{2+}_{LC} site is reached a reduction of 10 cm^{-1} can be observed.

This phenomenon has been demonstrated experimentally using two samples differing in surface area [5], varying in their densities of Mg^{2+}_{5C} sites. MgO prepared from magnesium ribbon possesses a large cube size, with the surface ions being predominantly 5 co-ordinated. Therefore as CO coverage is increased, the possibility of adsorbate-adsorbate interactions are enhanced. Conversely crystallites obtained by decomposing $Mg(OH)_2$ in vacuum at high temperatures are much smaller in size and highly faceted, hence are less populated in Mg^{2+}_{5C} sites. Results confirmed that dipolar coupling is more prominent on the MgO ribbon catalyst with an abundance of 5C ions. The IR band had a maximum of 2148 cm^{-1}, compared to that of the ex $Mg(OH)_2$ sample with a value at 2152 cm^{-1}.

4.5.1 CO Adsorption On 100 Å MgO Probing The Mg^{2+}_{LC} Sites

CO was admitted onto the clean MgO surface at 77 K at pressures ranging from 4×10^{-3} to 2 Torr. When further increasing the pressure, CO was not dosed until equilibrium between the surface and the gas phase was attained. Evolution of the different bands was followed in two stages, at intermediate and high pressures, probing different Mg^{2+}_{LC} environments.

Bands formed at low CO coverage on 100 Å MgO are shown below. All spectra are presented in terms of mass per cm^2, which allows direct comparison of all the Ube samples.
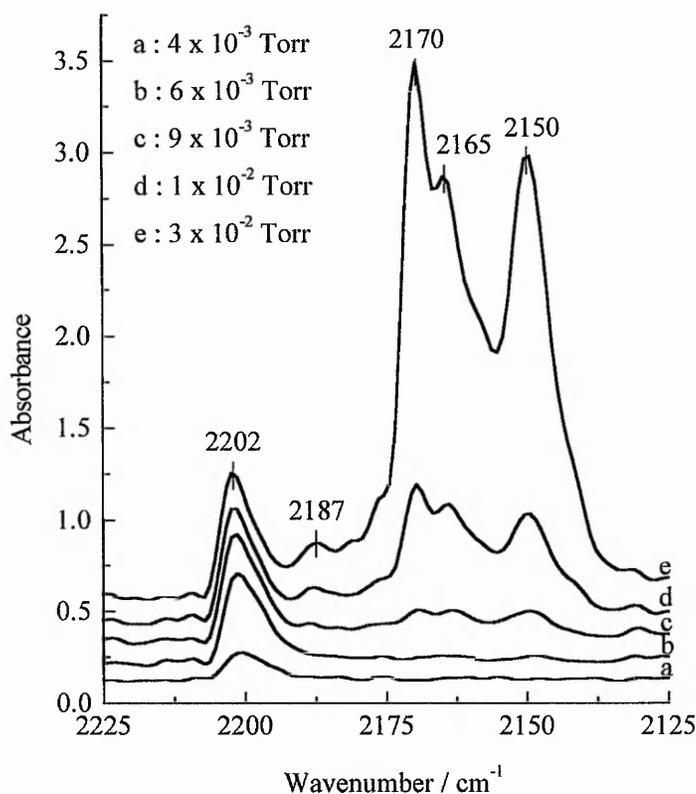
Fig 4.5.1.1   **FTIR Spectra Of CO Adsorbed On 100 Å MgO At 77 K At Low Pressures Probing Mg^{2+}_{LC} Sites.**

From Fig 4.5.1.1 at the lowest pressure of 4×10^{-3} Torr, only a band due to CO adsorbed on Mg^{2+}_{3C} cations is present. With further CO addition four new bands emerge at 2187, 2170, 2165 and 2150 cm^{-1}, their intensity increasing with pressure. The species at 2150 cm^{-1} is attributed to CO interactions with a Mg^{2+}_{LC} ion pair, agreeing with the value presented in

Table 4.5.1. Maxima at 2170 and 2165 cm^{-1} are due to contributions from 4 co-ordinated sites, the higher frequency band reflecting CO molecules adsorbed on isolated Mg$^{2+}_{4C}$ anions. As coverage of the 4C increases dipolar coupling contributions become evident, starting to shift the peak to lower wavenumbers.

Finally there is no reference in the literature to a species at 2187 cm^{-1}, therefore it is assumed to be the identification of a new surface CO species. This was shown to be reproducible as it was also present on the remainder of the Ube samples.

The stability of the surface species were tested by outgassing at 77 K in stages until the base pressure was reached.
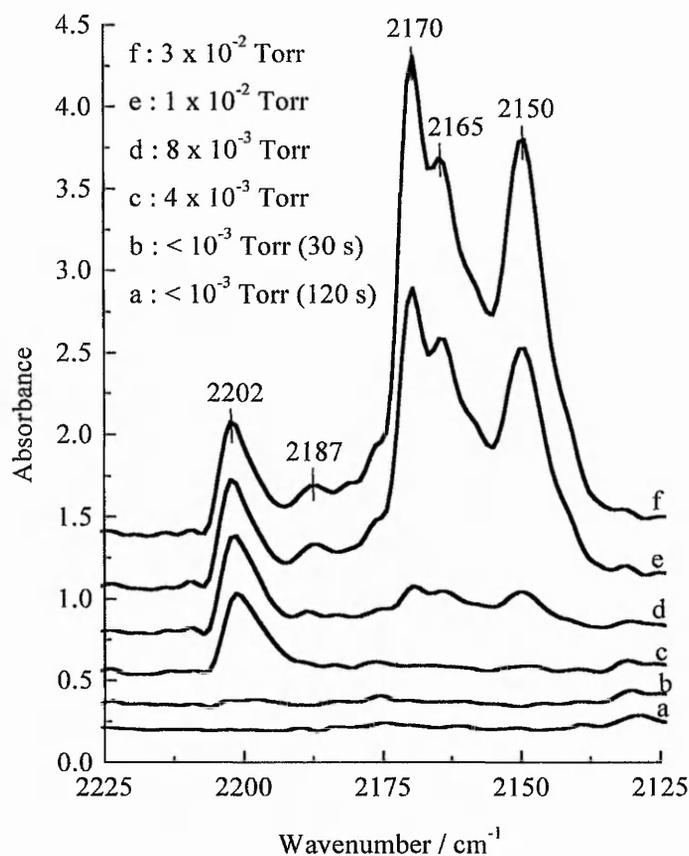
Fig 4.5.1.2   **FTIR Spectra Of CO Adsorbed On 100 Å MgO At 77 K During Outgassing At Low Pressures Probing Mg$^{2+}_{LC}$ Sites.**

As it can be seen all the bands are fully reversible, in accordance to previous observations [5, 115, 117, 118], indicating only a weak interaction with the surface. Comparison of Figs 4.5.1.1 and 4.5.1.2 shows each species to have a similar intensity at a given coverage, regardless of increasing or decreasing the pressure. Prolonged evacuation at $< 10^{-3}$ Torr gave a spectrum identical to that of the clean surface.

Further CO was contacted with the surface, up to pressures of 2 Torr, probing Mg^{2+}_{LC} site coverage.
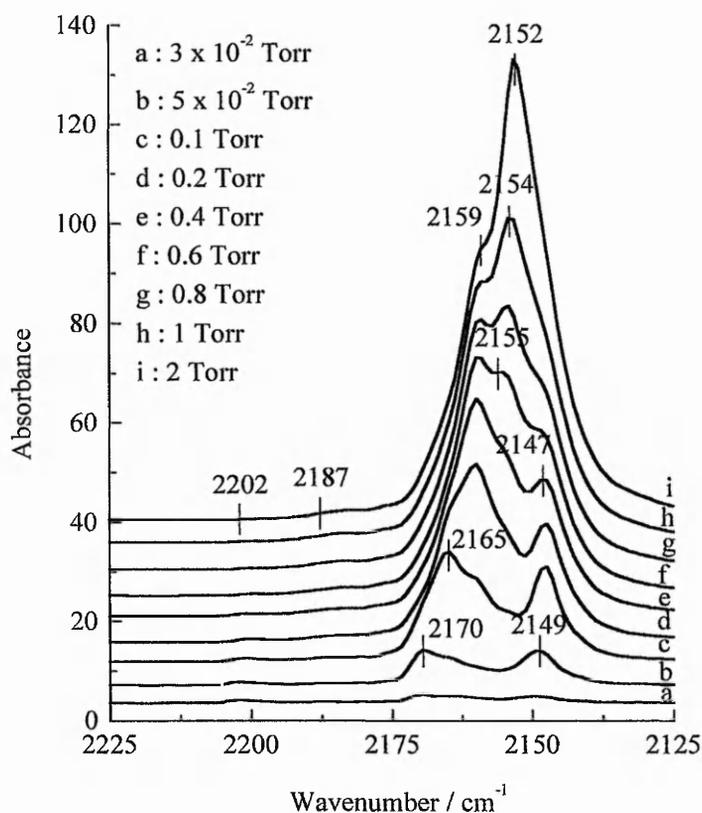
Fig 4.5.1.3   **FTIR Spectra Of CO Adsorbed On 100 Å MgO At 77 K At High Pressures Probing Mg^{2+}_{LC} Sites.**

Since the bands at 2202 (attributed to Mg^{2+}_{3C}) and 2187 cm^{-1} only contribute to a small proportion of the total surface sites, their intensities are negligible compared to the predominating 4 and 5 co-ordinated cations. Therefore they do not feature in the above figure.

At 5 x 10^{-2} Torr the band at 2170 cm^{-1} due to isolated 4C sites is still present but it gradually disappears as dipolar coupling effects shift it to lower wavenumbers. Adsorption on Mg^{2+}_{4C} cations reaches maximum intensity at 1 Torr (2159 cm^{-1}), where it then becomes a shoulder of the more abundant Mg^{2+}_{5C} band. The CO species coupled to two Mg^{2+}_{LC} ions suffers a similar fate, being lost into the low frequency tail of the increasing Mg^{2+}_{5C} peak at 0.6 Torr. The Mg^{2+}_{5C} band is also subject to dipolar coupling, decreasing from 2159 to 2152 cm^{-1} as saturation increases.

Subsequent evacuation again showed, as in Fig 4.5.1.2, that all the bands were unstable to outgassing, being fully reversible at 10^{-3} Torr.

4.5.2 CO Adsorption On The Ube MgO Samples Probing The Mg^{2+}_{LC} Sites

CO adsorption was performed on the remaining Ube MgO samples. The results are very similar to those obtained for 100 Å MgO, therefore detailed spectra will not be presented for the sake of brevity. However it is of interest to compare adsorption bands at various CO pressures, indicating differences in populations of the Mg^{2+}_{LC} sites between the samples. Spectra were recorded at 1 x 10^{-2}, 0.4 and 2 Torr, probing cations in 3, 4, and 5 fold co-ordination respectively.
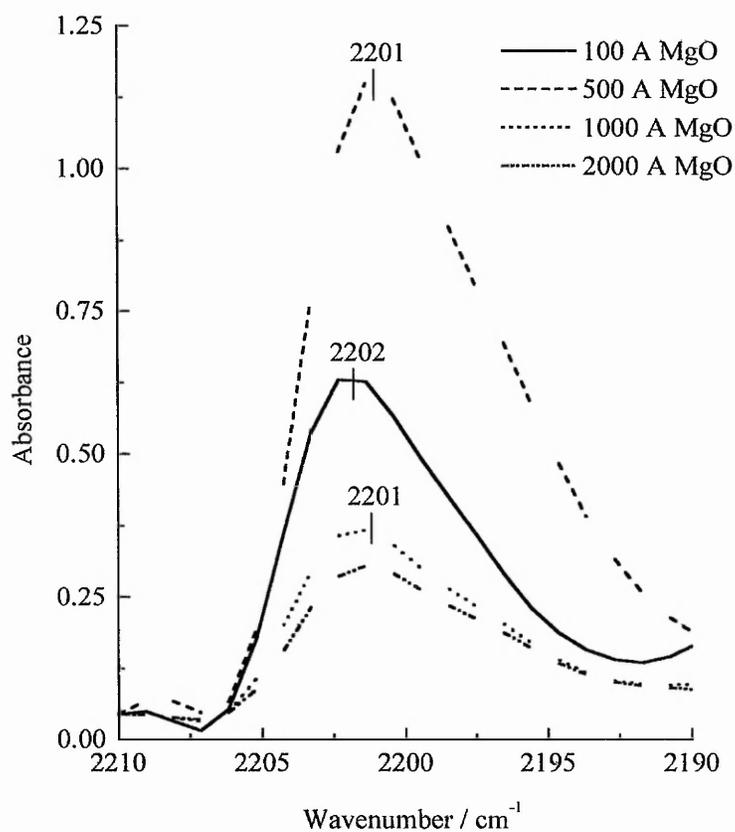
Fig 4.5.2.1   FTIR Spectra Of CO Adsorbed On The Ube MgO Samples At 1 x 10⁻² Torr Probing The Mg$^{2+}_{3C}$ Sites.
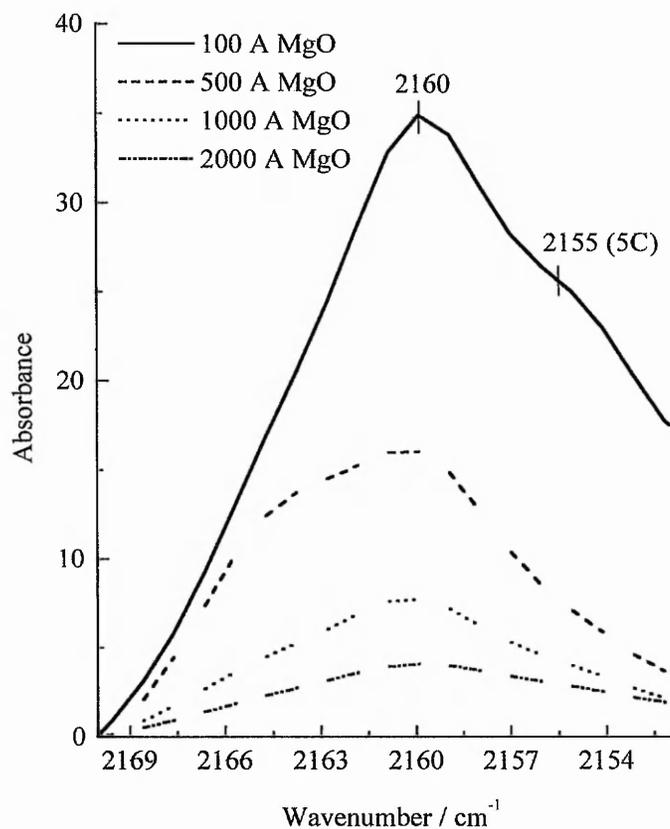
Fig 4.5.2.2   **FTIR Spectra Of CO Adsorbed On The Ube MgO Samples At 0.4 Torr Probing The Mg$^{2+}_{4C}$ Sites.**
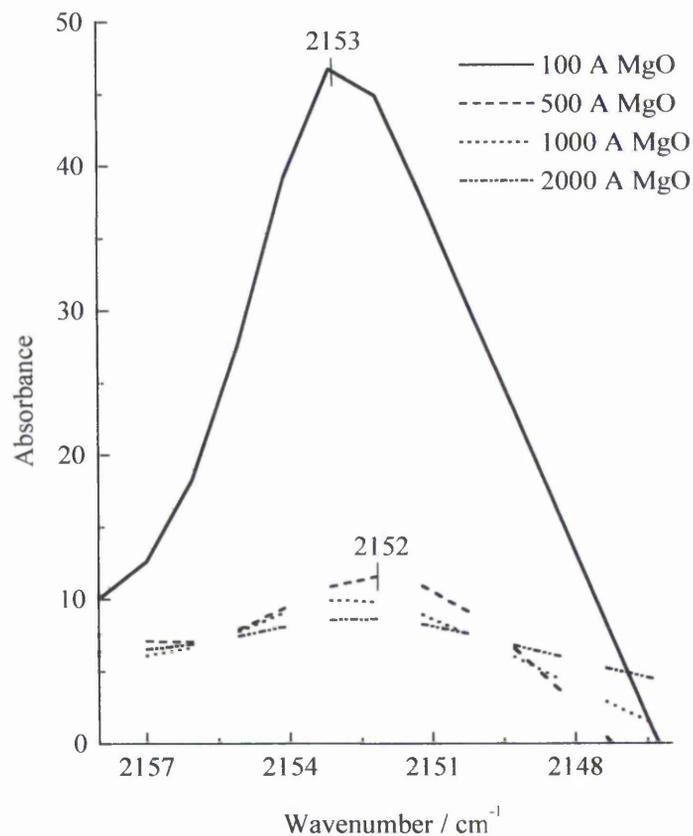
Fig 4.5.2.3   **FTIR Spectra Of CO Adsorbed On The Ube MgO Samples At 2 Torr Probing The Mg$^{2+}_{5C}$ Sites.**

From inspection of the above figures the following can be concluded.

Co-ord No	Figure	Sequence (Decreasing number of sites)
3	4.5.2.1	500 Å > 100 Å > 1000 Å > 2000 Å
4	4.5.2.2	100 Å > 500 Å > 1000 Å > 2000 Å
5	4.5.2.3	100 Å > 500 Å > 1000 Å > 2000 Å

Table 4.5.2.1   **Table Showing Differences In Population Of Surface Sites On The Ube MgO Samples Using FTIR Spectroscopy.**

These provide interesting results regarding the populations of the various co-ordinatively unsaturated surface sites on the Ube MgO samples.

4.5.3 CO Adsorption On 2000 Å MgO After Sintering Experiments

From Section 4.5.2 the spectra of 2000 Å MgO show a certain degree of complexity indicative of an irregular surface, unlike those of other low surface area MgO already reported [39]. This is attributed to kink and step formation, increasing populations low co-ordinated sites, probably as a result of water vapour attack. As a consequence of this sintering experiments were performed, reducing the surface area so that 5C ions become predominant, in an attempt to simplify the spectra. This was achieved by treating the sample in 200 Torr CO_2 known to aid the sintering process [22], for 16 hours at 1073 K, following the same procedure as Scarano *et al* [115]. Spectra were then recorded at various degrees of CO coverage, the figure below showing the different bands formed at low pressures.
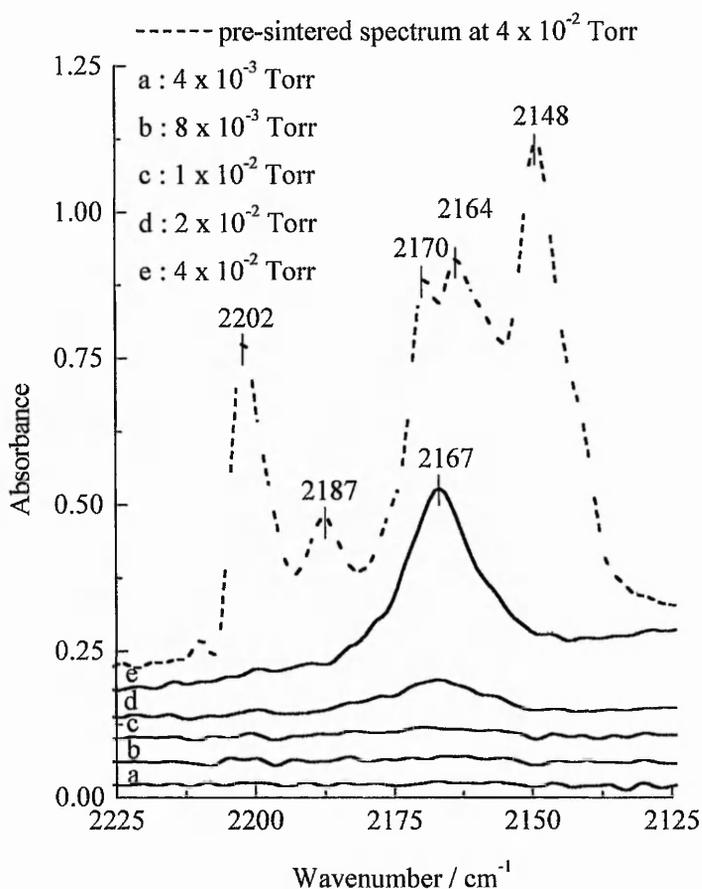
Fig 4.5.3.1   **FTIR Spectra Of CO Adsorbed On Sintered 2000 Å MgO At 77 K At Low Pressures.**

From Fig 4.5.3.1 it is apparent that the sintering process has a pronounced effect on the spectra. The only band evident at low coverage is that of CO bound to a Mg^{2+}_{4C} cation at ca. 2167 cm^{-1}, other species associated with an irregular surface previously observed at 2202, 2187, 2170 and 2148 cm^{-1} are not present. This is expected as it is well documented that low co-ordinated ions are destroyed preferentially over higher ones on heating MgO in CO_2 [115]. Therefore the surface of sintered 2000 Å MgO comprises of mainly 4 and 5 co-ordinated ions, as indicated by Fig 4.5.3.1.

To show the overall effect of the treatment the figure below shows a comparison of 2000 Å MgO at a pressure of 10 Torr CO, both before and after sintering.
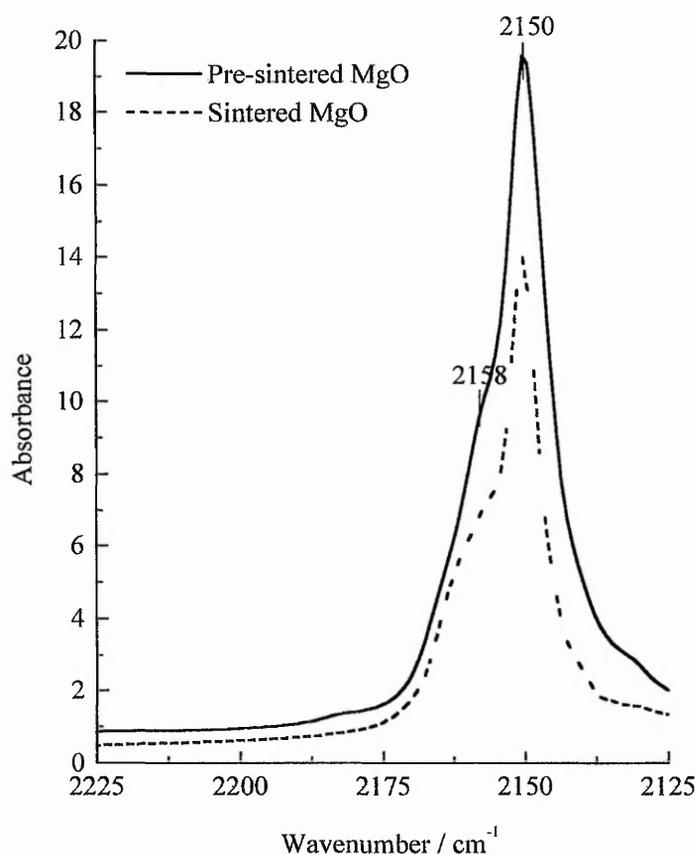
Fig 4.5.3.2 **FTIR Spectra Of 10 Torr CO Adsorbed On Sintered 2000 Å MgO At 77 K.**

A main feature of the pre-sintered sample is the broadness and intensity of the 2150 cm^{-1} Mg^{2+}_{5C} band and its Mg^{2+}_{4C} shoulder at 2158 cm^{-1}, normally associated with a relatively high surface area MgO from a hydroxide precursor [5, 114]. On sintering the width of the

2150 cm^{-1} peak becomes narrower and its maximum sharper, indicative of MgO with predominantly 5 co-ordinated sites [5]. This modification of the spectra on sintering shows the CO_2 treatment was successful in annealing the surface, leading to a decrease in surface area.

4.6   FTIR Spectra Of CO Interaction With O^{2-}_{3C} Sites

The use of FTIR spectroscopy to study the interaction of CO with 3 co-ordinated oxygen anions of MgO is well established [5, 114-116, 118, 119, 121, 123]. The position and assignment of all the observed bands are summarised below.

Position / cm^{-1}	Assignment	Suffix used by Zecchina[a]	Suffix used by Babaeva[b]	Temp Observed / K	Reference
1472, 1325, 1285.	Carbonite CO_2^{2-}	T', T	IIb	77	[5] [114] [118] [123]
2084-2108, 1358-1392, 1548-1582, 1160.	Ketenic $C_nO_{n+1}^{2-}$	KD	V	77, 298	[5] [114] [115] [116] [118] [119] [121]
1066, 1197, 1275, 1480.	Aromatic $C_nO_n^{2-}$	P	VI	298	[5] [144] [118] [119] [121]
1750-1550, 1400-1150.	Oxidised Species	O	VIII	77, 298	[114] [118] [119]
1870, 1760.	Reduced Species	Q	Not seen	77, 298	[114] [119]

a - taken from reference [114].

b - taken from reference [118].

Table 4.6.1   **Position And Assignment Of O^{2-}_{3C} Bands Of CO Adsorption On MgO From FTIR Spectroscopy.**

Both Zecchina [114] and Babaeva [118, 123] were in agreement that the carbonite ion was the first species to be formed on the MgO surface at 77 K, however their interpretation of the spectra regarding these bands slightly differed. Babaeva [118, 123] ascribed the maximum at 1472 cm^{-1} to this species, Zecchina [114] attributed it to a bidentate form of this ion transformed by the interaction of CO molecules with an adjacent Mg^{2+}_{LC} cation. This bidentate structure was postulated to originate from the carbonite ion, having a doublet at 1285 and 1325 cm^{-1} [114], hence giving it three bands in the spectrum. Interestingly Babaeva has no mention of these latter peaks. Excluding this minor discrepancy excellent correlation between the results of both workers was found.

Due to the extensive literature on this subject only reactions involving 100 Å MgO were followed, as a means of comparison of the Ube samples with the published results.

4.6.1 CO Adsorption On 100 Å MgO Probing The O^{2-}_{3C} Sites

In an attempt to determine the initial species formed on the O^{2-}_{3C} sites on MgO, small amounts of CO were brought into contact with the surface. Spectra obtained at low pressures are shown overleaf.

As expected when dosing at low pressures the T species are the first to become apparent, having maxima at 1315 and 1281 cm^{-1}. Even at this stage these carbonite ions have undergone further CO addition, indicated by KD bands present at 2094 and 1377 cm^{-1}. Increasing the pressure leads to the enhancement of these peaks, coupled with the appearance of two new KD bands at 1566 and 1169 cm^{-1}. Saturation of the O^{2-}_{3C} sites is realised at approximately 1 x 10^{-2} Torr as the T bands begin to lose intensity, undergoing transformations into KD species as they incorporate more CO. A sharp peak at 1475 cm^{-1} due to the T' structure and a final KD maximum at 1298 cm^{-1} are also evident. As pressures of 3 x 10^{-2} Torr are reached the KD bands dominate the spectrum, as the T bands virtually disappear, being converted into ketenic structures.
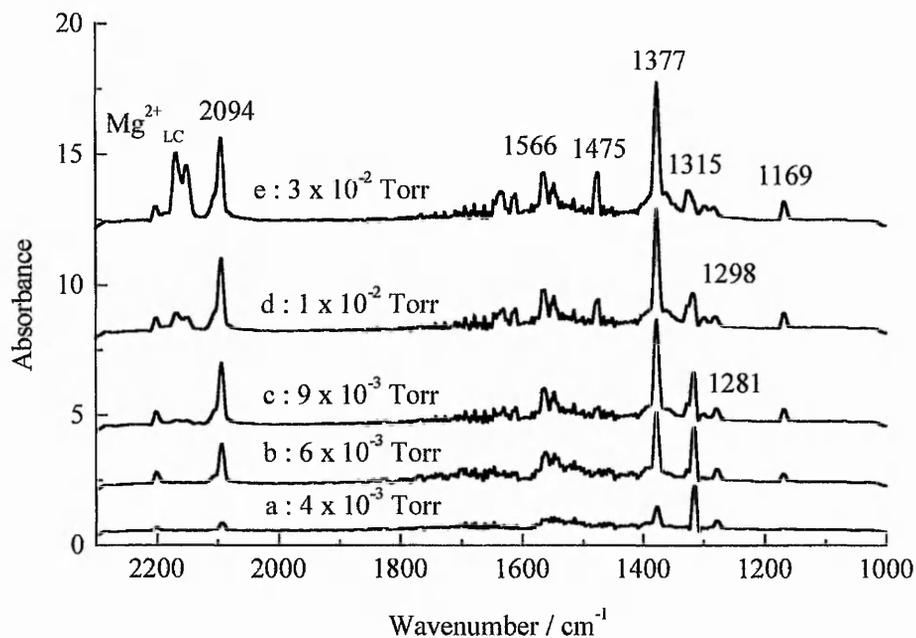
Fig 4.6.1.1   FTIR Spectra Of CO Adsorbed On 100 Å MgO At 77 K At Low Pressures Investigating The Formation Of Surface Structures.

Additional CO had little or no effect on the spectra as the reaction proceeds no further at 77 K [114, 116, 118, 122]. At this point the stability of the surface species were tested by evacuation to a system pressure of $< 10^{-3}$ Torr.

139
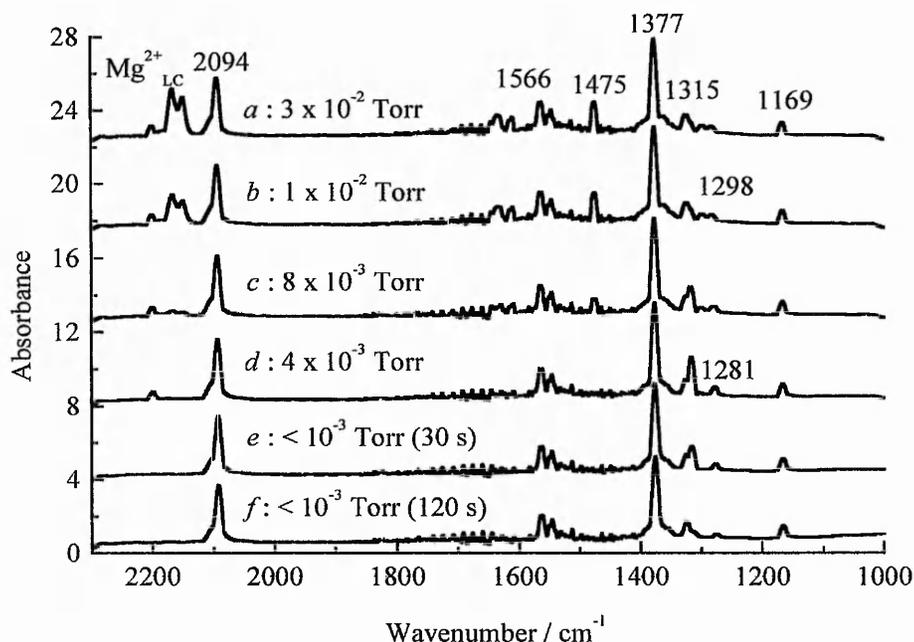
Fig 4.6.1.2   FTIR Spectra Of CO Adsorbed On 100 Å MgO At 77 K At Low Pressures Investigating The Stability Of The Surface Structures To Evacuation.

The results obtained are in agreement to those reported previously [114, 118, 119, 121, 123]. Throughout evacuation (Fig 4.6.1.2, *a-f*) intensities of the KD bands remain constant, indicating their relative stability. Conversely the carbonite ion is unstable to outgassing, showing a degradation of its peaks with decreasing pressure. Initially the bidentate species disappears, converted into the monodentate by the loss of CO from an adjacent Mg^{2+}_{LC} cation, seen in the reduction of the 1475 cm^{-1} band (*a-d*). Enhancement of the monodentate ion is shown by an increase of the T maximum at 1315 cm^{-1} (*a-d*), this is only temporary however as further pumping leads to its disappearance (*d-f*). Once the base pressure is reached (*f*), only contributions from the ketenic structures are evident in the spectrum.

On completion of desorption at 77 K the system was allowed to reach 298 K, upon which further CO was admitted, investigating the species formed at room temperature, as in the case of MgO prepared from the decomposition of $Mg(OH)_2$ [114].
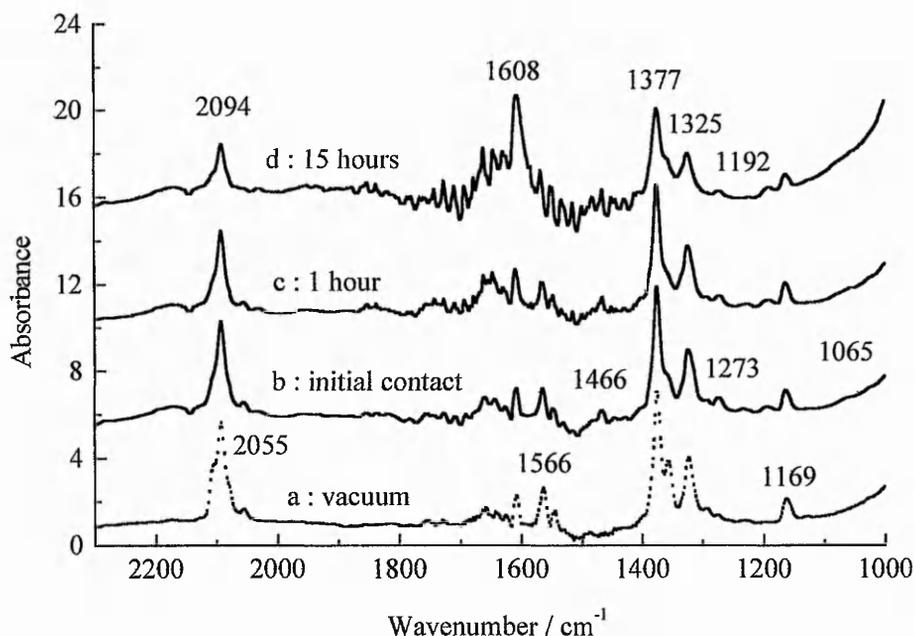
Fig 4.6.1.3   FTIR Spectra Of 10 Torr CO Adsorbed On 100 Å MgO At 298 K Investigating The Formation Of Surface Structures.

Contacting CO with the MgO surface at 298 K allows the formation of the aromatic ring structures [99, 100, 114, 120, 122]. Immediately, P bands at 1466, 1273, 1192 and 1065 cm^{-1} due to the rhodizonate ion become apparent, increasing in intensity with time. Zecchina *et al* [114] indicated that these species were the product of two neighbouring ketenic ions joining through incorporation of a further CO molecule. In the present case a slight decrease in KD bands at 2094, 1566, 1377, 1325 and 1169 cm^{-1} is observed, in parallel to the appearance of a band at 1608 cm^{-1}. On the basis of its position it is attributable to an oxidised species, produced through a disproportionation process of ketenic structures [114, 118, 119], increasing in intensity with reaction times of up to 15 hours.

This observation is quite interesting with respect to previous IR spectra published, of CO adsorbed on MgO from the decomposition of Mg(OH)$_2$ [114]. This sample has a high degree of O$^{2-}_{3C}$ anions and due to the bunching of many small crystallites therfore they can be found in close proximity on the surface. Consequently the incorporation of CO between two KD species on these sites, giving a cyclic ring structure (Fig 4.4.2.5), is enhanced.

　　　　Considering 100 Å MgO it is synthesised from magnesium vapour [84, 85] yielding
individual microcrystals, hence 3 co-ordinated sites, which are considerably high for MgO
generally prepared in this manner, will only be evident on the corners of cubes. Even
allowing for kink and step formation from water vapour attack, the number of these ions in
adjacent positions, able to bridge two KD species is minimal. This is illustrated well in
Fig 4.6.1.3. Bands associated with the rhodizonate ion are small on 100 Å MgO, compared
to those for the ex $Mg(OH)_2$ sample [114], indicating the ease of ring formation on the
latter. Consequently intensities of the KD structures are much higher on 100 Å MgO, as the
3C are isolated and they cannot be converted into cyclic ring species. Instead they undergo
disproportionation reactions giving oxidised species like that at 1608 cm^{-1}, which are not
evident on the ex $Mg(OH)_2$ catalyst [114].

　　　　Finally the reactivity of the ketenic and aromatic species towards oxygen was tested
after evacuating the excess CO.
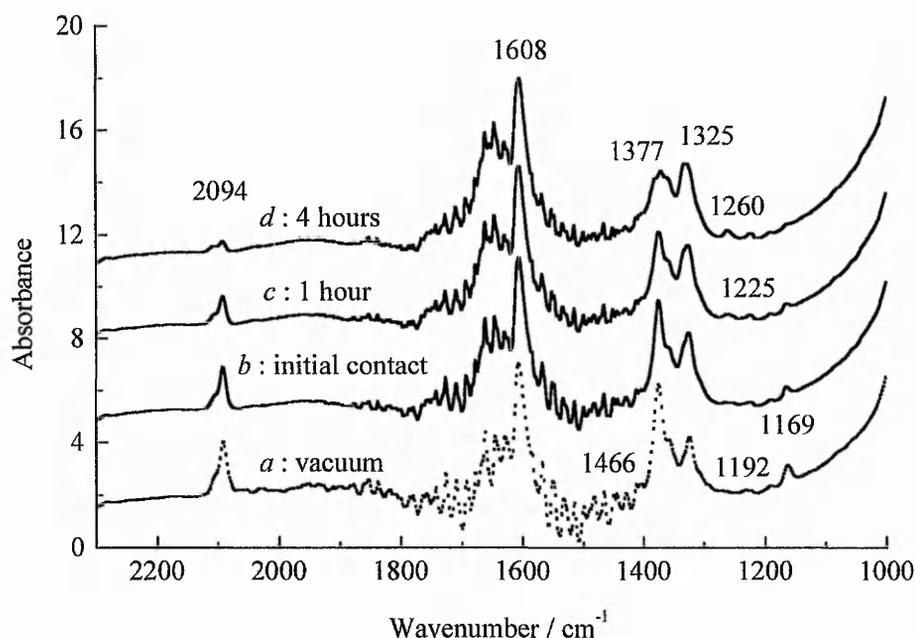
Fig 4.6.1.4　　　**FTIR Spectra Showing The Influence Of 60 Torr Oxygen On Surface CO Structures Formed On 100 Å MgO At 298 K.**

As Fig 5.6.1.4 indicates outgassing for short periods has no visible effect on the spectrum (*a*), with both the ketenic and aromatic ring structures retained on the surface. A similar observation is seen upon initial contact of the surface with 60 Torr oxygen (*b*). With increasing time the rhodizonate ion is oxidised (*c*), giving bands at 1225 and 1260 cm^{-1}. At this stage the KD species remain unreactive, however they are slowly attacked by oxygen (*d*), also being converted into oxidised species.

4.7 UV/VIS/NIR Diffuse Reflectance Spectra Of CO Interaction With O^{2-}_{3C} Sites

UV/VIS/NIR diffuse reflectance spectroscopy provides an alternative means of following the interaction of CO with highly co-ordinatively unsaturated oxygen anions [99, 100, 120, 121, 122]. An advantage of using this method over FTIR spectroscopy is that it gives simple spectra. Table 4.7.1 indicates the positions of the different structures formed, values for 3 and 4 co-ordinated oxygen anions are also presented.

Band Position / nm	Assignment	Reference
230	O^{2-}_{4C}	[4] [15] [28] [98] [99] [100]
270	O^{2-}_{3C}	[4] [15] [28] [98] [99] [100]
290	Ketenic species	[99] [100] [120] [121] [122]
340	Croconate ion	[100]
360	Carbonite ion	[122]
450	Rhodizonate ion	[99] [100] [120] [121] [122]

Table 4.7.1   Position And Assignment Of O^{2-}_{3C} Bands Of CO Adsorption On MgO From UV/VIS/NIR Diffuse Reflectance Spectroscopy.

In order to obtain a picture of the overall reactivity of MgO, CO adsorption, evacuation and oxygen admission were performed on 100 Å MgO at 298 K. Subsequently in an attempt to estimate the populations of 3 co-ordinated sites between the samples, reactions were followed on the 500, 1000 and 2000 Å Ube MgO.

4.7.1 UV/VIS/NIR Diffuse Reflectance Spectra Of CO Adsorbed On 100 Å MgO At 298 K

Prior to reaction with CO, the spectrum of the clean MgO surface, recorded under the influence of 10 Torr oxygen to quench fluorescence [98], was taken. This allows a comparison of the two types of spectra. After removal of the oxygen from the system CO was progressively dosed up to values of 100 Torr, the results of this are shown below.
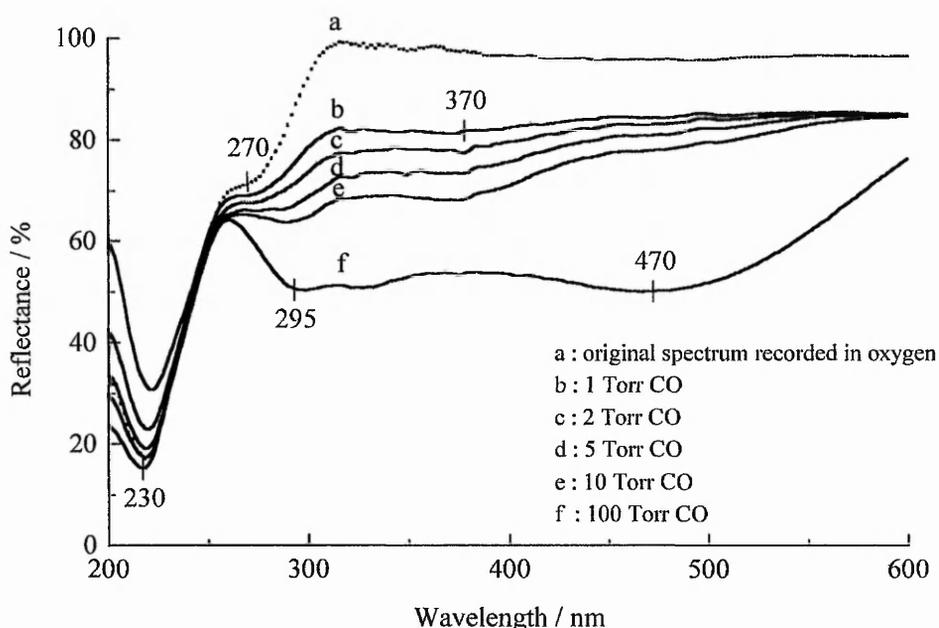
Fig 4.7.1.1   UV/VIS/NIR Diffuse Reflectance Spectra Of CO Adsorbed On 100 Å MgO At 298 K.

As described in detail previously (Section 4.2) two absorptions are present on the clean MgO surface at 230 and 270 nm, due to anions in 4 and 3 fold co-ordination respectively. Upon initial contact with CO the shoulder at 270 nm diminishes, being eroded preferentially over the 240 nm band. This indicates that only 3 co-ordinated ions are able to react with CO, the O^{2-}_{4C} sites remaining untouched throughout the experiment [99, 100, 120, 121]. The only changes of the latter observed during the reaction is a decrease in reflectance due to the increased efficiency of quenching of the fluorescence by CO.

Development of a band is observed at 370 nm as the CO pressure reaches 2 Torr. Bailes and Stone [122] associated this with the carbonite ion, requiring specific conditions for its occurrence at 298 K. The current investigations further support this claim, indicating it is only formed in this low pressure region.

Subsequent CO addition leads to the disappearance of the carbonite ion, as stepwise addition yields ketenic species, present at 295 nm. This band increases in intensity up until approximately 10 Torr, at which point their conversion into the aromatic ring structures is apparent [122]. As the CO pressure reaches 100 Torr a broad absorption envelope at 470 nm of the rhodizonate ion dominates the spectrum. At this point a pink colouration of the sample was visible, as seen many times previously [99, 100, 114, 120, 122]. Ketenic anions unable to incorporate further CO are also present at this stage. No changes in the absorption bands were observed when contact times in excess of 1 hour were used.

The stability of the surface species towards evacuation was then tested, the results of which are shown below.
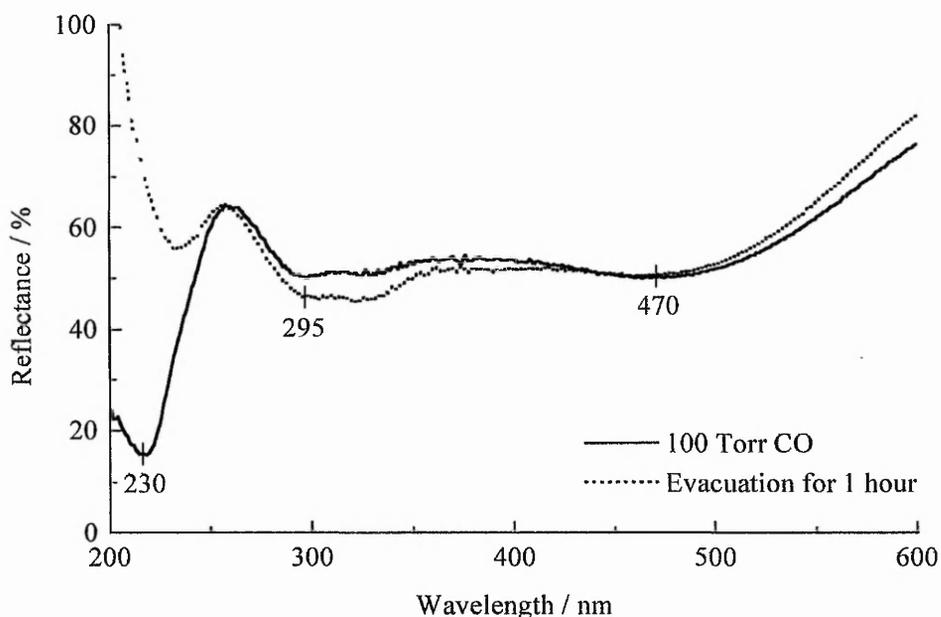
Fig 4.7.1.2   **Effect Of Evacuation On The UV/VIS/NIR Diffuse Reflectance Spectra Of CO Adsorbed On 100 Å MgO At 298 K.**

It is apparent from Fig 4.7.1.2 that the removal of CO has no effect upon the ketenic and aromatic structures. The only difference between the two spectra is that the fluorescence has returned, due to the fact that the quencher is no longer present. At this stage the reactivity of the surface species was tested by admitting 10 Torr oxygen into the system.

Reflectance / %

Wavelength / nm

a : Evacuation for 1 hour
b : 10 Torr O_2 immediately
c : 10 Torr O_2 1 hour
d : 10 Torr O_2 18 hours
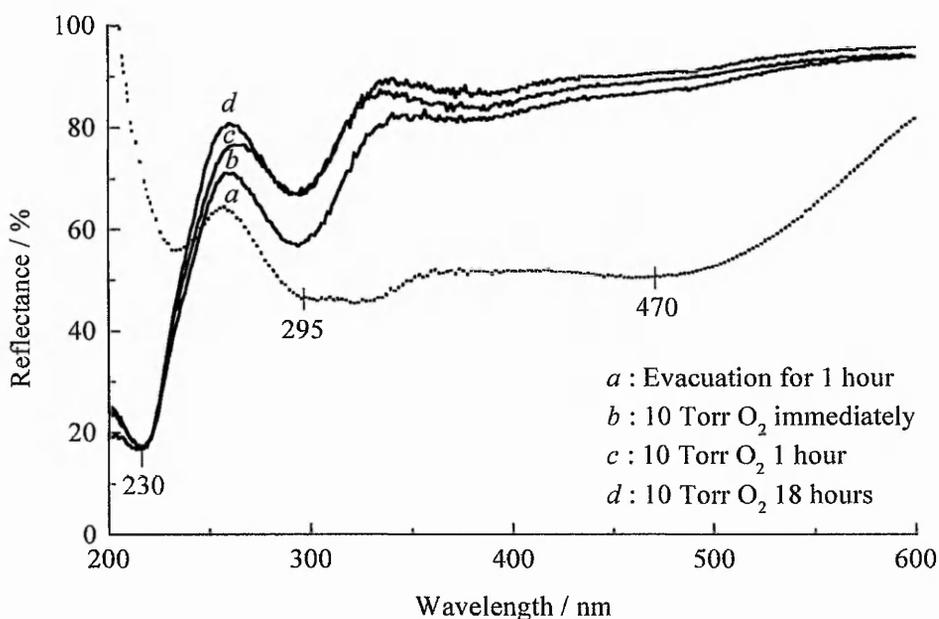
Fig 4.7.1.3   Effect Of Oxygen Admission On The UV/VIS/NIR Diffuse Reflectance Spectra Of CO Adsorbed On 100 Å MgO At 298 K.

Clearly the rhodizonate ion is highly reactive, disappearing immediately upon oxygen contact (*b*). The ketenic species are less sensitive to oxidation, requiring a period of 1 hour before any noticeable change is detected (*c*). Prolonging the reaction time has little or no effect on the spectrum, as indicated by absorptions obtained after 18 hours (*d*).

4.7.2 UV/VIS/NIR Diffuse Reflectance Spectra Of CO Adsorbed On The Ube Samples At 298 K

The adsorption of CO was subsequently followed on the remaining Ube samples, showing characteristics similar to that of 100 Å MgO. The only differences are the magnitudes of

absorbance maxima (reflectance minima) between the catalysts, attributed to varying populations of 3 co-ordinated sites available for reaction. Comparison of the bands formed at 100 Torr is shown below.
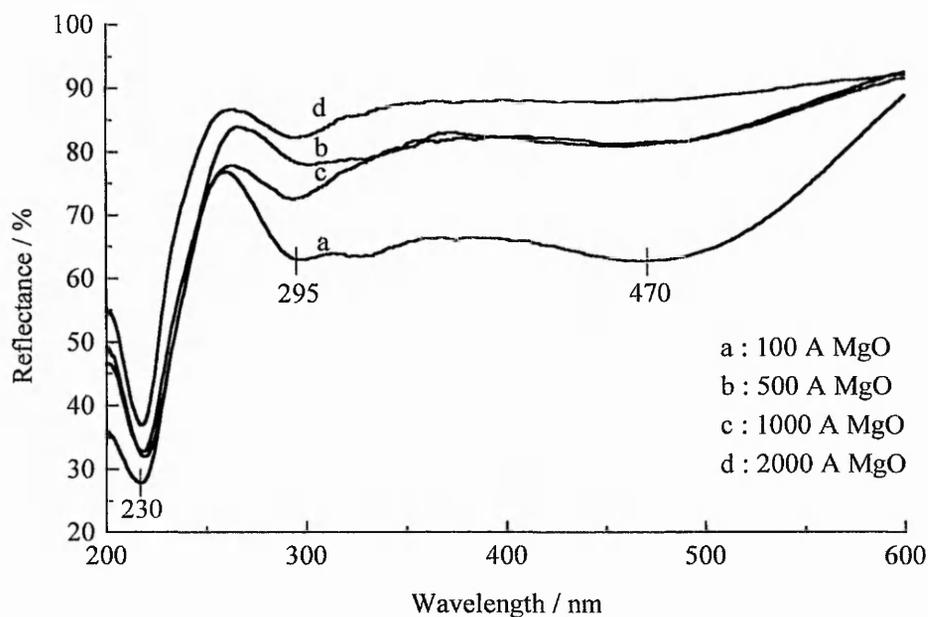
Fig 4.7.2.1   UV/VIS/NIR Diffuse Reflectance Spectra Of 100 Torr CO Adsorbed On The Ube MgO Samples At 298 K.

From Fig 4.7.2.1 it is clear that numbers of sites exhibiting the lowest co-ordination decrease according to the following sequence :

$$100 \text{ Å} > 1000 \text{ Å} > 500 \text{ Å} > 2000 \text{ Å}$$

As expected this is the same conclusion reached during UV/VIS/NIR diffuse reflectance experiments on the clean MgO surface (Fig 4.2.2.1). It is also possible to apply the Kulbelka-Munk function to the data, providing an alternative means of presenting the spectra. However for the sake of brevity they have been omitted, as they show the same results as outlined above.

4.8   Discussion

As this chapter shows the Ube samples exhibit characteristics indicative of MgO, comparing them to the vast amount of literature available, regarding UV/VIS/NIR diffuse reflectance, FTIR and photoluminescence spectroscopies. The main aim of undertaking these measurements was to determine differences in population of the various ions on the surface between the samples. Using a wide range of techniques has allowed this, enabling trends in 3, 4 and 5 co-ordinated sites on 100, 500, 1000 and 2000 Å MgO to be distinguished. A summary of the results obtained is tabulated below.

Co-ordination No	Experiment Type	Figure	Sequence (Decreasing Sites)
3	Photoluminescence	4.3.2.3	100 > 500 > 1000 > 2000
	Diffuse Reflectance	4.2.2.2	100 > 1000 > 500 > 2000
	FTIR - CO_{ads}	4.5.2.1	500 > 100 > 1000 > 2000
	Diffuse Reflectance - CO_{ads}	4.7.2.1	100 > 1000 > 500 > 2000
4	Photoluminescence	4.3.2.2	500 > 100 > 1000 > 2000
	Diffuse Reflectance	4.2.2.2	100 > 500 > 1000 > 2000
	FTIR - CO_{ads}	4.5.2.2	100 > 500 > 1000 > 2000
5	FTIR - CO_{ads}	4.5.2.3	100 > 500 > 1000 > 2000

Table 4.8.1   Table Showing The Variations In Co-ordinatively Unsaturated Surface Ions By The Use Of Different Spectroscopic Techniques.

Regarding the 3 co-ordinated ions it would be predicted that 100 Å MgO possesses the most and 2000 Å the least of these sites. Clearly photoluminescence spectroscopy results support this, which would be expected as it is the most sensitive of the techniques employed [103]. A minor discrepancy arises with the UV/VIS/NIR diffuse reflectance data, indicating 1000 Å MgO is richer in 3 co-ordinated ions than its 500 Å counterpart. Naturally both spectra of the clean and CO adsorbed surface reach the same conclusion, however closer inspection of Figs 4.2.2.2 and 4.7.2.1 indicate such differences are negligible. Lastly, FTIR

spectroscopy highlights 500 Å MgO as being the most abundant in 3 co-ordinated sites, a result which there is no apparent explanation for.

On inspecting the results regarding the 4 co-ordinated sites both UV/VIS/NIR diffuse reflectance and FTIR spectroscopy follow a sequence one would expect. Interestingly photoluminescence measurements indicate 500 Å MgO to be more highly populated in 4 co-ordinated ions than the 100 Å sample. At a first glance this would appear to be an error, however in light of the isotopic oxygen exchange results (Section 3.7.1), this subject warrants further discussion (see Section 4.8.2).

Finally when probing Mg^{2+}_{5C} cations by CO adsorption using FTIR spectroscopy, it appears that the experimental findings are in agreement with predicted values, thus requiring no further comment.

4.8.1 Determination Of The Difference In Populations Of Particular Site Types

Results obtained using both photoluminescence and UV/VIS/NIR diffuse reflectance spectroscopy (when applying the Kulbelka-Munk function to the data), allows the determination of differences in populations of ions in particular co-ordination environments. Unfortunately this is only possible for 3 and 4C sites. Contributions from 5C ions are not observed due to the low intensity of the excited light available in their absorption region (ca. 190 nm), with spectra only being obtainable at wavelengths greater than 230 nm [4, 13].

By taking maxima of the bands due to 3 and 4 co-ordinated sites from individual spectra for each catalyst, it is possible to calculate the ratio of these ions between the samples. This is of great interest as it can provide information regarding the structure sensitivity of isotopic oxygen exchange on MgO.

Similar work has been performed by Coluccia *et al* [4], comparing differences in 3 and 4C sites on a single MgO sample. The ratios of 3 and 4C sites have been determined experimentally relative to the 100 Å MgO sample. The results obtained are tabulated below, together with values calculated assuming a perfectly cubic surface.

Ratio	3 Co-ordinated			4 Co-ordinated			5 Co-ordinated	
	Expt[a]	Expt[b]	Calc	Expt[a]	Expt[b]	Calc	Expt	Calc
100:500	1.27	3	30	0.9	2.3	5	-	0.97
100:1000	1.66	3	100	1.24	3.25	11	-	0.96
100:2000	3.38	10.2	600	1.46	3.84	21	-	0.96

a - taken from photoluminescence measurements.

b - taken from UV/VIS/NIR diffuse reflectance measurements.

Table 4.8.1.1   Table Showing The Ratios Of Each Different Co-ordination Site Type From The Experimental Data And Theoretical Calculations.

From Table 4.8.1.1 it is apparent that the experimental and calculated values do not coincide. This is as expected as characterisation of the Ube samples shows that they do not exhibit a perfectly cubic morphology (Section 3.10.1). It was found the samples possessed an irregular surface, thought to be a consequence of water vapour attack, thus altering the populations of co-ordinatively unsaturated surface sites. Another feature of the catalysts was the crystallite size distribution from the quoted value, which again alters the numbers of 3, 4 and 5C sites from their predicted values.

However comparing the experimentally determined ratios of sites between the catalysts for each co-ordination environment, with the differences in rates of isotopic oxygen exchange, can help to confirm the findings of the previous chapter that isotopic oxygen exchange is structure insensitive on MgO.

4.8.2 Correlation Of Photoluminescence And Isotopic Oxygen Exchange Data

The main conclusion from performing isotopic oxygen exchange experiments on the set of Ube MgO samples (Section 3.10.4), was that the reaction is structure insensitive. Since there was a surface area difference of an order of magnitude between the 100 and 2000 Å samples, the latter would be expected to contain more ions of low co-ordination. As the initial rates of isotopic oxygen exchange did not vary significantly between the catalysts, it

was assumed that these sites did not participate in the reaction. Consequently comparisons of the ratios of 3 and 4C sites between the Ube samples (Table 4.8.1.1), with the initial rates of oxygen exchange can be made, determining if this conclusion is valid.

The initial rates of isotopic oxygen exchange on each of the samples at 80 torr, following vacuum pre-treatment at 733 K (Section 3.7.1), are given below.

Temperature / K	Specific Rate Of Isotopic Oxygen Exchange / x 10^{13} atoms s^{-1} / m^2			
	100 Å	500 Å	1000 Å	2000 Å
688	1.41 ± 0.32	2.34 ± 0.35	1.18 ± 0.54	1.02 ± 0.50
708	3.61 ± 0.33	3.74 ± 0.37	1.94 ± 0.23	1.73 ± 0.26
723	3.74 ± 0.37	6.12 ± 0.55	2.69 ± 0.30	2.35 ± 0.33
733	6.22 ± 0.44	8.52 ± 0.60	5.74 ± 0.40	4.96 ± 0.45

Table 4.8.2.1   Specific Rates Of Isotopic Oxygen Exchange On The Ube MgO Samples At An Oxygen Pressure Of 80 Torr Following Vacuum Pre-treatment At 733 K.

If exchange were to proceed through the involvement of 3 co-ordinated anions, the initial rate of exchange on 100 Å MgO, should be an order of magnitude greater than for 2000 Å MgO, according to UV/VIS/NIR diffuse reflectance spectroscopy. Similarly this value should be 3½ times greater when considering photoluminescence measurements. Clearly from Table 4.8.1.2 the initial rates of isotopic oxygen exchange, do not differ within the limits of experimental error, at each of the temperatures studied.

Subsequently if 4 co-ordinated sites were responsible for exchange 100 Å MgO should be a factor of 4 more active than its 2000 Å counterpart. It is interesting to compare exchange rates with photoluminescence results obtained for the 4C ions. Spectroscopy measurements indicated that 500 Å MgO possessed the highest number of 4 co-ordinated sites, whilst exchange experiments showed it to be the most active of the Ube catalysts. However no link between the two could be found and in light of the UV/VIS/NIR diffuse reflectance findings this correlation was deemed fortuitous.

These results confirm that neither 3 or 4 co-ordinated anions are involved in isotopic oxygen exchange, further re-iterating the earlier conclusions regarding the lack of structure sensitivity of isotopic oxygen exchange reactions on these samples.

4.8.3 FTIR Spectra Of CO Adsorbed On 100 Å MgO At 77 K At Low Pressures Probing Mg^{2+}_{LC} Sites

As mentioned previously in this chapter (Section 4.5.1), a new band at 2187 cm^{-1} has been identified on the MgO surface, following CO adsorption at 77 K at low pressures. Determination of the structure of this species is possible by the use of modelling techniques. Pelmenschikov *et al* [124] have already calculated positions of CO adsorbed on Mg^{2+}_{3C} and Mg^{2+}_{4C} to within ± 2 cm^{-1} of the experimental data. Also in related studies they have used the same approach using CD_3CN as a probe molecule, investigating the role of dual Mg^{2+}_{LC} sites in the adsorption process [125]. Further theoretical studies involving the CO — MgO system are currently in progress by our co-workers [126], which will help in understanding these observations.

5. Characterisation And Performance Of MgO Prepared From Different Precursors

5.1 Introduction

As shown in Chapter 3, the lack of structure sensitivity of isotopic oxygen exchange was determined on MgO prepared by the same technique but possessing varying crystallite sizes. Consequently it is of interest to investigate if the nature of the precursor effects the characteristics of MgO, leading to different rates of exchange. This has been attempted on MgO catalysts prepared from the thermal decomposition of magnesium hydroxide, magnesium basic carbonate and by igniting the ribbon in air and collecting the resultant ash.

There have been several reports concerned with the morphological features [3, 5] and quantifying populations of co-ordinatively unsaturated sites [4, 5, 8, 13] on the surface of MgO from various preparative routes. Activities of these catalysts have also been compared in specific cases, including the methane coupling reaction by this group [6, 7], cis-2-butene isomerisation and the phenol alkylation of methanol by Hattori *et al* [25] and propan-2-ol dehydration by Aramendía *et al* [34, 127]. Also an attempt has been made to synthesise MgO exhibiting (111) termination planes, by the decomposition of $Mg(OH)_2$ in air using differing calcination temperatures. Exposing this higher index plane enhances the populations of 3 co-ordinated sites at the surface. There are instances in the literature indicating the possibility of forming a (111) MgO surface from magnesium hydroxide [8, 10, 31, 128, 129] and magnesium basic carbonate [9], however it is often observed in conjunction with the more abundant (100).

All the samples studied were characterised by surface area determination, TEM, powder XRD and XPS. Rates of isotopic oxygen exchange will be measured at 80 torr and 708 K, following treatment in vacuum at 733 K for 16 hours.

5.2   Preparation Of MgO Catalysts From Different Precursors

Generally MgO can be prepared by the thermal decomposition of magnesium hydroxide [18, 19, 23, 89, 130] or magnesium basic carbonate [3, 9, 10, 25], at elevated temperatures in air or vacuum, both reactions proceeding above 623 K [86]. In the present study both precursors were calcined in air at 1073 K for 3 hours, giving a suitable means of comparison between catalysts. These are similar conditions to those adopted previously by this group [6, 7].

The magnesium hydroxide and magnesium basic carbonate precursors decompose giving MgO, with H_2O [19, 25] and H_2O and CO_2 [25] as by-products of each reaction respectively. The preparative route to MgO from magnesium ribbon is slightly different [3-8]. Initially the ribbon is ignited in air with the ensuing ash being collected, subsequently this was heated at 1073 K for 3 hours, removing any magnesium nitride which may have been formed [7].

5.3   Surface Areas Of The MgO Catalysts Prepared From Different Precursors

Surface areas of the three MgO catalysts and their precursors were measured by nitrogen physisorption at 77 K and the results are tabulated below.

Precursor	Surface Area / m^2g^{-1}	
	Precursor	MgO
Ribbon	-	8
Hydroxide	8	40
Basic Carbonate	12	35

Table 5.3.1   Measured Surface Areas Of The MgO Catalysts And Their Precursors.

Values obtained for MgO are consistent with those previously reported for the ex hydroxide [6-8, 89] and ex basic carbonate [6, 7, 131], following decomposition of the parent compound in air at elevated temperature, although no direct comparison can be drawn as

variations in calcination time and temperature affect the surface area [11, 18, 23, 89, 90, 130].

It is widely accepted that igniting magnesium ribbon in air yields an MgO powder possessing an area of roughly 10 m^2g^{-1} [3-8, 12, 31], the current value agreeing with this.

5.4 TEM Studies Of The MgO Catalysts Prepared From Different Precursors

Electron micrographs were obtained for the MgO samples from different preparative routes, examples of which are given below.
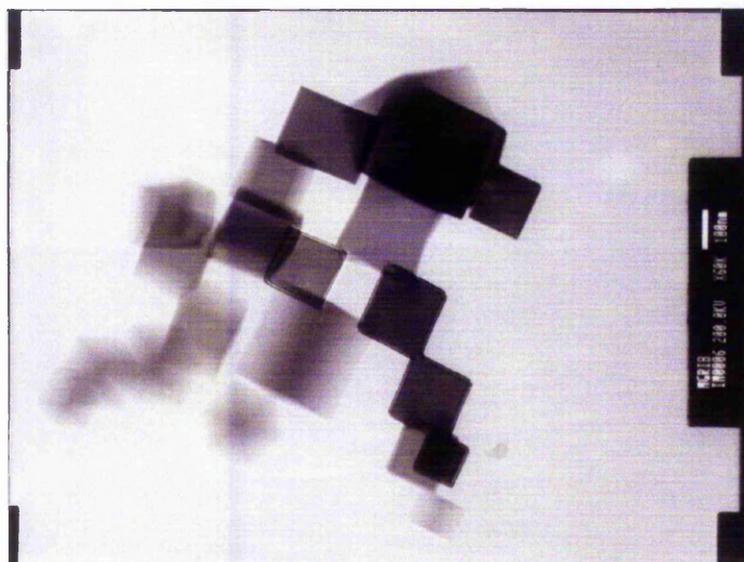
Fig 5.4.1   **Electron Micrograph Of MgO Prepared From Igniting Magnesium Ribbon In Air Then Calcining The Resultant Ash In Static Air At 1073 K For 3 Hours. - Magnification x 60 K. Scale 5mm = 100 nm.**

Preparation of MgO from the ribbon results in a sample possessing a near perfect cubic morphology, as Fig 5.4.1 shows. One feature of these crystals which is apparent is their broad size range, being in the region 1000-2000 Å [3-8, 31]. It is interesting to note the high degree of cubic morphology evident in this sample, compared to the Ube catalysts characterised by electron microscopy in Section 3.3. These showed a rounding at corners with kink formation indicative of water attack, possibly experienced during transportation

from Japan. Subsequently TEM of the MgO ex ribbon sample was performed immediately upon its preparation, allowing little opportunity for the adsorption of water vapour. Also as a further precaution the catalysts were stored in a dessicator when not in use, to minimise water vapour adsorption.
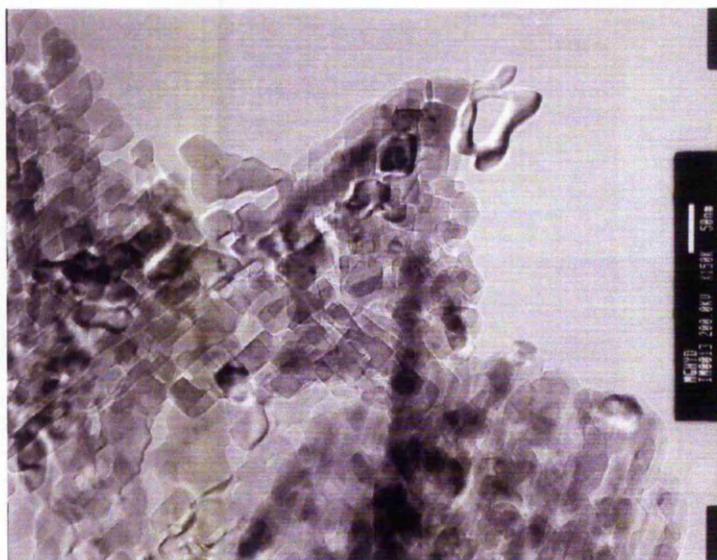
Fig 5.4.2   **Electron Micrograph Of MgO Prepared From Decomposing Magnesium Hydroxide In Static Air At 1073 K For 3 Hours. - Magnification x 150 K. Scale 7mm = 50 nm.**

Inspection of Fig 5.4.2 shows the decomposition of $Mg(OH)_2$ gives a morphology comparable to that of the ex ribbon (Fig 5.4.1), the only difference being a much smaller average cube size of 200-400 Å is obtained [6, 7]. A feature of MgO prepared in this manner is sintering where individual cubes agglomerate [3, 9], producing irregular shaped crystals. If imperfect alignment is observed as generally is the case, step, terrace and kink formation occurs. This leads to a greater number of 3 and 4 co-ordinated ions present at the surface, compared to the ribbon residue.
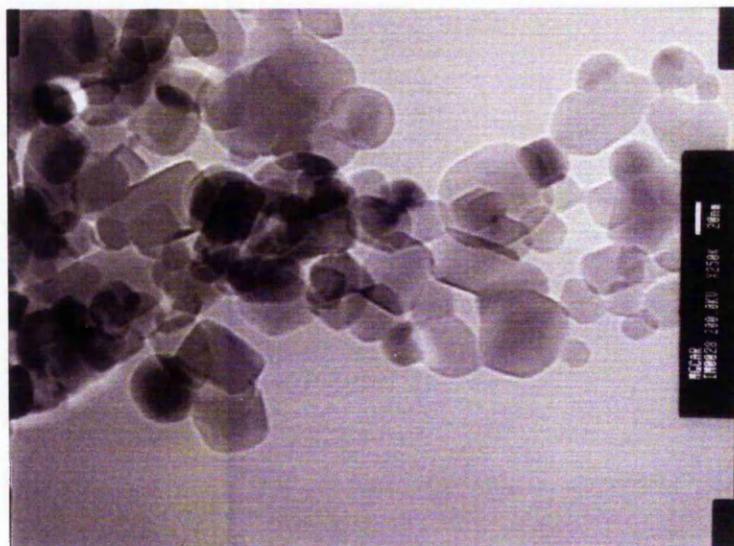
Fig 5.4.3   **Electron Micrograph Of MgO Prepared From Decomposing Magnesium Basic Carbonate In Static Air At 1073 K For 3 Hours. - Magnification x 250 K Scale 5mm = 20 nm.**

From the decomposition of magnesium basic carbonate (Fig 5.4.3) it is evident that the average crystallite size is in the range 200-400 Å with the majority exposing the (100) face, in accordance with previous studies [3, 6, 7]. These are also very similar to the micrographs of the decomposed $Mg(OH)_2$ sample. Microfaceting is apparent [3, 9] causing bunching. Due to individual crystallites connecting at different orientations, higher mean index planes such as the (110) and (111) have been observed [3, 6, 7, 9]. As a result of this a surface exhibiting a higher degree of irregularity compared to that for a predominantly cubic morphology (Figs 5.4.1 and 5.4.2) is produced. Consequently a higher proportion of co-ordinatively unsaturated surface sites will be evident.

5.5   Powder XRD Studies Of The MgO Catalysts Prepared From Different Precursors

Diffraction patterns of the magnesium hydroxide and basic carbonate precursors were recorded, together with those of the MgO produced. The results can highlight any impurity phases present, as magnesium nitride (Mg_3N_2) is a known product of igniting the ribbon in

air [7]. They also give a good indication that the transformation of the parent compounds to MgO is complete in each case.

5.5.1 Powder XRD Patterns Of The MgO Precursors

Patterns of the magnesium hydroxide and basic carbonate precursors are given below.
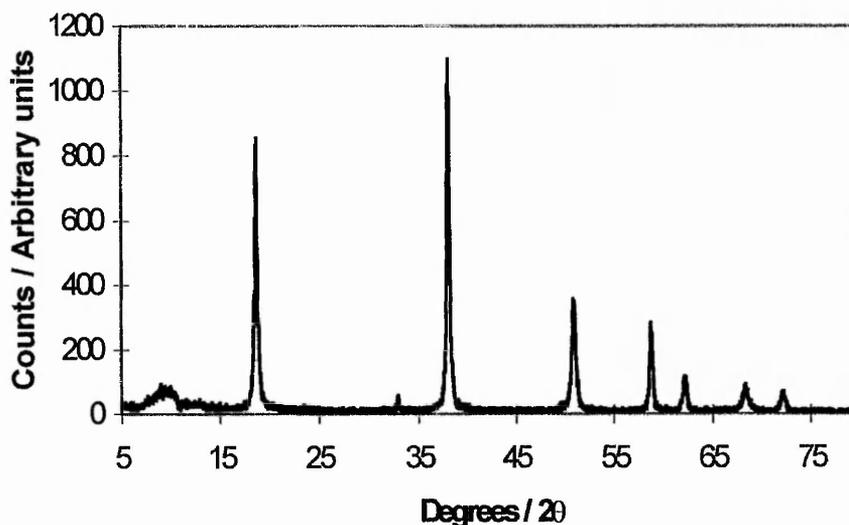
Fig 5.5.1.1   Powder X-Ray Diffraction Pattern Of The Magnesium Hydroxide Precursor.

158
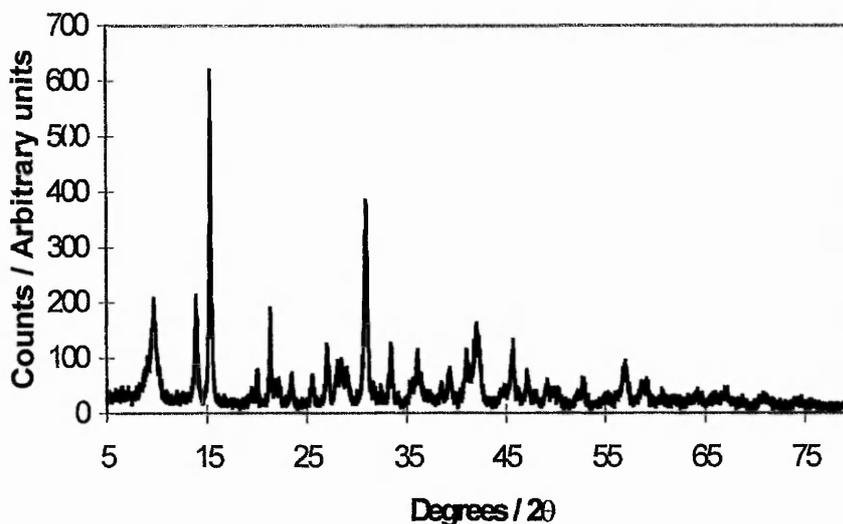
Fig 5.5.1.2   Powder X-Ray Diffraction Pattern Of The Magnesium Basic Carbonate Precursor.

5.5.2 Powder XRD Patterns Of The MgO Catalysts Prepared From Different Precursors

The powder XRD patterns of MgO prepared from magnesium ribbon, hydroxide and basic carbonate are illustrated below. As mentioned previously an anomaly is present at approximately $2\theta = 10°$ for all samples, attributed to an artefact of the diffractometer. Individual reflections can be compared to those tabulated in standard diffraction files [80], as shown in Table 5.5.2.1.

159
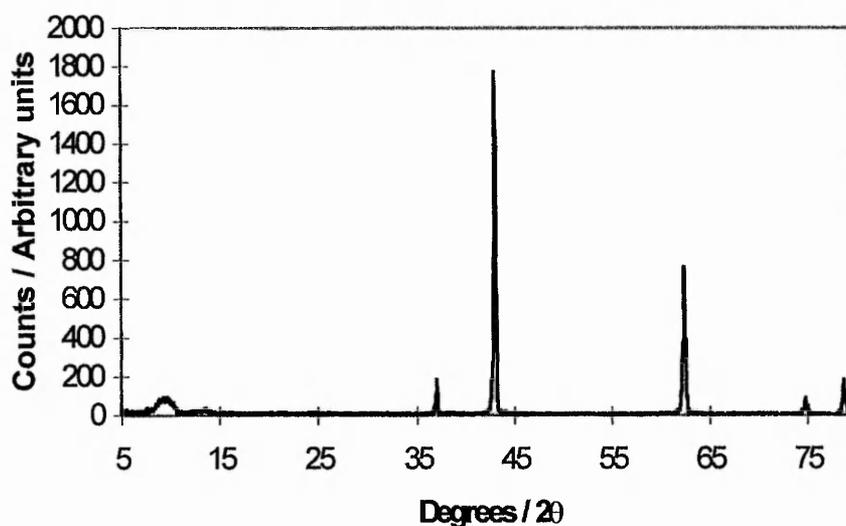
Fig 5.5.2.1   **Powder X-Ray Diffraction Pattern Of MgO Prepared By Igniting Magnesium Ribbon In Air Then Calcining The Resultant Ash At 1073 K For 3 Hours.**
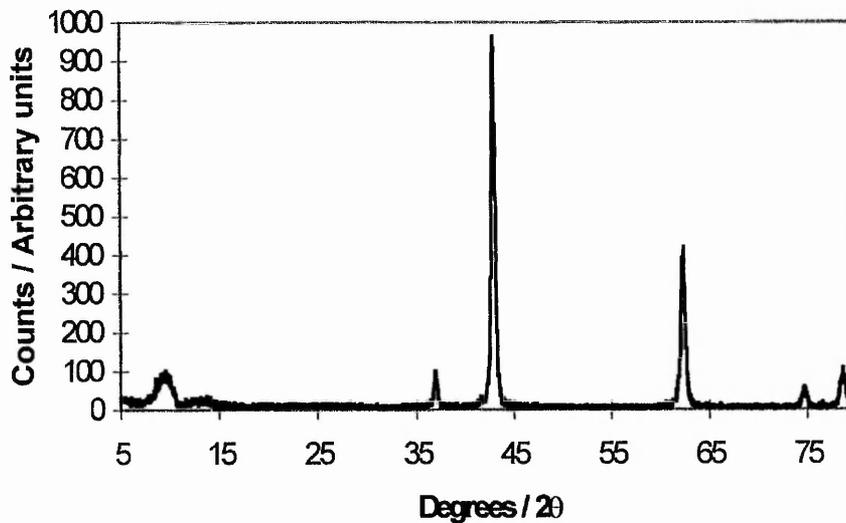
Fig 5.5.2.2   **Powder X-Ray Diffraction Pattern Of MgO Prepared From Decomposing Mg(OH)$_2$ In Air At 1073 K For 3 Hours.**
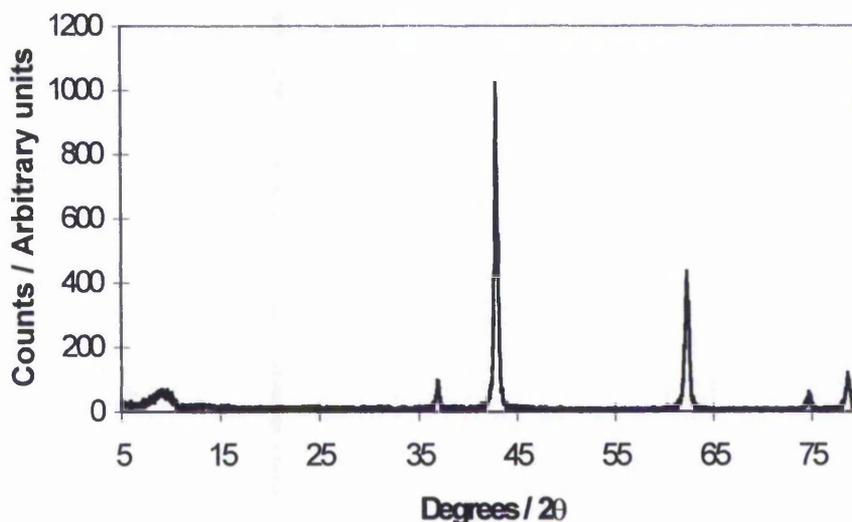
Fig 5.5.2.3   **Powder X-Ray Diffraction Pattern Of MgO Prepared From Decomposing**
Magnesium Basic Carbonate In Air At 1073 K For 3 Hours.

Tabulated[a]			Experimental					
			ex Ribbon		ex Hydroxide		ex Basic Carbonate	
{hkl}	d / Å	Int	d / Å	Int	d / Å	Int	d / Å	Int
{111}	2.431	10	2.428	11	2.433	10	2.439	10
{200}	2.106	100	2.102	100	2.105	100	2.107	100
{220}	1.489	52	1.488	43	1.489	44	1.490	43
{311}	1.270	4	1.269	5			1.270	5
{222}	1.216	12	1.215	10	1.216	11	1.217	12

a - Magnesium oxide JCPDS file no : 8-429 [80].

Table 5.5.2.1   **Comparison Of Tabulated And Experimental Reflections Obtained From The**
Powder XRD Patterns Of The MgO Samples Prepared From Different Precursors.

From Table 5.5.2.1 it is clear each reflection corresponds to that of MgO, indicating total decomposition of the precursors during 3 hours treatment in air at 1073 K. Also there are no signs of magnesium nitride (JCPDS file no : 35-778) [80] produced from igniting the ribbon in air [7], indicating it is removed during the calcination process. However powder

XRD will not detect it if it is lower than 5 %, but it is easily distinguishable being visible to the naked eye, having a yellow/green colour.

5.5.3 Determination Of The Degree Of Cubic Character From The Powder XRD Patterns

Berry [81] suggested that the average crystal morphology of a sample could be determined by application of a form of the Scherrer equation (Equation 2.3.1.1). If the relative breadth of two diffraction lines are calculated, the particle size can be eliminated, as shown by Equation 2.3.2.1. Berry [81] used this method in measuring the mean particle shape of a MgO powder, prepared from $MgCO_3$ decomposition, finding it to be cubic in nature.

This procedure was adopted to investigate the different morphologies of the samples. In order to quantify this, the full width-half maximum (FWHM) of the {200}, {220} and {222} reflections are required, together with a constant K, corresponding to the particle shape of the Miller indices. Such values are tabulated below.

Miller Index	K[a]	FWHM[b] / °		
		ex Ribbon	ex Hydroxide	ex Basic Carbonate
{200}	0.90	0.219	0.313	0.313
{220}	0.84	0.219	0.469	0.313
{222}	0.87	0.313	0.625	0.469

a - values taken from ref [81] corresponding to a cubic morphology.

b - FWHM values measured from Figs 5.5.2.1 to 5.5.2.3.

Table 5.5.3.1   FWHM Values Of The MgO Catalysts Prepared From Different Precursors.

By application of the data presented in Table 5.5.3.1 to Equation 2.3.2.1, it is possible to determine which of the three samples can be associated with the highest cubic order. This is associated with the material possessing an $R_{observed}/R_{calculated}$ ratio closest to unity [81].

Ratio	Catalyst		
	ex Ribbon	ex Hydroxide	ex Basic Carbonate
$R_{200} / R_{220\ observed}$ over $R_{200} / R_{220\ calculated}$	1.02	0.68	1.02
$R_{222} / R_{220\ observed}$ over $R_{222} / R_{220\ calculated}$	1.25	1.16	1.31
$R_{222} / R_{200\ observed}$ over $R_{222} / R_{200\ calculated}$	1.23	1.72	1.29
Average	1.17	1.19	1.21

Table 5.5.3.2   **Cubic Shape Factors Calculated For The MgO Catalysts Prepared From Different Precursors As A Means Of Determining Morphology.**

From Table 5.5.3.2 the following sequence is obtained, with cubic character decreasing from left to right.

ex Mg ribbon > ex Hydroxide > ex Basic Carbonate

This result is in agreement with electron microscopy experiments performed on the same catalysts. As mentioned earlier igniting magnesium ribbon in air leads to a sample exhibiting a near perfect cubic morphology (Fig 5.4.1). A similar observation is made with the ex $Mg(OH)_2$ sample (Fig 5.4.2), however due to sintering [1, 110] crystallites are formed with a slightly more irregular shape. Finally heating magnesium basic carbonate gives some rounded MgO particles, as illustrated by Fig 5.4.3, hence its cubic character would be expected to be poor.

5.6   XPS Studies Of The MgO Catalysts Prepared From Different Precursors

Spectra were obtained for each of the MgO samples prepared from the different precursors to investigate their purity. The results of this are shown below.

Peak	Tabulated BE[a] /	MgO From Different Precursors / BE / eV		
	eV	Ribbon	Hydroxide	Basic Carbonate
O 2s	23.0	-	-	-
Mg 2p	49.8	50.6	-	-
Mg 2s	90.0	88.1	87.0	87.5
C 1s	284.6	285.1	285.2	285.3
O 1s	531.0	530.9	531.3	531.0
Mg 1s	1305.0	1305.0	1305.0	1305.0
Unknown	-	None	None	None

a - Taken from the Handbook of Photoelectron Spectroscopy [82].

Table 5.6.1   Table Showing The Binding Energy Positions Of The Maxima Of The MgO Catalysts Prepared From Different Precursors - Highlighting Any Impurities.

Inspection of Table 5.6.1 leads to the conclusion that there are no impurities present within the limit of detection, in the outermost layers of the three samples studied, which could influence the rate of isotopic oxygen exchange. Hence the catalytically active site can be attributed to oxygen anions of the oxide, or as indicated previously, an O⁻ anion adsorbed on a surface Mg^{2+}_{5C} cation (Section 3.10.3).

5.7   Isotopic Oxygen Exchange Reactions On MgO Prepared From Different Precursors

Rates of isotopic oxygen exchange were measured on the MgO catalysts derived from the ribbon, hydroxide and basic carbonate. Reactions were followed at 80 torr and 708 K, after treatment in vacuum at 733 K for 16 hours.

An interesting feature apparent from the exchange reactions is that there is an increase in the mole fraction of mass 32 during an experiment on some of the samples, as shown below for the ex basic carbonate catalyst.
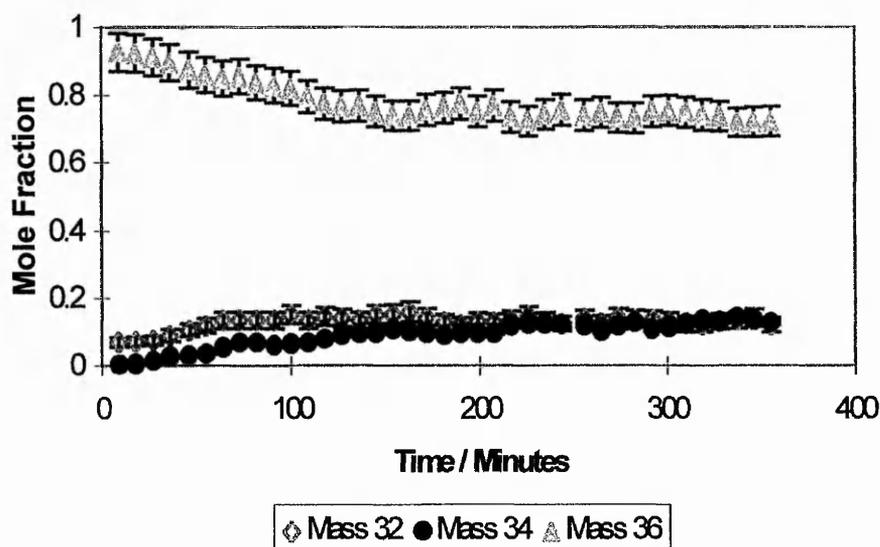
Fig 5.7.1   **Plot Showing How The Mole Fractions Of The Different Oxygen Species Vary During Exchange On The Ex Basic Carbonate Catalyst At 80 Torr And 708 K - Treated In Vacuum At 733 K.**

The increase in mole fraction of mass 32 was not due to an air leak in the system, as there were no fluctuations in mass 28 (nitrogen) inside the mass spectrometer. Also it is increasing above the limits of experimental error. Therefore it would appear that R_2 exchange was occurring on some of these catalysts. This is where two ^{18}O atoms exchange with the surface simultaneously, releasing $^{16}O_2$ into the gas phase (Section 1.4.2).

$$^{18}O_{2\,(g)} + 2\,^{16}O_{(surface)} \longrightarrow {}^{16}O_{2\,(g)} + 2\,^{18}O_{(surface)} \qquad (R_2)$$

Alternatively for reactions involving O^- species.

$$^{18}O_{2\,(g)} + 2\,^{16}O^-_{(surface)} \longrightarrow {}^{16}O_{2\,(g)} + 2\,^{18}O^-_{(surface)} \qquad (R_2)$$

Where R_2 was evident its initial rate of exchange was measured by following the evolution of $^{16}O_2$ molecules with time, in the same manner as R_1 rates were calculated previously (Section 3.6.2).

165

The results of the experiments are given below.

Catalyst	Ratio	Specific Rate of Exchange / x 10^{13} atoms s^{-1}/m^2		
	R_1:R_2	R_1	R_2	Total
Ribbon	-	4.05 ± 0.81	-	4.05 ± 0.81
Hydroxide	8:5	3.12 ± 0.22	2.37 ± 0.28	5.49 ± 0.50
Basic Carbonate	1:1	9.23 ± 1.85	11.9 ± 2.14	21.1 ± 3.99

Table 5.7.1 **Specific Rates Of Isotopic Oxygen Exchange Measured On The MgO Catalysts Prepared From Different Precursors At 80 Torr And 708 K Following Vacuum Treatment At 733K.**

The most important result from Table 5.7.1 is the apparent sensitivity of isotopic oxygen exchange over the MgO catalysts studied. From Table 5.7.1 it is clear that the sample derived from the basic carbonate is approximately a factor of 4 times more active than the hydroxide, which is comparable to the ribbon residue. Due to the similar specific rates in the case of the latter two catalysts it would appear low co-ordinated ions do not participate in isotopic oxygen exchange. These sites are more abundant on the ex hydroxide sample than the ribbon [4, 5, 8, 13], therefore one would expect a greater reactivity with the ex $Mg(OH)_2$ catalyst if they were active. This finding of the inertness of low co-ordinated sites towards exchange is in agreement with earlier work (Section 3.10.4), measuring exchange on the Ube MgO samples.

However this does not explain the enhanced performance of the basic carbonate sample, as this possesses a surface rich in low co-ordinated ions, similar to the ex hydroxide catalyst. Previous work by this group found a similar trend to that above for MgO samples during methane coupling experiments [7]. The higher reactivity of the ex basic carbonate was attributed to a feature of the irregular surface, but not ions in 3 and 4 co-ordination [7]. The active centre was assigned to a bottom step site. This assignment was only tentative as the ex basic carbonate catalyst was also shown to contain both calcium and sodium, which could influence the methane coupling results. Similarly the sample used in this investigation was taken from the same batch, but showed no impurities in XPS (Section 5.6), to the detectable limit of the ESCA 3 instrument.
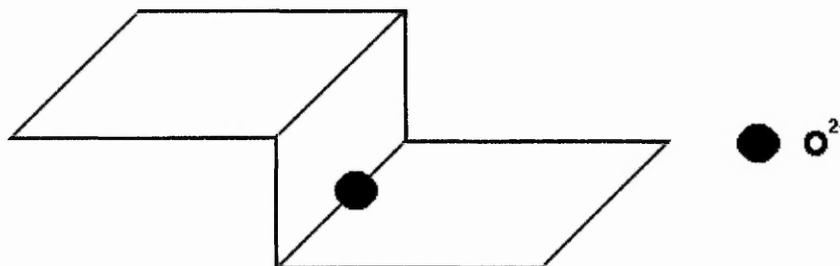
Fig 5.7.2   **A Bottom Step Site On An Irregular MgO Surface.**

Secondly it is interesting to note the occurrence of R_2 exchange on MgO from both the ex hydroxide and ex basic carbonate samples, but not magnesium ribbon. None of the Ube MgO catalysts showed evidence of R_2 reactions (Section 3.7.1), which were also derived from metallic magnesium. Various other workers have published results regarding the ability of MgO to promote R_2 exchange. Klier *et al* [45, 46] reported R_2 exchange on MgO, the rate of which was half that of R_1. Unfortunately there was no reference to the origin of the sample used. Both Winter [48], using MgO derived from $MgCO_3$, and Boreskov [38], could not find any contributions from R_2 during their isotopic oxygen exchange experiments.

5.8   Preparation Of (111) Terminated MgO

From the vast amount of literature available regarding MgO the most frequently exposed plane is the (100) [3-7, 12, 15, 84, 114, 128, 129]. Therefore it would be of great interest if MgO could be synthesised, with a different surface plane termination. Higher index planes than the (100) plane may show a different catalytic activity. Consequently an attempt has been made to produce (111) terminated MgO from the decomposition of magnesium hydroxide (brucite) in air at elevated temperatures. There are very few reports regarding the preparation of (111) terminated MgO as it is expected to be unstable, due to the fact that only one type of ion (either Mg^{2+}_{3C} or O^{2-}_{3C}) is exposed at the surface.

      There is substantial literature on the synthesis of MgO from the dehydration of brucite [14, 17, 23, 89, 96, 128-130] together with its reverse process, the hydroxylation of

MgO [8, 16, 18, 21, 31, 91, 129]. However there is little information available concerning the (111) terminated surface [10, 128, 129]. Boudart *et al* [10] proposed that 3 O^-_{3C} anions on a (111) microplane associated with a surface hydroxyl group, was the active site for hydrogen dissociation and subsequent H_2/D_2 exchange. Goodman [128] found on subjecting $Mg(OH)_2$ to the beam of an electron microscope, (111) orientated MgO was observed. The transition was thought to be consequence of the heat produced from the intensity of the focused beam. Recently Wogelius *et al* [129] performed calculations to determine the possibility of forming a (111) type surface of MgO.

It was proposed by Wogelius *et al* [129] that during initial dehydroxylation, Mg^{2+} cations are replaced by protons in the surface layer. From this the reaction proceeds by diffusion of Mg^{2+} out and $2H^+$ inwards parallel to the (111) plane, resulting in a stable charge balanced structure. Measurements showed this has a d-spacing within 2 % of the original brucite, of which the preferred orientation is the (0001) plane, being identical to that of the (111) of MgO. The hexagonal crystal structure of $Mg(OH)_2$ is shown diagramatically overleaf [132], exhibiting a CdI_2 type lattice.

Another conclusion from this work was that the (111) terminated surface was an intermediate between (100) MgO and brucite. It was found that either hydroxylation or dehydration of the appropriate starting material in air led to (111) plane formation, with the residual hydroxide groups providing stability. The ability of water vapour to initiate the reconstruction of (100) MgO was shown earlier by Kuroda *et al* [8], confirming the above result.
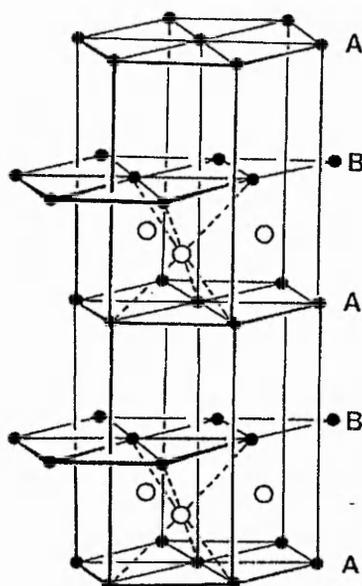
where closed circles represent Mg^{2+} cations and open circles represent OH^- anions.

Fig 5.8.1   The Crystal Structure Of Mg(OH)₂.

5.8.1 The Decomposition Of Brucite To MgO

Because the decomposition of brucite has been reported to produce MgO terminated by (111) planes in some instances [128], a study of MgO preparation by this process under these conditions has been undertaken. As described previously (Section 5.2) brucite starts to decompose at around 623 K, giving MgO and H_2O. An attempt was made to produce the (111) terminated phase of MgO from a series of catalysts, calcined in the range 623-1223 K at regular 100 K intervals, for 3 hours in static air. The heating of $Mg(OH)_2$ at variable temperatures and times in air [89] and vacuum [18, 23, 89, 130] has been studied earlier by several workers, measuring changes in surface area.

After preparation the samples were characterised by surface area determination, TEM, powder XRD and XPS. Initial rates of isotopic oxygen exchange were also measured at 80 torr and 708 K, following treatment in vacuum at 733 K.

5.8.2 Surface Areas Of The Dehydroxylated Brucite Samples

Surface area measurements of the seven MgO catalysts were made, together with that of the brucite precursor. The results of this are tabulated below.

Brucite Decomposition Temperature / K	Surface Area / m^2g^{-1}
623	64
723	63
823	72
923	69
1023	50
1123	48
1223	34
Brucite	8

Table 5.8.2.1   Measured Surface Areas Of The MgO Catalysts Prepared From Decomposing Magnesium Hydroxide At Varying Temperatures In Air For 3 Hours.

The above results are similar in magnitude to those found by Razouk and Mikhail [89], who also monitored brucite decomposition in air over similar time periods. A general trend of the surface area passing through a maximum at approximately 823 K, then tailing off with increasing temperature has been observed by many researchers [18, 23, 89, 130]. The results in Table 5.8.2.1 appear to follow this, however the surface area seems to be fairly constant at low decomposition temperatures before decreasing above 923 K.

An explanation for these observations was provided by Gregg [23, 90, 130] and Razouk and Mikhail [18, 89]. It was thought that the highest surface area corresponded to the temperature where decomposition was just complete, within the time span of the experiment. Below this temperature some of the parent brucite still remained, subsequently lowering the surface area. Above the maximum complete MgO formation was realised before the calcination ended, hence sintering was apparent for the remaining time, decreasing the surface area.

Even though the values in Table 5.8.2.1 appear to follow the described model, it is thought that it is incorrect in explaining the decomposition of brucite in air. Electron micrographs presented in the next section (5.8.3), provide an alternative means of describing the variations in surface area with calcination temperature.

5.8.3 TEM Studies Of The Dehydroxylated Brucite Samples

A micrograph of the Mg(OH)$_2$ starting material can be seen below.

Fig 5.8.3.1   Electron Micrograph Of The Magnesium Hydroxide Precursor. - Scale 29 mm = 200nm.

As expected inspection of Fig 5.8.3.1 indicates that the brucite exhibits a hexagonal platelet structure, exposing the (0001) plane.

Portions of this sample were then calcined in the range 623-1223 K, in static air for 3 hours (Section 5.8.1). A selection of micrographs obtained from different dehydration

temperatures are given below. However for the sake of brevity only those of significance in explaining changes in surface termination, will be presented.

TEM of the MgO catalyst prepared at 623 K is shown below.
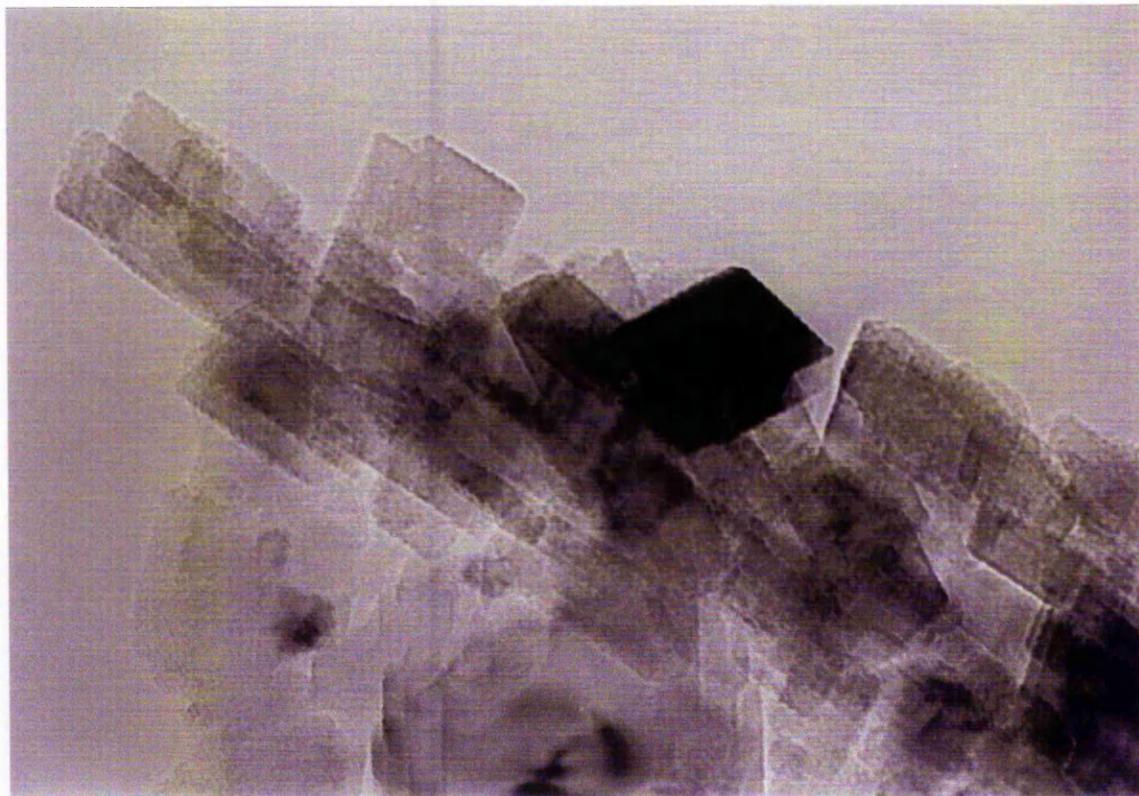
Fig 5.8.3.2   Electron Micrograph Of MgO Prepared From Decomposing Magnesium Hydroxide In Air At 623 K For 3 Hours. - Scale 13mm = 20nm.

From Fig 5.8.3.2 it appears that the platelet structure has recrystallised, giving rise to smaller crystals. It is interesting to note that the hexagonal $Mg(OH)_2$ relic structure has been retained, suggesting that the transition to MgO is incomplete. However powder XRD measurements (Section 5.8.4) show no sign of brucite in the diffraction pattern. Consequently it would seem the above crystallites represent (111) terminated MgO surfaces. Related studies by our co-workers [133] have confirmed the presence of (111) terminated MgO at this temperature, by calculating lattice spacings from electron diffraction patterns. Although total decomposition of the bulk $Mg(OH)_2$ phase has been realised, it is

probable surface hydroxyl groups remain at terminal positions, providing stability for the (111) plane.

As the calcination temperature is increased to 923 K the (111) terminated surface still remains, as indicated by the following micrograph.

Fig 5.8.3.3   **Electron Micrograph Of MgO Prepared From Decomposing Magnesium Hydroxide In Air At 923 K For 3 Hours. - Scale 28mm = 100nm.**

As Fig 5.8.3.3 shows (111) terminated MgO still dominates, however it appears that sintering between individual crystals is evident. It also thought the more stable (100) planes of MgO are becoming observable, arising from the damage of (111) orientated crystals in the electron beam of the microscope. This effect was seen by Goodman [128], attributing it heat produced by the intensity of the focused beam on the sample. Similar results are obtained from electron diffraction patterns [133], confirming the (111) planes are still present. However at this temperature lattice spacings indicative of (100) MgO are becoming evident.

As the next point in the series is reached at 1023 K, a reconstruction in morphology is observed.
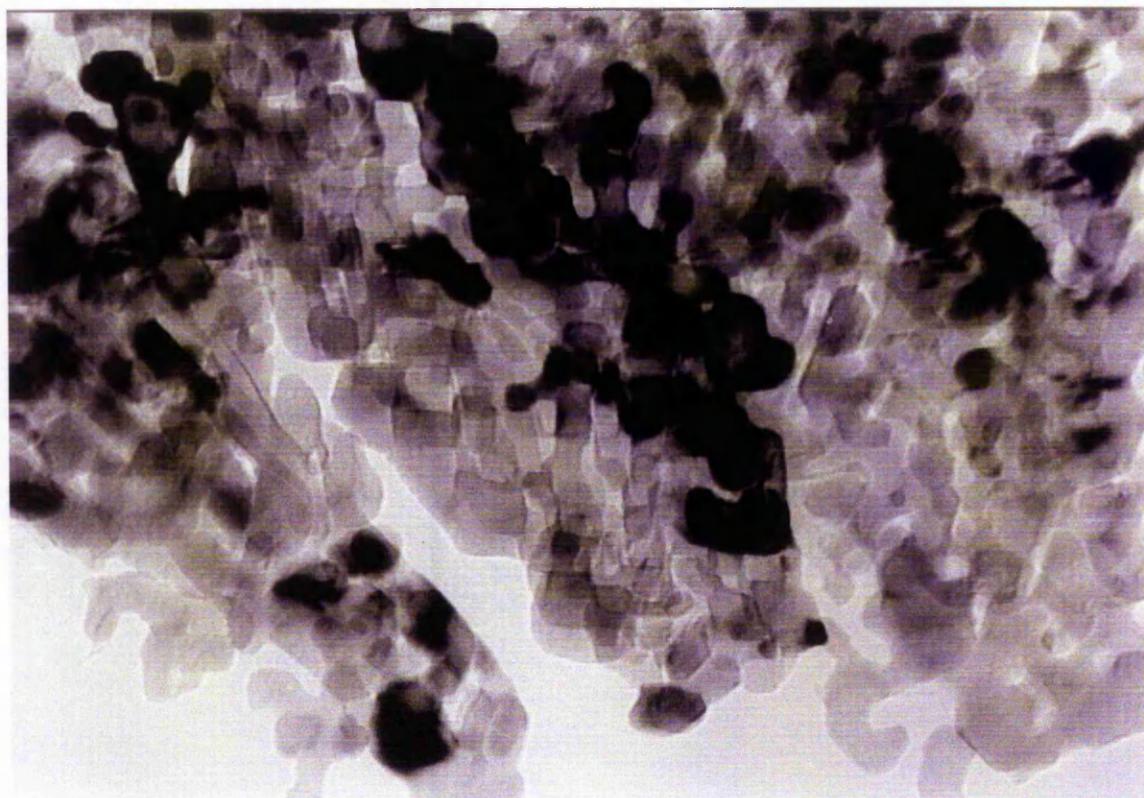
Fig 5.8.3.4 **Electron Micrograph Of MgO Prepared From Decomposing Magnesium Hydroxide In Air At 1023 K For 3 Hours. - Scale 28 mm = 100nm.**

From Fig 5.8.3.4 degradation of the (111) terminated planes is observed, giving way to the more stable (100) cubic orientation. This change in morphology can probably be explained in terms of hydroxyl desorption from the surface. It is well documented that on heating MgO to 1000-1100 K, hydroxyl coverage becomes negligible [4, 12, 13, 14, 17, 96, 102]. Since hydroxyls were thought to be responsible for stabilising the (111) terminated surface [129], their removal will signal the loss of this type of orientated crystals.

This transition also coincides with a decrease in surface area of the sample (Table 5.8.2.1), falling by 20 m^2g^{-1} compared with the previous calcination temperature. It is clear from Fig 5.8.3.4 that sintering between individual crystals is apparent, leading to an increase in crystallite size, which would account for the differences in surface area.

Further increasing the dehydration temperature to 1123 K leads to no noticeable changes in catalyst morphology. The main difference between this sample and that at 1023K is the increased crystallite size due to further sintering.
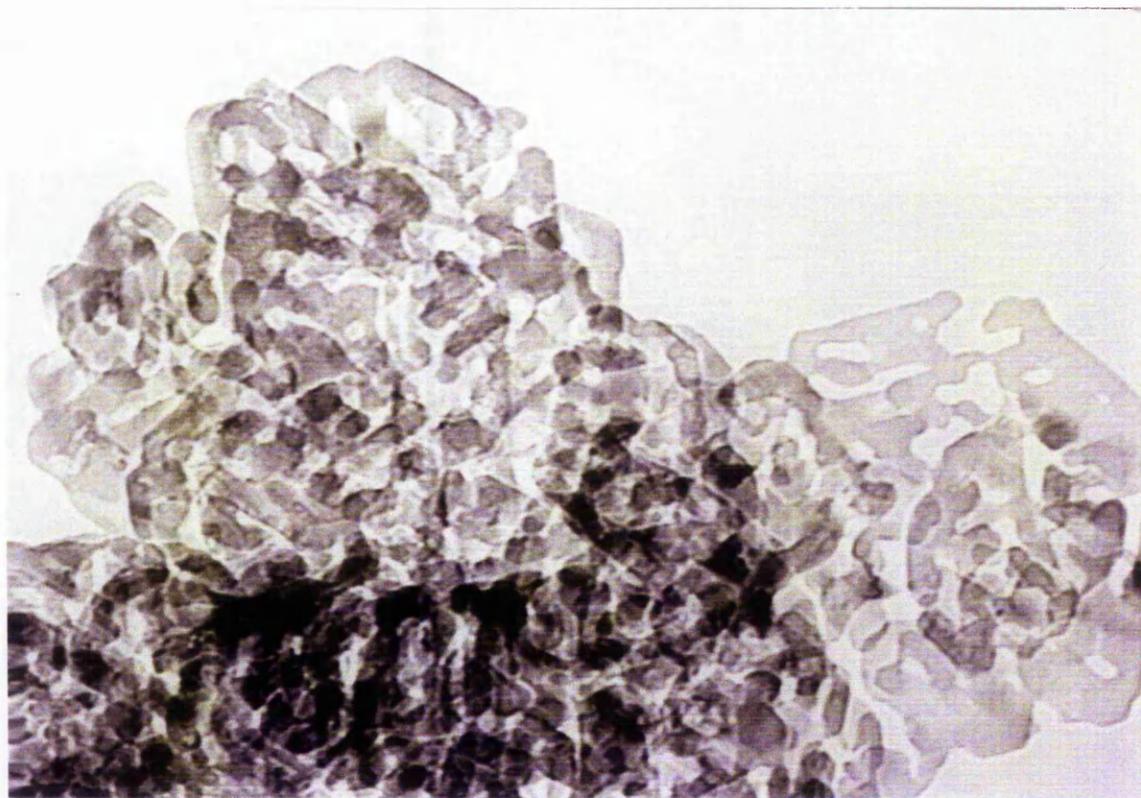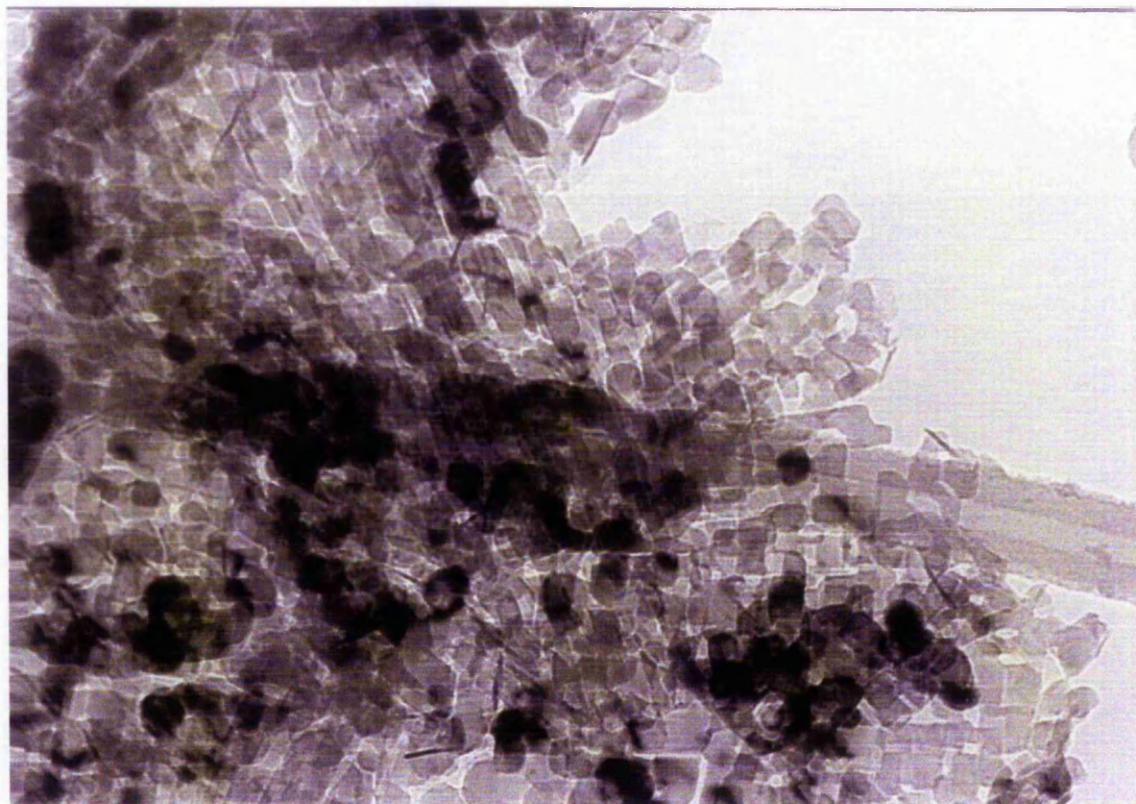

Fig 5.8.3.5   Electron Micrograph Of MgO Prepared From Decomposing Magnesium Hydroxide In Air At 1123 K For 3 Hours. - Scale 19mm = 100nm.

This sequence where a (111) terminated MgO surface is produced, which is subsequently destroyed upon heating giving the more stable cubic structure, was also observed by Moodie *et al* [9] during magnesium basic carbonate decomposition.

5.8.4 Powder XRD Studies Of The Dehydroxylated Brucite Samples

Powder XRD was performed on each of the MgO catalysts in the calcination series. These can then be compared to that of the parent brucite (Fig 5.5.1.1), to determine if the decomposition is complete. A typical diffraction pattern recorded following $Mg(OH)_2$

dehydration at 623 K in air for 3 hours is given below, the remainder are very similar but are not shown for the sake of brevity.
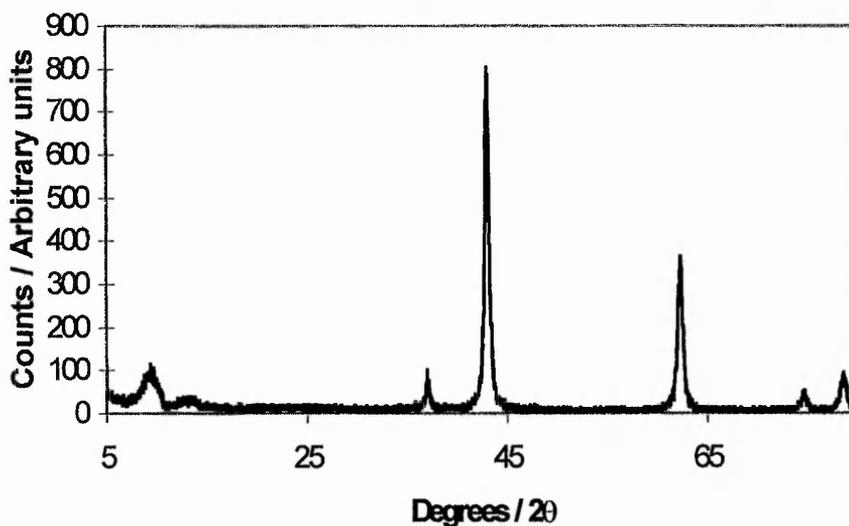
Fig 5.8.4.1   Powder X-Ray Diffraction Pattern Of MgO Prepared From Decomposing Magnesium Hydroxide In Air At 623 K For 3 Hours.

The positions of individual reflections of each of the samples are presented below, enabling the identification of any impurity phases or undecomposed brucite.

{hkl}	Tabulated[a]		623		723		823		923		1023		1123		1223	
	d / Å	Int	d / Å	Int	d / Å	Int	d / Å	Int	d / Å	Int	d / Å	Int	d / Å	Int	d / Å	Int
111	2.431	10	2.431	12	2.434	11	2.436	11	2.426	11	2.429	10	2.428	11	2.429	10
200	2.106	100	2.105	100	2.105	100	2.105	100	2.105	100	2.105	100	2.105	100	2.102	100
220	1.489	52	1.489	45	1.488	44	1.488	49	1.490	48	1.490	42	1.488	45	1.488	44
311	1.270	4	1.271	6							1.271	7	1.269	6	1.270	5
222	1.216	12					1.217	13	1.216	14	1.216	12	1.215	11	1.216	12

Mg(OH)$_2$ Decomposition Temperature / K

a - Magnesium oxide JCPDS file : 8-429 [80].

Table 5.8.4.1   Comparison Of Tabulated And Experimental Reflections Obtained From The Powder XRD Patterns Of The MgO Samples Prepared From Decomposing Magnesium Hydroxide In Air At Various Temperatures For 3 Hours.

The main result from the XRD is that the brucite dehydroxylation is complete in all cases, even at the lowest calcination temperature of 623 K. However any phase present at less than approximately 5 % will not be highlighted, due to the sensitivity of the technique. Earlier studies of Razouk and Mikhail [18, 89] claimed that roughly 5 % of the $Mg(OH)_2$ remained undecomposed after 5 hours at 623 K [18]. They found that temperatures in excess of 923 K were required to obtain 100 % conversion [89]. Similar work by Yoshida *et al* [134] showed the transition to MgO to be complete at 623 K.

5.8.5 XPS Studies Of The Dehydroxylated Brucite Samples

XP spectra of the MgO samples prepared from $Mg(OH)_2$ decomposition in air at 623, 923 and 1223 K for 3 hours were recorded. These catalysts were chosen for study as they were the ones on which isotopic oxygen exchange was subsequently performed.

Peak	Tabulated BE[a] /	MgO From Different Precursors / BE / eV		
	eV	Ribbon	Hydroxide	Basic Carbonate
O 2s	23.0		21.2	
Mg 2p	49.8	49.4	49.3	49.5
Mg 2s	90.0	88.1	88.3	87.7
C 1s	284.6	285.9	286.0	285.3
O 1s	531.0	531.6	531.2	531.4
Mg 1s	1305.0	1305.0	1305.0	1305.0
Unknown	-	None	None	None

a - Taken from the Handbook of Photoelectron Spectroscopy [82].

Table 5.8.5.1   Table Showing The Binding Energy positions Of The Maxima Of The MgO Catalysts Prepared From Decomposing Magnesium Hydroxide In Air At Various Temperatures For 3 Hours - Highlighting Any Impurities.

As Table 5.8.5.1 clearly shows there are no appreciable impurities present in the outermost layers of the MgO catalysts, prepared from brucite dehydroxylation, to the limit of

detection. Therefore measured rates of isotopic oxygen exchange can be explained in terms of reaction with the oxide layer, with foreign ions playing no part.

5.8.6 Isotopic Oxygen Exchange Reactions Of The Dehydroxylated Brucite Samples

Specific rates of isotopic oxygen exchange were measured on three of the MgO catalysts in the calcination series, samples decomposed at 623, 923 and 1223 K in static air for 3 hours. These were chosen as they represent the full range of the dehydroxylation temperatures studied.

Exchange was followed at 80 torr and 708 K after vacuum pre-treatment at 733 K for 16 hours, the results of which are tabulated below.

Decomposition Temperature / K	Ratio $R_1:R_2$	Specific Rate Of Exchange / x 10^{13} atoms s^{-1}/m^2		
		R_1	R_2	Total
623	3:2	0.75 ± 0.19	0.57 ± 0.19	1.32 ± 0.39
923	6:1	3.08 ± 0.19	0.55 ± 0.25	3.63 ± 0.44
1223	2:3	0.92 ± 0.16	1.22 ± 0.26	2.14 ± 0.41

Table 5.8.6.1   **Specific Rates Of Isotopic Oxygen Exchange Measured On The MgO Catalysts At 80 Torr And 708 K Prepared From Decomposing Magnesium Hydroxide In Air At Various Temperatures For 3 Hours.**

The most interesting result of these exchange reactions is the apparent structure sensitivity between the samples prepared at different dehydration temperatures. From Table 5.8.6.1 the MgO catalyst calcined at 923 K is more active than those at 623 and 1223 K, which are quite similar. It is also clear from Table 5.8.6.1 that R_2 exchange is occurring on each of these catalysts studied, with its initial rate increasing with calcination temperature.

From the present results it would appear that the most active catalyst is associated with a (111) terminated surface. It is to be expected that there would be a greater exposure of low co-ordinated sites when this (111) orientation is dominating. Since these ions were shown not to participate in exchange (Section 3.10.4), the structure sensitivity found is

quite suprising. However it has been demonstrated [10, 129], that the presence of hydroxyl groups are required, for stabilisation of the (111) plane. As concluded previously (Section 3.10.3), the active site for exchange on the Ube MgO samples was associated with an O^- anion, produced by the removal of atomic hydrogen from an adsorbed OH^- group. Therefore the abundance of these on the predominantly (111) terminated catalyst, could explain the higher specific rate observed, compared to the (100) orientated MgO, where hydroxyl coverage is considerably lower.

If the higher activity of dehydrated brucite samples was associated with (111) terminated surfaces, one would expect the initial rate of exchange to be higher on the 623 K calcined sample, which from Table 5.8.6.1 is not the case. The reason for the poor performance of this catalyst may lie in morphological and surface area changes, experienced during pre-treatment prior to exchange, as this temperature was 110 K greater than that used for decomposition. A more detailed study of this is given in the next section.

5.8.7 Characterisation After Exchange Of The Dehydroxylated Brucite Samples

Upon completion of a reaction the catalyst was removed from the reactor, allowing the characterisation of an exchanged sample. Both surface area and XPS measurements were obtained, the former being tabulated below.

Brucite Decomposition	Surface Area / m^2g^{-1}	
Temperature / K	Prior to exchange	Following exchange
623	64	46
923	69	71
1223	34	34

Table 5.8.7.1   Measured Surface Areas Of The MgO Catalysts Before And After Exchange Prepared From Decomposing Magnesium Hydroxide In Air At Varying Temperatures For 3 Hours.

As briefly mentioned in the previous section (Section 5.8.6), the rate of isotopic oxygen exchange on the 623 K prepared sample was unusually low, compared to the 923 K catalyst, which was considered to be of a similar nature. This may be explained in terms of the value taken for the surface area following treatment, but prior to exchange. With previous experiments run after heating in vacuum it was assumed this procedure caused no appreciable change in the specific area, as shown by several workers [58-60, 89], in the temperature region studied. However the 623 K decomposed catalyst is unique, as it is the only one where the treatment temperature is higher than that of formation.

Of the three catalysts tested it is expected that the 623 K decomposed sample has retained the greatest coverage of adsorbed hydroxyl groups at the surface. Therefore it is suggested that this sample will show the greatest loss in hydroxyl concentration during treatment. As a consequence of this there may be a change in morphology. Therefore the surface area both before and following treatment may not be the same. When normalising the initial rates of isotopic exchange the former value was taken, whereas it is probable that the surface area was different than this on the commencement of exchange. As a result of this the initial rate quoted in Table 5.8.6.1 may be inaccurate. Unfortunately there are no intermediate surface area measurements or electron micrographs to support this claim.

Finally it is interesting to note that there is no change in surface areas of the 923 and 1223 K powders both before and following a reaction. This is in disagreement with the observations made on the Ube MgO catalysts (Sections 3.7.3 and 3.8.4). It was found that the vacuum treatment had little effect on the measured surface area, but during exchange $^{18}O_2$ caused sintering. Currently there is no explanation for this.

It can also be seen that there is a slight increase in the surface area of the 923 K catalyst after exchange. This can be attributed to the limits in experimental error in using the Quantisorb instrument.

XP spectra of the three samples were recorded after completion of a reaction and are summarised below.

Peak	Tabulated BE[a]	Mg(OH)₂ Decomposition Temperature / BE / eV		
	/eV	623 K	923 K	1223 K
O 2s	23.0			
Mg 2p	49.8	49.2	49.8	
Mg 2s	90.0	88.3	87.7	87.9
C 1s	284.6	285.6	285.4	284.4
O 1s	531.0	531.6	531.2	531.5
Mg 1s	1305.0	1305.0	1305.0	1305.0
Unknown	-	None	None	None

a - taken from the Handbook of Photoelectron Spectroscopy [82].

**Table 5.8.7.2   Table Showing The Binding Energy Positions Of The Maxima Of The Exchanged
MgO Catalysts Prepared From Decomposing Magnesium Hydroxide In Air At
Various Temperatures For 3 Hours - Highlighting Any Impurities.**

From Table 5.8.7.2 as with the XP spectra of the unexchanged catalysts (Table 5.8.5.1), there are no impurities present in the outermost layers of the oxide, with the detection limits of the instrument Therefore exchange can be explained solely in terms of interaction with the oxide lattice.

5.9   Discussion

5.9.1 Characterisation Of MgO Prepared From Different Precursors

Characterisation of MgO catalysts prepared from magnesium ribbon, hydroxide and basic carbonate shows they exhibit properties very similar to those synthesised via the same route previously [3, 6, 8, 9, 18, 23, 89, 130]. In addition they have morphologies and surface areas directly comparable to ones published earlier by this group [6, 7].

Morphology has also been studied by the application of a method used by Berry [81], calculating the degree of cubic morphology for a MgO sample, which has been

adopted to test the current materials. The results of this (Section 5.5.3) showed excellent agreement with TEM studies (Section 5.4), indicating that MgO prepared from magnesium ribbon consists of near perfect cubes. The ex hydroxide sample is also cubic in nature, however some irregular crystallites are observed, due to the microfaceting of small cubes [3, 9]. Finally the crystals of the ex basic carbonate catalyst are poorly defined, with most of the cubelets present having rounded edges, many exhibiting a spherical like shape. Therefore it can be concluded that this procedure augments the electron microscopy findings very well.

5.9.2 Isotopic Oxygen Exchange On MgO Prepared From Different Precursors

MgO prepared from magnesium basic carbonate showed a specific rate 5 times greater than the other two catalysts, which were similar. For this material, the active site was tentatively assigned to a bottom step site associated with the irregular surface. It is thought that such a site is more abundant on this sample due to microfaceting as evidenced by TEM, leading to the exposure of higher index (110) and (111) mean planes. The similarity in overall specific rates between the ribbon residue and ex hydroxide, which both exhibit predominantly (100) faces but possess large differences in crystallite size, provides further confirmation for the absence of involvement of low co-ordination ions. Previous results by this group observed the same trend during methane coupling reactions using similarly derived catalysts [6, 7].

However unlike the ex ribbon and Ube samples, the R_2 reaction was additionally observed to occur on the ex hydroxide sample as well as the ex basic carbonate. This result is quite suprising as it appears to have a similar morphology to the these two materials. It is suggested that two active sites in close proximity are responsible for R_2 exchange.

Previous experiments of Klier *et al* [45, 46] also observed R_2 exchange on MgO in conjunction with R_1, however no reference to the origin of the MgO was made. Neither Winter [48], using an ex magnesium carbonate catalyst, or Boreskov [38], found any evidence of R_2 exchange on MgO. Therefore it seems the R_2 exchange characteristics may be influenced by the MgO precursor.

Again as with the Ube catalysts (Section 3.10.3) it is thought exchange is proceeding via interaction with oxygen of an adsorbed O^- species, resulting from the

dissociation of a surface OH⁻ group. Care was taken to minimise water vapour attack by storing the catalysts in a dessicator when not in use, however the presence of hydroxyl groups cannot be discounted.

Comparisons of the rates of isotopic oxygen exchange over a series of MgO catalysts prepared from different precursors, is the first known of its kind. As described above measurements show the reaction to be structure sensitive, depending upon the parent substance used, with the ex basic carbonate catalyst being most reactive. This result is very important when analysing previous literature on this subject, as all MgO was assumed to be equivalent, irrespective of its origin. This finding could explain discrepancies in activities reported by different workers.

Winter [48] found that his extrapolated initial rate at 573 K was approximately an order of magnitude greater than Boreskov [38], at the same temperature. Boreskov [38] attributed this to variations in pre-treatment conditions. However the current experiments indicate the answer may lie with the precursor used. Therefore these studies show that it is essential to stipulate the origin of the catalyst, when performing isotopic oxygen exchange on MgO.

5.9.3 Preparation And Isotopic Exchange Of (111) Terminated MgO

From Section 5.8 it is clear from TEM characterisation that the (111) plane of MgO has successfully been stabilised. Micrographs indicate that the (111) terminated planes are stable when heating in air, between the decomposition temperature of brucite and 923 K. Above this, reconstruction is observed, leading to the more commonly encountered (100) orientation. It is thought that the stability is provided by surface hydroxyl groups, adsorbed at terminal positions. It appears that the disappearance of (111) terminated planes coincide with increasing hydroxyl desorption on the surface, which is complete at ca. 1073 K [4, 12-14, 17, 96], a temperature where (100) crystals become evident.

A suprising result from isotopic oxygen exchange reactions on these catalysts is that there is an apparent structure sensitivity, observable with a (111) terminated MgO catalyst. This would not be expected as this orientation should lead to the exposure of more low co-ordinated ions. Therefore it appears that there is another feature of the (111) plane which promotes the active site responsible for isotopic oxygen exchange.

Since hydroxyl groups are present, especially with the (111) terminated planes, it would appear that they contribute to isotopic oxygen exchange. As mentioned previously with the Ube samples (Section 3.10.3), O^- from the disproportionation of adsorbed OH^- species, are thought to exchange preferentially before oxygen of the lattice. However the sample decomposed at 1223 K shows no sign of (111) surfaces, but it is still unclear if hydroxyl groups are available, offering a route for exchange with this catalyst.

Again as with the ex magnesium hydroxide sample decomposed at 1073 K (Section 5.9.3), R_2 exchange was evident on all the catalysts, irrespective of them comprising of predominantly (100) or (111) terminated surfaces.

6. Conclusions And Future Work

6.1   Conclusions

From performing isotopic oxygen exchange reactions on a set of Ube MgO samples possessing cube lengths in the range 100-2000 Å, it was found that this reaction was structure insensitive. A surface area difference of approximately an order of magnitude was measured between the 100 and 2000 Å catalysts, consequently the populations of 3 and 4 co-ordinated sites would be expected to be much higher on the former sample. Due to their similar specific rates of isotopic oxygen exchange, it would appear that ions exhibiting 3 and 4 co-ordination do not participate alone in this reaction. Further evidence of this was provided by both photoluminescence and UV/VIS/NIR diffuse reflectance spectroscopy, measuring the relative populations of 3 and 4 co-ordinated sites on the surface. Experiments showed that for 3 and 4 co-ordinated sites there was a difference of roughly a factor of 5 and 3 between the 100 Å and 2000 Å MgO catalysts respectively. Therefore if either of these co-ordination types were solely responsible for exchange, the rate should vary, whereas they were found to be equal within the limits of experimental error.

Even though isotopic oxygen exchange was found to be structure insensitive on the Ube MgO samples the rate of exchange progressively decreased during a reaction, indicating a fixed number of sites available for exchange. In all cases no more than 9 % of a monolayer was exchangeable at 733 K. An isotopic switching experiment was performed where an ^{18}O rich surface was re-exchanged with $^{16}O_2$. The kinetics of the forward and reverse reactions were very similar, indicating the equivalence of each active site and that exchange occurred in a sequential manner. This also shows that there are a fixed number of active sites which vary in direct proportion to surface area.

The nature of the active site was tentatively assigned to an O^- anion, formed from the dissociation of a surface OH^- species, adsorbed on an Mg^{2+}_{5C} cation. It is suggested that hydroxyl groups are present as the pre-treatment temperature used for isotopic oxygen exchange reactions was insufficient to remove them.

For exchange reactions involving MgO prepared from magnesium ribbon, magnesium hydroxide and magnesium basic carbonate differences in specific rate were

evident. MgO prepared from the basic carbonate showed a rate 5 times greater than the other two catalysts, which were very similar. Previous results by this group observed the same trend regarding methane coupling experiments on the same catalysts. Low co-ordination ions were shown not to facilitate the reaction as populations of these were much higher on the ex hydroxide sample. For the ex basic carbonate MgO the active site was tentatively assigned to a bottom step site, associated with the irregular surface. It was thought such a site was more abundant on this sample due to microfaceting, leading to the exposure of higher index (110) and (111) mean planes.

Another interesting result from these experiments was the occurrence of R_2 exchange on the ex hydroxide and ex basic carbonate samples. This result was quite suprising as the ex hydroxide sample exhibits a similar morphology to the ex ribbon and Ube samples, neither of which facilitated R_2 exchange. It is suggested that R_2 exchange occurs where two active sites could be in close proximity, where exchange could occur simultaneously. Also as with the Ube MgO samples it is thought exchange is occurring preferentially with adsorbed O^- species on these catalysts, rather than the surface layer of the oxide.

Finally the formation of (111) terminated MgO surfaces have been achieved, from decomposing brucite in air at various temperatures. Generally this orientation is not observed due to its relative instability, however it is suggested that hydroxyl groups adsorbed at terminal positions stabilise the structure. The (111) planes are only observed at calcination temperatures up to around 1023 K, above this reconstruction is evident leading to the formation of the more stable (100) orientation. This change in morphology is thought to be associated with the loss of hydroxyl groups from the surface. Isotopic oxygen exchange reactions on these catalysts shows a difference in specific rate, with a (111) terminated sample showing the highest activity. This is quite suprising since this catalyst would be expected to expose more lower co-ordinated ions, which are considered to be inactive for exchange. Therefore it is suggested that there is another feature of the (111) terminated planes which promotes active site formation. It is thought that exchange with O^- present from hydroxyl group decomposition may be evident here, as OH^- species are thought to be present at terminal positions, stabilising the (111) surface.

6.2   Future Work

In an attempt to determine if exchange occurs via interactions with hydroxyl groups or the oxide surface, isotopic hydrogen/deuterium exchange reactions can be performed on the MgO samples, similar to those by Cunningham *et al* [72] on CaO. Evidence of exchange would verify the presence of hydroxyl groups and the extent of reaction would enable their surface coverage.

An interesting IR experiment can be performed to determine if exchange occurs with 3 fold co-ordinated sites. In Chapter 4 the reactivity of O^{2-}_{3C} anions towards CO was extensively studied using FTIR spectroscopy. The first species observed on the surface at 77 K was the carbonite ion (CO_2^{2-}) at 1472 cm^{-1}. However if the surface anion was $^{18}O^{2-}_{3C}$, upon interaction with CO the band would be shifted to a wavenumber lower than 1472 cm^{-1} due to an isotope effect. Therefore if during an isotopic reaction ^{18}O exchanges with 3C sites the above result will be seen. This can be tested by carrying out an IR experiment on an exchanged sample. This type of reaction was attempted by Babaeva *et al* [118], using a CaO catalyst. In this study they found that a carbonite ion adsorbed on a $Ca^{18}O$ surface was 22 cm^{-1} lower than when using normal $Ca^{16}O$.

Clearly further work is required regarding exchange reactions on the MgO samples prepared from different precursors and the (111) terminated MgO surfaces. Exchange was only performed at a single temperature on each of these catalysts, therefore further experiments are required to obtain a better understanding of the exchange characteristics on these samples. It would be of interest to follow reactions over a range of temperatures, allowing the determination of activation energies and pre-exponential terms of exchange.

Regarding the (111) terminated MgO surfaces isotopic oxygen exchange was only measured on 3 of the 7 catalysts prepared, therefore a much more detailed study is warranted regarding this system. Also the rate of R_2 exchange varied between the samples, it would be interesting to know how temperature influenced this process

Finally it has recently been shown that MgO can be synthesised from precursors other than magnesium ribbon, magnesium hydroxide and magnesium basic carbonate. It has been demonstrated by Thoms *et al* [135, 136] that it is possible to prepare MgO from various magnesium alcoholates. SEM analysis showed differences in morphology and crystallinity, depending upon the alcoholate used. It would therefore be of interest to

investigate the isotopic exchange characteristics of these materials, comparing them to MgO obtained from the more conventional methods.

7. References

[1]   Henrich, V. E., and Cox, P. A., The Surface Science Of Metal Oxides, Cambridge University Press, (1994), 32-34.

[2]   The Chemical Society Of London, Tables Of Interatomic Distances And Configuration In Molecules And Ions, The Chemical Society Of London, (1958).

[3]   Moodie, A. F., and Warble, C. E., J. Cryst. Growth, 1971, **10**, 26-38.

[4]   Coluccia, S., Tench, A. J., and Segall, R. L., J. Chem. Soc., Faraday Trans. 1, 1979, **75**, 1769-1779.

[5]   Coluccia, S., Baricco, M., Marchese, L., Martra, G., and Zecchina, A., Spectrochim. Acta, 1993, **49A**, 1289-1298.

[6]   Hutchings, G. J., Hargreaves, J. S. J., Joyner, R. W., and Kiely, C. J., Chemtech, 1994, **11**, 25-29.

[7]   Hargreaves, J. S. J., Hutchings, G. J., Joyner, R. W., and Kiely, C. J., J. Catal., 1992, **135**, 576-595.

[8]   Kuroda, Y., Yasugi, E., Aoi, H., Miura, K., and Morimoto, T., J. Chem. Soc., Faraday Trans. 1, 1988, **84**, 2421-2430.

[9]   Moodie, A. F., Warble, C. E., and Williams, L.C., J. Am. Ceram. Soc., 1966, **49**, 676-677.

[10]   Boudart, M., Delbouille, A., Derouane, E., Indovina, V., and Walters, A. B., J. Am. Chem. Soc., 1972, **94**, 6622-6630.

[11]   Onishi, H., Egawa, C., Aruga, T., and Iwasawa, Y., Surf. Sci., 1987, **191**, 479-491.

[12]   Coluccia, S., Barton, A., and Tench, A., J., J. Chem. Soc., Faraday Trans. 1, 1981, **77**, 2203-2207.

[13]   Coluccia, S., Deane, A. M., and Tench, A. J., J. Chem. Soc., Faraday Trans. 1, 1978, **74**, 2913-2922.

[14]   Duley, W. W., J. Chem. Soc., Faraday Trans. 1, 1984, **80**, 1173-1179.

[15]   Zecchina, A., Lofthouse, M. G., and Stone, F. S., J. Chem. Soc., Faraday Trans. 1, 1975, **71**, 1476-1490.

[16]   Anderson, P. J., Horlock, R. F., and Oliver, J. F., Trans. Faraday Soc., 1965, **61**, 2754-2762.

[17]   Coluccia, S., Marchese, L., Lavagnino, S., and Anpo, M., Spectrochim. Acta, 1987, **43A**, 1573-1576.

[18]   Razouk, R. I., and Mikhail, R. S., J. Phys. Chem, 1955, **59**, 636-640.

[19]   Malinowski, S., Szczepanska, S., Bielanski, A., and Sloczynski, J., J. Catal., 1965, **4**, 324-331.

[20]   Gregg, S. J., and Ramsay, J. D., J. Chem. Soc. (A), 1970, 2784-2787.

[21]   Evans, J. V., and Whateley, T. L., Trans. Faraday Soc., 1967, **63**, 2769-2777.

[22]   Ito, T., J. Chem. Soc., Faraday Trans. 1, 1982, **78**, 1603-1613.

[23]   Gregg, S. J., Packer, R. K., and Wheatley, K. H., J. Chem. Soc., 1955, 46-50.

[24]   Smart, R. St. C., Slager, T. L., Little, L. H., and Greenler, R. G., J. Phys. Chem., 1973, **77**, 1019-1023.

[25]   Hattori, H., Shimazu, K., Yoshii, N., and Tanabe, K., Bull. Chem. Soc. Jpn., 1976, **49**, 969-972.

[26]   Tsuji, H., Shishido, T., Okamura, A., Gao, Y., Hattori, H., and Kita, H., J. Chem. Soc., Faraday Trans., 1994, **90**, 803-807.

[27]   Fukuda, Y., and Tanabe, K., Bull. Chem. Soc. Jpn., 1973, **46**, 1616-1619.

[28]   Garrone, E., Zecchina, A., and Stone, F. S., Philos. Mag., Sect. B, 1980, **42**, 683-703.

[29]   Dunski, H., Józwiak, W. K., and Sugier, H., J. Catal.,1994, **146**, 166-172.

[30]   Beruto, D., Searcy, A. W., Botter, R., and Giordani, M. J., J. Phys. Chem., 1993, **97**, 9201-9205.

[31]   Jones, C. F., Reeve, R. A., Rigg, R., Segall, R. L., Smart, R. St. C., and Turner, P. S., J. Chem. Soc., Faraday Trans. 1, 1984, **80**, 2609-2617.

[32]   Langel, W., and Parrinello, M., Phys. Rev. Lett., 1994, **73**, 504-507.

[33]   de Leeuw, N. H., Watson, G. W., and Parker, S. C., J. Phys. Chem., 1995, **99**, 17219-17225.

[34]   Aramendía, M. A., Borau, V., Jiménez, C., Marinas, J. M., Porras, A., and Urbano, F. J., J. Mater. Chem., 1996, **6**, 1943-1949.

[35]   Ito, T., Fujita, M., Watanabe, M., and Tokuda, T., Bull. Chem. Soc. Jpn., 1981, **54**, 2412-2419.

[36]   Allen, J. A., and Lauder, I., Nature, 1949, **164**, 142-143.

[37]   Winter, E. R. S., Adv. Catal., 1958, **10**, 196-241.

[38]   Boreskov, G. K., Adv. Catal., 1964, **15**, 285-339.

[39]   Nováková, J., Catal. Rev., 1970, **4**, 77-113.

[40]   Cunningham, J., Goold, E. L., and Leahy, E. M., J. Chem. Soc., Faraday Trans. 1, 1979, **75**, 305-313.

[41]   Cunningham, J., Goold, E. L., and Fierro, J. L. G., J. Chem. Soc., Faraday Trans. 1, 1982, **78**, 785-801.

[42]   Whalley, E., and Winter, E. R. S., J. Chem. Soc., 1950, 1175-1177.

[43]   Cameron, W. C., Farkas, A., and Litz, L. M., J. Phys. Chem., 1953, **57**, 229-238.

[44]   Guerro-Ruiz, A., Rodríguez-Ramos, I., Ferreira-Aparicio, P., and Volta, J. C., Catal. Lett., 1997, **45**, 113-118.

[45]   Muzykantov, V. S., Jíru, P., Klier., and Nováková, J., Collection Czech. Chem. Commun., 1968, **33**, 829-835.

[46]   Klier, K., Nováková, J., and Jíru, P., J. Catal., 1963, **2**, 479-484.

[47]   Muzykantov, V. S., Popovskii, V. V., and Boreskov, G. K., Kinet. Catal., 1964, **5**, 551-556.

[48]   Winter, E. R. S., J. Chem. Soc. (A), 1968, 2889-2902.

[49]   Winter, E. R. S., J. Catal., 1980, **61**, 562-564.

[50]   Margolis, L. Y., and Kiselev, V. A., Dokl. Acad. Nauk SSSR, 1960, **130**, 159-161.

[51]   Winter, E. R. S., J. Chem. Soc., 1954, 3342-3344.

[52]   Margolis, L. Y., Izvest. Akad. Nauk SSSR, 1959, 207-212.

[53]   Winter, E. R. S., J. Chem. Soc., 1955, 2726-2740.

[54]   Winter, E. R. S., J. Chem. Soc., 1955, 3824-3834.

[55]   Popovskii, V. V., and Boreskov, G. K., Kinet. Catal., 1960, **1**, 530-539.

[56]   Dzisyak, A. P., Boreskov, G. K., Kasatkina, L. A., and Kochurikhin, V. E., Kinet. Catal., 1961, **2**, 655-659.

[57]   Boreskov, G. K., Discuss. Faraday Soc., 1966, **41**, 263-276.

[58]   Winter, E. R. S., and Houghton, G., Mass Spectrometry - Inst. of Petroleum, 1952, 127-140.

[59]   Winter, E. R. S., Discuss. Faraday Soc., 1950, **8**, 231-237.

[60]   Houghton, G., and Winter, E. R. S., J. Chem. Soc.,1954, 1509-1516.

[61]   Winter, E. R. S., J. Chem. Soc., 1954, 1522-1527.

[62]   Winter, E. R. S., J. Chem. Soc., 1950, 1170-1175.

[63]   Barnard, J. A., Winter, E. R. S., and Briscoe, H. V. A., J. Chem. Soc.,1954, 1517-1521.

[64]   Boreskov, G. K., Kasatkina, L. A., and Popovskii, V. V., Kinet. Catal., 1960, **1**, 207-213.

[65]   Dzisyak, A. P., Boreskov, G. K., and Kasatkina, L. A., Kinet. Catal., 1962, **3**, 65-72.

[66]   Cunningham, J., and Goold, E. L., J. Chem. Soc, Faraday Trans. 1, 1981, **77**, 837-848.

[67]   Cunningham, J., Cullinane, D., Farrell, F., O'Driscoll, J. P., and Morris, M. A., J. Mater. Chem., 1995, **5**, 1027-1033.

[68]   Antoshin, G. V., Minachev, K. M., and Dmitrev, R. V., Kinet. Catal., 1968, **9**, 672-677.

[69]   Gorgoraki, V. I., Kasatkina, L. A., and Levin, V. Y., Kinet. Catal., 1963, **4**, 365-372.

[70]   Houghton, G., and Winter, E. R. S., Nature, 1949, **164**, 1130-1131.

[71]   Martin, D., and Duprez, D., J. Phys. Chem., 1996, **100**, 9429-9438.

[72]   Cunningham, J., and Healy, C. P., J. Chem. Soc., Faraday Trans. 1, 1987, **83**, 2973-2984.

[73]   Bond, G. C., Heterogenous Catalysis - Principles And Applications, Oxford Science Publications, 2nd Edition, (1987), 57-58.

[74]   Peil, K. P., Goodwin Jr, J. G., and Marcelin, G., J. Catal., 1991, **131**, 143-155.

[75]   Kalenik, Z., and Wolf, E. E., Catal. Lett., 1991, **9**, 441-450.

[76]   Mars, P., and van Krevelen, D. W., Chem. Eng. Sci. Sp. Suppl., 1954, **3**, pp41.

[77]   Brunauer, S., Emmet, P. H., and Teller, E., J. Am. Chem. Soc., 1938, **60**, 309-319.

[78]   Brunauer, S., Deming, L. S., Deming, W. E., and Teller, E., J. Am. Chem. Soc., 1940, **62**, 1723-1732.

[79]   Gregg, S. J., and Sing, K. W. S., Adsorption, Surface Area And Porosity, Academic Press Inc. Ltd, 2nd Edition, (1982), 4-5.

[80]   JCPDS International Centre For Diffraction Data, Selected Powder Diffraction Data For Education And Training - Search Manual And Data Cards, (1988).

[81]   Berry, C. R., Phys. Rev., 1947, **72**, 942-947.

[82]   Wagner, C. D., Riggs, W. M., Davis, L. E., Moulder, J. F., and Muilenberg, G. E.,
       Handbook Of X-Ray Photoelectron Spectroscopy, Perkin-Elmer Corporation,
       (1979), 187.

[83]   Scofield, J. H., J. Electron Spectrosc., 1976, **8**, 129-137.

[84]   Matsuura, I., Hashimoto, Y., Takayasu, O., Nitta, K., and Yoshida, Y., Appl. Catal.,
       1991, **74**, 273-280.

[85]   Hashimoto, Y., Takayasu, O., and Matsuura, I., Chem. Express, 1991, **6**, 81-84.

[86]   Lide, D. R., Handbook Of Chemistry And Physics, CRC Press Inc., 78th Edition,
       (1997).

[87]   Takayasu, O., Hata, T., and Matsuura, I., Chem. Express, 1990, **5**, 829-832.

[88]   Castanier, E., and Noguera, C., Surf. Sci., 1996, **364**, 1-16.

[89]   Razouk, R. I., and Mikhail, R. S., J. Phys. Chem., 1957, **61**, 886-891.

[90]   Gregg, S. J., J. Chem. Soc., 1953, 3940-3944.

[91]   Coluccia, S., Deane, A. M., and Tench, A. J., Proc. 6th Int. Congress on Catalysis,
       London, 1976, **1**, 171-182.

[92]   Coluccia, S., and Tench, A. J., Proc. 7th Int. Congress on Catalysis, Tokyo, 1981,
       1, 1154-1163.

[93]   Coluccia, S., Boccuzzi, F., Ghiotti, G., and Mirra, C., Z. Phys. Chem., 1980, **121**,
       141-143.

[94]   Coluccia, S., Boccuzzi, F., Ghiotti, G., and Morterra, C., J. Chem. Soc., Faraday
       Trans. 1, 1982, **78**, 2111-2119.

[95]   Anpo, M., Yamada, Y., and Kubokawa, Y., J. Chem. Soc., Chem. Commun., 1986,
       714-716.

[96]   Martens, R., Gentsch, H., and Freund, F., J. Catal., 1976, **44**, 366-372.

[97]   Kantorovich, L. N., Gillan, M. J., and White, J. A., J. Chem. Soc., Faraday Trans.,
       1996, **92**, 2075-2080.

[98]   Nelson, R. L., and Hale, J. W., Discuss. Faraday Soc., 1971, **52**, 77-88.

[99]   Zecchina, A., and Stone, F. S., J. Chem. Soc., Chem. Commun., 1974, 582-584.

[100] Garrone, E., and Stone, F. S., J. Chem. Soc., Faraday Trans. 1, 1987, **83**, 1237-
       1251.

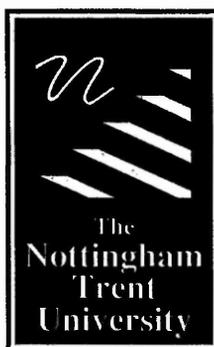[101] Tench, A. J., and Pott, G. T., Chem. Phys. Lett., 1974, **26**, 590-592.

[102] Anpo, M., Yamada, Y., Kubokawa, Y., Coluccia, S., Zecchina, A., and Che, M., J. Chem. Soc., Faraday Trans. 1, 1988, **84**, 751-764.

[103] Coluccia, S., Adsorption and Catalysis on Oxide Surfaces, Elsevier Science Publishers B. V., Amsterdam, (1985), 59-69.

[104] Shvets, V. A., Kuznetsov, A. V., Fenin, V. A., and Kazansky, V. B., J. Chem. Soc. Faraday Trans. 1, 1985, **81**, 2913-2919.

[105] Coluccia, S. and Tench, A. J., J. Chem. Soc., Faraday Trans. 1, 1983, **79**, 1881-1889.

[106] Duley, W. W., Philos. Mag., Sect. B, 1984, **49**, 159-170.

[107] Yanagisawa, Y., and Huzimura, R., J. Phys. Soc. Jpn., 1984, **53**, 66-69.

[108] Coluccia, S., and Borello, E., Proc. 8th Int. Congress on Catalysis, Berlin, 1984, **3**, 69-79.

[109] Knözinger, E., Jacob, K. H., and Hofmann, P., J. Chem. Soc., Faraday Trans. 1, 1993, **89**, 1101-1107.

[110] Cordischi, D., Indovina, V., and Occhiuzzi, M., J. Chem. Soc., Faraday Trans. 1, 1978, **74**, 456-465.

[111] Ito, T., Sekino, T., Moriai, N., and Tokuda, T., J. Chem. Soc., Faraday Trans. 1, 1981, **77**, 2181-2192.

[112] Ito, T., Kuramoto, M., Yoshioka, M., and Tokuda, T., J. Phys. Chem., 1983, **87**, 4411-4416.

[113] Ito, T., Yoshioka, M., and Tokuda, T., J. Chem. Soc., Faraday Trans. 1, 1983, **79**, 2277-2287.

[114] Zecchina, A., Coluccia, S., Spoto, G., Scarano, D., and Marchese, L., J. Chem. Soc., Faraday Trans. 1, 1990, **86**, 703-709.

[115] Scarano, D., Spoto, G., Bordigo, S., Coluccia, S., and Zecchina, A., J. Chem. Soc., Faraday Trans. 1, 1992, **88**, 291-296.

[116] Zecchina, A., Spoto, G., Coluccia, S., and Guglielminotti, E., J. Phys. Chem., 1984, **88**, 2575-2581.

[117] Escalona Platero, E., Scarano, D., Spoto, G., and Zecchina, A., Faraday Discuss. Chem. Soc., 1985, **80**, 183-193.

[118] Babaeva, M. A., Bystrov, D. S., Kovalgin, A. Y., and Tsyganenko, A. A., J. Catal., 1990, **123**, 396-416.

[119] Guglielminotti, E., Coluccia, S., Garrone, E., Cerruti, L., and Zecchina, A., J. Chem. Soc., Faraday Trans. 1, 1979, **75**, 96-108.

[120] Zecchina, A., and Stone, F. S., J. Chem. Soc., Faraday Trans. 1, 1978, **74**, 2278-2292.

[121] Garrone, E., Zecchina, A., and Stone, F. S., J. Chem. Soc., Faraday Trans. 1, 1988, **84**, 2843-2854.

[122] Bailes, M., and Stone, F. S., Mater. Chem. Phys., 1991, **29**, 489-501.

[123] Babaeva, M. A., and Tsyganenko, A. A., React. Kinet. Catal. Lett., 1987, **34**, 9-14.

[124] Pelmenschikov, A. G., Morosi, G., Gamba, A., and Coluccia, S., J. Phys. Chem., 1995, **99**, 15018-15022.

[125] Pelmenschikov, A. G., Morosi, G., Gamba, A., Coluccia, S., Martra, G., and Paukshtis, E. A., J. Phys. Chem., 1996, **100**, 5011-5016.

[126] Coluccia, S., Personal Communication.

[127] Aramendía, M. A., Borau, V., Jiménez, C., Marinas, J. M., Porras, A., and Urbano, F. J., J. Catal., 1996, **161**, 829-838.

[128] Goodman, J. F., Proc. R. Soc. London, Ser. A, 1958, **247**, 346-352.

[129] Wogelius, R. A., Refson, K., Fraser, D. G., Grime, G. W., and Goff, J. P., Geochim. Cosmochim. Acta, 1995, **59**, 1875-1881.

[130] Gregg, S. J., and Packer, R. K., J. Chem. Soc., 1955, 51-55.

[131] Britton, H. T. S., Gregg, S. J., and Winsor, G. W., J. Appl. Chem., 1952, **2**, 693-697.

[132] Massey, A. G., Main Group Chemistry, Ellis Horwood, (1990), 511.

[133] Kiely, C. J., Personal Communication.

[134] Yoshida, T., Tanaka, T., Yoshida, H., Funabiki, T., and Murata, T., J. Phys. Chem., 1995, **99**, 10890-10896.

[135] Thoms, H., Epple, M., Viebrock, H., and Reller, A., J. Mater. Chem., 1995, **5**, 589-594.

[136] Thoms, H., Epple, M., and Reller, A., Solid State Ionics, 1997, **101-103**, 79-84.

[137] Karasuda, T., and Aika, K., J. Catal., 1997, **171**, 439-448.

[138] Karasuda, T., Nagaoka K., and Aika, K., Stud. Surf. Sci. Catal., 1998, **119**, 283-288.

[139] Stockenhuber M., Personal Communication.

[140] Kellner, R., Mermet, J. M., Otto, M., and Widmer, H. M., Analytical Chemistry, Wiley-VCH, (1998), 557.

[141] Che, M., and Tench, A. J. Adv. Catal., 1982, **31**, 77-133.

[142] Che, M., and Tench, A. J. Adv. Catal., 1983, **32**, 1-148.

[143] Tench, A. J., and Lawson, T., Chem. Phys. Lett., 1970, **7**, 459-460.

[144] Naccache, C., Chem. Phys. Lett., 1971, **11**, 323-325.

[145] Tench, A. J., Lawson, T., and Kibblewhite, J. F. J., J. Chem. Soc. Faraday Trans. 1, 1972, **68**, 1169-1180.

[146] Tench, A. J., J. Chem. Soc. Faraday Trans. 1, 1972, **68**, 1181-1189.

[147] Naccache, C., and Che, M., 5th Int. Congress on Catalysis, Miami, 1972, **2**, 1389-1398.

[148] Nikisha, V. V., Shelimov, B. N., Shvets, V. A., Griva, A. P., and Kazansky, V. B., J. Catal., 1973, **28**, 230-235.

[149] Kazansky, V. B., Shvets, V. A., Kon, M. Y., Nikisha, V. V., and Shelimov, B. N., 5th Int. Congress on Catalysis, Miami, 1972, **2**, 1423-1433.